The Dissertation Committee for Irvin Allen Chen Certifies that this is the approved version of the following dissertation:

Synthesis of Portland Cement and Calcium Sulfoaluminate-Belite Cement for Sustainable Development and Performance

Committee:

Maria C.G. Juenger, Supervisor

Desiderio Kovar

Kevin J. Folliard

Harovel G. Wheat

J. Steven Swinnea

Synthesis of Portland Cement and Calcium Sulfoaluminate-Belite Cement for Sustainable Development and Performance

by

Irvin Allen Chen, B.S.

Dissertation

Presented to the Faculty of the Graduate School of

The University of Texas at Austin

in Partial Fulfillment

of the Requirements

for the Degree of

Doctor of Philosophy

The University of Texas at Austin

December 2009

Dedication

This dissertation is dedicated to my parents.

Acknowledgements

My deepest appreciation goes to my advisor, Dr. Maria Juenger, for her guidance, support, and encouragement during my doctoral study. Dr. Juenger allows me the freedom to grow as a researcher. I would also like to thank my committee, Dr. Kevin Folliard, Dr. Desiderio Kovar, Dr. Harovel Wheat, and Dr. Steven Swinnea for their valuable suggestions and insights.

I am grateful to the Cockrell School of Engineering and the Graduate School Office at the University of Texas at Austin for awarding me fellowships that allowed me to put full efforts into research and study.

I would also like to acknowledge Mr. Michael Rung and Mr. Chris Clement for providing technical support, Ms. Sherian Williams and Ms. Clarissa Peña for administrative assistance, and Mr. Ryan Chancey and Ms. Katherine Gustashaw for assisting on cement analysis work.

Finally, I would like to thank my parents, David Chen and Chenghwa Hsu, my sister, Arlene Chen, and my fiancé, I-Yun Wang, for their unconditional love and support.

This research was funded by the National Science Foundation, Project Number CMMI 0448983 and Portland Cement Association Education Foundation Research Fellowship, Project Number F08-07.

Synthesis of Portland Cement and Calcium Sulfoaluminate-Belite Cement for Sustainable Development and Performance

Publication No._____

Irvin Allen Chen, PhD

The University of Texas at Austin, 2009

Supervisor: Maria C.G. Juenger

Portland cement concrete, the most widely used manufactured material in the world, is made primarily from water, mineral aggregates, and portland cement. The production of portland cement is energy intensive, accounting for 2% of primary energy consumption and 5% of industrial energy consumption globally. Moreover, portland cement manufacturing contributes significantly to greenhouse gases and accounts for 5% of the global CO_2 emissions resulting from human activity. The primary objective of this research was to explore methods of reducing the environmental impact of cement production while maintaining or improving current performance standards. Two approaches were taken, 1.) incorporation of waste materials in portland cement synthesis, and 2.) optimization of an alternative environmental friendly binder, calcium sulfoaluminate-belite cement. These approaches can lead to less energy consumption, less emission of CO_2, and more reuse of industrial waste materials for cement manufacturing. In the portland cement part of the research, portland cement clinkers conforming to the compositional specifications in ASTM C 150 for Type I cement were

successfully synthesized from reagent-grade chemicals with 0% to 40% fly ash and 0% to 60% slag incorporation (with 10% intervals), 72.5% limestone with 27.5% fly ash, and 65% limestone with 35% slag. The synthesized portland cements had similar early-age hydration behavior to commercial portland cement. However, waste materials significantly affected cement phase formation. The C_3S–C_2S ratio decreased with increasing amounts of waste materials incorporated. These differences could have implications on proportioning of raw materials for cement production when using waste materials. In the calcium sulfoaluminate-belite cement part of the research, three calcium sulfoaluminate-belite cement clinkers with a range of phase compositions were successfully synthesized from reagent-grade chemicals. The synthesized calcium sulfoaluminate-belite cement that contained medium $C_4A_3\overline{S}$ and C_2S contents showed good dimensional stability, sulfate resistance, and compressive strength development and was considered the optimum phase composition for calcium sulfoaluminate-belite cement in terms of comparable performance characteristics to portland cement. Furthermore, two calcium sulfoaluminate-belite cement clinkers were successfully synthesized from natural and waste materials such as limestone, bauxite, flue gas desulfurization sludge, Class C fly ash, and fluidized bed ash proportioned to the optimum calcium sulfoaluminate-belite cement synthesized from reagent-grade chemicals. Waste materials composed 30% and 41% of the raw ingredients. The two calcium sulfoaluminate-belite cements synthesized from natural and waste materials showed good dimensional stability, sulfate resistance, and compressive strength development, comparable to commercial portland cement.

Table of Contents

List of Tables xii

List of Figures xiv

Chapter 1: Introduction 1

1.1 Research Objective 1

1.2 Research Plan 2

1.2.1 Portland Cement 2

1.2.2 Calcium Sulfoaluminate-Belite Cement 4

1.3 Overview of Dissertation 8

1.4 Notations 8

1.4.1 Cement Chemistry Notations 8

1.4.2 Acronyms 9

Chapter 2: Background and Literature Review 10

2.1 Portland Cement 10

2.1.1 Background 10

2.1.2 Waste Materials Incorporation 11

2.2 Calcium Sulfoaluminate-Belite Cement 12

2.2.1 Background 12

2.2.2 History and Potential 14

2.2.3 Synthesis 15

2.2.4 Hydration 18

2.2.5 Porosity Development 21

2.2.6 Dimensional Stability 22

2.2.7 Strength Development 23

2.2.8 Sulfate Resistance 25

2.2.9 Corrosion Resistance 25

Chapter 3: Incorporation of Waste Materials into Portland Cement Clinker Synthesized from Reagent-Grade Chemicals 28
3.1 Introduction 28
3.2 Experimental 29
3.2.1 Materials 29
3.2.2 Synthesis 30
3.2.3 Analysis 32
3.2.3.1 X-Ray Diffraction 32
3.2.3.2 Scanning Electron Microscopy 33
3.2.3.3 Isothermal Conduction Calorimetry 33
3.3 Results and Discussion 34
3.3.1 Phase Composition 34
3.3.2 Microstructure 39
3.3.3 Early-Age Hydration Behavior 45
3.4 Conclusions 49
Chapter 4: Incorporation of Waste Materials into Portland Cement Clinker Synthesized from Natural Materials 50
4.1 Introduction 50
4.2 Experimental 50
4.2.1 Materials 50
4.2.2 Synthesis 52
4.2.3 Analysis 53
4.2.3.1 X-Ray Diffraction 53
4.2.3.2 Scanning Electron Microscopy 54
4.2.3.3 Isothermal Conduction Calorimetry 55
4.3 Results and Discussion 55
4.3.1 Phase Composition 55
4.3.2 Microstructure 61
4.3.3 Early-Age Hydration Behavior 67
4.4 Conclusions 71

Chapter 5: Calcium Sulfoaluminate-Belite Cement: Synthesis 73
5.1 Introduction 73
5.2 Materials Proportioning 74
5.3 Synthesis 75
5.4 Analysis 76
5.4.1 Thermogravimetric Analysis 76
5.4.2 Particle Fineness and Particle Size distribution 77
5.4.3 X-Ray Diffraction 77
5.4.4 Scanning Electron Microscopy 78
5.5 Results and Discussion 79
5.5.1 Thermogravimetric Analysis 79
5.5.2 Particle Fineness and Distribution 80
5.5.3 Phase Composition 82
5.5.4 Phase Distribution 85
5.6 Conclusions 89

Chapter 6: Calcium Sulfoaluminate-Belite Cement: Effects of Phase Composition on Hydration and Properties 90
6.1 Introduction 90
6.2 Analysis 91
6.2.1 Isothermal Conduction Calorimetry 91
6.2.2 X-Ray Diffraction 91
6.2.3 Scanning Electron Microscopy 92
6.2.4 Dimensional Stability and Sulfate Resistance 93
6.2.5 Compressive Strength Development 93
6.3 Results and Discussion 94
6.3.1 Early-Age Hydration Behavior 94
6.3.2 Hydration Product Development 104
6.3.3 Dimensional Stability 115
6.3.4 Sulfate Resistance 121
6.3.5 Compressive Strength Development 127

6.4 Conclusion 128

Chapter 7: Calcium Sulfoaluminate-Belite Cement: Incorporation of Waste Materials. 131

7.1 Introduction 131

7.2 Materials Selection and Proportioning 132

7.3 Synthesis 135

7.4 Analysis 136

7.4.1 Particle Fineness and Particle Size distribution 136

7.4.2 X-Ray Diffraction 136

7.4.3 Scanning Electron Microscopy 137

7.4.4 Isothermal Conduction Calorimetry 138

7.4.5 Dimensional Stability and Sulfate Resistance 138

7.4.6 Compressive Strength Development 139

7.5 Results and Discussion 139

7.5.1 Particle Size and Distribution 139

7.5.2 Phase Composition and Distribution 141

7.5.3 Early-Age Hydration Behavior and Hydration Product Development 149

7.5.4 Dimensional Stability and Sulfate Resistance 170

7.5.5 Compressive Strength Development 172

7.6 Conclusions 173

Chapter 8: Conclusions and Future Research 176

8.1 Conclusions 176

8.2 Future Research 179

Appendix A: X-Ray Patterns for the Hydrated Synthesized Calcium Sulfoaluminate-Belite Cements 181

Bibliography 188

Vita 195

List of Tables

Table 2.1 – Cement phases lime contents (Mehta, 1980)....13
Table 3.1 – Chemical compositions (%) of the fly ash and slag used....30
Table 3.2 – Phase content (%) of clinker samples synthesized by reagent-grade chemicals (RG) with waste materials incorporation....35
Table 3.3 – Comparison of image and Rietveld analysis results (%) for clinker samples synthesized by reagent-grade chemicals (RG), 40% fly ash incorporation, and 60% slag incorporation....45
Table 3.4 – Blaine fineness values for a commercial Type I/II portland cement (control) and clinker samples synthesized using reagent-grade chemicals (RG) with waste materials incorporation....46
Table 4.1 – Chemical compositions of the natural materials and industrial waste materials used....51
Table 4.2 – Comparison of Bogue calculation and Rietveld analysis results for clinker samples synthesized from reagent-grade chemicals (RG), GLS with 27.5% YLS, GLS with 27.5% fly ash, and GLS with 35% slag....57
Table 4.3 – Comparison of multispectral (MS) and Rietveld analysis results for clinker samples synthesized GLS with 27.5% YLS, GLS with 27.5% fly ash, and GLS with 35% slag....67
Table 4.4 – Blaine fineness values for a commercial Type I/II portland cement (control) and clinker samples synthesized from reagent-grade chemicals, GLS with 27.5% YLS, GLS with 27.5% fly ash, and GLS with 35% slag....68
Table 5.1 – Target phase compositions for the CSAB cement clinkers synthesized from reagent-grade chemicals....75
Table 5.2 – Blaine fineness values for a commercial Type I/II portland cement (PC) and the CSAB cement clinkers synthesized from reagent-grade chemicals....81
Table 5.3 – Phase compositions for the CSAB cement clinkers synthesized from reagent-grade chemicals (TG: target calculated from the Bogue equations; R: Rietveld analysis)....85
Table 6.1 – Calculated and measured optimum gypsum contents for the CSAB cement clinkers synthesized from reagent-grade chemicals and their relevant phase contents....98
Table 6.2 – Phase compositions for the hydrated synthesized CSAB cements from reagent-grade chemicals....105
Table 7.1 – Chemical compositions for the natural materials and industrial waste materials used....133
Table 7.2 – Proportion of raw ingredients for the CSAB cement clinkers synthesized from Class C fly ash (MC) and fluidized bed ash (MF)....135
Table 7.3 – Blaine fineness values for a commercial Type I/II portland cement (PC) and the CSAB cement clinkers synthesized from reagent-grade chemicals (MS) Class C fly ash (MC), and fluidized bed ash (MF)....140

Table 7.4 – Phase compositions for the CSAB cement clinkers synthesized from reagent-grade chemicals (MS), Class C fly ash (MC), and fluidized bed ash (MF) (TG: target calculated from the Bogue equations; R: Rietveld analysis)..... 145
Table 7.5 – Calculated and measured optimum gypsum contents for the synthesized CSAB cements from reagent-grade chemicals (MS), Class C fly ash (MC), and fluidized bed ash (MF) and their relevant phase contents for ettringite formation 152
Table 7.6 – Phase compositions for the hydrated synthesized CSAB cements from reagent-grade chemicals (MS), Class C fly ash (MC), and fluidized bed ash (MF) 156
Table 7.7 – Phase compositions for the hydrated synthesized CSAB cements from reagent-grade chemicals (MS), Class C fly ash (MC), and fluidized bed ash (MF); MC and MF with 1% citric acid (retarder) addition..... 161

List of Figures

Figure 1.1 – Experimental flow chart for the portland cement part of the research 4
Figure 1.2 – Experimental flow chart for the reagent-grade chemicals CSAB cement research 6
Figure 1.3 – Experimental flow chart for the natural and waste materials CSAB cement research 7
Figure 2.1 – Schematic phase diagram of ternary system representing CSAB cement; slow, normal, and rapid refer to hardening rates (adapted from Metha, 1980).....24
Figure 3.1 – Rietveld refinement for a clinker sample synthesized by reagent-grade chemicals.....36
Figure 3.2 – X-ray patterns for clinker samples synthesize by reagent-grade chemicals, 20% fly ash incorporation, and 40% fly ash incorporation 37
Figure 3.3 – X-ray patterns for clinker samples synthesized by reagent-grade chemicals, 30% slag incorporation, and 60% slag incorporation.....37
Figure 3.4 – Elemental maps for a clinker sample synthesized by reagent-grade chemicals (left-right, top-bottom orientation: secondary electron image, Ca, Si, Al, and Fe; field width: 450 μm) 41
Figure 3.5 – Multispectral image for a clinker sample synthesized by reagent-grade chemicals (C_3S blue, C_2S green, C_3A red, and C_4AF yellow; field width: 450 μm)42
Figure 3.6 – Multispectral image for a clinker sample synthesized by reagent-grade chemicals with 40% fly ash incorporation (C_3S blue, C_2S green, C_3A red, C_4AF yellow, and periclase purple; field width: 450 μm).....43
Figure 3.7 – Multispectral image for a clinker sample synthesized by reagent-grade chemicals with 60% slag incorporation (C_3S blue, C_2S green, C_3A red, C_4AF yellow, and periclase purple; field width: 450 μm).....44
Figure 3.8 – Rate of heat evolution for a commercial Type I/II portland cement (control) and cement samples synthesized by reagent-grade chemicals (RG) with fly ash (F) and slag (S) incorporation.....47
Figure 3.9 – Cumulative heat evolved for a commercial Type I/II portland cement (control) and cement samples synthesized by reagent-grade chemicals (RG) with fly ash (F) and slag (S) incorporation 48
Figure 4.1 – Rietveld refinement for a clinker sample synthesized from GLS with 27.5% YLS.....57
Figure 4.2 – Rietveld refinement for a clinker sample synthesized from GLS with 27.5% fly ash.....59
Figure 4.3 – Rietveld refinement for a clinker sample synthesized from GLS with 35% slag.....59
Figure 4.4 – Elemental maps for a clinker sample synthesized from GLS with 27.5% YLS (left-right, top-bottom orientation: secondary electron image, Ca, Si, Al, Fe, and Mg; field width: 450 μm).....63

Figure 4.5 – Multispectral image for a clinker sample synthesized from GLS with 27.5% YLS (C_3S blue, C_2S green, C_3A red, C_4AF yellow, and periclase purple; field width: 450 μm) 64
Figure 4.6 – Multispectral image for a clinker sample synthesized from GLS with 27.5% fly ash (C_3S blue, C_2S green, C_3A red, C_4AF yellow, and periclase purple; field width: 450 μm) 65
Figure 4.7 – Multispectral image for a clinker sample synthesized from GLS with 35% slag (C_3S blue, C_2S green, C_3A red, C_4AF yellow, and periclase purple; field width: 450 μm) 66
Figure 4.8 – Rate of heat-evolution for a commercial Type I/II portland cement (control) and cement samples synthesized from reagent-grade chemicals (RG), GLS with 27.5% YLS, GLS with 27.5% fly ash (F), and GLS with 35% slag (S) 69
Figure 4.9 – Cumulative heat evolved for a commercial Type I/II portland cement (control) and cement samples synthesized from reagent-grade chemicals (RG), GLS with 27.5% YLS, GLS with 27.5% fly ash (F), and GLS with 35% slag (S) 70
Figure 5.1 – Schematic and picture of the SEM sample disk (Chancey, 2008) 78
Figure 5.2 – Thermogravimetric analysis for the raw ingredients of the CSAB cement clinkers synthesized from reagent-grade chemicals 80
Figure 5.3 – Particle size distribution for a commercial Type I/II portland cement (PC) and the CSAB cement clinkers synthesized from reagent-grade chemicals 81
Figure 5.4 – Rietveld analysis results for the HS CSAB cement clinker synthesized from reagent-grade chemicals 83
Figure 5.5 – Rietveld analysis results for the MS CSAB cement clinker synthesized from reagent-grade chemicals 83
Figure 5.6 – Rietveld analysis results for the LS CSAB cement clinker synthesized from reagent-grade chemicals 84
Figure 5.7 – X-ray diffraction patterns comparison for the CSAB cement clinkers synthesized from reagent-grade chemicals 84
Figure 5.8 – Backscattered electron image for the HS CSAB cement clinker synthesized from reagent-grade chemicals [a (light gray): C_2S, b (dark gray): $C_4A_3\overline{S}$, and c (white): C_4AF] 86
Figure 5.9 – Backscattered electron image for the MS CSAB cement clinker synthesized from reagent-grade chemicals [a (light gray): C_2S, b (dark gray): $C_4A_3\overline{S}$, and c (white): C_4AF] 87
Figure 5.10 – Backscattered electron image for the LS CSAB cement clinker synthesized from reagent-grade chemicals [a (light gray): C_2S, b (dark gray): $C_4A_3\overline{S}$, and c (white): C_4AF] 88
Figure 6.1 – Rate of heat evolution for the HS CSAB cement clinker synthesized from reagent-grade chemicals with different amounts of gypsum (G) addition 95
Figure 6.2 – Rate of heat evolution for the MS CSAB cement clinker synthesized from reagent-grade chemicals with different amounts of gypsum (G) addition 95
Figure 6.3 – Rate of heat evolution for the LS CSAB cement clinker synthesized from reagent-grade chemicals with different amounts of gypsum (G) addition 96

Figure 6.4 – Cumulative heat for the HS CSAB cement clinker synthesized from reagent-grade chemicals with different amounts of gypsum (G) addition 97
Figure 6.5 – Cumulative heat for the MS cement clinker synthesized from reagent-grade chemicals with different amounts of gypsum (G) addition 97
Figure 6.6 – Cumulative heat for the LS CSAB cement clinker synthesized from reagent-grade chemicals with different amounts of gypsum (G) addition 98
Figure 6.7 – Rate of heat evolution for a commercial Type I/II portland cement (PC) and the synthesized CSAB cements from reagent-grade chemicals 99
Figure 6.8 – Cumulative heat for a commercial Type I/II portland cement (PC) and the synthesized CSAB cements from reagent-grade chemicals 100
Figure 6.9 – Rate of heat evolution for the synthesized CSAB cements from reagent-grade chemicals at 5˚C, 23˚C, and 38˚C 101
Figure 6.10 – Cumulative heat for the synthesized CSAB cements from reagent-grade chemicals at 5˚C, 23˚C, and 38˚C 102
Figure 6.11 – X-ray diffraction patterns for the HS CSAB cement after 7 days of hydration at 5˚C, 23˚C, and 38˚C 103
Figure 6.12 – X-ray diffraction patterns for the MS CSAB cement after 7 days of hydration at 5˚C, 23˚C, and 38˚C 103
Figure 6.13 – X-ray diffraction patterns for the LS CSAB cement after 7 days of hydration at 5˚C, 23˚C, and 38˚C 104
Figure 6.14 – Backscattered electron images for the hydrated HS CSAB cement from reagent-grade chemicals [a (black): pores and cracks, b (dark gray background): ettringite and amorphous content, c (dark gray particles): gypsum, d (gray): $C_4A_3\overline{S}$, and e (light gray): C_2S; field width: 1250 μm] 109
Figure 6.15 – Backscattered electron images for the hydrated MS CSAB cement from reagent-grade chemicals [a (black): pores and cracks, b (dark gray background): ettringite and amorphous content, c (dark gray particles): gypsum, d (gray): $C_4A_3\overline{S}$, and e (light gray): C_2S; field width: 1250 μm] 111
Figure 6.16 – Backscattered electron images for the hydrated LS CSAB cement from reagent-grade chemicals [a (black): pores and cracks, b (dark gray background): ettringite and amorphous content, c (dark gray particles): gypsum, d (gray): $C_4A_3\overline{S}$, and e (light gray): C_2S; field width: 1250 μm] 114
Figure 6.17 – Dimensional stability for a commercial Type I/II portland cement (PC) and the synthesized CSAB cements from reagent-grade chemicals cured in ultra-pure water after demolding at 1 day of hydration 116
Figure 6.18 – Picture of a slightly cracked small bar made from the HS CSAB cement from reagent-grade chemicals after 7 days of hydration 116
Figure 6.19 – Dimensional stability for the HS CSAB cement from reagent-grade chemicals using 0.45 and 0.7 water-to-cement ratio (w/c) cured in ultra-pure water after demolding at 1 day of hydration 118
Figure 6.20 – Dimensional stability for the HS CSAB cement clinker synthesized from reagent-grade chemicals with different amounts of gypsum (G) addition cured in ultra-pure water after demolding at 1 day of hydration 119

Figure 6.21 – X-ray diffraction patterns for the HS CSAB cement clinker with 10% and 25% gypsum (G) addition after 7 days of hydration; no calcium monosulfoaluminate formed 120
Figure 6.22 – Sulfate resistance for a commercial Type I/II portland cement (PC) and the synthesized CSAB cements from reagent-grade chemicals stored in 5% Na_2SO_4 solution after 7 days of hydration 122
Figure 6.23 – Pictures of the small bars made from the synthesized CSAB cements from reagent-grade chemicals stored in 5% Na_2SO_4 solution; HS for 5 days (failed), MS and LS for 90 days 123
Figure 6.24 – X-ray diffraction patterns for the HS CSAB cement after 7 days of hydration and stored in 5% Na_2SO_4 solution and ultra-pure water for 3 days..... 124
Figure 6.25 – Sulfate resistance for the HS CSAB cement from reagent-grade chemicals using 0.45 and 0.7 water-to-cement ratio (w/c) stored in 5% Na_2SO_4 solution after 7 days of hydration 125
Figure 6.26 – Sulfate resistance for the HS CSAB cement clinker synthesized from reagent-grade chemicals with different amounts of gypsum (G) addition stored in 5% Na_2SO_4 solution after 7 days of hydration 126
Figure 6.27 – Sulfate resistance for the HS CSAB cement from reagent-grade chemicals stored in 5% Na_2SO_4 solution and saturated $CaSO_4$ solution after 7 days of hydration 127
Figure 6.28 – Compressive strength development for a commercial Type I/II portland cement (PC) and the synthesized CSAB cements from reagent-grade chemicals . 128
Figure 7.1 – Particle size distribution for a commercial Type I/II portland cement (PC) and the CSAB cement clinkers synthesized from reagent-grade chemicals (MS), Class C fly ash (MC), and fluidized bed ash (MF)..... 141
Figure 7.2 – Rietveld analysis results for the MC CSAB cement clinker synthesized from Class C fly ash 143
Figure 7.3 – Rietveld analysis results for the MF CSAB cement clinker synthesized from fluidized bed ash 143
Figure 7.4 – X-ray diffraction patterns comparison for the CSAB cement clinkers synthesized from reagent-grade chemicals (MS), Class C fly ash (MC), and fluidized bed ash (MF)..... 144
Figure 7.5 – Backscattered electron image for the MC CSAB cement clinker synthesized from Class C ash [a (light gray): C_2S, b (dark gray): $C_4A_3\overline{S}$, and c (white): C_4AF] 146
Figure 7.6 – Backscattered electron image for the MF CSAB cement clinker synthesized from fluidized ash [a (light gray): C_2S, b (dark gray): $C_4A_3\overline{S}$, and c (white): C_4AF] 147
Figure 7.7 – Backscattered electron image for the MS CSAB cement clinker synthesized from reagent-grade chemicals [a (light gray): C_2S, b (dark gray): $C_4A_3\overline{S}$, and c (white): C_4AF] 148
Figure 7.8 – Rate of heat evolution for the MC CSAB cement clinker synthesized from Class C fly ash with different amounts of gypsum (G) addition..... 150

Figure 7.9 – Cumulative heat for the MC CSAB cement clinker synthesized from Class C fly ash with different amounts of gypsum (G) addition 150
Figure 7.10 – Rate of heat evolution for the MF CSAB cement clinker synthesized from fluidized bed ash with different amounts of gypsum (G) addition..... 151
Figure 7.11 – Cumulative heat for the MF CSAB cement clinker synthesized from fluidized bed ash with different amounts of gypsum (G) addition..... 151
Figure 7.12 – Rate of heat evolution for a commercial Type I/II portland cement (PC) and the synthesized CSAB cements from reagent-grade chemicals (MS), Class C fly ash (MC), and fluidized bed ash (MF)..... 153
Figure 7.13 – Cumulative heat for a commercial Type I/II portland cement (PC) and the synthesized CSAB cements from reagent-grade chemicals (MS), Class C fly ash (MC), and fluidized bed ash (MF)..... 154
Figure 7.14 – Pictures for the hydrated synthesized CSAB cement samples from Class C fly ash (MC) and fluidized bed ash (MF) after 3 days of hydration..... 155
Figure 7.15 – Rate of heat evolution for the MS CSAB cement from reagent-grade chemicals with 1%, 2%, and 5% NaOH addition and the CSAB cements form Class C fly ash (MC) and fluidized bed ash (MF)..... 158
Figure 7.16 – Rate of heat evolution for the MS CSAB cement from reagent-grade chemicals and the CSAB cements form Class C fly ash (MC) and fluidized bed ash (MF) with 0.5%, 1%, and 2% citric acid (retarder) addition 159
Figure 7.17 – Cumulative heat for the MS synthesized CSAB cement from reagent-grade chemicals and CSAB cements form Class C fly ash (MC) and fluidized bed ash (MF), respectively, with 0.5%, 1%, and 2% citric acid (retarder) addition..... 159
Figure 7.18 – Backscattered electron images for the hydrated MC CSAB cement from Class C fly ash [a (black): pores and cracks, b (dark gray background): ettringite and amorphous content, c (dark gray particles): gypsum, d (gray): $C_4A_3\overline{S}$, and e (light gray): C_2S; field width: 1250 μm]..... 165
Figure 7.19 – Backscattered electron images for the hydrated MF CSAB cement from fluidized bed ash [a (black): pores and cracks, b (dark gray background): ettringite and amorphous content, c (dark gray particles): gypsum, d (gray): $C_4A_3\overline{S}$, and e (light gray): C_2S; field width: 1250 μm]..... 167
Figure 7.20 – Backscattered electron images for the hydrated MS CSAB cement from reagent-grade chemicals [a (black): pores and cracks, b (dark gray background): ettringite and amorphous content, c (dark gray particles): gypsum, d (gray): $C_4A_3\overline{S}$, and e (light gray): C_2S; field width: 1250 μm]..... 170
Figure 7.21 – Dimensional stability for a commercial Type I/II portland cement (PC) and the synthesized CSAB cements from reagent-grade chemicals (MS), Class C fly ash (MC), and fluidized bed ash (MF) stored in ultra-pure water after demolding at 1 day of hydration; MC and MF with 1% citric acid (retarder) addition 171
Figure 7.22 – Sulfate resistance for a commercial Type I/II portland cement (PC) and the synthesized CSAB cements from reagent-grade chemicals (MS), Class C fly ash (MC), and fluidized bed ash (MF) stored in 5% sodium sulfate solution after 7 days of hydration; MC and MF with 1% citric acid (retarder) addition..... 172

Figure 7.23 – Compressive strength development for a commercial Type I/II portland cement (PC) and the synthesized CSAB cements from reagent-grade chemicals (MS), Class C fly ash (MC), and fluidized bed ash (MF); MC and MF with 1% citric acid (retarder) addition..... 173

Chapter 1: Introduction

1.1 RESEARCH OBJECTIVE

Portland cement concrete, the most widely used manufactured material in the world, is made primarily from water, mineral aggregates, and portland cement. Portland cement clinker is produced from high temperature firing and grinding of mineral deposits such as limestone and clay; the clinker is then ground with gypsum to make cement. Global production of portland cement is estimated about 1.7×10^9 tonnes per year (Gartner, 2004). The production of portland cement is energy intensive, accounting for 2% of primary energy consumption and 5% of industrial energy consumption globally (Hendricks et al., 1999). Moreover, portland cement manufacturing contributes significantly to greenhouse gases and accounts for 5% of the global CO_2 emissions resulting from human activity. Half of this CO_2 comes from the use of fossil fuels to heat the kilns, and the other half is produced through the calcination of limestone ($CaCO_3 \rightarrow CaO + CO_2$).

The primary objective of this research was to explore methods of reducing the environmental impact of cement production while maintaining or improving current performance standards. Two approaches were taken, 1.) incorporation of waste materials in portland cement synthesis, and 2.) optimization of an alternative environmental friendly binder, calcium sulfoaluminate-belite cement. These approaches can lead to less energy consumption, less emission of CO_2, and more reuse of industrial waste materials for cement manufacturing.

1.2 RESEARCH PLAN

1.2.1 Portland Cement

One method of reducing energy consumption and CO_2 emissions from cement manufacturing is to reduce or eliminate the use of limestone, replacing it with materials high in CaO rather than $CaCO_3$ ($CaCO_3 \rightarrow CaO + CO_2$, $\Delta H = 178$ kJ/mol). Viable alternatives to limestone are calcium oxide-bearing waste materials such as fly ash from coal burning power plants and blast furnace slag from steel production. The reuse of these waste materials from other industries reduces landfilling, thereby further reducing the environmental impact of cement manufacturing.

In this part of the research, portland cement clinker was synthesized from reagent-grade chemicals, natural materials, industrial waste materials, and combinations of these. The primary goal was to demonstrate the feasibility of using industrial waste materials in cement manufacturing. As part of this process, it is important to develop an understanding of the phases that form in the presence of the large quantities of impurities present in waste materials. Therefore, reagent-grade chemicals were first chosen to create a model system with no impurities, thereby establishing a baseline for the composition and the synthesis procedure. After successful synthesis of portland cement clinker from reagent-grade chemicals, waste materials, specifically fly ash and slag, were incorporated in increments up to the maximum content while the target clinker composition and the synthesis procedure remained unchanged. The only impurities in the system came from the waste materials, allowing investigation into the effects of these waste-specific impurities on phase formation.

Portland cement clinker was then synthesized from a gray limestone (GLS) and an argillaceous yellow limestone (YLS) acquired from a cement manufacturing plant to form a portland cement clinker with a similar composition to the clinker sample

synthesized from reagent-grade chemicals. Portland cement clinker can be synthesized by combining only these two natural materials because the YLS used contained high amounts of silicon, aluminum, and iron. After successful synthesis of portland cement clinker from natural materials, several ingredient proportions of GLS and fly ash or slag were fired in the furnace. The fly ash and slag used contained similar oxide composition to YLS except for impurities, whose effects on phase formation are not well known. The final goals were to synthesize portland cement clinkers with minimal limestone content and maximal waste material content, and to evaluate the effects of impurities on phase formation.

All the resulting synthetic portland cement clinkers were ground, tested for particle fineness by Blaine fineness (ASTM C 204, 2007), and analyzed for phase composition using X-ray diffraction (XRD) and phase distribution using scanning electron microscopy (SEM). Finally, the synthetic clinkers were made into cements by adding gypsum to control their hydration reactions. Their early-age hydration behavior was investigated using isothermal conduction calorimetry. The results were compared to a commercially produced portland cement. Figure 1.1 shows the experimental flow chart for the portland cement part of the research.

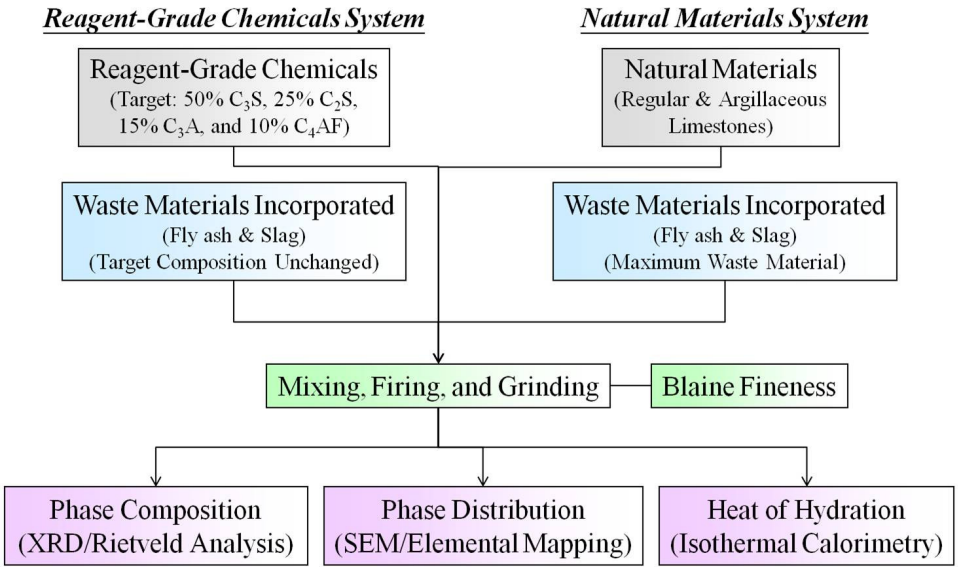

Figure 1.1 – Experimental flow chart for the portland cement part of the research

1.2.2 Calcium Sulfoaluminate-Belite Cement

Another method of reducing the environmental impact of cement manufacturing is the use and adoption of an alternative environmental friendly binder, calcium sulfoaluminate-belite (CSAB) cement. CSAB cement has a different phase assemblage to portland cement which requires less lime for its formation. The relatively low lime requirement for CSAB cement production reduces energy consumption and CO_2 emissions ($CaCO_3 \rightarrow CaO + CO_2$, $\Delta H = 178$ kJ/mol) from cement manufacturing. Moreover, CSAB cement can form and is stable approximately 200ºC lower than the temperature used for portland cement production, which further reduces energy consumption and CO_2 emissions from cement manufacturing. The lower synthesis temperature not only further lowers energy consumption and CO_2 emissions from cement manufacturing but the resulting clinker is more friable (due to high porosity), which reduces the energy needed for grinding. Additionally, CSAB cement contains high amounts of sulfur, which makes high sulfur-containing waste materials such as fluidized

bed ash and waste gypsum suitable for its production. The reuse of these waste materials in CSAB cement production decreases landfilling, thereby further reducing the environmental impact of cement manufacturing.

In this part of the research, three CSAB cement clinkers with different phase compositions were first synthesized from reagent-grade chemicals to tightly control compositional variables. The range of phase compositions was chosen because it allows full evaluation of the inter-relationship between phase composition and performance of the CSAB cement system. The synthetic CSAB cement clinkers were analyzed for phase composition using X-ray diffraction (XRD) and phase distribution using scanning electron microscopy (SEM). The synthetic clinkers were ground and tested for particle fineness and distribution by Blaine fineness (ASTM C 204, 2007) and laser light scattering particle size distribution analysis (Laser PSD). Different amounts of gypsum were added to the synthetic CSAB cement clinkers to control their hydration reactions and tested with isothermal conduction calorimetry to investigate their optimum gypsum contents and early-age hydration behavior. The synthetic clinkers were made into cements by adding their optimum gypsum contents and the resulting cements were monitored for hydration product development using XRD and SEM.

The hydration products of CSAB cement could be expansive and could significantly affect property development. Therefore, the dimensional stability along with sulfate resistance and compressive strength development of the synthesized CSAB cements were studied. The results were compared to a commercially produced portland cement. The primary goal was to determine the optimum CSAB cement phase composition for performance. Figure 1.2 shows the experimental flow chart for the reagent-grade chemicals CSAB cement research.

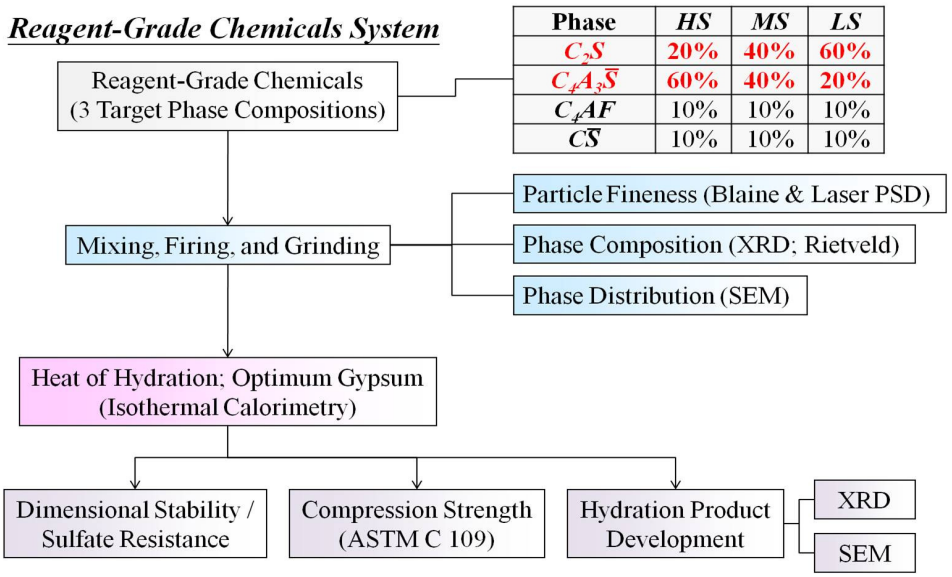

Figure 1.2 – Experimental flow chart for the reagent-grade chemicals CSAB cement research

A potential problem facing the widespread adoption and production of CSAB cement is the cost and availability of raw materials. Natural deposits containing calcium and silicon oxides are plentiful throughout most of the world, making it possible to produce portland cement cheaply in most areas using local materials. The production of CSAB cement requires more alumina than does portland cement. Bauxite deposits, generally reserved for use in aluminum and alumina production, are not widespread and the extracted alumina can be expensive. Therefore, it is desirable to find alternative raw materials for CSAB cement production to keep costs competitive. If the raw materials are waste products of other industries, then the environmental benefit of CSAB cement becomes even greater than simply a reduction of energy consumption and CO_2 emissions because cement becomes a useful repository for waste materials that would otherwise enter landfills. Moreover, incorporating waste materials high in CaO rather than $CaCO_3$ further reduces CO_2 emissions, making CSAB cement even more attractive.

Therefore, different waste materials such as fly ash, fluidized bed ash, and waste gypsum were combined with limestone and bauxite to synthesize CSAB cement. The raw ingredients were proportioned according to the optimum phase composition determined from the synthesized CSAB cements from reagent-grade chemicals. The synthesized CSAB cements from waste materials were again studied for phase composition and distribution, hydration chemistry, and properties. The results were compared to the optimum synthesized CSAB cement from reagent-grade chemicals and a commercially produced portland cement. The final goals were to produce satisfactory CSAB cements with minimal limestone and bauxite contents and maximal waste material content, and to evaluate the effects of impurities from the natural and waste materials used on phase formation, hydration chemistry, and properties. Figure 1.3 shows the experimental flow chart for the natural and waste materials CSAB cement research.

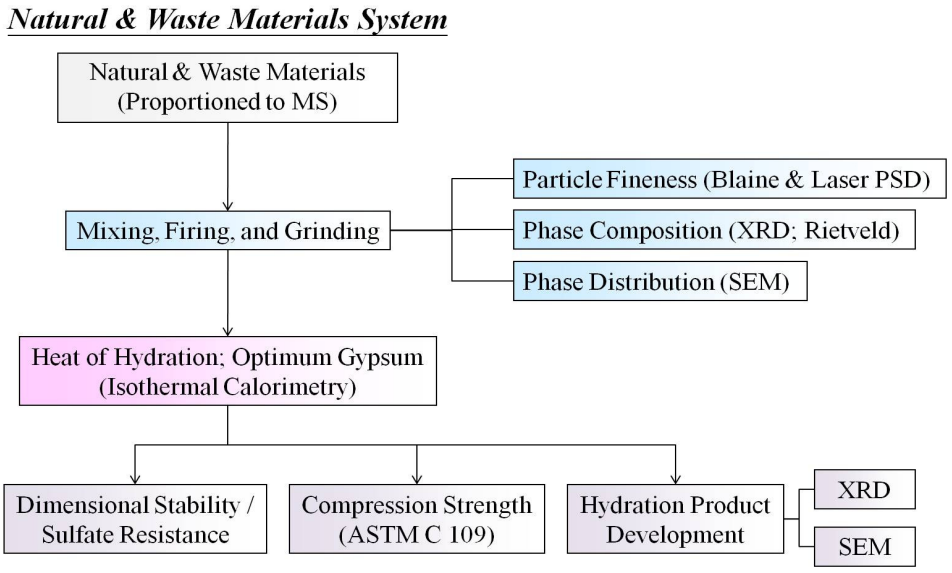

Figure 1.3 – Experimental flow chart for the natural and waste materials CSAB cement research

1.3 OVERVIEW OF DISSERTATION

This dissertation includes 8 chapters. Chapter 1 provides an overview on the research objective, research plan, and layout of this dissertation. Chapter 2 provides background and reviews the pertinent literature on portland cement and calcium sulfoaluminate-belite cement. Chapter 3 presents the results of synthesized portland cement from reagent-grade chemicals and industrial waste materials. Chapter 4 presents the results of synthesized portland cement from natural materials and industrial waste materials. Chapter 5 presents the results of calcium sulfoaluminate-belite cement synthesis. Chapter 6 presents the results of the effects of calcium sulfoaluminate-belite cement composition on hydration and properties. Chapter 7 presents the results of waste materials incorporation in calcium sulfoaluminate-belite cement. Finally, Chapter 8 provides a summary, and discusses the implications and future recommendations from this research.

1.4 NOTATIONS

All the notations and acronyms used throughout this dissertation are listed in Sections 1.4.1 and 1.4.2, respectively.

1.4.1 Cement Chemistry Notations

A	Al_2O_3
C	CaO
F	Fe_2O_3
H	H_2O
S	SiO_2
$\overline{S}$	SO_3
M	MgO

1.4.2 Acronyms

CSA	Calcium Sulfoaluminate
CSAB	Calcium Sulfoaluminate-Belite
G	Gypsum
GLS	Gray Limestone
HS	Synthesized CSAB Cement from Reagent-Grade Chemicals with High $C_4A_3\overline{S}$ content
LS	Synthesized CSAB Cement from Reagent-Grade Chemicals with Low $C_4A_3\overline{S}$ content
LSF	Lime Saturation Factor
MC	Synthesized CSAB Cement from Class C Fly Ash with Medium $C_4A_3\overline{S}$ content
MF	Synthesized CSAB Cement from Fluidized Bed Ash with Medium $C_4A_3\overline{S}$ content
MS	Synthesized CSAB Cement from Reagent-Grade Chemicals with Medium $C_4A_3\overline{S}$ content
MSWI	Municipal Solid Waste Incineration
PC	Portland Cement
PSD	Particle Size Distribution
SAB	Sulfoaluminate-Belite
SEM	Scanning Electron Microscopy
SCMs	Supplementary Cementing Materials
XRD	X-Ray Diffraction
w/c	Water-to-Cement Ratio
YLS	Yellow Limestone

Chapter 2: Background and Literature Review

2.1 PORTLAND CEMENT

2.1.1 Background

Portland cement concrete, the most widely used manufactured material in the world, is made primarily from water, mineral aggregates, and portland cement. Modern portland cement was first produced by Isaac Johnson in 1845 and has been used in a form without many changes to its physical and chemical characteristics for the past 164 years (Mindess et al., 2003).

Portland cement clinker is produced from high temperature firing (approximately 1450ºC) and grinding of mineral deposits such as limestone and clay; the clinker is then ground with gypsum to make cement. The production of portland cement is energy intensive, accounting for 2% of primary energy consumption and 5% of industrial energy consumption globally (Hendricks et al., 1999). Moreover, portland cement manufacturing contributes significantly to greenhouse gases and accounts for 5% of the global CO_2 emissions resulting from human activity. Half of this CO_2 comes from the use of fossil fuels to heat the kilns, and the other half is produced through the calcination of limestone.

A typical portland cement contains approximately: 55% tricalcium silicate (alite; Ca_3SiO_5; C_3S)*, 20% dicalcium silicate (belite; Ca_2SiO_4; C_2S), 10% tricalcium aluminate ($Ca_3Al_2O_6$; C_3A), 8% calcium aluminoferrite ($Ca_4Al_2Fe_2O_{10}$; C_4AF), and 6% gypsum ($CaSO_4 \cdot 2H_2O$; $C\overline{S}H_2$) (Mindess et al., 2003). C_3S reacts with water rapidly and contributes to the early-age property development in portland cement. The hydration reaction of C_2S is slower, but it eventually catches up and contributes to the long-term

*In cement chemistry notation, oxides are abbreviated by the first capital letter: C = CaO, S = SiO_2, A = Al_2O_3, F = Fe_2O_3, H = H_2O, $\overline{S}$ = SO_3, M = MgO

property development in portland cement. C_3S and C_2S composed of approximately 75% of portland cement and their hydration reactions to form calcium silicate hydrate (C-S-H) are primarily responsible for the mechanical property development in portland cement, e.g., setting and strength. Calcium silicate hydrate is usually referred to as C-S-H because its composition is variable depending on formation conditions. Gypsum is added to portland cement clinker to regulate the hydration reactions of C_3A and C_4AF. The hydration reactions of C_3A and C_4AF with gypsum to form ettringite ($Ca_6Al_2(SO_4)_3(OH)_{12} \cdot 26H_2O$; $C_6A\overline{S}_3H_{32}$) contribute to the early-age property development in portland cement to some extent.

2.1.2 Waste Materials Incorporation

One method of reducing the environmental impact of cement manufacturing is the use of waste materials as raw materials for portland cement production. Incorporating waste materials high in CaO rather than $CaCO_3$ such as fly ash and slag also reduces CO_2 emissions from cement manufacturing. Komljenovic et al. (2007) successfully synthesized portland cement clinker using limestone and a Class F fly ash (ASTM C 618, 2007). The synthetic portland cement clinker from fly ash had similar phase composition to a reference portland cement clinker. Monshi and Asgarani (1999) showed that slags from blast furnace (iron slag) and steel converter (steel slag) can be used as raw materials for portland cement production. The synthesized portland cements had higher C_3S contents and showed better mechanical properties when raw ingredients were proportioned at higher lime saturation factor (LSF). Shih et al. (2003) showed that municipal solid waste incineration (MSWI) ash can be used as a replacement of portland cement raw mix after removing its metallic content with a magnetic separator. However, compressive strength of the synthesized portland cements decreased significantly with

MSWI ash replacement higher than 5% due to the lower LSF of the MSWI ash replaced portland cement raw mix, which reduced the C_3S contents in the synthesized portland cements. Other research has shown that special cements can be synthesized using waste materials such as red mud (from aluminum industry; mainly containing silicon oxide, aluminum oxide, and iron oxide) (Singh et al., 1996), rice hull ash (from agriculture industry; mainly containing silicon oxide) (Rodrigues, 2003), and phosphogypsum (from fertilizer industry; mainly containing gypsum) (Singh and Garg, 2000).

2.2 CALCIUM SULFOALUMINATE-BELITE CEMENT

2.2.1 Background

Another method of reducing energy consumption and CO_2 emissions from cement manufacturing is to modify the portland cement phase assemblage to lower the limestone requirement (Mehta, 1980). Table 2.1 shows the lime contents of the cement phases. Alite (Ca_3SiO_5; C_3S), the most dominant phase in portland cement, has the highest lime content and requires the highest formation temperature. Substituting C_3S with belite (Ca_2SiO_4; C_2S) in cement can lower the limestone requirement and temperature for cement manufacturing, thereby reducing energy consumption and CO_2 emissions while maintaining satisfying long-term properties. However, substituting C_3S with C_2S compromises the early-age property development due to the slow reacting C_2S. This renders the high-C_2S cement unusable in nearly any field of practice.

Table 2.1 – Cement phases lime contents (Mehta, 1980)

Cement Phase	Lime Content (weight%)
C_3S	73.7
C_2S	65.1
C_3A	62.2
C_4AF	46.2
$C_4A_3\overline{S}$	36.7

In order to compensate for the slow reacting C_2S, a fast reacting calcium sulfoaluminate (mineral name Ye'elimite; $Ca_4Al_6SO_{16}$; $C_4A_3\overline{S}$) phase is incorporated, thus creating an aptly named calcium sulfoaluminate-belite cement (Mehta, 1980). $C_4A_3\overline{S}$ is known as Klein's compound and was invented by Alexander Klein in 1966 as an additive to portland cement to make expansive cement (Klein, 1966). $C_4A_3\overline{S}$ has the lowest lime content of any cement phase (Table 2.1), which reduces the limestone requirement for cement manufacturing. Calcium sulfoaluminate-belite cement also goes by names such as sulfoaluminate-belite (SAB) cement and calcium sulfoaluminate (CSA) cement. However, since the main components of this type of cement are calcium sulfoaluminate ($C_4A_3\overline{S}$) and belite (C_2S), the name calcium sulfoaluminate-belite (CSAB) cement, is the most representative.

CSAB cement might also contain calcium aluminoferrite (C_4AF) and calcium sulfates (Metha, 1980); calcium sulfates can either be formed as anhydrite ($CaSO_4$; $C\overline{S}$) in clinker or be interground as gypsum ($CaSO_4 \cdot 2H_2O$; $C\overline{S}H_2$) after clinkering, or some combination of the two (Glasser and Zhang, 2001). C_3A usually does not form in CSAB cement due to the lower production temperature; however, other aluminum-containing phases such as $C_{12}A_7$, CA, and C_2AS might form depending on the raw materials composition (Sharp et al., 1999). Other minor phases might form in CSAB cement

including $C_5S_2\overline{S}$ and free lime (C) (Roy et al., 1999). Unlike portland cement, CSAB cement does not have a defined phase composition range. CSAB cement generally refers to cements that have the same basic components of $C_4A_3\overline{S}$ and C_2S, but the minor phases and the amounts of the phases present vary significantly.

All the phases in CSAB cement can form and are stable at a temperature of approximately 1250ºC, which is about 200ºC lower than the temperature used for portland cement production (Mehta, 1980). The lower formation temperature not only further lowers the energy requirement and CO_2 emissions from cement manufacturing, but the resulting clinker is more friable (due to high porosity), which reduces the energy needed for grinding (Glasser and Zhang, 2001). The high sulfate requirement for CSAB cement production allows calcium sulfate-containing industrial byproducts such as fluidized bed ash and flue gas desulfurization sludge to be used as raw materials for CSAB cement production (Phair, 2006). These high sulfate containing industrial byproducts are not suitable to be used as either raw materials for portland cement production or supplementary cementing materials (SCMs) to directly replace a portion of the portland cement in concrete. Furthermore, incorporating C_4AF in CSAB cement allows the use of iron-containing industrial byproducts as raw materials (Palou and Majling, 1995). Most industrial byproducts suitable for cement manufacturing contain some amount of iron. The reuse of industrial byproducts that would otherwise go into landfill could further reduce the environmental impact of cement production.

2.2.2 History and Potential

CSAB cement was first put into industrial production in China under the name "Third Cement Series" in the 1970s (Zhang et al., 1999). Third Cement Series includes sulfoaluminate cement and ferroaluminate cement, which have the same basic

components: $C_4A_3\overline{S}$, C_2S, C_4AF, and calcium sulfates ($C\overline{S}$ and $C\overline{S}H_2$), only with different proportions depending on applications. In China, CSAB cements have been produced in a similar manner to portland cement with a slightly lower firing temperature of 1325ºC. Annual production of the CSAB cements in China was estimated about 1 million tonnes in 1997. The CSAB cements have exhibited rapid setting, high early-age strength, self stressing, and shrinkage compensating properties due to the fast reacting $C_4A_3\overline{S}$ and the expansive nature of ettringite. Furthermore, in field practices, the CSAB cements have been used mainly in pre-cast concrete applications and cold environments and have shown good dimensional stability, low permeability, low alkalinity, good durability, and comparable compressive strength to portland cement concrete. However, despite the increasing interests in CSAB cement, industrial scale production and usage are still limited in China (Gartner, 2004). A potential problem facing the widespread adoption and production of CSAB cement is the cost and availability of raw materials. Natural deposits containing calcium and silicon oxides are plentiful throughout most of the world, making it possible to produce portland cement cheaply in most areas using local materials. However, the CSAB cements produced and used in China contain high $C_4A_3\overline{S}$ contents which require higher amount of aluminum oxide for production than does portland cement. Bauxite deposits, generally reserved for use in aluminum and alumina production, are not widespread and the extracted alumina can be expensive. The increased cost in raw materials could inhibit the widespread adoption and production of CSAB cement, unless alternative raw materials are available.

2.2.3 Synthesis

Majling et al. (1993) adapted the generalized Bogue method to predict the phase assemblage and composition in CSAB cement clinker from raw materials oxide

composition using knowledge of phase equilibria and solving linear equations. This method also allows assessment of suitable raw materials for CSAB cement production.

CSAB cement can be produced by combing limestone, clay, bauxite, and gypsum to provide the necessary CaO, SiO_2, Al_2O_3, and SO_3 required for phase formation, respectively. However, for environmental and cost concerns, CSAB cement is mostly produced by combining natural and waste materials. Majling et al. (1999) suggested that fly ash, even though it has a wide range of oxide compositions, could be potential raw materials for CSAB cement production because of its generally high CaO, SiO_2, Al_2O_3, and Fe_2O_3. Beretka et al. (1992) showed that blast furnace slag can be used to synthesized CSAB cement clinker due to its high CaO, SiO_2, and Al_2O_3 contents. Phair (2006) suggested that calcium sulfate containing industrial byproducts such as fluidized bed ash and flue gas desulfurization sludge could be suitable raw materials for CSAB cement production because of its high sulfate requirement. Arjunan et al. (1999) showed that lime dust can be used to synthesize CSAB cement clinkers due to its high CaO and SiO_2 contents. Majling (1995) showed that high iron-containing industrial byproduct, brown mud, can be used to synthesize high C_4AF CSAB cement clinker. Natural materials such as limestone, clay, bauxite, and gypsum were combined with waste materials to provide the additional CaO, SiO_2, Al_2O_3, and SO_3 required for CSAB cement production.

CSAB cement generally refers to cements that have the same basic components of $C_4A_3\overline{S}$ and C_2S, but the minor phases and the amounts of the phases present vary significantly. Sahu and Majling (1994) successfully synthesized CSAB cement clinkers from limestone, fly ash, and gypsum. The main phases formed in these synthetic CSAB cement clinkers were $C_4A_3\overline{S}$, C_2S, $C\overline{S}$, C_4AF, C_2AS, and unreacted free lime (C). The phase compositions of the synthetic CSAB cement clinkers showed good agreement with

their estimated phase compositions obtained from the adapted generalized Bogue method developed by Majling et al. (1993). Aujunan et al. (1999) successfully synthesize CSAB cement clinkers from lime dust, fly ash, and flue gas desulfurization sludge. The main phases formed in these synthetic CSAB cement clinkers were also $C_4A_3\overline{S}$, C_2S, $C\overline{S}$, C_4AF, and C_2AS. However, the contents of C_2AS decreased while $C_4A_3\overline{S}$ increased when prolonging the firing time. Roy et al. (1999) successfully synthesized CSAB cement clinkers from lime dust, fly ash, and fluidized bed ash. The main phases formed in these synthetic CSAB cement clinkers were also $C_4A_3\overline{S}$, C_2S, $C\overline{S}$, C_4AF. However, surplus SO_3 in the raw materials resulted in the formation of $C_5S_2\overline{S}$, which required a synthesis temperature higher than 1250ºC or longer firing time to decompose it. In these studies, a 1250ºC synthesis temperature was shown to be sufficient for CSAB cement clinker synthesis.

Palou and Majling (1995) successfully synthesized CSAB cement clinkers with high C_4AF contents from limestone, bauxite, gibbsite, gypsum, fly ash, blast furnace slag, and brown mud. Different raw materials were proportioned for the same oxide composition and the raw mixtures were expected to have the same clinker phase composition using the adapted generalized Bogue method developed by Majling et al. (1993). The main phases formed in these synthetic CSAB cement clinkers were $C_4A_3\overline{S}$, C_2S, $C\overline{S}$, C_4AF, and $C_5S_2\overline{S}$. However, the synthetic CSAB cement clinkers with the same estimated phase composition showed distinct hydration behavior and compressive strength development. The differences are perhaps caused by the different minor impurities contained in the waste materials used, which might affect the final CSAB cement phase composition and properties.

The generalized Bogue method does not take into account of the impurities contained in the system and assumes that the cement phases are in their stoichiometric

forms, which is usually not realistic because these phases can accommodate a large amount of substitute ions. Strigac et al. (2000) studied the actual composition of the CSAB cement phases. The results showed that ferrite phase formed a solid solution and accommodated some SiO_2. The actual composition of the ferrite phase solid solution can range from C_4AF to C_6AF_2. $C_4A_3\overline{S}$ accommodated some SiO_2 and up to 2% Fe_2O_3. C_2S and $C\overline{S}$, on the other hand, formed more homogenous compositions with minor substitute ions. This information can be used to refine the adapted generalized Bogue method developed by Majling et al. (1993) to better predict the clinker phase compositions from its oxide composition (Strigac et al., 1997). However, Strigac et al. did not study the effect of impurities on the actual composition of CSAB cement phases.

2.2.4 Hydration

The hydration reaction of $C_4A_3\overline{S}$ with calcium sulfates ($C\overline{S}$ and $C\overline{S}H_2$) initiates rapidly and forms ettringite ($C_6A\overline{S}_3H_{32}$) and AH_3, which contributes to the early-age property development in CSAB cement, as shown in Equations 2.1-2.4 (Mehta 1980; Kasselouri et al., 1995):

$$C\overline{S} + 2H \rightarrow C\overline{S}H_2 \quad (2.1)$$

$$C_4A_3\overline{S} + 2C\overline{S}H_2 + 34H \rightarrow C_6A\overline{S}_3H_{32} + 2AH_3 \quad (2.2)$$

$$C_4A_3\overline{S} + 8C\overline{S}H_2 + 6CH + 74H \rightarrow 3C_6A\overline{S}_3H_{32} \quad (2.3)$$

$$AH_3 + 3CH + 3C\overline{S}H_2 + 20H \rightarrow C_6A\overline{S}_3H_{32} \quad (2.4)$$

The CH in Equations 2.3 and 2.4 can be derived from the hydration reaction of C_2S, as shown in Equation 2.5:

$$C_2S + 2H \rightarrow CH + C\text{-}S\text{-}H \quad (2.5)$$

The hydration reaction of C_2S also forms C-S-H, which contributes to the long-term property development in CSAB cement. If there are insufficient calcium sulfates in the

system to complete the reaction in Equation 2.2, calcium monosulfoaluminate ($C_4A\overline{S}H_{12}$) forms (Glasser and Zhang, 2001).

Kasselouri et al. (1995) studied the hydration product development in a CSAB cement that contained 20.1% $C_4A_3\overline{S}$, 47.1% C_2S, 19.8% $C\overline{S}$, and 13.8% C_4AF using a water-to-cement ratio of 0.4. The results show that $C_4A_3\overline{S}$ reacted with $C\overline{S}$ and formed ettringite within 6 h of hydration following Equations 2.1 and 2.2. Ettringite was the main hydration product formed and it continued to form at later ages from AH_3, CH, and $C\overline{S}H_2$ according to Equations 2.3 and 2.4. $C_4A_3\overline{S}$ totally reacted at 7 days of hydration; however, there was small amount of unreacted $C\overline{S}H_2$ present at 90 days of hydration. Valenti et al. (2007) showed that $C_4A_3\overline{S}$ reacted with $C\overline{S}H_2$ and formed ettringite within 3 h of hydration in a CSAB cement that contained 32.8% $C_4A_3\overline{S}$, 39.3% C_2S, and 13.7% $C\overline{S}H_2$ using a water to cement ratio of 0.5 Ettringite was the main hydration product formed and showed a needle-like morphology observed under scanning electron microscopy. $C_4A_3\overline{S}$ and $C\overline{S}H_2$ totally reacted at 28 days of hydration perhaps due to the higher water-to-cement ratio and lower $C\overline{S}H_2$ content compared to the cement of Kasselouri et al. Beretka et al. (1993) showed a similar hydration product development in a CSAB cement that contained 43.0% $C_4A_3\overline{S}$, 28.5% C_2S, and 28.5% $C\overline{S}$ using a water-to-cement ratio of 0.5. $C_4A_3\overline{S}$ reacted rapidly with $C\overline{S}$ and formed ettringite, which was the main hydration product formed. However, small amounts of $C_4A_3\overline{S}$ and $C\overline{S}H_2$ remained unhydrated at 28 days of hydration perhaps due to the higher $C_4A_3\overline{S}$ and $C\overline{S}$ contents of the CSAB cement used compared to the cements of Kasselouri et al. and Valenti et al. In all these studies, C_2S remained mostly unhydrated even at later ages.

The other hydration product from the hydration reaction of $C_4A_3\overline{S}$ with calcium sulfates, AH_3, appears to be amorphous, cannot be detected by X-ray diffraction and can hardly be identified by microscopy (Kasselouri et al., 1995). However, Valenti et al.

(2007) showed that thermogravimetric analysis successfully detects AH_3, which formed along with ettringite following Equation 2.2 in a CSAB cement that contained 32.8% $C_4A_3\overline{S}$, 39.3% C_2S, and 13.7% $C\overline{S}H_2$.

Kasselouri et al. (1995) showed that no calcium monosulfoaluminate formed in a CSAB cement that contained 20.1% $C_4A_3\overline{S}$, 47.1% C_2S, 19.8% $C\overline{S}$, and 13.8% C_4AF due to the sufficient amount of $C\overline{S}$ in the system. However, Valenti et al. (2007) showed that no calcium monosulfoaluminate formed in a CSAB cement that contained 32.8% $C_4A_3\overline{S}$; 39.3% C_2S, and 13.7% $C\overline{S}H_2$ even though the $C\overline{S}H_2$ content was insufficient in the system. Wang et al. (1992) showed that the hydration reaction of $C_4A_3\overline{S}$ accelerated with increasing amount of $C\overline{S}H_2$ in the system and eventually reached a higher degree of hydration. However, at lower $C\overline{S}H_2$ content, more $C_4A_3\overline{S}$ remained unhydrated instead of forming calcium monosulfoaluminate.

Glasser and Zhang (2001) showed that CSAB cement required a higher water-to-cement ratio for complete hydration than portland cement because the formation of ettringite requires large amount of water according to Equation 2.2. At lower water-to-cement ratio, CSAB cement underwent self-desiccation and more cement phases remained unhydrated even at later ages.

CSAB cement might also contain minor phases such as calcium aluminoferrite (C_4AF), calcium aluminates ($C_{12}A_7$ and CA), gehlenite (C_2AS), and calcium sulfosilicate ($C_5S_2\overline{S}$) (Mehta, 1980; Sharp et al., 1999; Roy et al., 1999). The hydration reactions of C_4AF, $C_{12}A_7$, and CA with calcium sulfates form ettringite and can contribute to the early-age property development in CSAB cement (Evju and Hansen, 2001). Beretka et al. (1993) showed that $C_5S_2\overline{S}$ reacts with water very slowly (almost inert), but can contribute to the long-term property development in CSAB cement. Palou et al. (2005)

showed that the hydration reaction of C_2AS forms gehlenite hydrate (mineral name: Strätlingite; C_2ASH_8) at later ages, which is well crystalline and stable.

2.2.5 Porosity Development

The porosity development in CSAB cement is generally different to portland cement due to the different hydration chemistry. Bernardo et al. (2006) applied mercury intrusion porosimetry to a CSAB cement that contained 53.0% $C_4A_3\overline{S}$, 13.2% C_2S, 18.6% $C\overline{S}$, and 10.3% $C_{12}A_7$ using a water-to-cement ratio of 0.5 and compared the results to portland cement. The CSAB cement hardened rapidly due to the fast formation of ettringite and AH_3 from the hydration reaction of $C_4A_3\overline{S}$ and $C\overline{S}$ following Equations 2.1 and 2.2. The initial hydration products quickly reduced the internal pore space. After 6 hours of hydration, the smaller pores (~25 nm) dominated over the capillary pores (~200 nm) and the system developed a bimodal pore structure, which generally correlates to a disconnected pore structure and a denser microstructure. Portland cement, on the other hand, showed a unimodal or continuous pore structure at early ages, which generally correlates to a more porous microstructure. It only developed a bimodal pore structure after 7 days of hydration, demonstrating the disconnected nature of the pore system as the larger pore volume decreases. Contrarily, Janotka et al. (2007) showed that a mortar made from a CSAB cement that contained low $C_4A_3\overline{S}$ (20.2% $C_4A_3\overline{S}$, 50.3% C_2S, 9.7% $C\overline{S}$, and 19.5% C_4AF) using a water-to-cement ratio of 0.5 had higher porosity and coarser pore structure than portland cement mortar at 90 days of hydration. The hydration reaction of $C_4A_3\overline{S}$ with calcium sulfates ($C\overline{S}$ and $C\overline{S}H_2$) to form ettringite and AH_3 is responsible for the early-age property development in CSAB cement and their contents have a large impact on pore structure development in CSAB cement.

2.2.6 Dimensional Stability

The formation of ettringite from the hydration reactions of $C_4A_3\overline{S}$ with calcium sulfates ($C\overline{S}$ and $C\overline{S}H_2$) and CH, as shown in Equations 2.1-2.4, can be expansive (Kasselouri et al., 1995). If most of the ettringite forms before the paste hardens, then non-expansive and rapid hardening CSAB cement can be achieved. However, significant ettringite formation after hardening could cause expansion and cracking (Ogawa and Roy, 1982).

Beretka et al. (1996) showed that CSAB cements that mainly contained $C_4A_3\overline{S}$, $C_5S_2\overline{S}$, and $C\overline{S}$ expanded and cracked with $C_4A_3\overline{S}$ contents higher than 50% using a water-to-cement ratio of 0.4. Kasselouri et al. (1995) studied the expansibility of a CSAB cement with low $C_4A_3\overline{S}$ (20.1% $C_4A_3\overline{S}$, 47.1% C_2S, 19.8% $C\overline{S}$, and 13.8% C_4AF) using a water-to-cement ratio of 0.4. The CSAB cement showed no expansion, comparable to portland cement. Janotka et al. (2007) showed that mortar made from a CSAB cement with low $C_4A_3\overline{S}$ (20.2% $C_4A_3\overline{S}$, 50.3% C_2S, 9.7% $C\overline{S}$, and 19.5% C_4AF) using a water-to-cement ratio of 0.5 had limited expansion (0.25%), but was higher than portland cement mortar (-0.10%). The CSAB cements of Kasselouri et al. and Janotka et al. had similar phase compositions. The differences in dimensional stability could be caused by the different water-to-cement ratios, curing conditions, and test methods used. These studies show that dimensional stability of CSAB cement is dependent on its $C_4A_3\overline{S}$ content.

Glasser and Zhang (2001) showed that a CSAB cement clinker that mainly contained $C_4A_3\overline{S}$, C_2S, $C\overline{S}$, C_4AF shrunk slightly at 18% $C\overline{S}H_2$ addition, showed zero dimensional change at 22-24% $C\overline{S}H_2$ addition, and became expansive at 24-25% of $C\overline{S}H_2$ addition, which suggests that dimensional stability of CSAB cement is also dependent on the amount of $C\overline{S}H_2$ available in the system.

Beretka et al. (1996) showed that CSAB cements that mainly contained $C_4A_3\overline{S}$, $C_5S_2\overline{S}$, and $C\overline{S}$ expanded and cracked with $C_4A_3\overline{S}$ contents higher than 50% because the initial water-to-cement ratio (0.4) was not enough for large amount of $C_4A_3\overline{S}$ to completely react according to Equation 2.2. Secondary ettringite formed from the unhydrated $C_4A_3\overline{S}$ and $C\overline{S}$ during curing in 100% relative humidity after the paste hardened, causing expansion and cracking at later ages. However, when using higher water-to-cement ratios (0.65-0.7), the high $C_4A_3\overline{S}$ cements remained dimensionally stable during curing in 100% relative humidity because water in the system was sufficient for $C_4A_3\overline{S}$ to fully react at early ages. Furthermore, Odler and Colan-Subauste (1999) showed that ettringite formation and expansion depended on the curing environment. When curing at low humidity, ettringite formation stopped after a few days of hydration due to the loss of free water in the system. The availability of water is critical for ettringite formation and dimensional stability of CSAB cement.

2.2.7 Strength Development

Mehta (1980) suggested that CSAB cements can be produced with a wide range of properties from rapid to slow hardening and good to poor durability depending on their phase compositions, as shown in Figure 2.1. Mortars made from CSAB cements that contained 20% $C_4A_3\overline{S}$, 25-30% C_2S, 15-20% $C\overline{S}$, and 30-40% C_4AF using a water-to-cement ratio of 0.4 set rapidly and showed good 1-day (31 MPa) and 120-day (53 MPa) compressive strength. The hydration reactions of the fast-reacting $C_4A_3\overline{S}$ and C_4AF with $C\overline{S}$ to form ettringite and AH_3 (Equations 2.1 and 2.2) resulted in rapid setting and contributed to the high early-age strength development, while the hydration reaction of the slow-reacting C_2S to form C-S-H (Equation 2.5) contributed to the long-term strength development. However, mortars made from CSAB cements that contained 10% $C_4A_3\overline{S}$,

50-65% C_2S, 10% $C\overline{S}$, and 15-30% C_4AF using a water-to-cement ratio of 0.4 were slow hardening and showed poor early-age and long-term compressive strength perhaps due to their low $C_4A_3\overline{S}$, C_4AF, and $C\overline{S}$ contents and high C_2S contents. Compressive strength development of CSAB cement is strongly dependent on its phase composition.

Other research also showed that CSAB cements exhibited rapid setting and high early-age strength development. Glasser and Zhang (2001) showed that mortar made from a CSAB cement that mainly contained $C_4A_3\overline{S}$, C_2S, $C\overline{S}$, and C_4AF with 18% $C\overline{S}H_2$ addition set rapidly and showed excellent 1 and 3-day compressive strength (44 and 54 MPa, respectively) and flexural strength (7.6 and 7.5 MPa, respectively). Quillin (2001) showed that concretes made from two CSAB cements that mainly contained $C_4A_3\overline{S}$, C_2S, $C\overline{S}$, C_4AF, and $C\overline{S}H_2$ set rapidly and showed good 1-day (33-42 MPa) and 90-day (49-55 MPa) compressive strength.

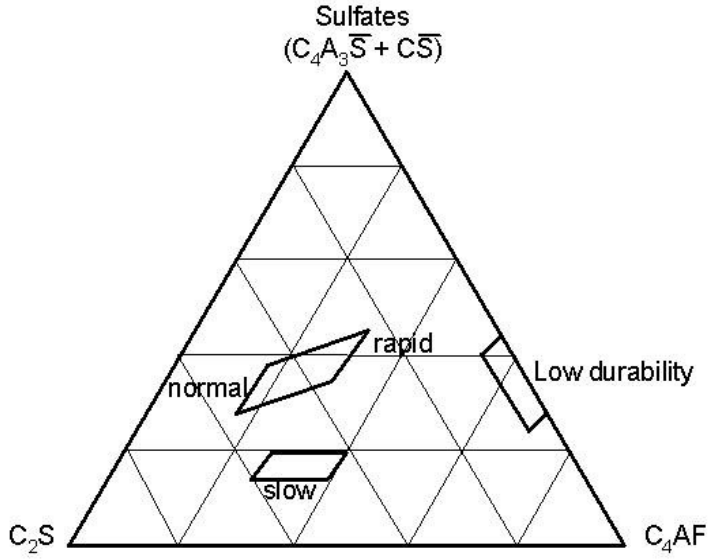

Figure 2.1 – Schematic phase diagram of ternary system representing CSAB cement; slow, normal, and rapid refer to hardening rates (adapted from Metha, 1980)

2.2.8 Sulfate Resistance

Glasser and Zhang (2001) calculated the mineralogical balances for CSAB cement hydration and showed that if there are insufficient calcium sulfates ($C\overline{S}$ and $C\overline{S}H_2$) in the system to complete the reaction in Equation 2.2, calcium monosulfoaluminate ($C_4A\overline{S}H_{12}$) forms. It is also known that in portland cement, if insufficient gypsum ($C\overline{S}H_2$) is added, ettringite reacts with the aluminum containing phases (C_3A and C_4AF) to form calcium monosulfoaluminate ($C_4A\overline{S}H_{12}$) (Mindess et al., 2003). Calcium monosulfoaluminate is subject to transform back to ettringite in the presence of environmental sulfate, causing cracking. However, CSAB cement generally shows good sulfate resistance. Kurtis et al. (2001) showed that a CSAB cement that mainly contained $C_4A_3\overline{S}$ and C_2S had excellent sulfate resistance. Quillin (2001) showed that two concretes made from CSAB cements that mainly contained $C_4A_3\overline{S}$, C_2S, C_4AF, $C\overline{S}$, and $C\overline{S}H_2$ exhibited excellent sulfate resistance. Dan and Janotka (2003) showed that mortar made from a CSAB cement that contained 29% $C_4A_3\overline{S}$, 55.2% C_2S, 5.3% $C\overline{S}$, and 10.5% C_4AF was more resistant to sulfate attack compared to portland cement mortar even though the $C\overline{S}$ content was insufficient in the system.

2.2.9 Corrosion Resistance

The pore solution pH in CSAB cement is generally lower than in portland cement due to its different hydration chemistry. Less CH forms in CSAB cement than in portland cement and results in a lower pore solution pH (Kalogridis et al., 2000). Furthermore, ettringite, the main hydration product in CSAB cement, is susceptible to carbonation, which further lowers the pore solution pH in CSAB cement at later ages (Quillin, 2001). In steel reinforced concrete, a passivated oxide layer forms on the reinforcement steel surface and protects it from corrosion when the pH of the surrounding pore solution is high (Jones, 1996). However, this passivated layer breaks down when

the surrounding pore solution pH is below approximately 11.5. The low pore solution pH in CSAB cement might not be high enough to protect the reinforcement steel, leading to corrosion in the reinforcement steel and cracking in the concrete.

Kalogridis et al. (2000) showed that the pore solution pH in steel reinforced mortar made from a CSAB cement that contained 21.0% $C_4A_3\overline{S}$, 44.5% C_2S, 19.8% $C\overline{S}$, and 15.8% C_4AF using a water-to-cement ratio of 0.45 was lower than a steel reinforced portland cement mortar. The reinforcement steel in the CSAB cement mortar showed a higher corrosion rate than the reinforcement steel in the portland cement mortar stored either in continuous or intermittent exposure to 3.5% NaCl solution by direct measurement of weight loss of the reinforcement steel. Half cell potential measurement of the reinforcement steel showed that the lower pH in the CSAB cement mortar pore solution depassivated the reinforcement steel and caused the higher corrosion rate either in continuous or intermittent exposure to 3.5% NaCl solution.

Quillin (2001) showed that two concretes made from CSAB cements that mainly contained $C_4A_3\overline{S}$, C_2S, C_4AF, $C\overline{S}$, and $C\overline{S}H_2$ carbonated more rapidly compared to portland cement concrete. These two CSAB cement concretes also showed higher chloride diffusion coefficients compared to portland cement concrete and resulted in deeper chloride penetration depth. These results suggest that reinforcement steel in these two concretes might be prone to corrosion because of the chloride availability and the decrease in pore solution pH from carbonation. Glasser and Zhang (2001) showed that chlorides were able to penetrate a CSAB cement concrete pipe used in a marine environment for 14 years. The penetrated chloride altered the concrete outer layer microstructure; however, the reinforcement steel was found to be uncorroded. Zhang and Glasser (2005) showed that the carbonation of CSAB cement concrete can be controlled by the water-to-cement ratio. At low water-to-cement ratio, the concrete underwent self-

desiccation and eliminated the availability of pore water that can transport CO_2, thereby limiting the potential depth of carbonation.

Chapter 3: Incorporation of Waste Materials into Portland Cement Clinker Synthesized from Reagent-Grade Chemicals

3.1 INTRODUCTION

As reviewed in Chapter 2, previous research has shown that waste materials can be used as raw materials for portland cement production. However, a thorough, quantitative investigation on cement phase composition, phase distribution, and hydration behavior was not performed in these studies. The portland cement part of the research performed for this dissertation aimed to address these gaps in our knowledge.

In this chapter, portland cement clinkers were synthesized from reagent-grade chemicals and waste materials. A primary goal was to demonstrate the feasibility of using waste materials in cement manufacturing. As part of this process, it is important to develop an understanding of the phases that form in the presence of the large quantities of impurities present in waste materials. Reagent-grade chemicals were chosen in order to create a model system with no impurities, thereby establishing a baseline for the composition and the synthesis procedure. Then, calcium oxide-bearing waste materials, specifically fly ash and blast furnace slag, were combined with the reagent-grade chemicals to synthesize portland cement clinkers. The only impurities in the system came from the waste materials, allowing investigation into the effects of these waste-specific impurities on phase formation. The resulting synthetic clinkers were analyzed for phase content using X-ray diffraction and phase distribution using scanning electron microscopy. Finally, the early-age hydration behavior of the synthesized cements was investigated using isothermal conduction calorimetry.

3.2 EXPERIMENTAL

3.2.1 Materials

In this study, portland cement clinker was synthesized from reagent-grade chemicals with industrial waste material incorporation. The reagent-grade chemicals used were calcium oxide (96%+ CaO; Acros), silica gel (100% SiO_2; Fisher), aluminum oxide (100% Al_2O_3; Acros), and ferric oxide (100% Fe_2O_3; Fisher). The industrial waste materials used, specifically fly ash and ground granulated blast furnace slag, were those already marketed and distributed for use as supplementary cementing materials (SCMs) for concrete, meaning that they can be used to directly replace a portion of the portland cement in concrete. The fly ash (Class C; Headwaters/ISG) and blast furnace slag (Holnam, Dundee, MI) were chosen for their high calcium oxide, silicon oxide, and aluminum oxide content which are all necessary for portland cement manufacturing (oxide compositions from X-ray fluorescence analysis shown in Table 3.1) (ASTM C 618, 2005). Furthermore, in order to stabilize the desired β-C_2S phase, 0.1 wt% boron oxide (98.5% B_2O_3; Alfa Aesar) was added to the raw mix (Fierens and Trilocq, 1983).

Table 3.1 – Chemical compositions (%) of the fly ash and slag used

Oxides	Fly Ash	Slag
SiO_2	33.58	34.48
Al_2O_3	18.51	11.35
Fe_2O_3	6.56	0.67
CaO	27.08	41.73
MgO	6.10	7.32
Na_2O	1.89	0.14
K_2O	0.39	0.38
TiO_2	1.34	0.46
MnO_2	0.03	0.56
P_2O_5	1.15	0
SrO	0.48	0.10
BaO	0.74	0.11
SO_3	1.83	1.88
LOI	0.34	0.83
Moisture	0.07	0.28

Note: LOI is mass lost on ignition to 750°C

3.2.2 Synthesis

First, reagent-grade chemicals were used to synthesize portland cement clinker (with 0.1 wt% boron oxide addition). Chemicals were proportioned for a target clinker composition of 50% C_3S, 25% C_2S, 15% C_3A, and 10% C_4AF using the standard Bogue calculation (Bogue, 1929; Taylor, 1997). A portland cement clinker with this composition is classified as Type I according to ASTM C 150 (2005). The C_3A and C_4AF content are at the maximum limit because this allows for a higher amount of waste material incorporation.

Raw materials were dispersed in ultra-pure water (1:10 ratio) and mixed in a rotary jar mill (U.S. Stoneware; East Palestine, OH) for 24 h at 120 rpm in a HDPE bottle using 2 mm high-purity ZrO_2 (Y_2O_3-stabilized) grinding media (Richerson, 1992). The solution was poured in a beaker and dried in a 105˚C oven. The resulting product was hand crushed into fine powder form using a mortar and pestle. The materials were placed in platinum crucibles and fired in an electric muffle furnace (Sentrotech, Berea, OH). Two cycles of firing were run, with a 5˚C/min heating rate and a 2˚C/min cooling rate. In the first cycle, the materials were fired at 850˚C for 2 h to dehydrate and calcine the materials. They were then fired at 1200˚C for 8 h, from 1200˚C to 1250˚C for 8 h, and at 1250˚C for another 8 h. An intermediate grinding by hand was performed between cycles to homogenize the materials. In the second cycle, the materials were fired at 1300˚C for 8 h, from 1300˚C to 1350˚C for 8 h, and at 1350˚C for another 8 h (Fierens and Trilocq, 1983; Mohamed and Sharp, 2002; Stephan and Wilhelm, 2004). If the fired product contained excess free lime (>1 wt%, determined by X-ray diffraction), the materials were fired again at 1400˚C for 12 h. Finally, the resulting clinker was hand ground and passed through a #325 sieve (45 μm).

The goal of the laboratory synthesis processes was to mimic the processes that take place in industrial manufacturing. Raw ingredients much be homogenized and then fired at high temperature. The firing time in the furnace was much longer compared to the firing time in a rotary kiln used in industrial manufacturing because the raw ingredients remained stationary inside the crucible during the firing process, which prevented materials from properly reacting with each other. Furthermore, the maximum firing temperature used in the laboratory synthesis processes was 1400˚C which was about 50˚C lower than the maximum temperature used in industrial manufacturing. Under lower firing temperature, the required phases might take longer to form (Mindess,

2003).

After successful synthesis of portland cement clinker from reagent-grade chemicals, waste materials were incorporated in increments up to the maximum content while the target clinker composition and the synthesis procedure remained unchanged. To satisfy the target clinker composition, 40% fly ash and 60% slag incorporation were the maximum incorporation amounts for this specific fly ash and slag because of the high aluminum content in fly ash and slag. The percentage of incorporation represents the amount of waste materials in the final product. For example, if 20 g of clinker was being produced, a 40% waste materials incorporation means that 8 g of waste materials was put into the raw mix, and the remaining oxides needed for the target clinker composition were supplied by reagent-grade chemicals. Impurities from waste materials were taken as additives and were not included in the proportioning calculations. Therefore, all clinker samples contained the same amount of calcium, silicon, aluminum, and iron. This approach helps clarify how waste materials and impurities affect the formation mechanisms of the four major clinker phases.

3.2.3 Analysis

3.2.3.1 X-Ray Diffraction

All of the synthetic clinkers were tested by X-ray diffraction (Siemens D500 Powder Diffractometer; Cu $K_{\alpha 1}$, λ=1.5046 Å) to determine phase formation. The instrument was operated under 40 keV and 30 mA, the step size used was 0.02˚/6 s, and the scan range was 20˚–80˚ 2θ. Test samples were prepared by dispersing clinkers in ethanol and pouring the solution on quartz low background sample holders. Thin layers of solid materials were left on the sample holders after the samples dried.

Qualitative information of phases present in the sample was obtained using the

Hanawalt manual and the Jade program (MDI) (JCPDS–International Centre for Diffraction Data, 1989). Quantitative information was collected using the Rietveld method (accuracy about 1%) which was performed with the TOPAS-Academic software (Bruker AXS, Karlsruhe, Germany) (Young, 1995; Stutzman and Leigh, 2002).

3.2.3.2 Scanning Electron Microscopy

Phase distribution in several selected synthetic clinkers was studied using scanning electron microscopy (LEO 1530 Thermally-Assisted Field Emission SEM, Zeiss, Peabody, MA). Test samples were prepared by mixing clinker powders with optical-grade epoxy (Epotek 353ND) and casting in cylindrical molds. The samples were cured in a 40˚C oven for 24 h, and their cross sections were polished and coated with carbon before imaging and compositional examination by energy dispersive spectroscopy (Stutzman, 2004). Elemental maps were collected (Ca, Si, Al, Fe, Mg, S, Na, and K). The elemental maps collected have a resolution of 512 pixels over a 450 µm field width. This is equivalent to about 0.9 µm per pixel, approximately the spatial resolution of elemental mapping. The elemental maps were then preprocessed with ImageJ software to reduce noise (Rasband, 1997-2009; Abramoff et al., 2004). Multispectral images were then prepared by overlaying the separate elemental maps and processing using Multispec software (©Purdue Research Foundation), which allowed quantitative assessment of the spatial distribution of phases (Lydon, 2005).

3.2.3.3 Isothermal Conduction Calorimetry

To determine if the synthesized cements exhibited similar behavior to traditional cement, the rate of reaction with water was evaluated. The heat produced by cementitious materials in exothermic hydration reactions is a good indication of their early-age hydration behavior (Gartner et al., 2002). In this study, several selected

synthesized cements as well as a commercially produced Type I/II cement (TXI Hunter Cement) were tested for heat evolution using an isothermal conduction calorimetry (Thermometric TAM Air). Cements were made from the synthetic clinkers by adding 12.5 wt% gypsum (100% $CaSO_4 \cdot 2H_2O$; USG) to control setting of C_3A (Odler, 1998). Gypsum content was determined by adding a range of gypsum to the synthetic clinkers and testing for hydration behavior. 12.5 wt% gypsum addition compared best to the commercial cement and was considered the optimum gypsum content. The fineness of the synthetic clinkers were tested by an air-permeability test, called Blaine fineness, according to ASTM C 204 (2007) to assure uniform of particle fineness. Hydration was evaluated for 3 days at 23˚C using a water-to-cement ratio of 0.45.

3.3 RESULTS AND DISCUSSION

3.3.1 Phase Composition

Quantitative X-ray diffraction results obtained through Rietveld analysis for the clinker sample synthesized using only reagent-grade chemicals are shown in Table 3.2 and the refined X-ray diffraction pattern is shown in Figure 3.1. All four major clinker phases (C_3S, C_2S, C_3A, and C_4AF) formed in the sample. The free lime content of the sample was very low (0.5%), indicating that the materials completely reacted in the furnace. The sample contained 15.5% C_3A and 8.5% C_4AF, which nearly matches the target composition (15% C_3A and 10% C_4AF). In contrast, the sample contained much higher C_3S (65.2%) and much lower C_2S (10.3%) than its target composition (50% C_3S and 25% C_2S). The differences may be attributed to errors in the standard Bogue calculation used to proportion the raw materials. The standard Bogue calculation is a method used to estimate the amount of the four major phases in clinker from the oxide contents in the raw mix using knowledge of phase equilibria and by solving linear

equations (Bogue, 1929; Taylor, 1997). This method assumes that the four major cement phases are in their stoichiometric forms, which is usually not realistic because these phases can accommodate a large amount of substitute ions. Moreover, the synthesis environment is not always in an equilibrium state. Nevertheless, the results demonstrate that the synthesis procedure is appropriate for producing portland cement clinker in the laboratory from reagent-grade chemicals.

Table 3.2 – Phase content (%) of clinker samples synthesized by reagent-grade chemicals (RG) with waste materials incorporation

Sample	**C_3S**	**C_2S**	**C_3A**	**C_4AF**	**Lime**	**Periclase**
Target (Bogue)	50	25	15	10	0	0
100% RG	65.2	10.3	15.5	8.5	0.5	0
10% Fly ash	63.3	15.2	12.2	7.9	0.8	0.6
20% Fly ash	60.4	18.9	10.8	8.2	0.6	1.1
30% Fly ash	51.5	25.2	10.9	10.2	0.5	1.7
40% Fly ash	43.0	36.2	9.4	8.5	0.2	2.7
10% Slag	56.6	17.3	14.5	9.8	0.2	1.6
20% Slag	57.5	17.1	13.8	9.4	0.1	2.1
30% Slag	54.3	23.2	10.9	9.3	0.1	2.2
40% Slag	50.0	26.6	11.6	8.9	0.4	2.5
50% Slag	43.1	30.4	12.5	9.9	0.4	3.7
60% Slag	42.6	31.7	11.8	9.8	0.4	3.7

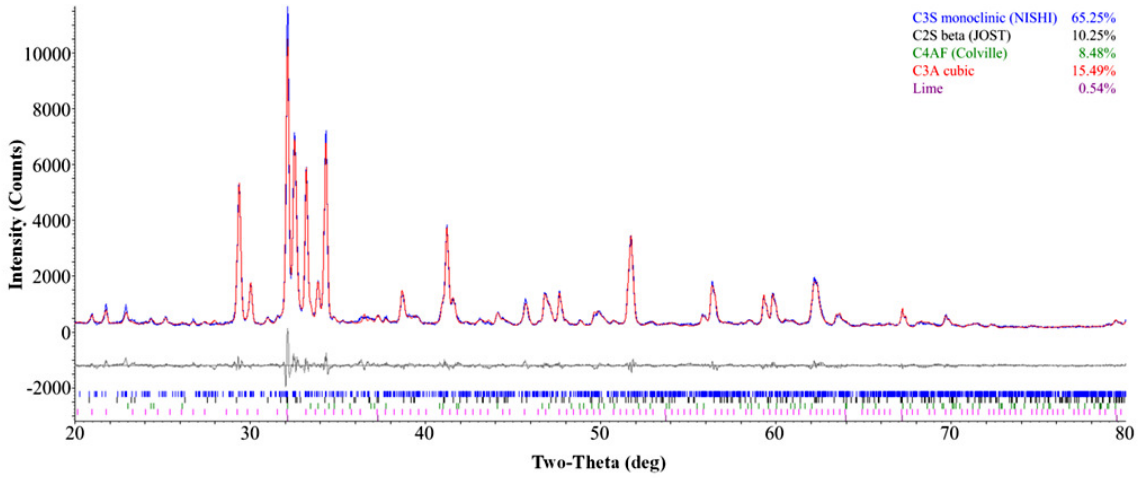

Figure 3.1 – Rietveld refinement for a clinker sample synthesized by reagent-grade chemicals

Rietveld analysis results for clinker samples synthesized with 0–40% fly ash and 0–60% slag incorporation (with 10% intervals) are shown in Table 3.2. The X-ray patterns for clinker samples synthesized by reagent-grade chemicals, 20% fly ash incorporation, and 40% fly ash incorporation; reagent-grade chemicals, 30% slag incorporation, and 60% slag incorporation are shown in Figures 3.2 and 3.3.

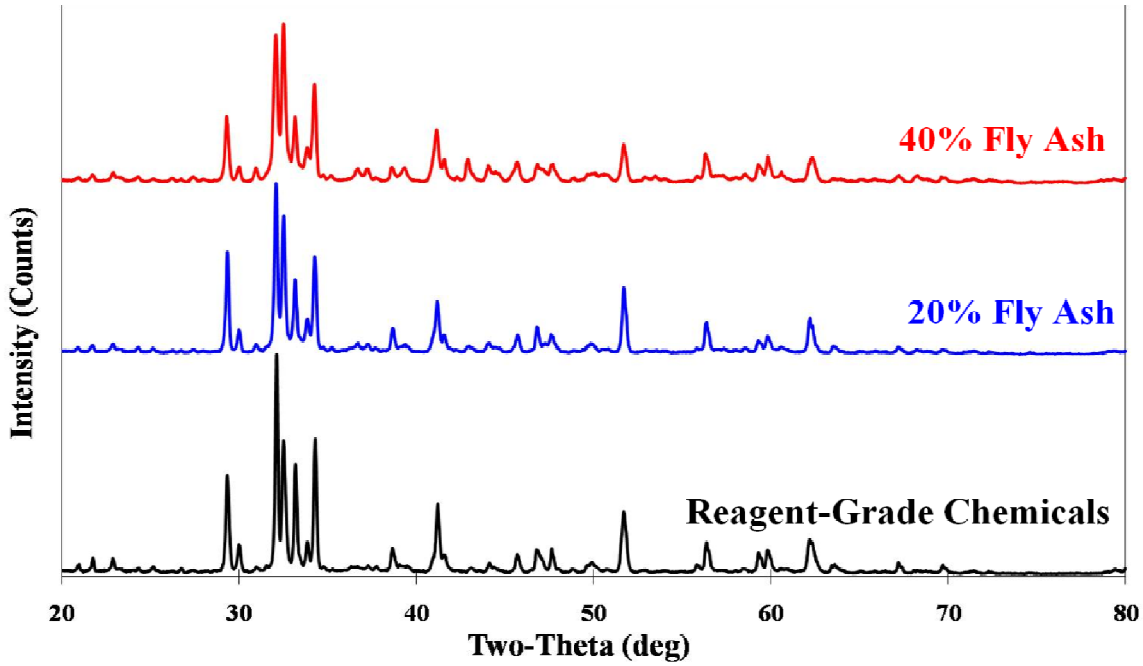

Figure 3.2 – X-ray patterns for clinker samples synthesize by reagent-grade chemicals, 20% fly ash incorporation, and 40% fly ash incorporation

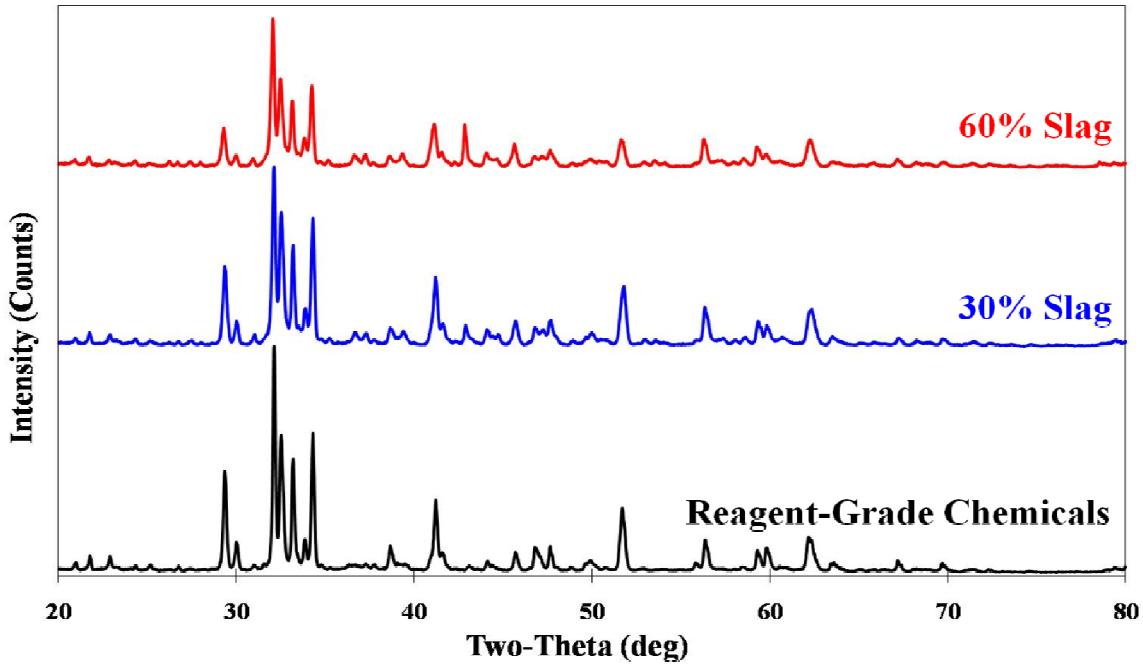

Figure 3.3 – X-ray patterns for clinker samples synthesized by reagent-grade chemicals, 30% slag incorporation, and 60% slag incorporation

The phase analysis results show that the four major cement phases formed in every sample. All of the clinker samples had low free lime contents indicating that the materials completely reacted in the furnace. The only impurity phase that can be detected by X-ray diffraction was periclase (MgO), which increased with increasing amount of waste materials incorporated (both fly ash and slag). The maximum amount of periclase in Type I cement allowed by ASTM C 150 (2005) is 6%; all synthetic clinkers had periclase contents lower than this limit.

The content of C_3S decreased with increasing amount of waste materials incorporated while the content of C_2S increased with increasing amount of waste materials incorporated (both fly ash and slag). According to the work of Uda et al. (1998), this effect could be due to the changes in equilibrium states in the $CaO–SiO_2–Al_2O_3–Fe_2O_3$ system caused by sulfur impurities; both the fly ash and the slag used had approximately 1.8% SO_3 (Table 3.1). Uda et al. also showed that C_2S can accommodate more sulfur than C_3S, which may be another reason for the observed change in $C_3S–C_2S$ ratio.

The results in Table 3.2 also show that the content of C_3A decreased as the amount of waste materials increased. Uda et al. (1998) showed that C_2S can accommodate more Al than C_3S, therefore a decrease in the $C_3S–C_2S$ ratio enables the incorporation of more aluminum in the silicate phases, leaving less available for formation of C_3A and C_4AF (Uda et al. 1998).

In spite of the changes in phase content with increasing incorporation of waste materials, Type I portland cement clinkers conforming to the compositional guidelines in ASTM C 150 (2005) were successfully made with reagent-grade chemicals and waste materials. Although the waste materials changed the proportions of the major cement phases, they remained in an acceptable range. However, the lower $C_3S–C_2S$ ratio in

clinker samples with high amounts of waste materials incorporation might result in lower early strength and could significantly affect the performance of concrete.

It is interesting to note that waste materials changed the C_3S–C_2S ratio considerably, as well as the amount of C_3A. These changes could have significant implications on proportioning raw materials when using wastes, since it may make it difficult to predict phase contents accurately. However, the current standard practice in proportioning raw materials and predicting phase content is antiquated and flawed. This is typically done using Bogue equations, as discussed earlier (Bogue, 1929; Taylor, 1997). These equations relate the oxide content of the raw materials to phase contents in a clinker using phase equilibria concepts and by solving linear equations. However, the present study demonstrates that Bogue equations poorly predict phase formation even in a pure system. The variation in product formation introduced through waste materials is not any more significant than that introduced through error in the Bogue equations. Therefore, changes in phase content due to waste material incorporation may not significantly affect cement production practices until more advanced methods of phase prediction or analysis are adopted.

3.3.2 Microstructure

The synthetic clinkers were examined under a microscope to determine if the incorporation of waste materials affects the spatial distribution of phases. Elemental maps for the clinker sample synthesized by reagent-grade chemicals are shown in Figure 3.4. Only the Ca, Si, Al, and Fe maps are revealed because other elements showed little signal except noise. Multispectral images were assembled from these elemental maps, and the multispectral images for clinker samples synthesized by reagent-grade chemicals, 40% fly ash incorporation, and 60% slag incorporation are shown in Figures 3.5-3.7. In

these multispectral images, colors were assigned to each individual phase (C_3S blue, C_2S green, C_3A red, C_4AF yellow, and periclase purple) facilitating quantitative examination of phase distribution. Periclase was the only impurity phase that can be identified in the samples with waste materials incorporation. The content of other impurities might have been too low to be identified. The clinker sample synthesized by reagent-grade chemicals contained more C_3S and less C_2S than the clinker samples synthesized by reagent-grade chemicals with 40% fly ash and 60% slag incorporation, respectively (image appears bluer). This result agrees with the X-ray diffraction results that showed a lower C_3S–C_2S content in clinker samples with high amounts of waste materials incorporation. The comparison of image and Rietveld analysis results for the clinker samples are shown in Table 3.3. The image and Rietveld analysis results agree with each other well except that the image analysis results showed a slightly lower C_3A, C_4AF, and periclase content in the samples with waste materials incorporation. Nevertheless, all of these samples showed similar spatial distribution of phases.

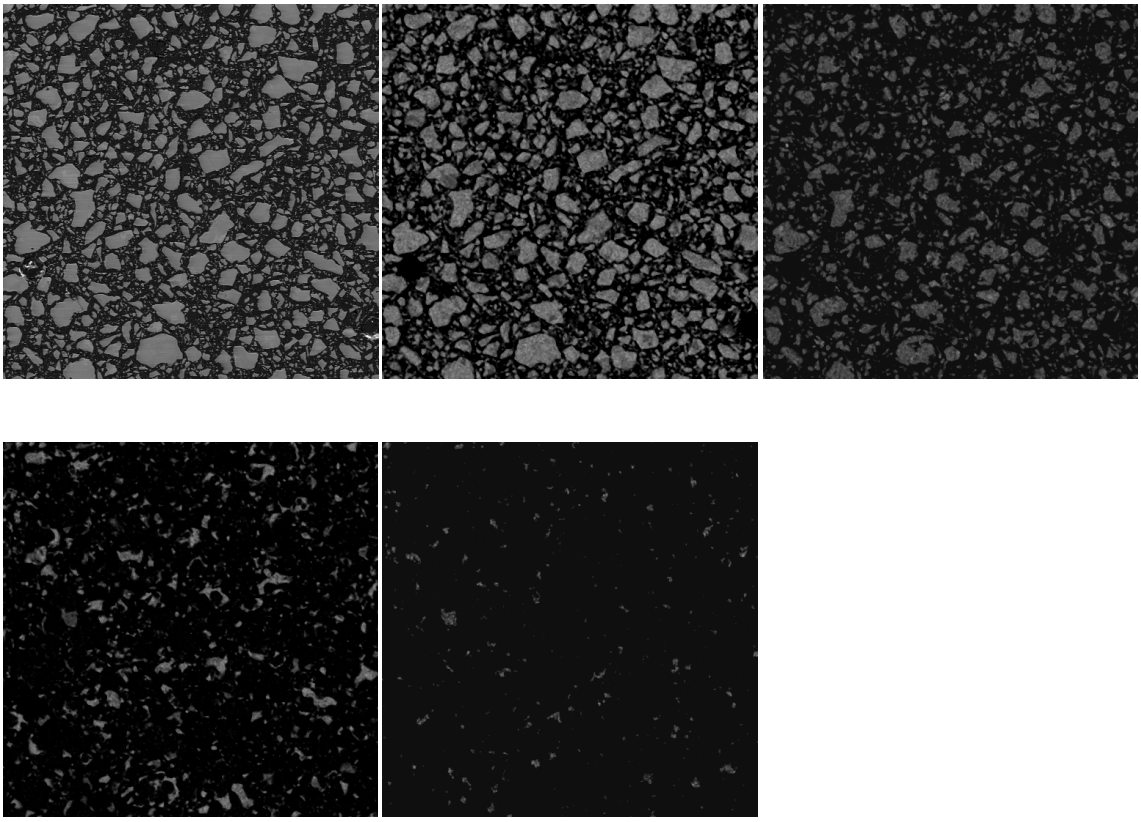

Figure 3.4 – Elemental maps for a clinker sample synthesized by reagent-grade chemicals (left-right, top-bottom orientation: secondary electron image, Ca, Si, Al, and Fe; field width: 450 μm)

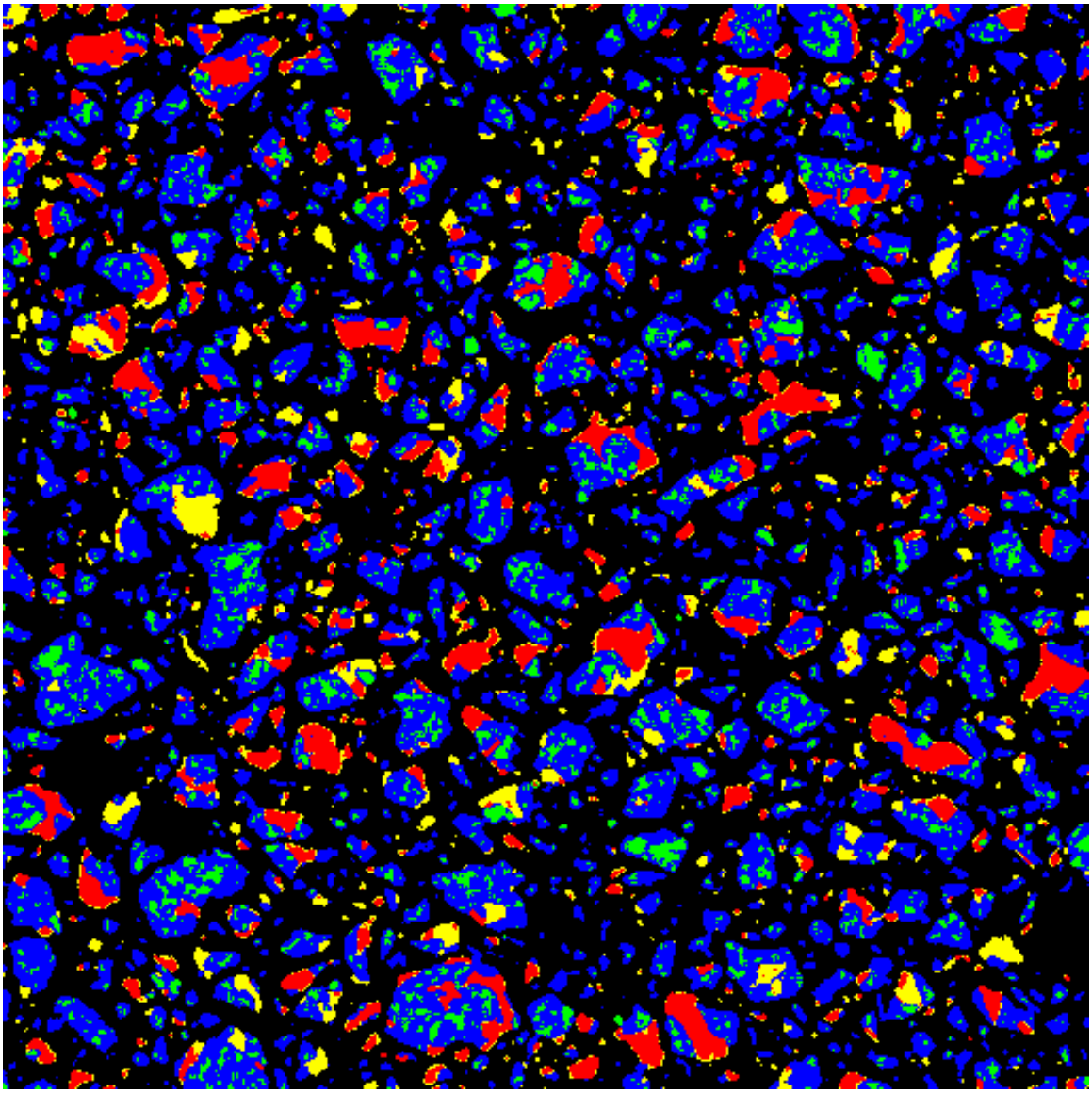

Figure 3.5 – Multispectral image for a clinker sample synthesized by reagent-grade chemicals (C_3S blue, C_2S green, C_3A red, and C_4AF yellow; field width: 450 μm)

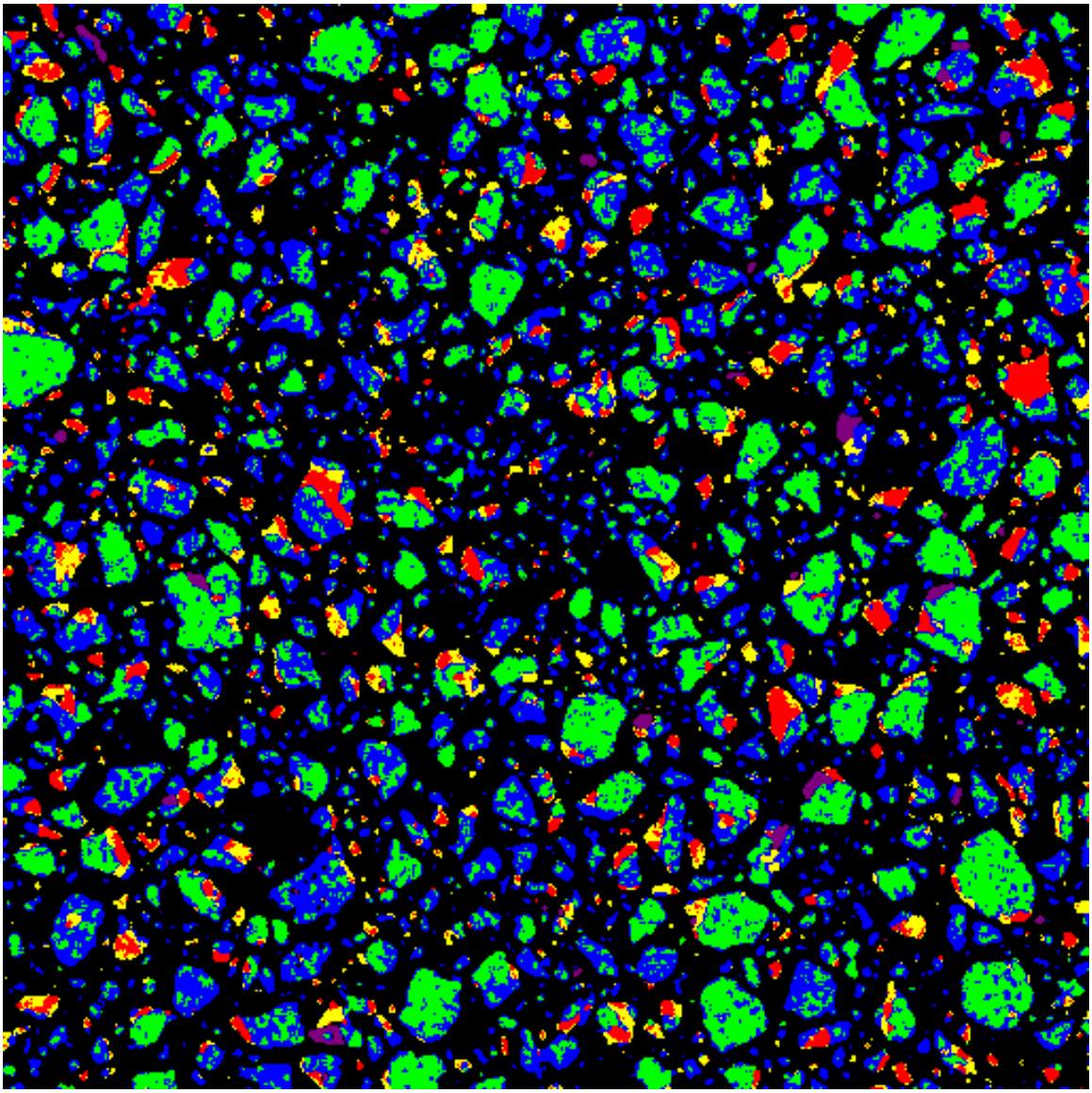

Figure 3.6 – Multispectral image for a clinker sample synthesized by reagent-grade chemicals with 40% fly ash incorporation (C_3S blue, C_2S green, C_3A red, C_4AF yellow, and periclase purple; field width: 450 μm)

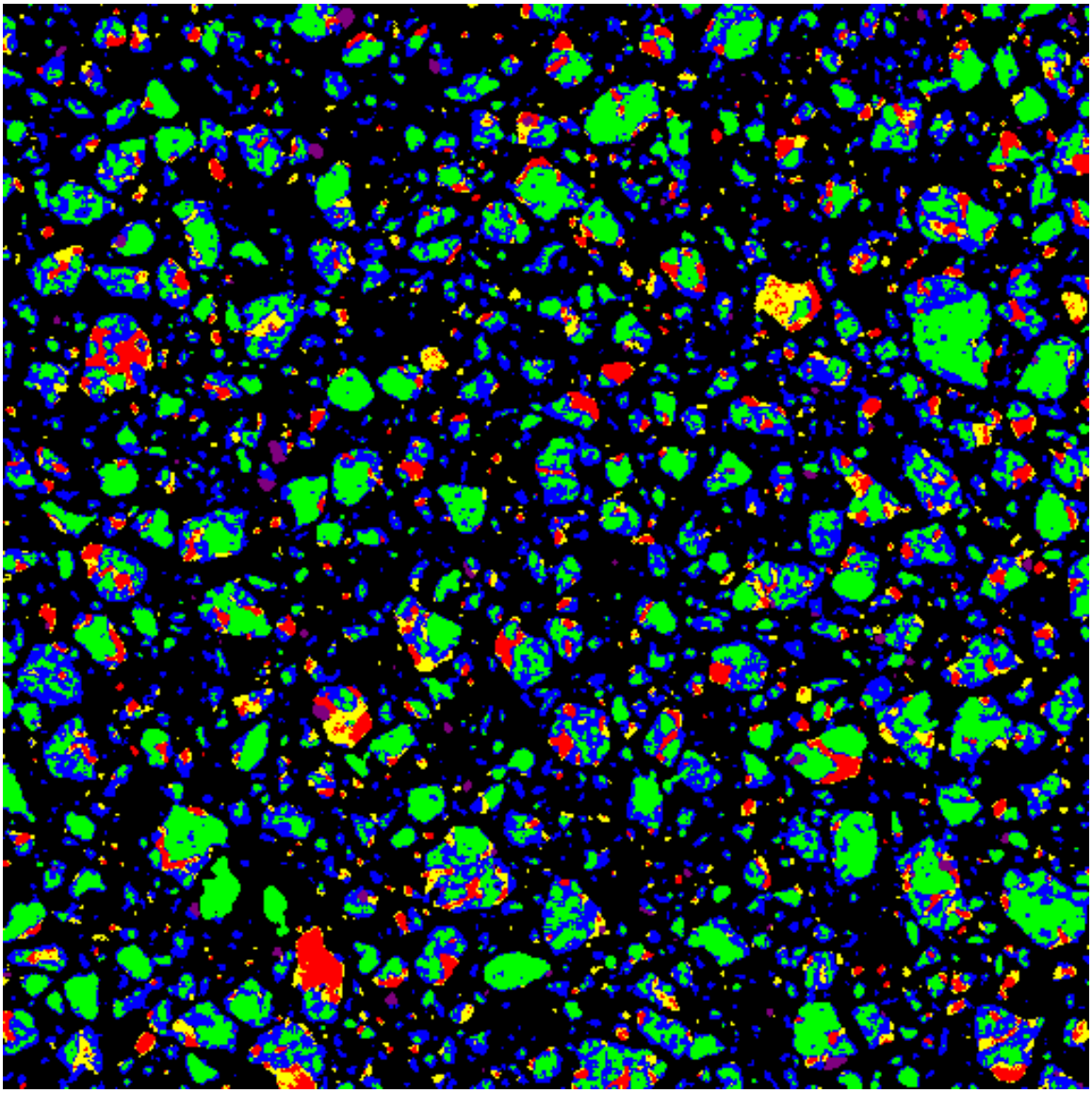

Figure 3.7 – Multispectral image for a clinker sample synthesized by reagent-grade chemicals with 60% slag incorporation (C_3S blue, C_2S green, C_3A red, C_4AF yellow, and periclase purple; field width: 450 μm)

Table 3.3 – Comparison of image and Rietveld analysis results (%) for clinker samples synthesized by reagent-grade chemicals (RG), 40% fly ash incorporation, and 60% slag incorporation

Phase	RG		40% Fly Ash		60% Slag	
	Image	Rietveld	Image	Rietveld	Image	Rietveld
C_3S	64.6	65.2	47.7	43.0	45.4	42.6
C_2S	10.3	10.3	35.4	36.2	37.5	31.7
C_3A	16.5	15.5	8.9	9.4	9.3	11.8
C_4AF	8.6	8.5	7.1	8.5	6.9	9.8
Lime	N/A	0.5	N/A	0.2	N/A	0.4
Periclase	N/A	N/A	0.9	2.7	0.9	3.7

3.3.3 Early-Age Hydration Behavior

In order to compare hydration behavior between commercial portland cement and the synthetic clinkers, the clinkers were made into cements by grinding to a comparable fineness and adding gypsum (12.5%). The Blaine fineness values for the synthetic clinkers ranged from 298.4 to 318.1 m^2/kg and are shown in Table 3.4. The differences in Blaine fineness between samples were perhaps caused by the grinding and sieving process. However, the differences are <10% and should not seriously affect the early-age hydration behavior. All of the clinker samples were hand ground and passed through a #325 sieve (45 μm); however, their Blaine fineness results were still significantly lower than the commercial Type I/II portland cement (405.5 m^2/kg).

Table 3.4 – Blaine fineness values for a commercial Type I/II portland cement (control) and clinker samples synthesized using reagent-grade chemicals (RG) with waste materials incorporation

Sample	Specific Surface (m^2/kg)
Control	405.5
RG	298.4
RG + 20% Fly ash	301.6
RG + 40% Fly ash	308.1
RG + 30% Slag	298.4
RG + 60% Slag	318.1

The rates of heat evolution for the commercial Type I/II portland cement and several of the synthesized cement samples are shown in Figure 3.8, and the cumulative heat-evolved curves are shown in Figure 3.9. The rates of heat evolution results show that the synthesized cements possessed hydration behavior similar to a commercial Type I/II portland cement because the shapes of the curves are similar.

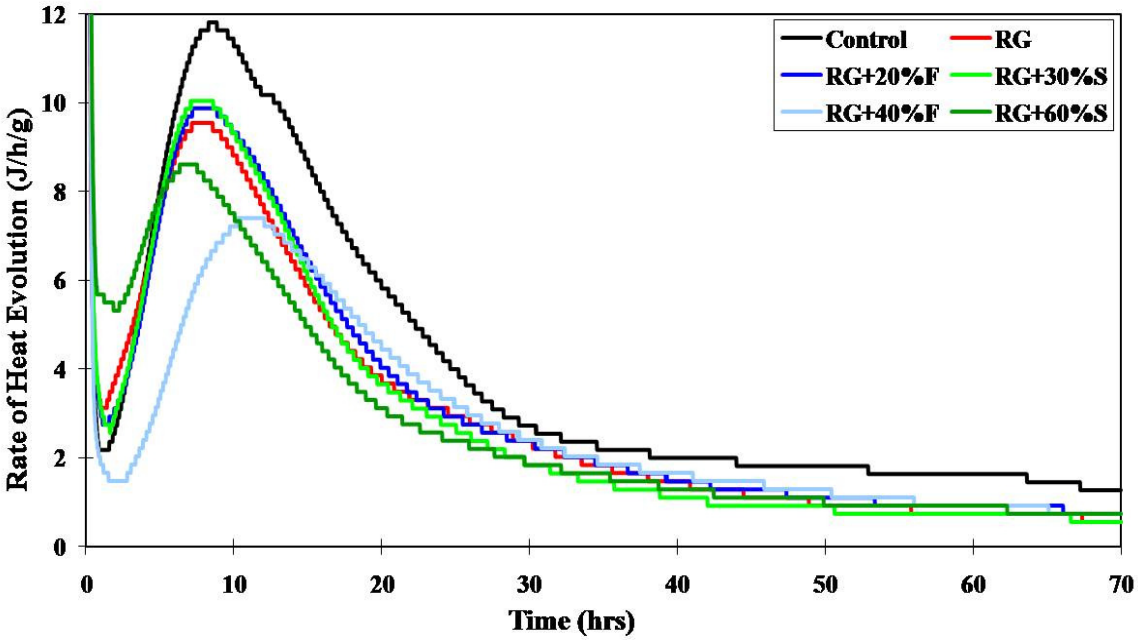

Figure 3.8 – Rate of heat evolution for a commercial Type I/II portland cement (control) and cement samples synthesized by reagent-grade chemicals (RG) with fly ash (F) and slag (S) incorporation

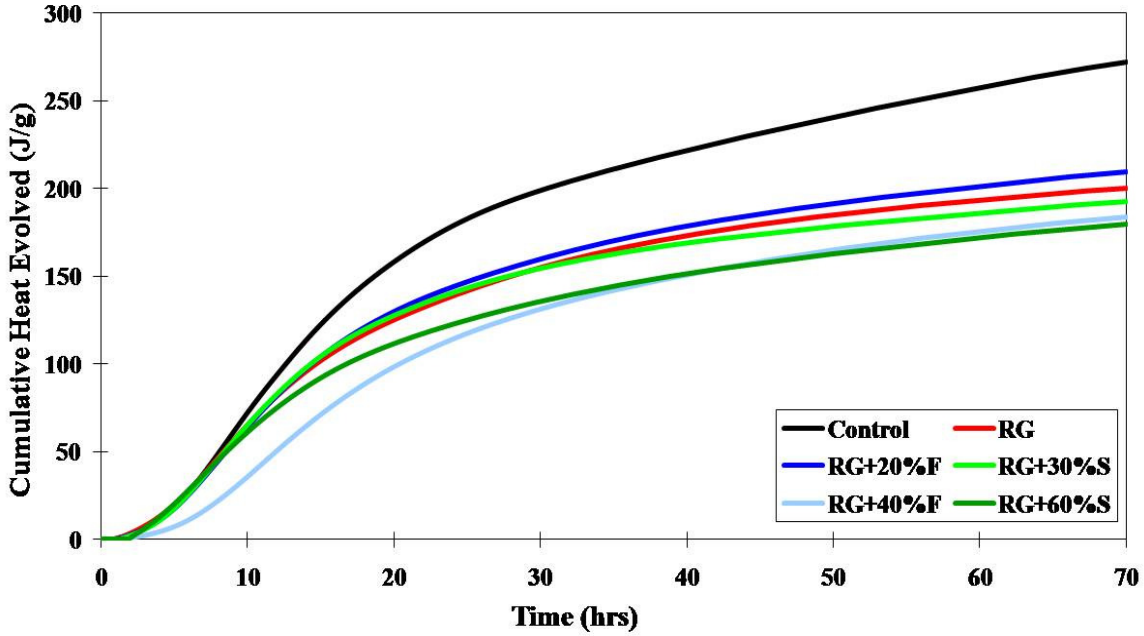

Figure 3.9 – Cumulative heat evolved for a commercial Type I/II portland cement (control) and cement samples synthesized by reagent-grade chemicals (RG) with fly ash (F) and slag (S) incorporation

One striking difference between the synthesized cements and the commercial cements is that the synthesized cements had lower maximum heat evolution rates and cumulative heat. The lower heat evolution rate was most likely caused by the differences in particle size; the Blaine fineness of the synthetic clinkers is about 25% lower than that of the commercial cement. Previous research has also shown that coarser cements reach lower degree of hydration compared to finer cements even after a long period of time, which agrees with the hydration results of the synthetic clinkers that showed an overall lower heat released compared to the commercial cement (Bentz et al., 1999).

Another noticeable difference in behavior is that the cement samples synthesized from reagent-grade chemicals with 40% fly ash and 60% slag incorporation had lower heat evolution rates and lower cumulative heat than the other synthesized cements. Since

the hydration of C_3S dominates the early-age hydration behavior of cement, this phenomenon agrees with the X-ray diffraction results which showed a decreasing C_3S and increasing C_2S content when incorporating more waste materials in the raw mix. However, the cement samples synthesized from reagent-grade chemicals, 20% fly ash incorporation, and 30% slag incorporation showed similar heat evolution rates and cumulative heat regardless of their differences in C_3S content (65.2%, 60.4%, and 54.3%, respectively). Furthermore, the clinker samples synthesized from reagent-grade chemicals with 40% fly ash incorporation reacted slower than the clinker samples synthesized from reagent-grade chemicals with 60% slag incorporation. These effects may have been caused by the minor impurities in these two waste materials.

3.4 CONCLUSIONS

Portland cement clinkers conforming to the compositional specifications in ASTM C 150 for Type I cement were successfully synthesized by combining reagent-grade materials with up to 40% fly ash and 60% slag incorporation. Periclase (MgO) was the only impurity phase formed, and the quantities formed were less than the limit specified in ASTM C 150. It was observed that waste materials significantly affected formation of the four major cement phases. The amount of C_2S increased with increasing amounts of waste materials incorporated, while the amounts of C_3S and C_3A decreased with increasing amounts of waste materials incorporated. These differences could have implications on proportioning of raw materials for cement production when using waste materials. On the other hand, the incorporation of waste materials had little to no effect on the spatial distribution of phases. Furthermore, the synthesized cements had similar early-age hydration behavior to commercial cement; however, their heat evolution rates and cumulative heat were lower.

Chapter 4: Incorporation of Waste Materials into Portland Cement Clinker Synthesized from Natural Materials

4.1 INTRODUCTION

In this chapter, portland cement clinkers were synthesized from natural materials and waste materials, specifically fly ash and blast furnace slag. A primary goal was to synthesize portland cement clinker with minimal limestone content and maximal waste material content. Portland cement clinker was first synthesized from natural materials and then from natural materials partially replaced by waste materials using the synthesis procedures developed in Chapter 3. The resulting clinkers were analyzed for phase contents using X-ray diffraction and phase distribution using scanning electron microscopy. The synthetic clinkers were then made into cements by adding gypsum to control hydration reactions. Finally, the early-age hydration behavior of the synthesized cements was investigated using isothermal conduction calorimetry.

4.2 EXPERIMENTAL

4.2.1 Materials

The natural materials used to synthesize portland cement clinker were obtained from Texas Lehigh Cement Company (Buda, Texas). These were a gray limestone and an argillaceous yellow limestone that is rich in aluminum and iron; their oxide compositions from X-ray fluorescence analysis are shown in Table 4.1. The industrial waste materials used, specifically fly ash and ground granulated blast furnace slag, were those already marketed and distributed for use as supplementary cementing materials for concrete, meaning that they can be used directly to replace a portion of the portland cement in concrete. The fly ash (Class C; Headwaters/ISG) and slag (Holnam) were chosen for their high calcium oxide, silicon oxide, and aluminum oxide contents which

are all necessary for portland cement manufacture (oxide compositions from X-ray fluorescence analysis shown in Table 4.1) (ASTM C 618, 2005). Furthermore, 0.1 wt% boron oxide (98.5% B_2O_3; Alfa Aesar) and 0.25 wt% lithium borate (75% $Li_2B_4O_7$, 25% $LiBO_2$; SPEX CertiPrep) were added to the raw ingredients in order to stabilize the desired β-C_2S phase and to lower the clinkering temperature, respectively (Fierens and Trilocq, 1983).

Table 4.1 – Chemical compositions of the natural materials and industrial waste materials used

Oxide	**Amount in sample (weight %)**			
	Gray limestone	**Yellow limestone**	**Fly ash**	**Slag**
SiO_2	5.95	38.44	33.58	34.48
Al_2O_3	1.69	10.51	18.51	11.35
Fe_2O_3	0.64	3.23	6.56	0.67
CaO	49.02	22.74	27.08	41.73
MgO	0.94	0.98	6.10	7.32
Na_2O	0.07	0.23	1.89	0.14
K_2O	0.29	1.66	0.39	0.38
TiO_2	0.04	0.48	1.34	0.46
MnO_2	0.02	0.03	0.03	0.56
P_2O_5	0.08	0.18	1.15	0
SrO	0.07	0.08	0.48	0.10
BaO	0.02	0.06	0.74	0.11
SO_3	0.77	0.08	1.83	1.88
LOI*	40.39	21.3	0.34	0.83
Moisture	0.49	0.71	0.07	0.28

*LOI is mass lost on ignition to 750°C

4.2.2 Synthesis

Portland cement clinker was first synthesized from gray limestone along with 20–40% yellow limestone (in 2.5% increments) with 0.1 wt% boron oxide and 0.25 wt% lithium borate additions. The goal was to synthesize a portland cement clinker with a similar phase composition to the portland clinker synthesized in Chapter 3 using reagent-grade chemicals. Portland cement clinker can be synthesized by combining only these two natural materials because the yellow limestone contained high amounts of silicon, aluminum, and iron (Table 4.1).

Materials were dispersed in ultra-pure water (1:10 ratio) and mixed by a rotary jar mill (U.S. Stoneware) for 24 h at 120 rpm in a HDPE bottle using 2-mm sphere high-purity ZrO_2 (Y_2O_3 stabilized) grinding media (Richerson, 1992). The solution was poured in a beaker and dried in a 105˚C oven. The resulting product was hand-crushed into fine powder form using a mortar and pestle. The materials were placed in platinum crucibles and fired in an electric muffle furnace (Sentrotech). Two cycles of firing were run, with a 5˚C/min heating rate and a 2˚C/min cooling rate. In the first cycle, the materials were fired at 850˚C for 2 h to dehydrate and calcine the materials. They were then fired at 1200˚C for 8 h, from 1200˚C to 1250˚C for 8 h, and at 1250˚C for another 8 h. An intermediate grinding by hand was performed between cycles to homogenize the materials. In the second cycle, the materials were fired at 1300˚C for 8 h, from 1300˚C to 1350˚C for 8 h, and at 1350˚C for another 8 h (Fierens and Trilocq, 1983; Mohamed and Sharp, 2002; Stephan and Wilhelm, 2004). If the fired product contained excess free lime (>1 wt%, determined by X-ray diffraction), the materials were fired again at 1400˚C for 12 h. Finally, the resulting clinker was hand-ground and passed through a #325 sieve (45 μm).

The goal of the laboratory synthesis processes was to mimic the processes that take place in industrial manufacturing. Raw ingredients must be homogenized and then fired at high temperature. The firing time in the furnace was much longer compared to the firing time in a rotary kiln used in industrial manufacturing because the raw ingredients remained stationary inside the crucible during the firing process, which prevented materials from properly reacting with each other. Furthermore, the maximum firing temperature used in the laboratory synthesis processes was 1400˚C which is about 50˚C lower than the maximum temperature used in industrial manufacturing (Mindess, 2003). Under lower firing temperature, the desired phases may take longer to form.

After successful synthesis of portland cement clinker from natural materials, portland cement clinker was synthesized from natural materials partially replaced by waste materials. The fly ash and slag used had similar oxide compositions to the yellow limestone except for impurities. Several ingredient proportions were fired in the furnace using the same synthesis procedure (gray limestone along with 20–40% fly ash or 20–60% slag; in 2.5% increments; with 0.1 wt% boron oxide and 0.25 wt% lithium borate additions). The primary goal was to synthesize portland cement clinker with minimal limestone content and maximal waste material content.

4.2.3 Analysis

4.2.3.1 X-Ray Diffraction

The synthetic clinkers were tested by X-ray diffraction (Siemens D500 Powder Diffractometer; Cu $K_{\alpha 1}$, λ=1.5046 Å) to determine phase formation. The instrument was operated under 40 keV and 30 mA, the step size used was 0.02˚/6 sec, and the scan range was 20˚–80˚ 2θ. Test samples were prepared by dispersing clinkers in ethanol and pouring the solution on quartz low background sample holders. Thin layers of solid

materials were left on the sample holders after the samples dried.

Qualitative information of phases present in the sample was obtained using the Hanawalt manual and the Jade program (MDI) (JCPDS–International Centre for Diffraction Data, 1989). Quantitative information was collected using the Rietveld method (accuracy about 1%) which was performed with the TOPAS-Academic software (Bruker AXS) (Young, 1995; Stutzman and Leigh, 2002; Whitfield and Mitchell, 2003).

4.2.3.2 Scanning Electron Microscopy

Phase distribution in the synthetic clinkers was studied using scanning electron microscopy (LEO 1530 Thermally-Assisted Field Emission SEM). Test samples were prepared by mixing clinker powders with optical-grade epoxy (Epotek 353ND) and casting in cylindrical molds (30 mm diameter). The samples were cured in a 40˚C oven for 24 h, and their cross-sections were polished and coated with carbon before imaging and compositional examination by energy dispersive spectroscopy (Stutzman, 2004). Elemental maps were collected for Ca, Si, Al, Fe, Mg, S, Na, and K. The elemental maps collected have a resolution of 512 pixels over a 450 µm field width. This is equivalent to about 0.9 µm per pixel, approximately the spatial resolution of elemental mapping. The elemental maps were then preprocessed with ImageJ software to reduce noise (Rasband, 1997-2009; Abramoff et al., 2004). Multispectral images were then prepared by overlaying the separate elemental maps and processing using Multispec software (©Purdue Research Foundation), which allowed quantitative assessment of the spatial distribution of phases (Lydon, 2005). The quantitative spatial distribution of phases was later converted to weight distribution by normalizing it with the density of the phases. The quantitative results determined from scanning electron microscopy were compared with those from quantitative X-ray diffraction.

4.2.3.3 Isothermal Conduction Calorimetry

To determine if the synthesized cements exhibited similar behavior to traditional cement, the rate of reaction with water was evaluated. The heat produced by cementitious materials in exothermic hydration reactions is a good indication of their early-age hydration behavior (Gartner et al., 2002). In this study, the synthesized cements were tested for heat evolution rate using isothermal conduction calorimeter (TAM Air, Thermometric). The results were compared to the synthesized portland cement from reagent-grade chemicals and a commercially-produced Type I/II cement (TXI Hunter). Cements were made from the synthetic clinkers by adding 12.5 wt% gypsum (100% $CaSO_4 \cdot 2H_2O$; USG) to control the reaction of C_3A (Odler, 1998). The synthetic clinkers were tested by an air-permeability test, called Blaine fineness, according to ASTM C 204 (2007) to assure uniform particle fineness. Hydration was evaluated for 3 days at 23˚C using a water-to-cement ratio by weight of 0.45.

4.3 RESULTS AND DISCUSSION

4.3.1 Phase Composition

Portland cement clinker was more difficult to synthesize from gray limestone (GLS) and yellow limestone (YLS) than from reagent-grade chemicals and required a higher synthesis temperature. The higher synthesis temperature was due to the large amount of quartz in the YLS, which is less reactive because of its crystalline structure compared to the amorphous reagent-grade silica gel. Therefore, in order to keep the synthesis procedure consistent, 0.25% lithium borate, which is a chemical commonly used as fusion flux for X-ray fluorescence analysis, was added to the system to allow phases to form at a relatively lower temperature.

GLS along with 20–40% YLS (in 2.5% increments) were fired in the furnace. The best result is from using 72.5% GLS and 27.5% YLS. Quantitative X-ray diffraction results obtained through Rietveld analysis for this clinker sample are shown in Table 4.2 and the refined X-ray diffraction pattern is shown in Figure 4.1. The refined X-ray diffraction pattern shows that the calculated pattern from the lattice parameters of the phases present (red line in Figure 4.1) agrees with their X-ray diffraction pattern (blue line in Figure 4.1) well, which means the quantitative results should be reliable. The gray line that shows negative intensities in Figure 4.1 represents the differences in intensities of the two patterns. The quantitative X-ray diffraction results show that all the four major clinker phases (C_3S, C_2S, C_3A, and C_4AF) formed in the sample. The free lime content of the sample was low (0.5%), indicating that the materials completely reacted in the furnace. The only impurity phase that can be detected by X-ray diffraction was periclase (MgO). However, periclase content (0.2%) is minimal. The maximum amount of periclase in Type I cement allowed by ASTM C 150 (2005) is 6%. The sample contained 16.6% C_3A and 6.3% C_4AF, which nearly matches the estimated phase composition from Bogue calculation (13.3% C_3A and 6.4% C_4AF). In contrast, the sample contained much higher C_3S (58.6%) and much lower C_2S (17.8%) than its estimated phase composition from Bogue calculation (42.3% C_3S and 33.9% C_2S). The differences may be attributed to errors in the standard Bogue calculation used to proportion the raw materials. The standard Bogue calculation is a method used to estimate the amount of the phases in portland cement clinker from the oxide contents in the raw ingredients using knowledge of phase equilibria and by solving linear equations (Bogue, 1929; Taylor, 1997). This method assumes that the four major clinker phases are in their stoichiometric forms, which is usually not realistic because these phases can accommodate a large amount of substitute ions. Moreover, the synthesis environment is not always in an equilibrium

state. Nevertheless, the sample had a very similar phase composition to the portland cement clinker synthesized from reagent-grade chemicals (Table 4.2), which exactly conforms to the synthesis goal.

Table 4.2 – Comparison of Bogue calculation and Rietveld analysis results for clinker samples synthesized from reagent-grade chemicals (RG), GLS with 27.5% YLS, GLS with 27.5% fly ash, and GLS with 35% slag

Sample	**Phase (weight %)**					
	C_3S	**C_2S**	**C_3A**	**C_4AF**	**Lime**	**Periclase**
RG (Bogue)	50	25	15	10	0	0
Rietveld	65.2	10.3	15.5	8.5	0.5	0
GLS + YLS (Bogue)	42.3	33.9	13.3	6.4	0	0
Rietveld	58.6	17.8	16.6	6.3	0.5	0.2
GLS + Fly ash (Bogue)	37.3	26.8	18.3	9.8	0	0
(Rietveld)	46.1	24.2	16.7	10.2	0.8	2.0
GLS + Slag (Bogue)	45.0	28.2	16.8	2.7	0	0
(Rietveld)	44.4	31.6	17.6	2.1	0.1	4.2

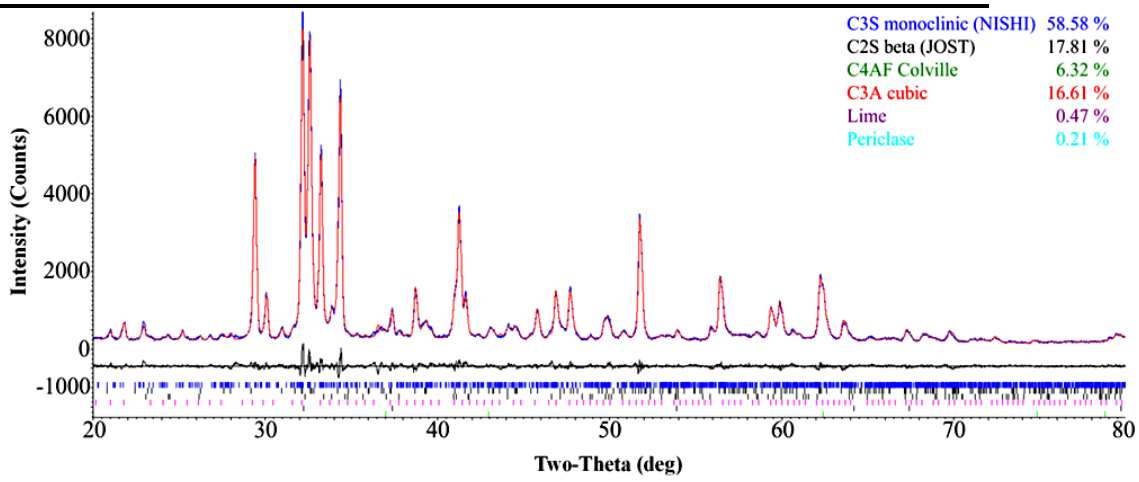

Figure 4.1 – Rietveld refinement for a clinker sample synthesized from GLS with 27.5% YLS

After successful synthesis of portland cement from natural materials, GLS along with 20–40% fly ash and 20–50% slag (in 2.5% increments) were fired in the furnace. The maximum amounts of waste materials that can be used for portland cement clinker synthesis with acceptable compositions were 27.5% fly ash and 35% slag. Quantitative X-ray diffraction results obtained through Rietveld analysis for these two clinker samples are shown in Table 4.2 and their refined X-ray diffraction patterns are shown in Figures 4.2 and 4.3, respectively. The four major clinker phases (C_3S, C_2S, C_3A, and C_4AF) formed in these two samples. The clinker samples contained low free lime contents, indicating that the materials completely reacted in the furnace. The clinker sample synthesized from GLS with 35% slag had a low C_4AF content because the slag used contained a low amount of iron. The only impurity phase that can be detected in these two clinker samples by X-ray diffraction was periclase. The clinker sample synthesized from GLS with 35% slag contained higher periclase content (4.2%) than the clinker sample synthesized from GLS with 27.5% fly ash (2.0%) because the slag used contained higher amount of magnesium than the fly ash (Table 4.1); moreover, slag was used at a higher amount for portland cement clinker synthesis than fly ash. However, these two synthetic clinkers had periclase contents lower than the ASTM C 150 (2005) limit (6%). Furthermore, even though the clinker samples with waste materials incorporation had lower C_3S, higher C_2S and C_3A contents than an ordinary portland cement clinker, they are still in the acceptable range specified by ASTM C 150. The low C_3S–C_2S ratio in portland cement clinker can be easily increased by increasing the GLS-waste ratio in the raw ingredients.

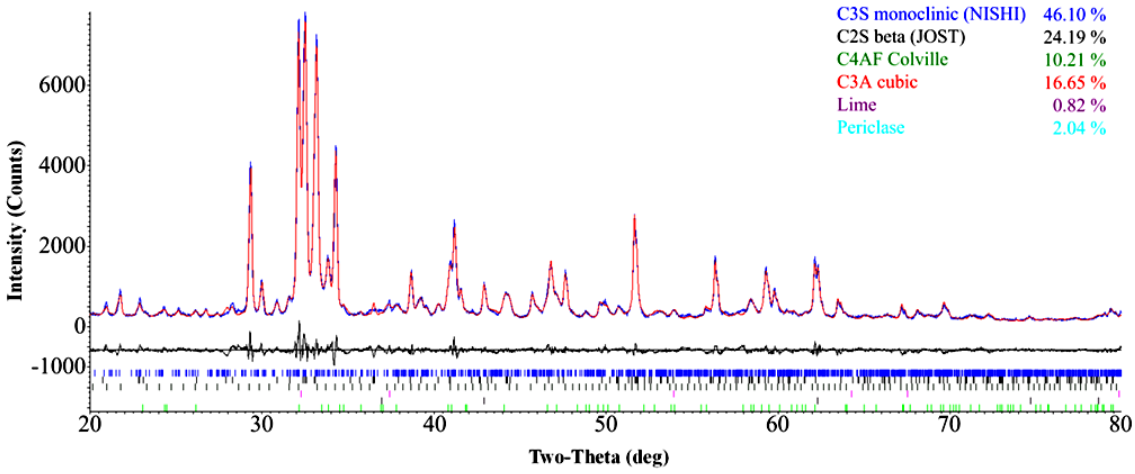

Figure 4.2 – Rietveld refinement for a clinker sample synthesized from GLS with 27.5% fly ash

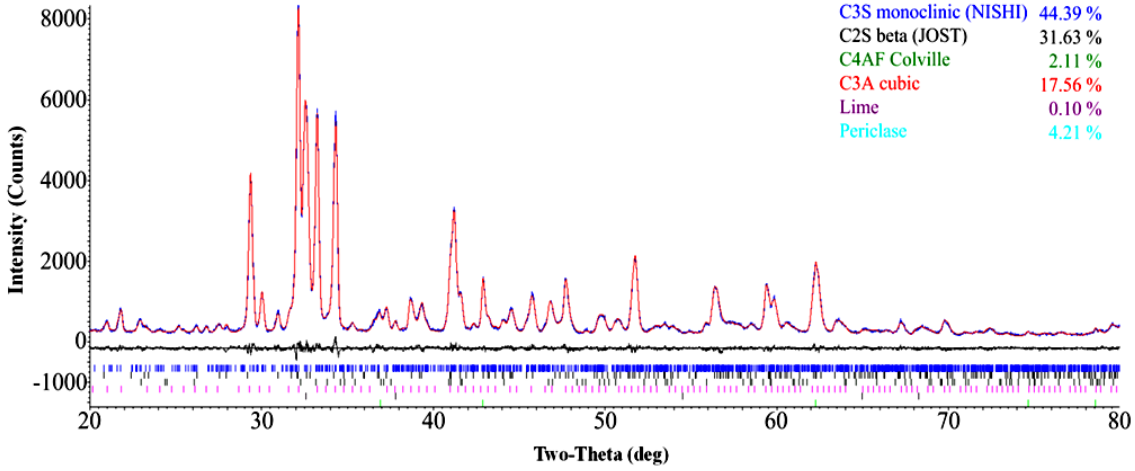

Figure 4.3 – Rietveld refinement for a clinker sample synthesized from GLS with 35% slag

Rietveld analysis results for the clinker sample synthesized from GLS with 27.5% YLS show that its C_3S content is about 16% higher than what the standard Bogue calculation estimated. For the cement sample synthesized from GLS with 27.5% fly ash, it is about 9% higher, and for the cement sample synthesized from GLS with 35% slag, the two values are nearly identical. This is because the waste materials used contained

higher impurity contents than YLS; moreover, the slag was used at a higher percentage for portland cement clinker synthesis than fly ash. According to the sutdy of Uda et al. (1998), this effect could be due to changes in phase equilibria in the $CaO–SiO_2–Al_2O_3–Fe_2O_3$ system caused by sulfur impurities; the contents of C_2S and CaO will increase, while the content of C_3S will decrease when increasing amount of SO_3 is incorporated in portland cement clinker synthesis. In the study, both the fly ash and the slag used contained approximately 1.8% SO_3 (Table 4.1). The portland cement clinkers synthesized in Chapter 3 using reagent-grade chemicals and waste materials with controlled calcium, silicon, aluminum, and iron oxide contents also showed that the sulfur impurities contained in the waste materials significantly affected formation of the four major clinker phases. The content of C_2S increased, while the content of C_3S decreased when increasing amounts of waste materials were used in portland cement clinker synthesis. Moreover, Uda et al. showed that C_3S no longer formed when the SO_3 content in the raw ingredients exceeded 2.6 wt%. Therefore, it is critical to evaluate the SO_3 content in materials before using them as raw ingredients in portland cement clinker production.

The modified Bogue calculation might be a better method than the standard Bogue calculation to accurately estimate the proportion of phases in portland cement clinker because it takes into account of the substitute ions in each of the major cement phases instead of assuming their stoichiometric forms (Bogue, 1929; Taylor, 1997). However, performing the modified Bogue calculation is not simple because they require intensive study of the actual contents of CaO, SiO_2, Al_2O_3, Fe_2O_3, and other impurities within each of the major cement phases, which might change when different types of materials are used in portland cement clinker production. Moreover, the modified Bogue equations still will not explain the changes in thermodynamics and kinetics of the CaO–

SiO_2–Al_2O_3–Fe_2O_3 system caused by sulfur impurities. Therefore, a model that is more precise than the currently used Bogue method in addition to empirical experience will be necessary to accurately predict clinker phase compositions when using materials with high SO_3 content as raw ingredients. Finally, because the properties of portland cement are mainly governed by its phase composition, the direct phase proportion quantitative X-ray diffraction technique provides a powerful means for cement manufacturers to better assess their products. Detailed aspects regarding the quantitative X-ray diffraction technique were recently specified by ASTM C 1365 (2006).

4.3.2 Microstructure

The synthetic clinkers were examined under a scanning electron microscope to determine the spatial distribution of phases. Elemental maps for the clinker sample synthesized from GLS with 27.5% YLS are shown in Figure 4.4. Only the Ca, Si, Al, Fe, and Mg maps are revealed because other elements showed little signal except noise. Multispectral images were obtained from overlaying and processing these elemental maps. Multispectral images for clinker samples synthesized from GLS with 27.5% YLS, GLS with 27.5% fly ash, and GLS with 35% slag are shown in Figures 4.5-4.7. In these multispectral images, colors were assigned to each individual phase (C_3S blue, C_2S green, C_3A red, C_4AF yellow, and periclase purple). Periclase was the only impurity phase that can be identified in the clinker samples with waste materials incorporation. The content of other impurities may have been too low to be identified. The clinker samples synthesized from natural materials contained more C_3S and less C_2S than the clinker samples with waste materials incorporation (images appear bluer), which agrees with the X-ray diffraction results that showed a lower C_3S–C_2S ratio in clinker samples with waste materials incorporation. Furthermore, quantitative information of the spatial distribution of

phases in these multispectral images was obtained by calculating the number of pixels of the different colors. The space fraction was later converted to weight fraction by normalizing it with the density of the phases. The comparison of multispectral and Rietveld analysis results for the synthetic clinkers are shown in Table 4.3. The multispectral and Rietveld analysis results agree with each other well except that the multispectral analysis results showed a higher C_3S and C_2S, and a lower C_3A, C_4AF, and periclase contents. This is because the multispectral analysis method quantifies the spatial distribution of phases which were later converted to weight distribution by normalizing it with the density of the phases. However, space distribution may not represent volume distribution due to the different morphology of the phases, and therefore may have caused errors in the analysis. Furthermore, C_3S and C_2S, C_3A and C_4AF formed together and are sometimes really difficult to differentiate due to the resolution of the elemental maps, which may have also induced errors in the analysis. Nevertheless, all of these samples showed similar spatial distribution of phases.

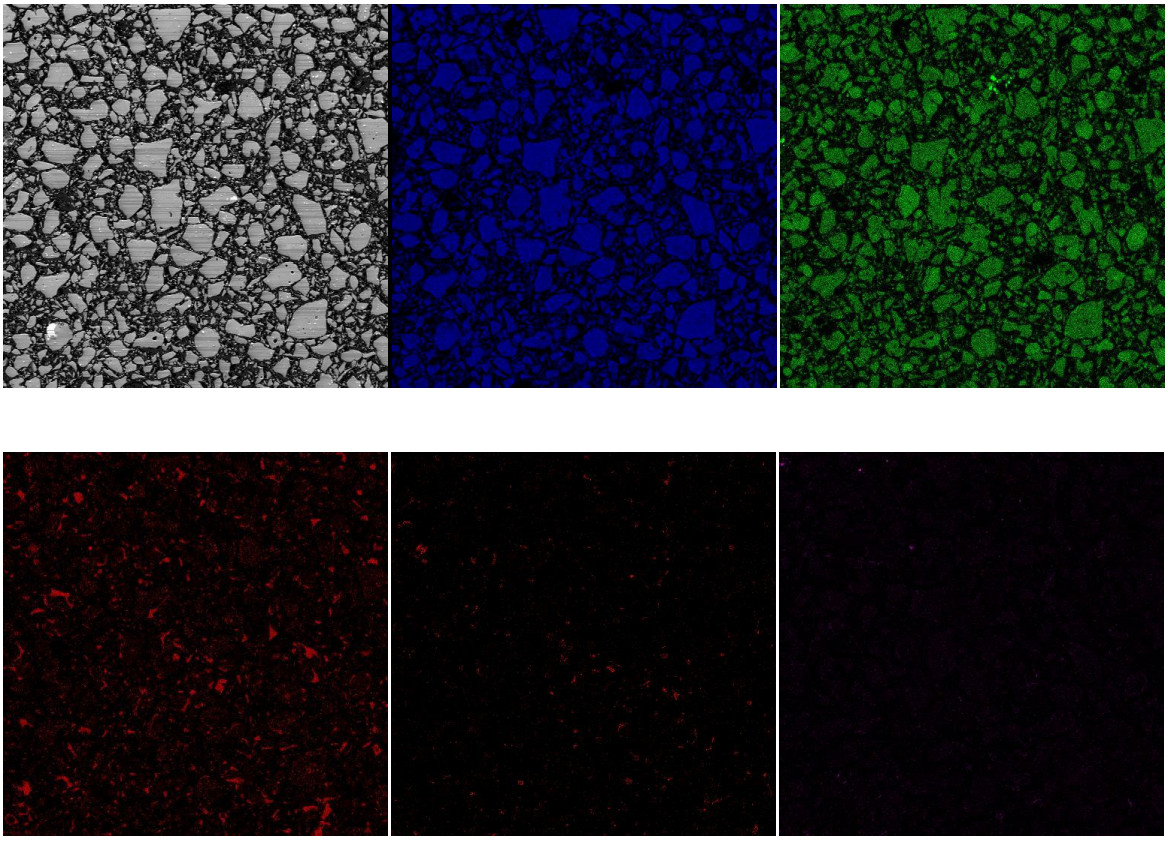

Figure 4.4 – Elemental maps for a clinker sample synthesized from GLS with 27.5% YLS (left-right, top-bottom orientation: secondary electron image, Ca, Si, Al, Fe, and Mg; field width: 450 μm)

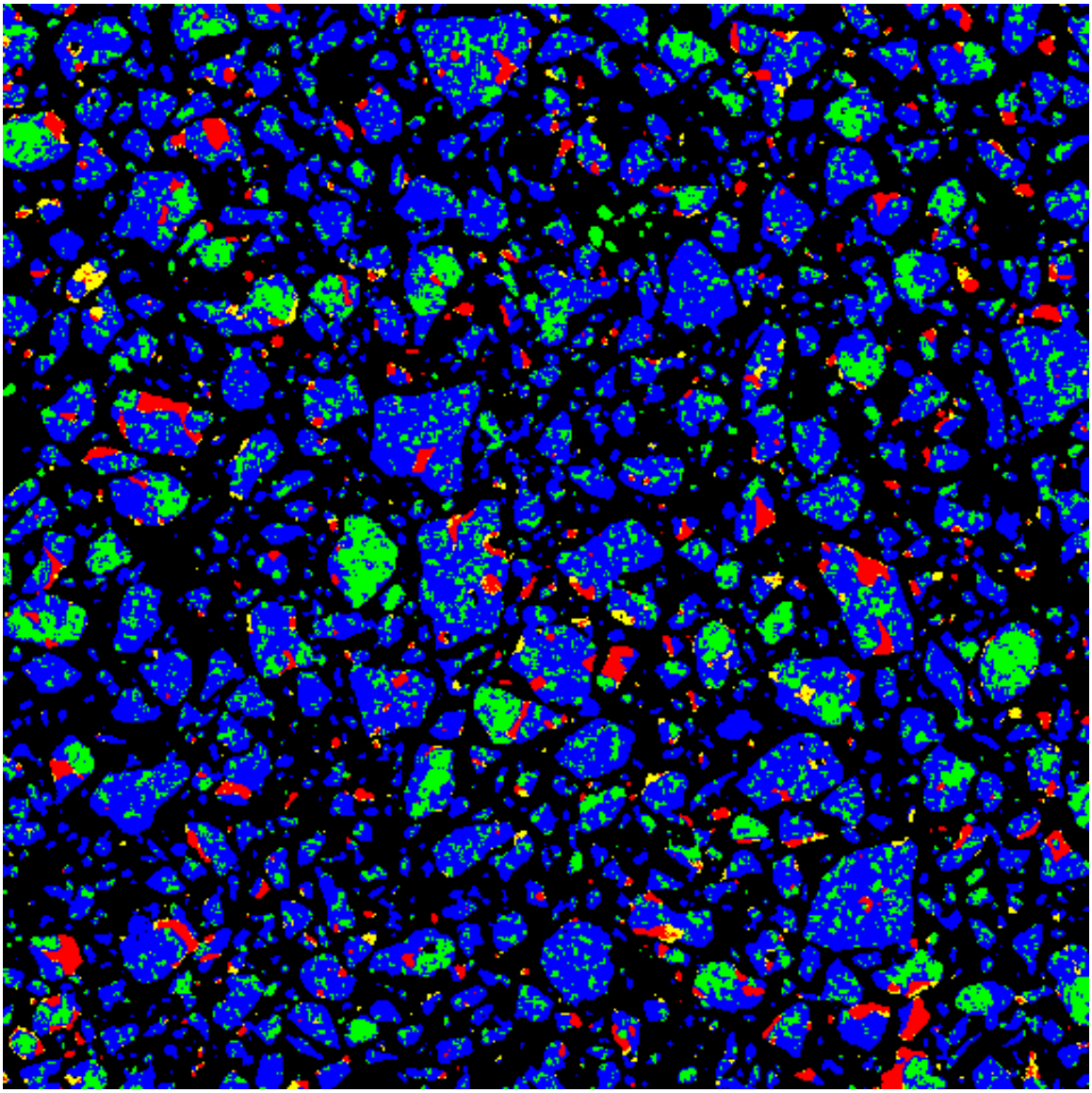

Figure 4.5 – Multispectral image for a clinker sample synthesized from GLS with 27.5% YLS (C_3S blue, C_2S green, C_3A red, C_4AF yellow, and periclase purple; field width: 450 μm)

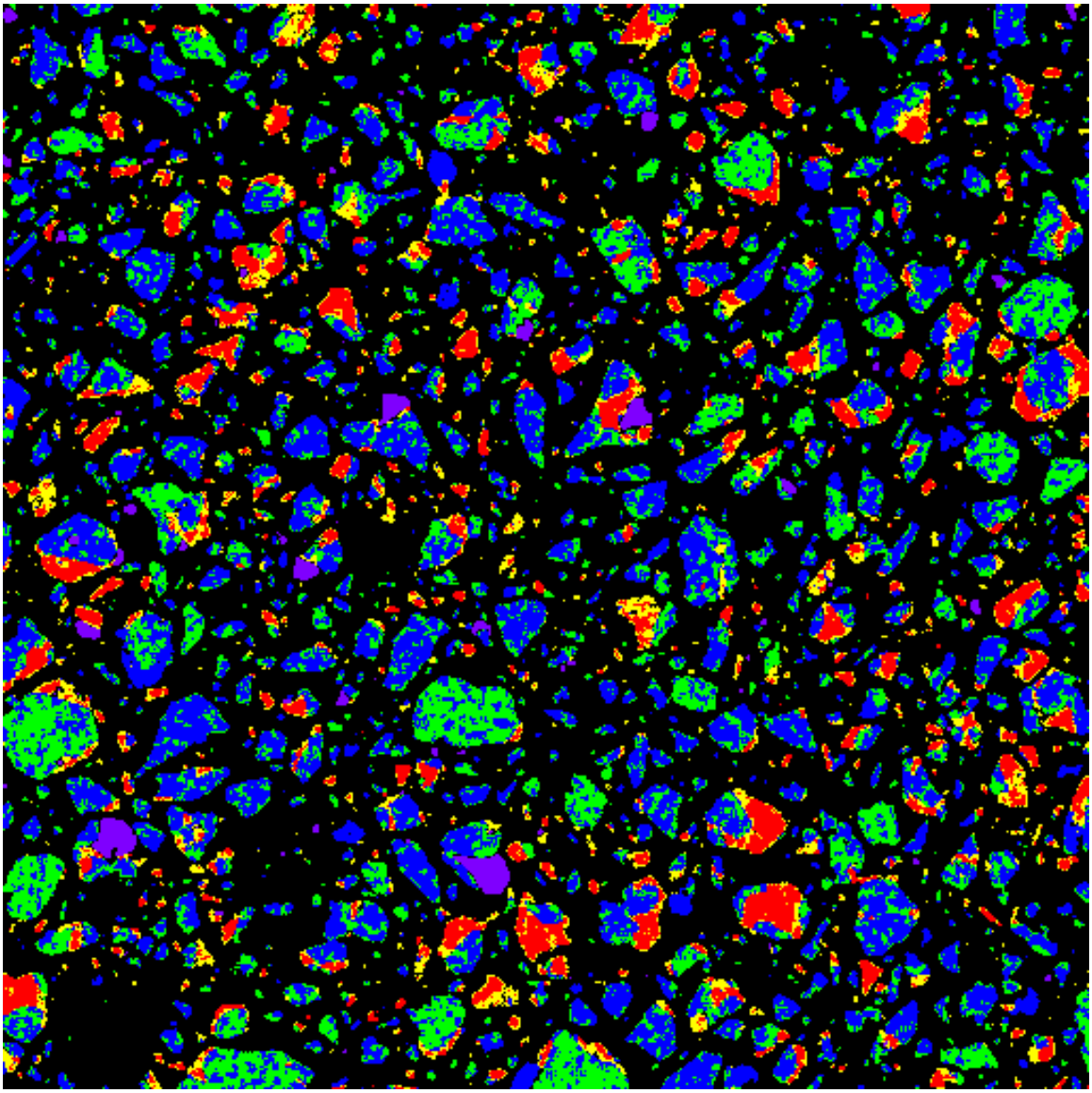

Figure 4.6 – Multispectral image for a clinker sample synthesized from GLS with 27.5% fly ash (C_3S blue, C_2S green, C_3A red, C_4AF yellow, and periclase purple; field width: 450 μm)

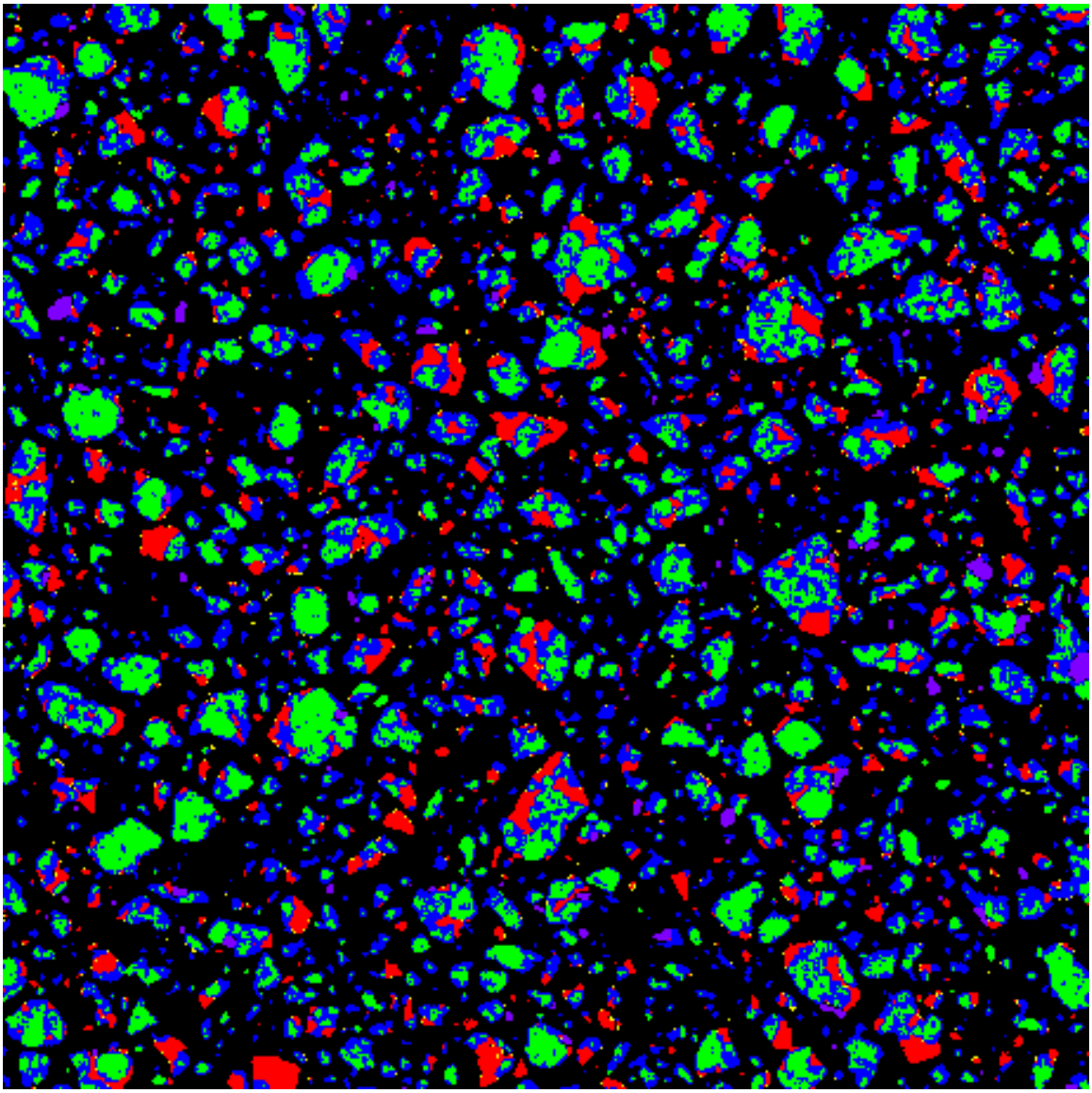

Figure 4.7 – Multispectral image for a clinker sample synthesized from GLS with 35% slag (C_3S blue, C_2S green, C_3A red, C_4AF yellow, and periclase purple; field width: 450 μm)

Table 4.3 – Comparison of multispectral (MS) and Rietveld analysis results for clinker samples synthesized GLS with 27.5% YLS, GLS with 27.5% fly ash, and GLS with 35% slag

Phase	Amount in sample (weight %)					
	GLS + YLS		GLS + Fly ash		GLS + Slag	
	MS	Rietveld	MS	Rietveld	MS	Rietveld
C_3S	65.6	58.6	46.5	46.1	49.8	44.4
C_2S	21.6	17.8	27.7	24.2	32.0	31.6
C_3A	10.2	16.6	15.1	16.7	15.8	17.6
C_4AF	2.6	6.3	9.0	10.2	0.8	2.1
Lime	N/A	0.5	N/A	0.8	N/A	0.1
Periclase	N/A	0.2	1.7	2.0	1.6	4.2

4.3.3 Early-Age Hydration Behavior

The reactivity of cement is strongly affected by its particle size. Therefore, in order to compare hydration behavior between commercial portland cement and the synthetic clinkers, the synthetic clinkers were first ground to a comparable fineness and tested for Blaine fineness. The Blaine fineness values for the synthetic clinkers ranged from 275.1 to 311.0 m^2/kg and are shown in Table 4.4. The differences in Blaine fineness between the synthetic clinkers were perhaps caused by the grinding and sieving process. However, the differences are about 10% and should not seriously affect the early-age hydration behavior. All of the clinker samples were hand-ground and passed through a #325 sieve (45 μm); however, their Blaine fineness results were still significantly lower than the commercial Type I/II portland cement (405.5 m^2/kg).

Table 4.4 – Blaine fineness values for a commercial Type I/II portland cement (control) and clinker samples synthesized from reagent-grade chemicals, GLS with 27.5% YLS, GLS with 27.5% fly ash, and GLS with 35% slag

Sample	Specific surface area (m^2/kg)
Control	405.5
RG	298.4
GLS +YLS	275.1
GLS + Fly ash	311.0
GLS + Slag	304.9

The synthetic clinkers were then made into cements by adding 12.5 wt% gypsum. The gypsum addition content was determined by adding a range of gypsum content to the synthetic clinkers and testing for early-age hydration behavior using isothermal conduction calorimetry. The addition of 12.5 wt% gypsum was considered as the optimum gypsum content. The optimum gypsum content represents the lowest amount of gypsum that results in only one main hydration peak from the hydration reaction of C_3S, and the shape of the peak no longer changes with additional amount of gypsum added (Lerch, 1947). An additional hydration peak generally indicates the formation of calcium monosulfoaluminate ($C_4A\overline{S}H_{12}$) from ettringite ($C_6A\overline{S}_3H_{32}$) due to insufficient gypsum ($C\overline{S}H_2$) in the system:

$$C_3A + 3C\overline{S}H_2 + 26H \rightarrow C_6A\overline{S}_3H_{32} \quad (4.1)$$

$$C_6A\overline{S}_3H_{32} + 2C_3A + 4H \rightarrow 3C_4A\overline{S}H_{12} \quad (4.2)$$

The rates of heat-evolution for a commercial Type I/II portland cement and the synthesized cements are shown in Figure 4.8, and the curves for the cumulative heat evolved are shown in Figure 4.9. The rates of heat-evolution results show that the synthesized cements possessed hydration behavior similar to a commercial Type I/II portland cement because the shapes of the curves are similar.

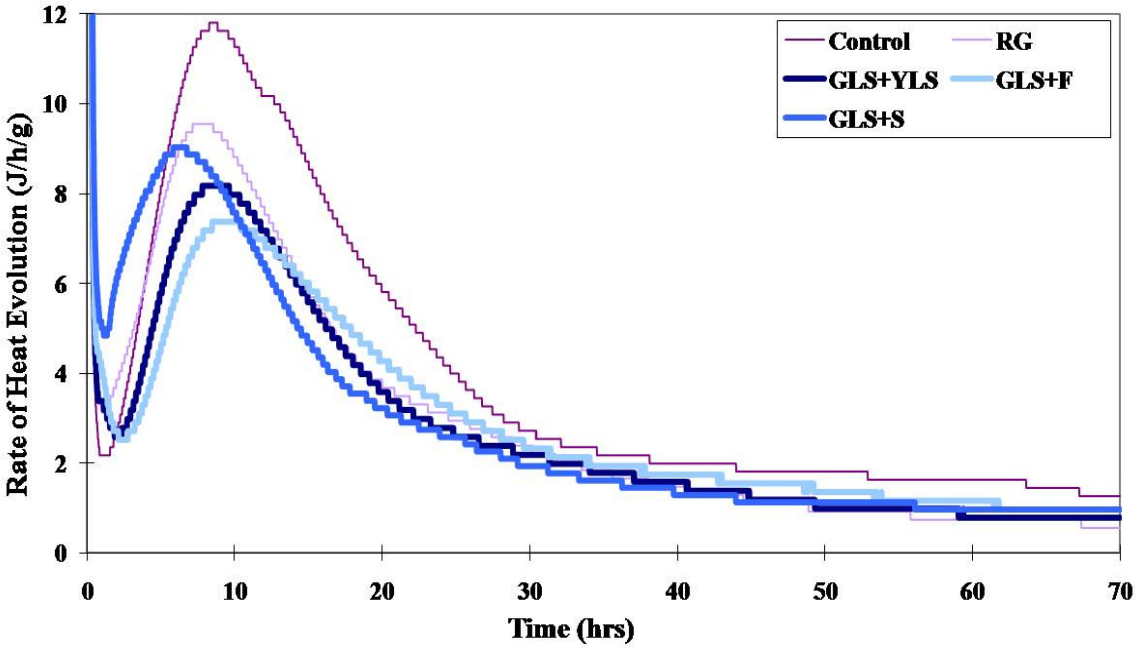

Figure 4.8 – Rate of heat-evolution for a commercial Type I/II portland cement (control) and cement samples synthesized from reagent-grade chemicals (RG), GLS with 27.5% YLS, GLS with 27.5% fly ash (F), and GLS with 35% slag (S)

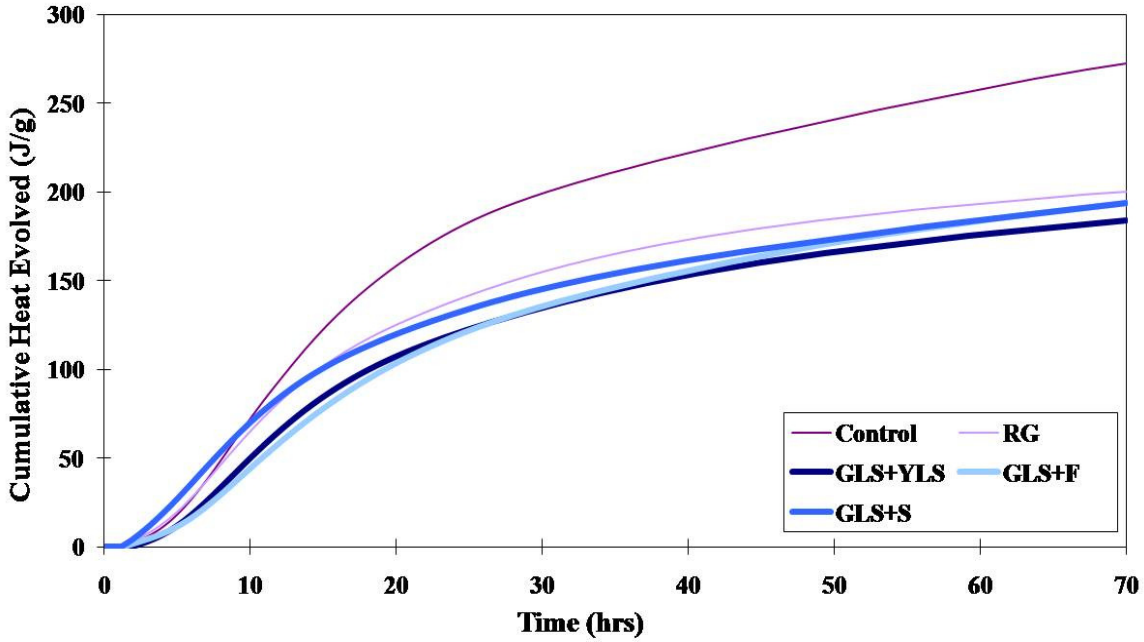

Figure 4.9 – Cumulative heat evolved for a commercial Type I/II portland cement (control) and cement samples synthesized from reagent-grade chemicals (RG), GLS with 27.5% YLS, GLS with 27.5% fly ash (F), and GLS with 35% slag (S)

The synthesized cements had lower maximum heat evolution rates and cumulative heat than the commercial cement. The lower heat evolution rate was most likely caused by the differences in particle size; the Blaine fineness of the synthetic clinkers is about 25% lower than that of the commercial cement. Previous research has shown that coarser cements reach lower degree of hydration than when compared with finer cements even after a long period of time, which agrees with the hydration results of the synthesized cements, which showed an overall lower heat released than when compared with the commercial cement (Bentz et al., 1999).

The cement samples synthesized from GLS with 27.5% YLS, GLS with 27.5% fly ash, and GLS with 35% slag had lower heat evolution rates and lower cumulative heat than the synthesized portland cement from reagent-grade chemicals. The phase

composition of the clinker sample synthesized from GLS with 27.5% YLS is similar to the portland cement clinker synthesized from reagent-grade chemicals. However, the Blaine fineness of the clinker sample synthesized from GLS with 27.5% YLS is about 8% lower than the portland cement clinker synthesized from reagent-grade chemicals which may be the primary reason that causes its lower heat evolution rate and cumulative heat. On the other hand, the cement samples synthesized from GLS with 27.5% fly ash and GLS with 35% slag also had lower heat evolution rates and lower cumulative heat than the synthesized portland cement from reagent-grade chemicals. Since the hydration of C_3S dominates the early-age hydration behavior of cement, this phenomenon agrees with the X-ray diffraction results that showed a lower C_3S and higher C_2S in clinker samples with waste materials incorporation.

4.4 CONCLUSIONS

Portland cement clinker was successfully synthesized from gray limestone (GLS) with yellow limestone (YLS), GLS with fly ash, and GLS with slag. The maximum amounts of waste materials that can be used for portland cement clinker synthesis with acceptable compositions were 27.5% fly ash and 35% slag. The clinker samples synthesized from GLS with 27.5% fly ash and GLS with 35% slag had lower C_3S–C_2S ratios than the clinker samples synthesized from reagent-grade chemicals and GLS with 27.5% YLS. However, the phase compositions of all the synthetic clinkers still conformed to the compositional specifications in ASTM C 150 for Type I cement. The low C_3S–C_2S ratio in the synthetic clinkers with waste materials incorporated can be easily increased by increasing the GLS-waste ratio in the raw ingredients. The synthetic clinkers with waste materials incorporated had high periclase (MgO) contents; however, the quantities formed were less than the limit specified in ASTM C 150. On the other

hand, the incorporation of waste materials had little to no effect on the spatial distribution of phases. The quantitative multispectral and Rietveld analysis results agree with each other well. Finally, the synthesized cements had similar early-age hydration behavior to commercial cement; however, their heat evolution rates and cumulative heat were lower.

Manufacturing portland cement with waste materials incorporation can reduce energy consumption, CO_2 emissions, and landfilling of wastes, thereby reducing the environmental impact of the portland cement production. Moreover, manufacturing portland cement from waste materials does not preclude it from being replaced with SCMs in concrete. These two methods can be applied simultaneously to further reduce the environmental impact of the concrete production. However, the presence of sulfur impurities in waste materials can significantly affect phase formation in portland cement clinker. The contents of C_2S and CaO will increase, while the content of C_3S will decrease when increasing amount of SO_3 is incorporated in portland cement clinker synthesis due to the changes in phase equilibria in the $CaO–SiO_2–Al_2O_3–Fe_2O_3$ system, which renders the standard and modified Bogue method inaccurate. Therefore, it is critical to evaluate SO_3 content in materials before using them as raw materials in portland cement clinker production. Furthermore, a model that is more precise than the currently used Bogue method in addition to empirical experience will be necessary to accurately predict clinker phase compositions when using materials with high SO_3 content as raw ingredients. Finally, because the properties of the portland cement are mainly governed by its phase composition, the direct phase proportion quantitative X-ray diffraction technique provides a powerful mean for cement manufacturers to better assess their products.

Chapter 5: Calcium Sulfoaluminate-Belite Cement: Synthesis

5.1 INTRODUCTION

As reviewed in Chapter 2, previous research has shown successful production of calcium sulfoaluminate-belite (CSAB) cement from reagent-grade chemicals, natural materials, and waste materials. However, there are many unanswered questions about this system. First, the effects of raw material composition and temperature on phase formation in clinkers are not well defined, which limits our ability to predict phase composition in the final cement. Second, the hydration chemistry is not nearly as well explored as that of portland cement, which hinders our ability to understand property development. Finally, the inter-relationship between phase composition and performance is underdeveloped, limiting our ability to optimize performance through proper proportioning of raw materials. The CSAB cement part of the research performed for this dissertation aimed to address these questions. The ultimate goals were to determine the optimum CSAB cement phase composition for performance and to synthesize satisfactory CSAB cements with comparable performance to portland cement using minimal limestone and bauxite contents and maximal waste material content in order to maximize the environmental benefits of CSAB cement.

This chapter reports on the use of reagent-grade chemicals to synthesize CSAB cement clinkers in order to tightly control compositional variables. Three target CSAB cement clinkers were synthesized because they allow evaluation of the inter-relationship between phase composition and performance of the CSAB cement system. The mass losses occurring with temperature during the firing process were followed with thermogravimetric analysis. The synthetic clinkers were ground into fine powder form and tested for particle fineness and particle size distribution by Blaine fineness and laser

light scattering particle size distribution analysis, respectively. Finally, the synthetic clinkers were analyzed for phase composition using X-ray diffraction and phase distribution using scanning electron microscopy.

5.2 MATERIALS PROPORTIONING

The reagent-grade chemicals used to synthesize CSAB cement clinkers were calcium oxide (96%+ CaO; Arcos), silica gel (100% SiO_2; Fisher), aluminum oxide (100% Al_2O_3; Fisher), ferric oxide (100% Fe_2O_3; Fisher), and calcium sulfate dihydrate (99% $CaSO_4 \cdot 2H_2O$; Arcos). Materials were proportioned using the Bogue method adapted for CSAB cement clinker assuming the phase assemblage of C_2S– $C_4A_3\overline{S}$ – C_4AF–$C\overline{S}$ –C, as shown in Equations 5.1-5.5. This phase assemblage was determined from review of the literature and preliminary testing and should be reasonable for CSAB cement (Mehta, 1980; Majling et al., 1993; Sharp, 1999). The Bogue method is a technique used in cement industry to estimate phase composition in portland cement clinker from the raw materials oxide composition using knowledge of phase equilibria and by solving linear equations (Bogue, 1929; Taylor, 1997).

$$\%C_4AF = 3.043(\%Fe_2O_3) \tag{5.1}$$

$$\%C_4A_3\overline{S} = 1.995(\%Al_2O_3) - 1.273(\%Fe_2O_3) \tag{5.2}$$

$$\%C_2S = 2.867(\%SiO_2) \tag{5.3}$$

$$\%C\overline{S} = 1.700(\%SO_3) - 0.445(\%Al_2O_3) + 0.284(\%Fe_2O_3) \tag{5.4}$$

$$\%C = 1.000(\%CaO) - 1.867(\%SiO_2) - 1.054(\%Fe_2O_3) - 0.550(\%Al_2O_3) - 0.700(\%SO_3) \tag{5.5}$$

Three target CSAB cement clinkers with different proportions of C_2S and $C_4A_3\overline{S}$ were synthesized (Table 5.1). These three phase compositions were chosen from preliminary testing (not reported) that worked with more phase compositions. C_2S is

slow reacting and contributes to the long-term property development in CSAB cement while $C_4A_3\overline{S}$ is fast reacting and contributes to the early-age property development (Mehta, 1980). This range of phase compositions allows evaluation of the inter-relationship between phase composition and performance of the CSAB cement system. The target C_4AF content was controlled at 10% for the CSAB cement clinkers because most natural and waste materials suitable for cement manufacturing contain some amount of iron; however, it is unusual to have suitable high iron-containing natural and waste materials to produce high C_4AF cement. The target $C\overline{S}$ content was controlled at 10% because it strongly affects hydration behavior (Kasselouri et al., 1995); instead, the optimum gypsum ($C\overline{S}H_2$) content was evaluated and added to the synthetic clinkers before performance testing, discussed in Chapter 6, similar to the process used for gypsum additions in portland cement.

Table 5.1 – Target phase compositions for the CSAB cement clinkers synthesized from reagent-grade chemicals

Phase	**Target Composition (weight %)**		
	HS	***MS***	***LS***
C_2S	20	40	60
$C_4A_3\overline{S}$	60	40	20
C_4AF	10	10	10
$C\overline{S}$	10	10	10

5.3 SYNTHESIS

The laboratory synthesis processes mimicked the processes that take place in industrial manufacturing, only on a much smaller scale. The proportioned raw ingredients were dispersed in ultra-pure water (1:2 ratio) and mixed using a rotary jar mill

(U.S. Stoneware) for 8 h at 120 rpm in an HDPE bottle using 5-15 mm sphere high-purity ZrO_2 (Y_2O_3 stabilized) grinding media (Richerson, 1992). The solution was poured in a steel pan and dried in a 105˚C oven for 72 h. The resulting product was hand-crushed into fine powder form using a mortar and pestle. The raw ingredients were then placed in alumina crucibles and fired in an electric muffle furnace (Sentrotech). Alumina crucibles can be used instead of platinum crucibles because the synthesis temperature for CSAB cement clinker is about 200˚C lower than portland cement clinker. The lower synthesis temperature prevents alumina from reacting with the raw ingredients, thereby contaminating the samples and destroying the crucibles. Two cycles of firing were run, with a 5˚C/min heating rate and a 2˚C/min cooling rate. In the first cycle, the raw ingredients were fired at 850˚C for 4 h to dehydrate and calcine the raw ingredients. Intermediate grinding by hand was performed between cycles to homogenize the raw ingredients. In the second cycle, covers were applied to the alumina crucibles to prevent sulfur emissions and the raw ingredients were fired at 1250˚C for 12 h. The firing time in the furnace was much longer compared to the firing time in a rotary kiln used in industrial manufacturing because the raw ingredients remained stationary inside the crucibles during the firing process, which prevented materials from efficiently reacting with each other. Finally, the resulting clinker was ground into fine powder form using a micro mill grinder (Scienceware/Bel-Art).

5.4 ANALYSIS

5.4.1 Thermogravimetric Analysis

Thermogravimetric analysis (Netzsch STA 409 PC Luxx) was used to follow the mass loss occurring with temperature for the raw ingredients of the CSAB cement clinkers during the firing process (Ramachandran, 1969). The instrument was operated

from 25˚C to 1300˚C, which is comparable to the temperature range in the furnace. A 10˚C/min heating rate was used for the testing. Nitrogen gas filled the sample chamber to prevent oxidation during the testing.

5.4.2 Particle Fineness and Particle Size distribution

The ground synthetic clinkers were tested by an air-permeability test, called Blaine fineness, according to ASTM C 204 (2007) to assure uniform median particle fineness before testing with the laser light scattering particle size distribution analysis. Blaine fineness measures the rate of air passing thorough pressed powder and is the most common technique used by cement manufacturers to measure cement fineness. A laser light scattering particle size distribution analyzer (Fritsch Analysette 22) was used to study the particle size distribution for the CSAB cement clinkers (Ferraris et al., 2006). Both the Blaine fineness and the particle size distribution results were compared to a commercially-produced Type I/II portland cement (TXI Hunter).

5.4.3 X-Ray Diffraction

X-ray diffraction (Siemens D500 Powder Diffractometer; Cu $K_{\alpha 1}$, λ=1.5046 Å) was used to determine phase compositions for the CSAB cement clinkers. The instrument was operated under 40 keV and 30 mA, the step size used was 0.02˚/6 sec, and the scan range used was 10˚–80˚ 2θ. Qualitative information for the phases present in the CSAB cement clinkers was obtained using the Hanawalt manual and the Jade program (MDI) (JCPDS–International Centre for Diffraction Data, 1989). Quantitative information was collected using Rietveld analysis (accuracy about 1%) by fitting the lattice parameters of the phases present in the synthetic clinkers to their X-ray diffraction patterns, which was performed with TOPAS-Academic software (Bruker AXS) (Young, 1995; Stutzman and Leigh, 2002).

5.4.4 Scanning Electron Microscopy

Scanning electron microscopy (JEOL JSM-5610 SEM) was used to study phase distribution in the CSAB cement clinkers. Test samples were prepared by mixing the ground synthetic clinkers with optical-grade epoxy and casting in cylindrical epoxy sample disks that had four holes drilled into the surface (Figure 5.1). Test samples were then cured in a 40˚C oven for 24 h, and the surface was polished and coated with silver before backscattered electron imaging and compositional examination by energy dispersive spectroscopy (Stutzman, 2004).

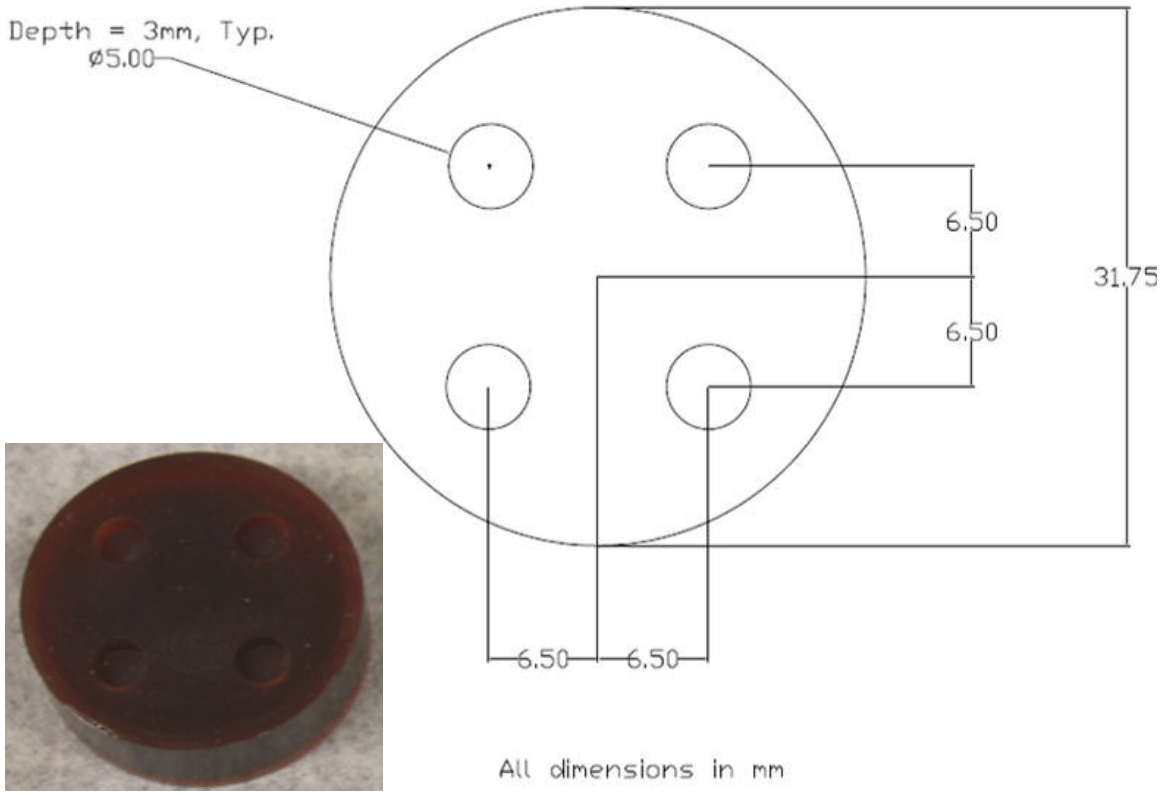

Figure 5.1 – Schematic and picture of the SEM sample disk (Chancey, 2008)

5.5 RESULTS AND DISCUSSION

5.5.1 Thermogravimetric Analysis

The mass loss occurring with temperature for the raw ingredients of the CSAB cement clinkers during the firing process, obtained through thermogravimetric analysis, is shown in Figure 5.2. Thermogravimetric analysis showed weight loss at 450˚C and 750˚C indicating the dissociation of water from $Ca(OH)_2$ and the calcination of $CaCO_3$, respectively. $Ca(OH)_2$ and $CaCO_3$ both formed from CaO contained in the raw ingredients during the mixing process. The raw ingredients for the CSAB cement clinkers with higher target C_2S contents contained more CaO and showed higher mass losses at 450˚C and 750˚C, indicating that more $Ca(OH)_2$ and $CaCO_3$ formed during the mixing process. Furthermore, thermogravimetric analysis showed that a substantial amount of sulfur contained in the raw ingredients was emitted at temperatures above 1200˚C, which can affect phase formation in CSAB cement clinker and the ability to predict phase composition from the initial raw materials composition. The raw ingredients for the CSAB cement clinkers with higher target $C_4A_3\overline{S}$ contents contained more sulfur and showed higher mass losses at temperatures above 1200˚C. Therefore, during clinkering in the laboratory furnace, the raw ingredients were fired in covered alumina crucibles to prevent sulfur emissions during the firing process.

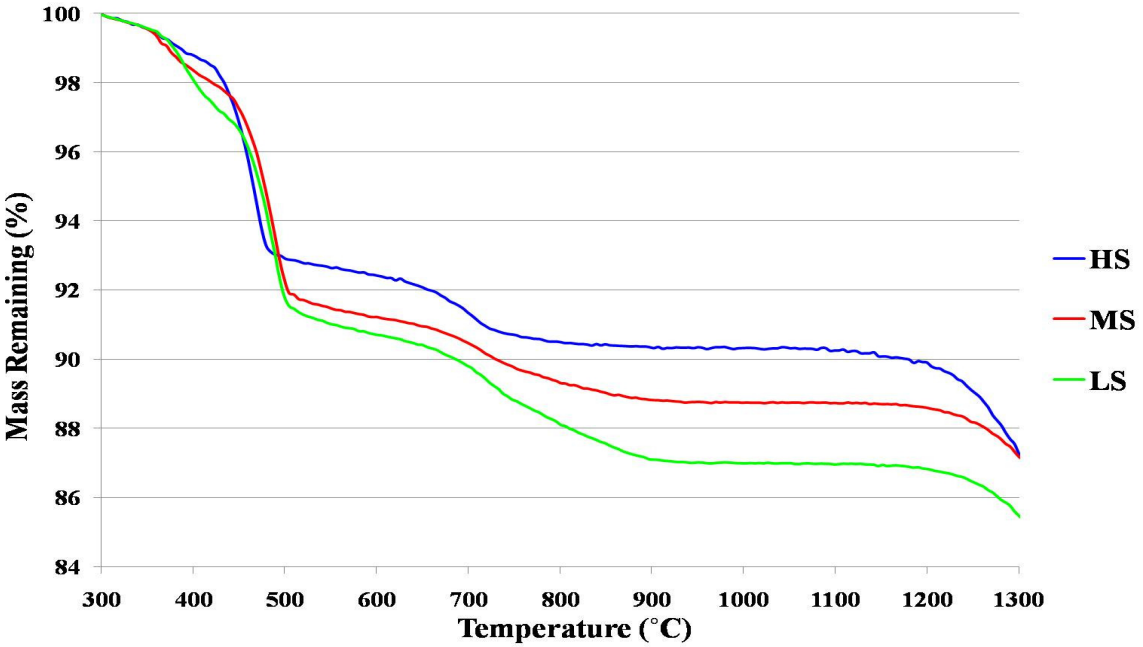

Figure 5.2 – Thermogravimetric analysis for the raw ingredients of the CSAB cement clinkers synthesized from reagent-grade chemicals

5.5.2 Particle Fineness and Distribution

Measuring the particle fineness and distribution of the synthetic clinkers is critical because these factors strongly affect property development. The ground CSAB cement clinkers had uniform Blaine fineness after grinding with the micro mill grinder, as shown in Table 5.2. Their Blaine values were about 325 m^2/kg, which conformed to the minimum portland cement Blaine value (280 m^2/kg) specified in ASTM C 150 (2005). However, the synthetic clinkers had Blaine values about 20% lower than the commercial Type I/II portland cement used for comparison purpose in this study (403.4 m^2/kg). Curiously, the particle size distributions obtained from laser light scattering particle size distribution analysis for the synthetic clinkers were similar to that of the commercial Type I/II portland cement; all had median particle sizes (d_{50}) of approximately 45 µm, as shown in Figure 5.3.

Table 5.2 – Blaine fineness values for a commercial Type I/II portland cement (PC) and the CSAB cement clinkers synthesized from reagent-grade chemicals

Sample	Specific Surface Area (m^2/kg)
PC	403.4
HS	325.0
MS	322.6
LS	322.3

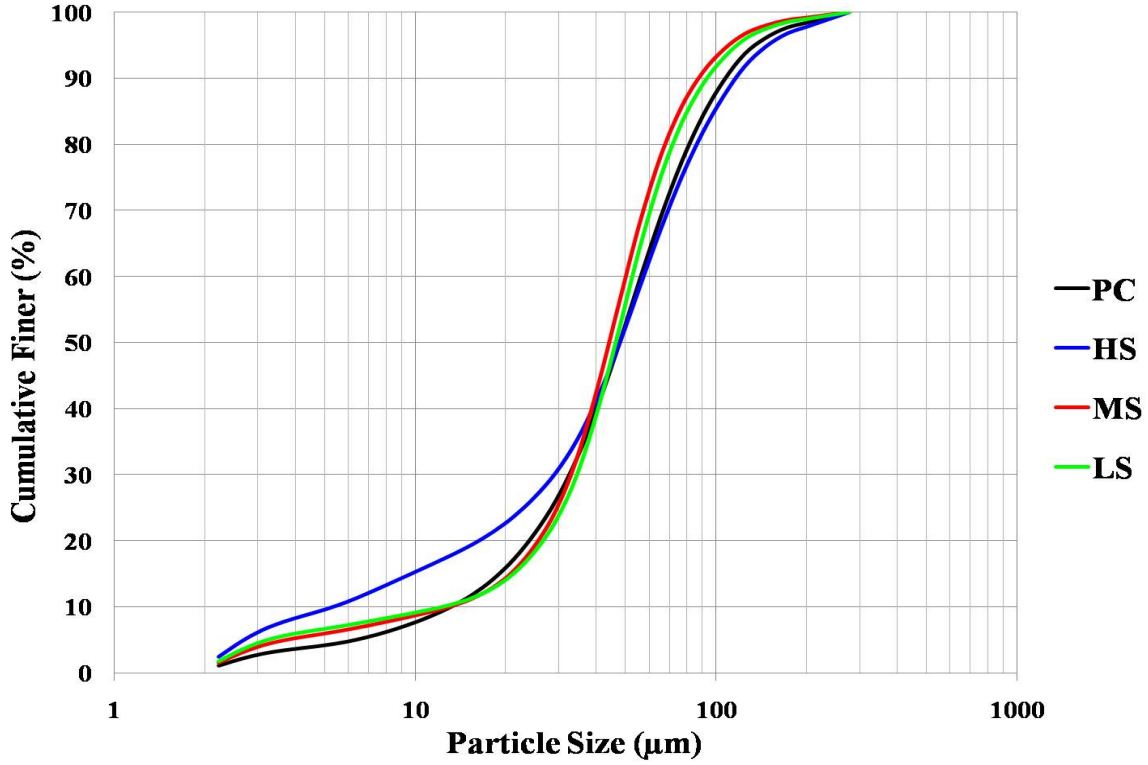

Figure 5.3 – Particle size distribution for a commercial Type I/II portland cement (PC) and the CSAB cement clinkers synthesized from reagent-grade chemicals

Blaine fineness measures the rate of air passing through pressed powder and its results could be affected by particle surface chemistry, morphology, and porosity, which could be different between CSAB cement and portland cement, resulting in different measured surface area values (Iyer and Stanmore, 1995).

5.5.3 Phase Composition

The refined X-ray diffraction patterns for the CSAB cement clinkers obtained through Rietveld analysis are shown in Figures 5.4-5.6. The patterns calculated from the lattice parameters of the phases present in the synthetic clinkers (red) agreed with the measured X-ray diffraction patterns (blue) very well, an indication of the reliability of the quantitative results. A comparison of the X-ray diffraction patterns for the synthetic clinkers is shown in Fig. 5.7 and their quantitative phase compositions are shown in Table 5.3. The phase analysis results show that the four major CSAB cement phases formed in every synthetic clinker. All the synthetic clinkers had low free lime (C) contents indicating that the 1250˚C firing temperature was sufficient for the raw ingredients to completely react in the furnace. The phase compositions for the synthetic clinkers were reasonably close to their target phase compositions, indicating that the Bogue method refined for this research can effectively predict CSAB cement clinker phase composition from its raw materials oxide composition. The slight deviations from the target phase compositions were perhaps caused by the ability of phases to accommodate substitute ions (Taylor, 1997). Furthermore, the synthetic clinkers with higher $C_4A_3\overline{S}$ contents had lower C_4AF contents than predicted by the proposed Bogue-type equations (Equations 5.1-5.5). Strigac et al. (2000) showed that $C_4A_3\overline{S}$ was able to accommodate up to 2% Fe_2O_3 substitute ions, which could therefore explain the low C_4AF content in high $C_4A_3\overline{S}$ -containing synthetic clinker.

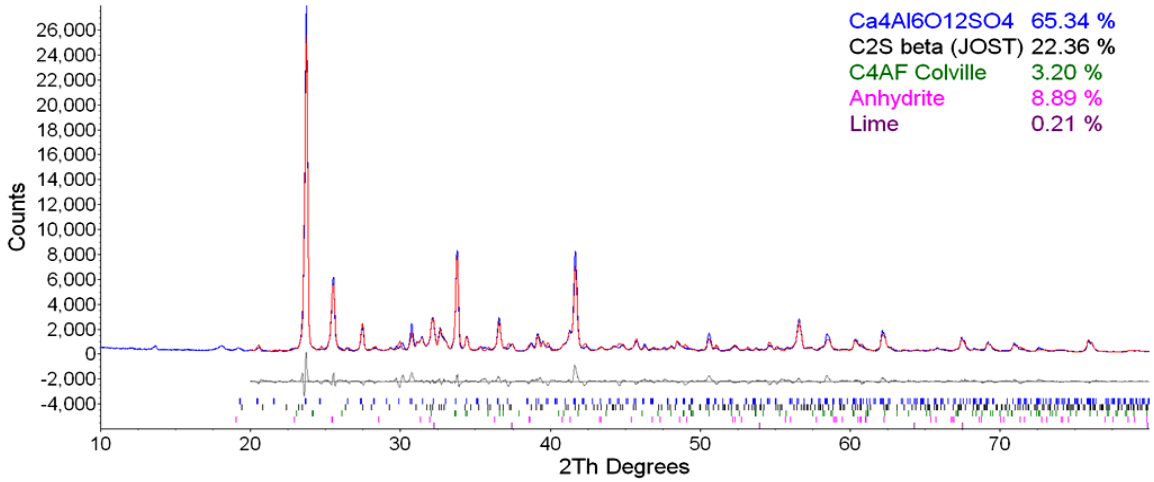

Figure 5.4 – Rietveld analysis results for the HS CSAB cement clinker synthesized from reagent-grade chemicals

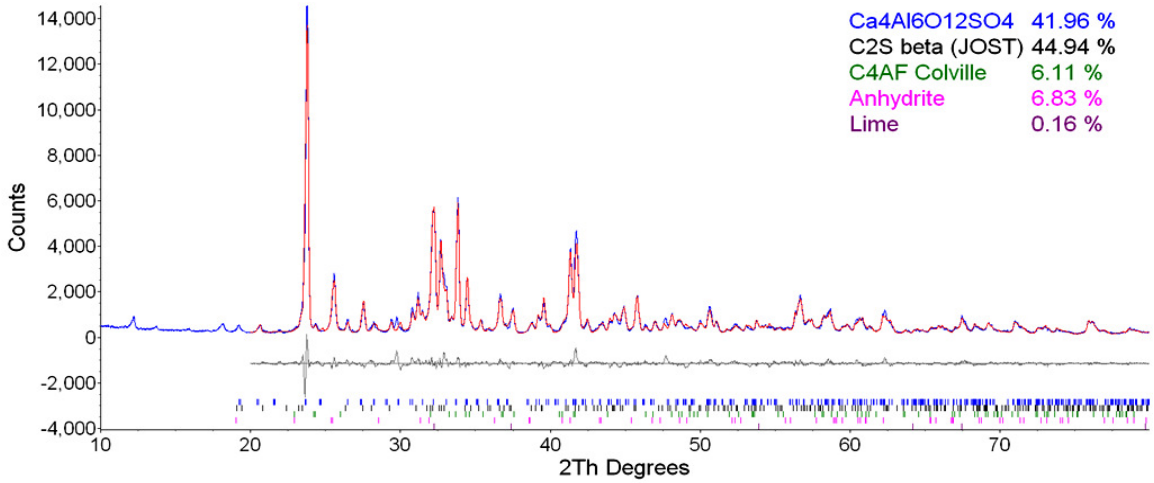

Figure 5.5 – Rietveld analysis results for the MS CSAB cement clinker synthesized from reagent-grade chemicals

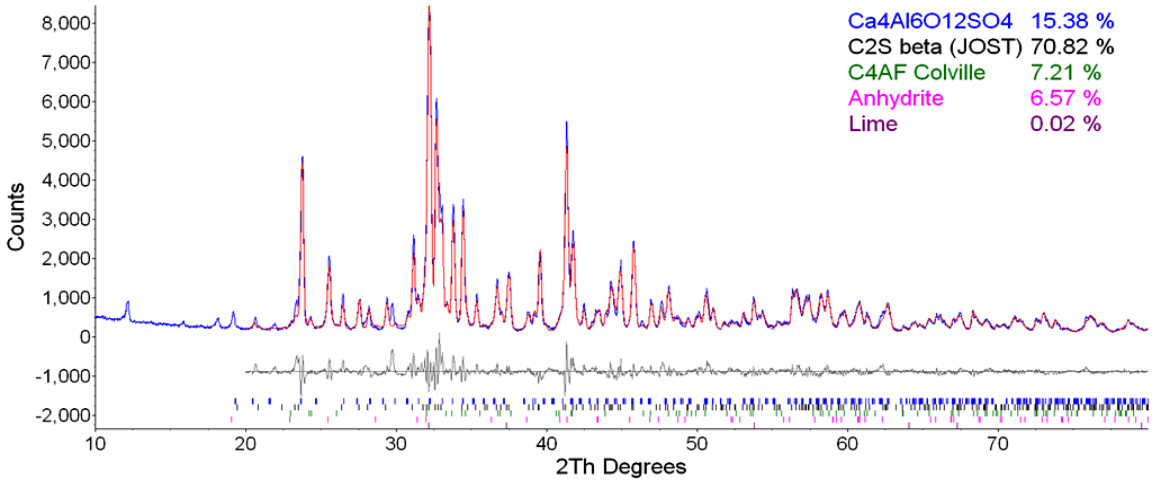

Figure 5.6 – Rietveld analysis results for the LS CSAB cement clinker synthesized from reagent-grade chemicals

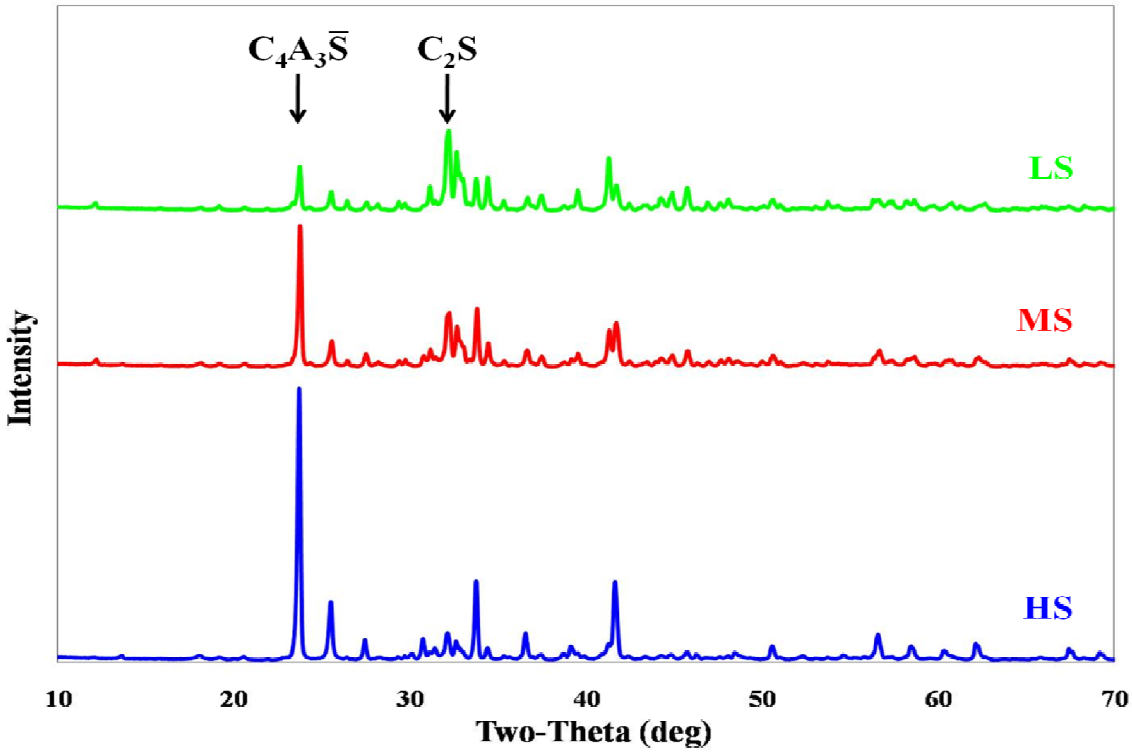

Figure 5.7 – X-ray diffraction patterns comparison for the CSAB cement clinkers synthesized from reagent-grade chemicals

Table 5.3 – Phase compositions for the CSAB cement clinkers synthesized from reagent-grade chemicals (TG: target calculated from the Bogue equations; R: Rietveld analysis)

Phase	**Phase Composition (weight %)**					
	HS		***MS***		***LS***	
	TG	***R***	***TG***	***R***	***TG***	***R***
C_2S	20	22.4	40	44.9	60	70.8
$C_4A_3\overline{S}$	60	65.3	40	42.0	20	15.4
C_4AF	10	3.2	10	6.1	10	7.2
$C\overline{S}$	10	8.9	10	6.8	10	6.6
C	0	0.2	0	0.2	0	0

5.5.4 Phase Distribution

Backscattered electron images clearly show phase distribution in the CSAB cement clinkers, as shown in Figures 5.8-5.10. The lighter gray areas in these images represent C_2S while the darker gray areas represent $C_4A_3\overline{S}$, as indicated in Figures 5.8-5.10. The synthetic clinkers that contained higher C_2S and lower $C_4A_3\overline{S}$ showed more light gray areas and less dark gray areas while the synthetic clinkers that contained higher $C_4A_3\overline{S}$ and lower C_2S showed more dark gray areas and less light gray areas, which agree with the quantitative X-ray diffraction results (Table 5.3). The small amount of white areas that formed individually and inside the light gray (C_2S) and dark gray ($C_4A_3\overline{S}$) areas represent C_4AF (indicated in Figures 5.8-5.10). The synthetic clinkers with higher $C_4A_3\overline{S}$ contents had fewer white areas. Energy dispersive spectroscopy analysis showed that $C_4A_3\overline{S}$ was able to accommodate up to 1.5% Fe_2O_3, which again explains the low C_4AF contents in high $C_4A_3\overline{S}$-containing synthetic clinkers. The synthetic clinkers showed similar particle size distribution in these images, which

conform to the Blaine fineness and laser light scattering particle size distribution analysis results (Table 5.2 and Figure 5.3, respectively).

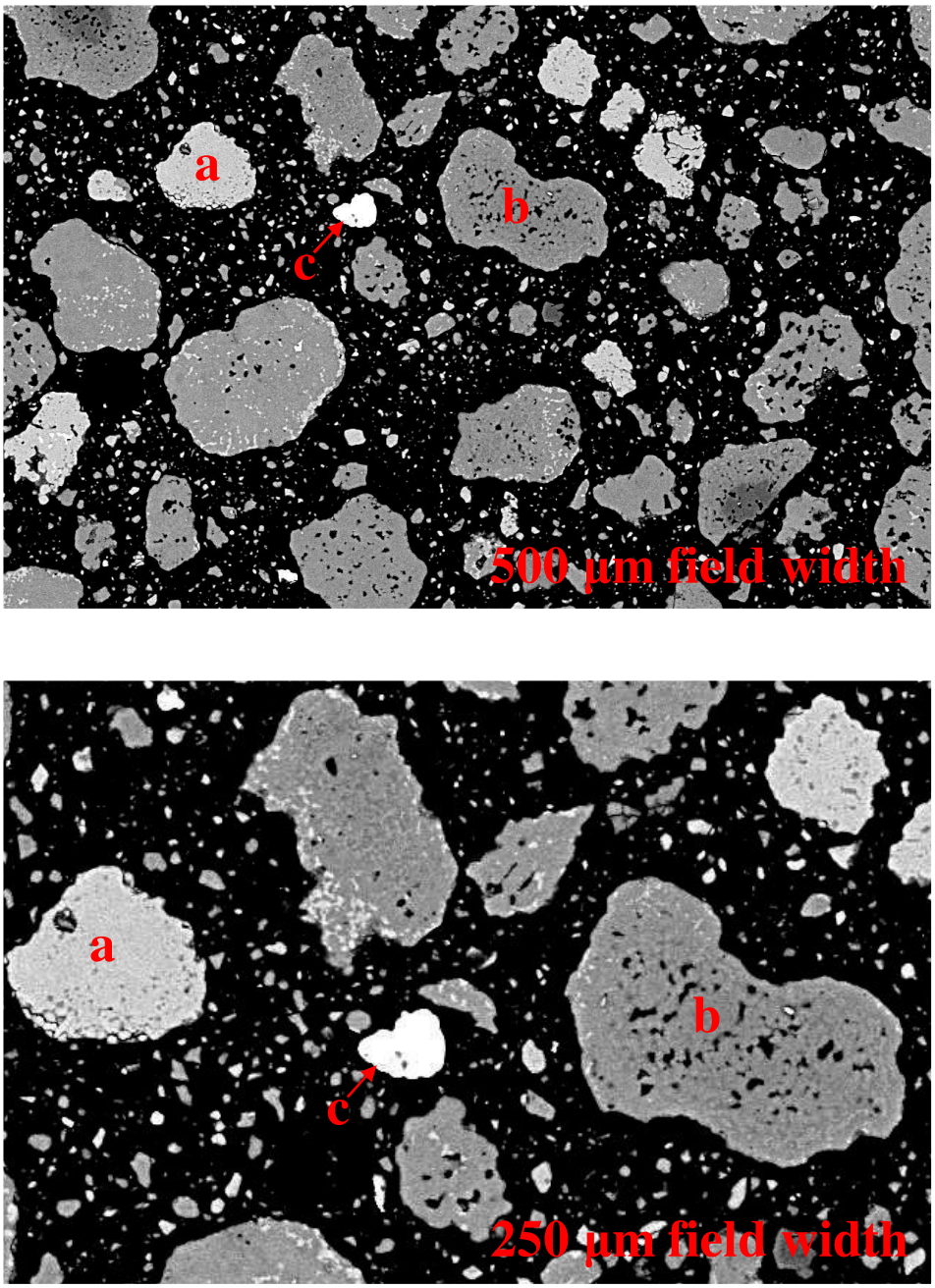

Figure 5.8 – Backscattered electron image for the HS CSAB cement clinker synthesized from reagent-grade chemicals [a (light gray): C_2S, b (dark gray): $C_4A_3\overline{S}$, and c (white): C_4AF]

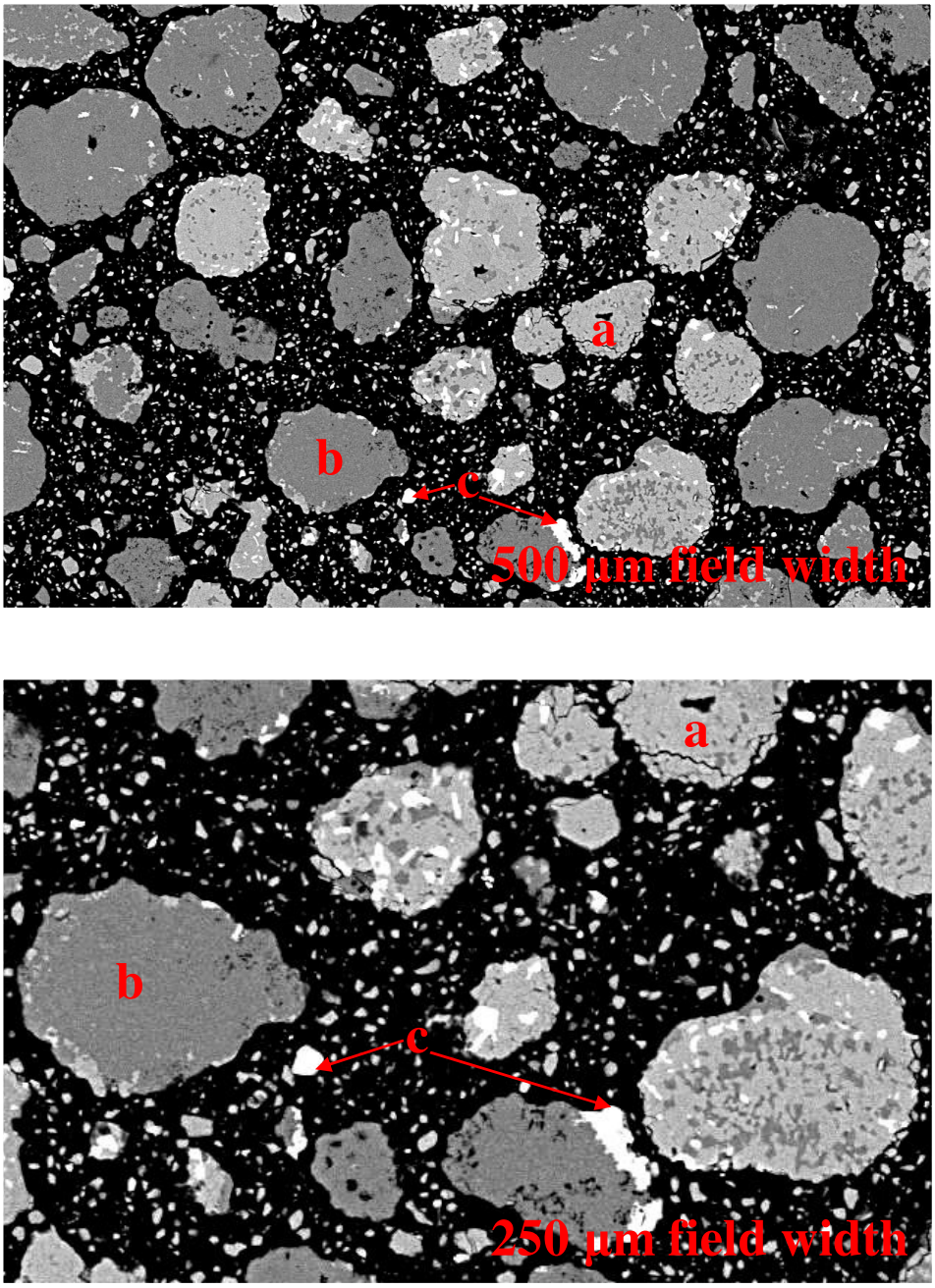

Figure 5.9 – Backscattered electron image for the MS CSAB cement clinker synthesized from reagent-grade chemicals [a (light gray): C_2S, b (dark gray): $C_4A_3\overline{S}$, and c (white): C_4AF]

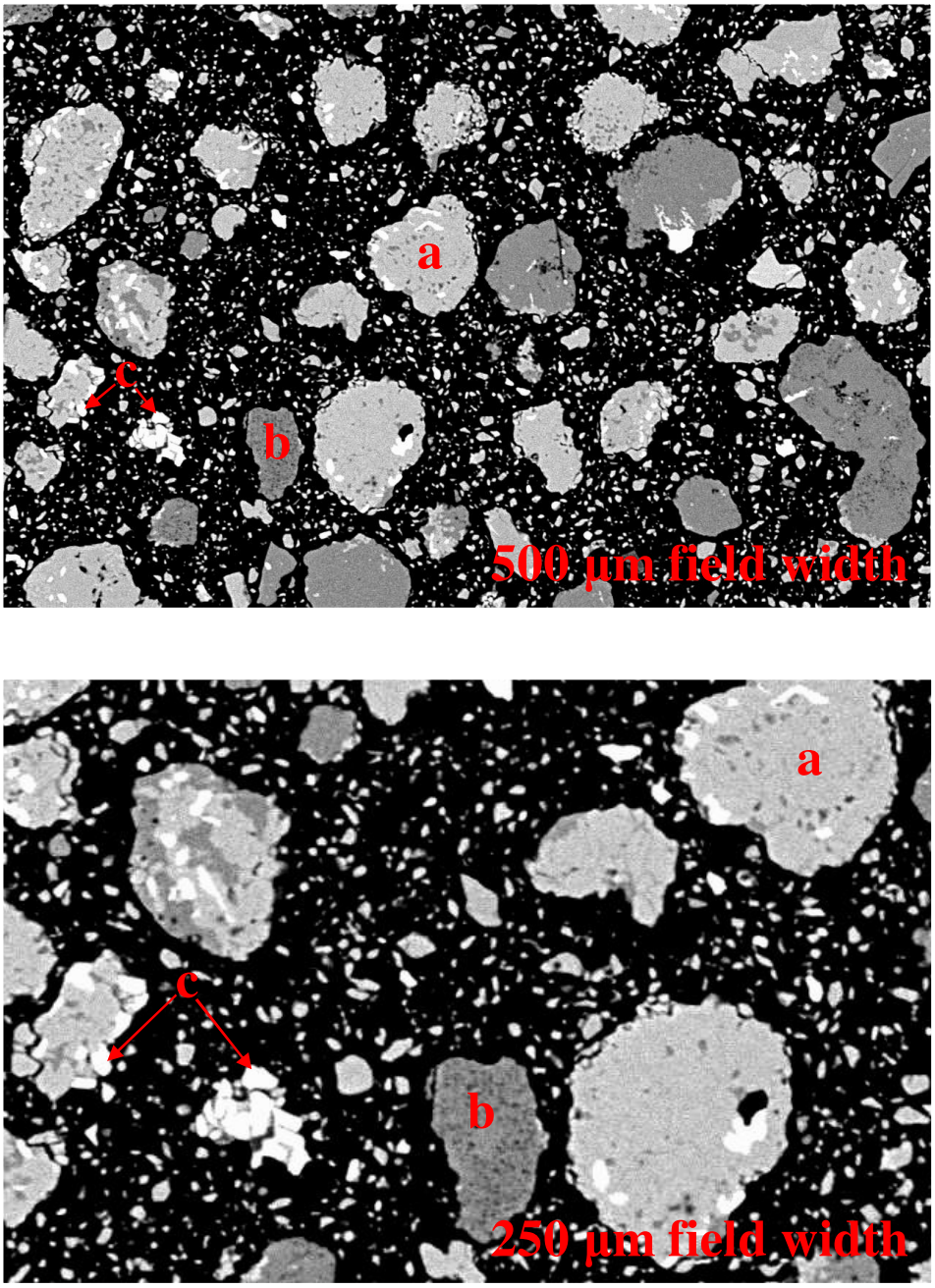

Figure 5.10 – Backscattered electron image for the LS CSAB cement clinker synthesized from reagent-grade chemicals [a (light gray): C_2S, b (dark gray): $C_4A_3\overline{S}$, and c (white): C_4AF]

5.6 CONCLUSIONS

The primary goal of this study was to synthesized CSAB cement clinkers from reagent-grade chemicals with a range of phase compositions for later evaluation of the inter-relationship between phase composition and performance of the CSAB cement system. In was observed that sulfur contained in the raw ingredients of the CSAB cement clinkers evaporated at temperature above 1200˚C. Therefore, special care should be taken during the firing process. The ground CSAB cement clinkers had similar particle fineness and distribution and were comparable to commercial portland cement as shown in the Blaine fineness and laser light particle size distribution analysis. Three CSAB cement clinkers with a range of target phase compositions were successfully synthesized from reagent-grade chemicals. The phase compositions for the CSAB cement clinkers were reasonably close to their target phase compositions, indicating that the adapted Bogue method can effectively predict CSAB cement clinker phase composition from its raw materials oxide composition. However, the synthetic clinkers with higher $C_4A_3\overline{S}$ contents had lower C_4AF contents than predicted by the proposed Bogue-type equations because $C_4A_3\overline{S}$ was able to accommodate up to 1.5% Fe_2O_3, as shown in the energy dispersive spectroscopy analysis. Some adjustments to the adapted Bogue method might be necessary to accurately predict CSAB cement clinker phase composition from its raw materials oxide composition. On the other hand, backscattered electron images clearly show phase distribution in the CSAB cement clinkers and agree with the X-ray diffraction results.

Chapter 6: Calcium Sulfoaluminate-Belite Cement: Effects of Phase Composition on Hydration and Properties

6.1 INTRODUCTION

The three calcium sulfoaluminate-belite (CSAB) cement clinkers synthesized from reagent-grade chemicals with different proportions of C_2S and $C_4A_3\overline{S}$ discussed in Chapter 5 were used to study the hydration chemistry and the inter-relationship between phase composition and performance of the CSAB cement system. Because the effects of added gypsum on early-age hydration behavior of CSAB cement are not well known, different amounts of gypsum were added to the synthetic clinkers and the resulting cements were tested for heat evolution rate using isothermal conduction calorimetry to study the effect of gypsum content on early-age hydration behavior and to determine the optimum gypsum content. The synthesized CSAB cements containing optimum gypsum contents were monitored for hydration product development using X-ray diffraction and scanning electron microscopy. Phase composition and phase distribution information for the hydrated synthesized cements were collected.

Monitoring the formation of ettringite ($C_6A\overline{S}_3H_{32}$), the main hydrated phase of CSAB cement system from the hydration reaction of $C_4A_3\overline{S}$ and gypsum, is critical for understanding the performance of CSAB cement. Ettringite formation has shown to be expansive in previous research and could cause cracking (Ogawa and Roy, 1982; Glasser and Zhang, 2001). Furthermore, it is known that in portland cement, if insufficient gypsum is added, ettringite reacts with the aluminum containing phases (C_3A and C_4AF) to form calcium monosulfoaluminate ($C_4A\overline{S}H_{12}$) (Mindess et al., 2003). Calcium monosulfoaluminate is subject to transform back to ettringite in the presence of environmental sulfate, causing cracking. Therefore, the dimensional stability and

environmental sulfate resistance of the synthesized CSAB cements were studied. Finally, compressive strength development of the synthesized cements was investigated. The dimensional stability, sulfate resistance, and compressive strength development results were compared to a commercial Type I/II portland cement. The final goal was to determine the optimum phase composition for CSAB cement performance.

6.2 ANALYSIS

6.2.1 Isothermal Conduction Calorimetry

The heat produced by cementitious materials in exothermic hydration reactions is a good indication of their early-age hydration behavior (Gartner et al., 2002). The CSAB cement clinkers were made into cements by adding different amounts of gypsum (99% $CaSO_4 \cdot 2H_2O$; Arcos) to control the hydration reaction of $C_4A_3\overline{S}$. The resulting cements were tested for heat evolution rate using isothermal conduction calorimetry (Thermometric TAM Air) to determine their optimum gypsum contents (percentage of cement) and to study early-age hydration behavior. Hydration was evaluated for 3 days at 23˚C using a water-to-cement ratio of 0.45. The results were compared to a commercially-produced Type I/II portland cement (TXI Hunter Cement). After determining the optimum gypsum contents for the synthetic clinkers, the synthesized CSAB cements containing their optimum gypsum contents were tested for heat evolution rate at 5˚C and 38˚C to study the hydration temperature dependency of the CSAB cement system.

6.2.2 X-Ray Diffraction

X-ray diffraction (Siemens D500 Powder Diffractometer; Cu $K_{\alpha 1}$, λ=1.5046 Å) was used to determine phase compositions for the hydrated synthesized CSAB cements at 3 h, 1, 3, 7, 28, and 90 days hydration. The synthesized cements were cast in plastic cups

using a water-to-cement ratio of 0.45, demolded at 1 day of hydration, and stored in ultra-pure water at room temperature until testing. Hydration of the synthesized cements was stopped using ethanol and a vacuum dessicator. The instrument was operated under 40 keV and 30 mA, the step size used was 0.02˚/6 sec, and the scan range used was 5˚–70˚ 2θ. 10% rutile (TiO_2) was ground into the hydrated synthesized cements to serve as an internal standard in order to quantify their amorphous contents. Qualitative information for the phases present in the CSAB cement clinkers was obtained using the Hanawalt manual and the Jade program (MDI) (JCPDS–International Centre for Diffraction Data, 1989). Quantitative information was collected using Rietveld analysis (accuracy about 1%) by fitting the lattice parameters of the phases present in the synthetic clinkers to their X-ray diffraction patterns, which was performed with TOPAS-Academic software (Bruker AXS) (Young, 1995; Stutzman and Leigh, 2002).

6.2.3 Scanning Electron Microscopy

Scanning electron microscopy (JEOL JSM-5610 SEM) was used to study phase distribution of the hydrated synthesized CSAB cements. Test samples were prepared by placing a slice of paste at the bottom of a cylindrical mold (30 mm diameter). 1, 3, 7, 28, and 90 day old paste samples were prepared. The synthesized cements were cast in plastic cups using a water-to-cement ratio of 0.45, demolded at 1 day of hydration, and stored in ultra-pure water at room temperature until testing. Hydration of the synthesized cements was stopped using ethanol and a vacuum dessicator. Optical-grade epoxy was then slowly poured in the cylindrical mold to cover the paste. The samples were then placed under vacuum to draw the remaining air out of the samples and were brought back to atmospheric pressure to allow epoxy to fill in the voids of the paste. The samples were then cured in a 40˚C oven for 24 hrs, and the surface was polished and coated with silver

before backscattered electron imaging and compositional examination by energy dispersive spectroscopy (Stutzman, 2004).

6.2.4 Dimensional Stability and Sulfate Resistance

Dimensional stability and sulfate resistance of the synthesized CSAB cements were tested by adapting a new test method for concrete sulfate resistance developed at the National Institute of Standards and Technology (Ferraris et al. 2006). Small bars (40×10×10 mm) were made from the synthesized cement using a water-to-cement ratio of 0.45, demolded at 1 day of hydration, and cured in ultra-pure water from 1 to 7 days of hydration at room temperature. Dimensional stability of the synthesized CSAB cements was tested by measuring expansion of the small bars from 1 to 4 days of hydration.

At 7 days of hydration, two threaded studs were screwed into the pins embedded in each end of the small bars and sealed with epoxy to prevent sulfate penetration from the ends. The small bars were stored in 5% Na_2SO_4 solution at room temperature. Sulfate resistance of the synthesized CSAB cements was tested by measuring the expansion of the small bars from 7 to 97 days of hydration. For both the dimensional stability and the sulfate resistance tests, six small bars were measured from each batch of paste and the expansion was averaged. The results were compared to a commercially-produced Type I/II portland cement (TXI Hunter).

6.2.5 Compressive Strength Development

Compressive strength development of the synthesized CSAB cements was tested with cubes (50×50×50 mm) of standard mortar (cement + sand + water; water-to-cement ratio of 0.45) according to ASTM C 109 (2007). The mortar cubes were demolded at 1 day of hydration and cured in ultra-pure water at room temperature. Compressive strength was tested at 1, 3, 7, 28, and 90 days. Three mortar cubes were tested at each

age for each sample type and the strengths were averaged. The results were compared to a commercially-produced Type I/II portland cement (TXI Hunter).

6.3 RESULTS AND DISCUSSION

6.3.1 Early-Age Hydration Behavior

Rate of heat evolution results for the CSAB cement clinkers with different amounts of gypsum addition are shown in Figures 6.1-6.3. The optimum gypsum content (percentage of cement) was taken to be the lowest amount of gypsum that produced only one main heat evolution peak, as shown by Lerch (1947) for portland cement clinker. The shape of the main heat evolution peak no longer changes with gypsum addition higher than the optimal amount. For CSAB cement, the main heat evolution peak is from the hydration reaction of $C_4A_3\overline{S}$ with calcium sulfates to form ettringite ($C_6A\overline{S}_3H_{32}$) and AH_3. Calcium sulfates are a combination of anhydrite ($C\overline{S}$) formed in clinker and gypsum ($C\overline{S}H_2$) interground after clinkering; anhydrite transforms to gypsum when reacting with water. The hydration reaction of $C_4A_3\overline{S}$ with gypsum initiates rapidly and dominates the early-age hydration behavior and property development of CSAB cement, as shown in Equation 6.1 (Kasselouri et al., 1995):

$$C_4A_3\overline{S} + 2C\overline{S}H_2 + 34H \rightarrow C_6A\overline{S}_3H_{32} + 2AH_3 \quad (6.1)$$

The hydration reaction of C_4AF contained in the synthetic clinkers with gypsum also contributes to ettringite formation, as shown in Equation 6.2 (Mindess et al., 2003):

$$C_4AF + 3C\overline{S}H_2 + 21H \rightarrow C_6(A,F)\overline{S}_3H_{32} + 2(A,F)H_3 \quad (6.2)$$

In the portland cement system, the additional heat evolution peak at gypsum addition lower than the optimal amount indicates the depletion of gypsum and the formation of calcium monosulfoaluminate ($C_4A\overline{S}H_{12}$) due to the lack of gypsum in the system, as shown by Tenoutasse (1968) and Gaidis and Gartner (1989). Calcium

monosulfoaluminate is subject to transform back to ettringite in the presence of environmental sulfate, causing cracking and therefore should be avoided (Mindess et al., 2003).

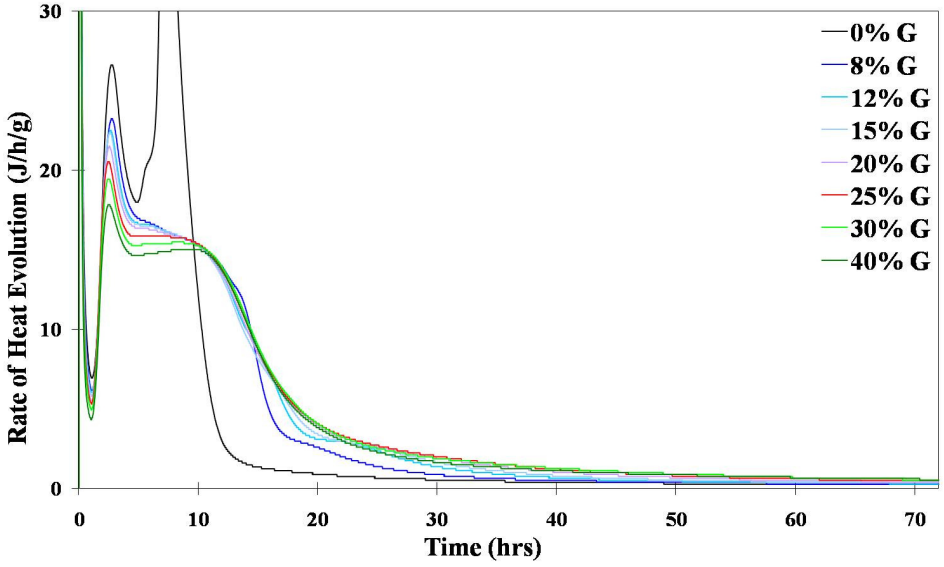

Figure 6.1 – Rate of heat evolution for the HS CSAB cement clinker synthesized from reagent-grade chemicals with different amounts of gypsum (G) addition

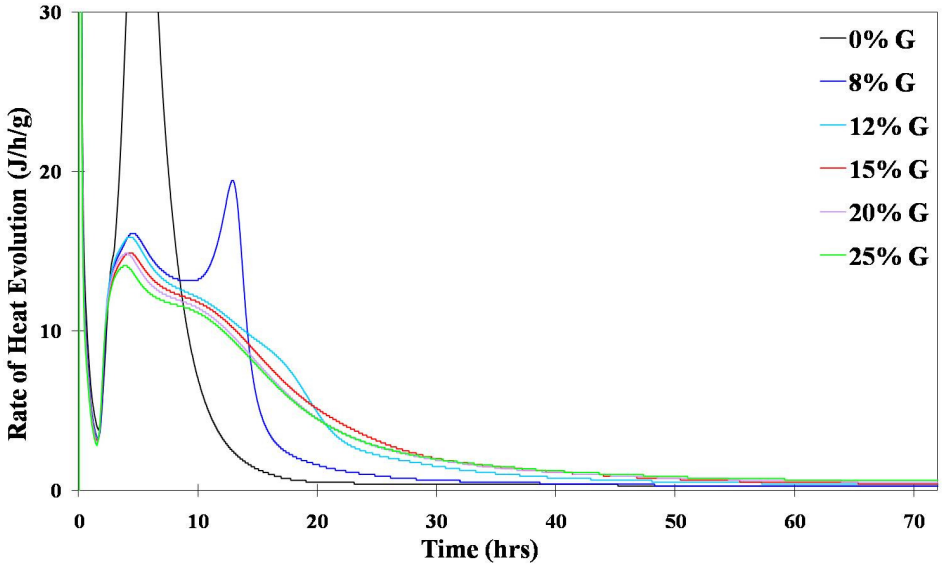

Figure 6.2 – Rate of heat evolution for the MS CSAB cement clinker synthesized from reagent-grade chemicals with different amounts of gypsum (G) addition

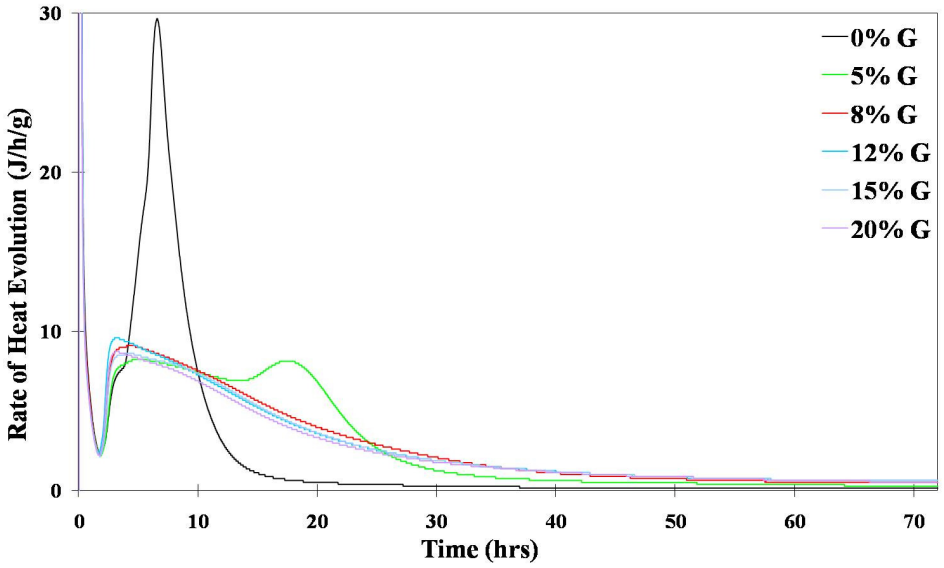

Figure 6.3 – Rate of heat evolution for the LS CSAB cement clinker synthesized from reagent-grade chemicals with different amounts of gypsum (G) addition

With the optimum gypsum content added, the synthetic CSAB cement clinkers also showed the highest cumulative heat, as shown in Figures 6.4-6.6. The optimum gypsum contents for all the synthetic clinkers and their relevant phase contents for ettringite formation are shown in Table 6.1. It was observed that the optimum gypsum contents for the CSAB cement clinkers mainly depended on their $C_4A_3\overline{S}$ contents. An equation for calculating the optimum gypsum content for CSAB cement clinker was developed for future reference based on the $C\overline{S}$ content of CSAB cement clinker and the hydration reactions of $C_4A_3\overline{S}$ and C_4AF with gypsum to form ettringite and AH_3 (Equations 6.1 and 6.2) and, as shown in Equation 6.3:

$$126.45 \times [0.4461(\%C_4A_3\overline{S}) + 0.8403(\%C_4AF) - 1.000(\%C\overline{S})] / \{100 + 1.2645 \times [0.4461(\%C_4A_3\overline{S}) + 0.8403(\%C_4AF) - 1.000(\%C\overline{S})]\} \quad (6.3)$$

The calculated optimum gypsum contents for the synthetic clinkers agreed with their measured optimum gypsum contents from the heat evolution rate results well, as shown in Table 6.1.

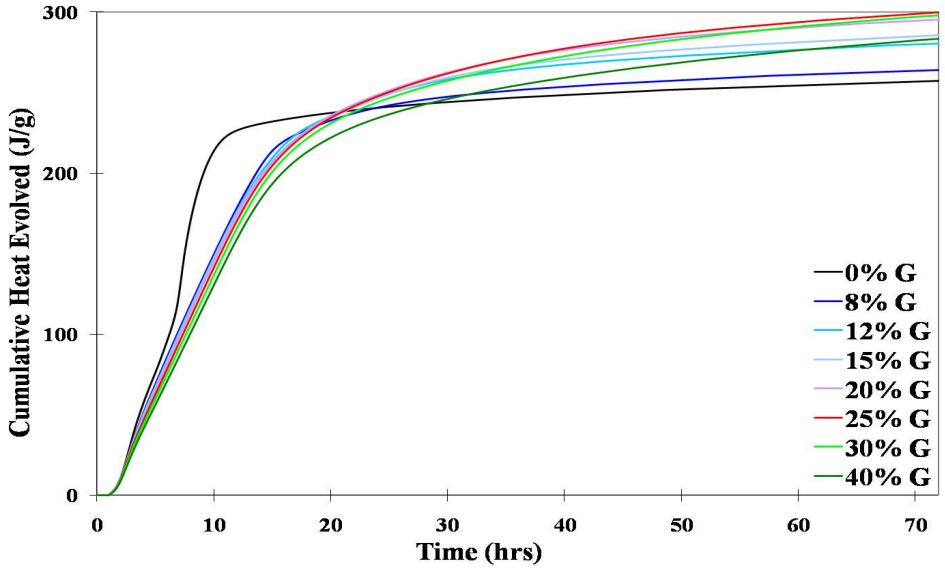

Figure 6.4 – Cumulative heat for the HS CSAB cement clinker synthesized from reagent-grade chemicals with different amounts of gypsum (G) addition

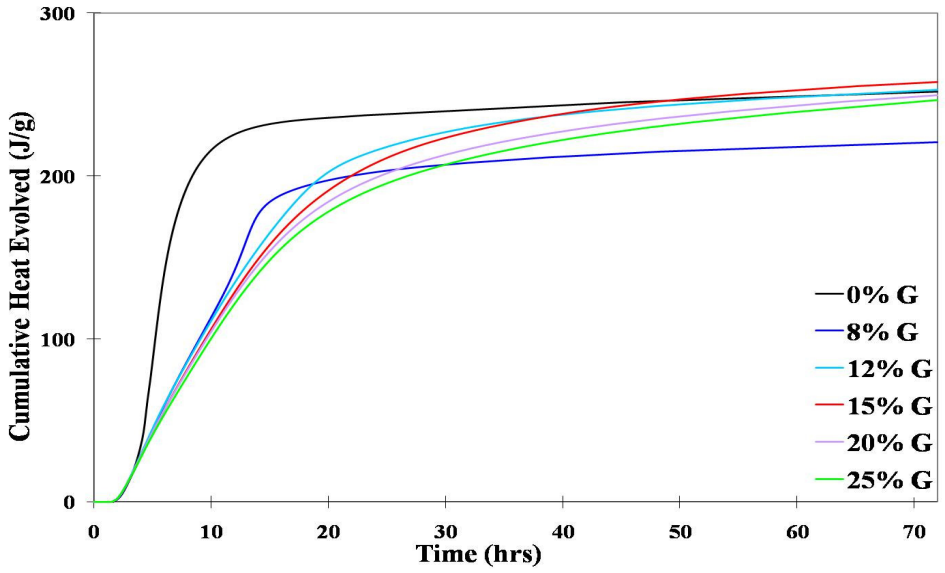

Figure 6.5 – Cumulative heat for the MS cement clinker synthesized from reagent-grade chemicals with different amounts of gypsum (G) addition

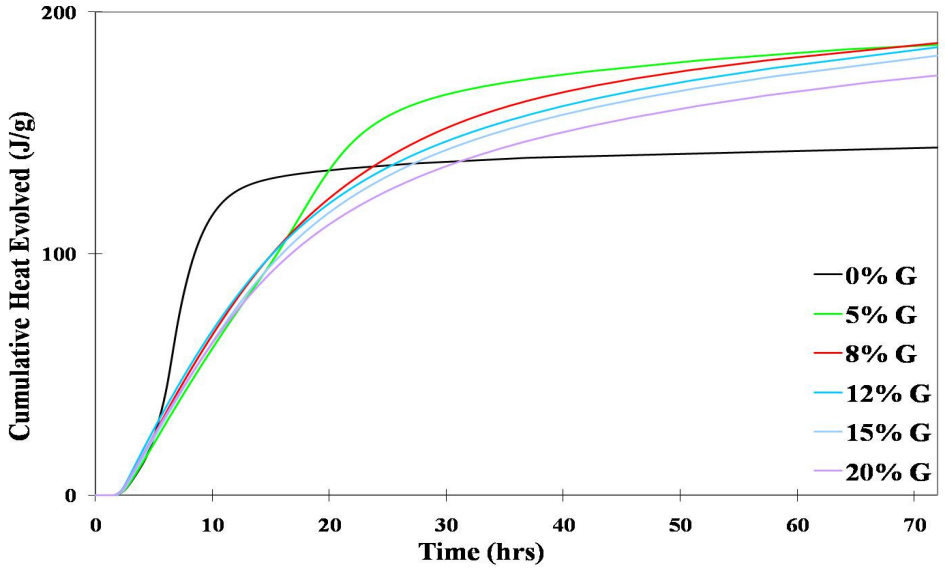

Figure 6.6 – Cumulative heat for the LS CSAB cement clinker synthesized from reagent-grade chemicals with different amounts of gypsum (G) addition

Table 6.1 – Calculated and measured optimum gypsum contents for the CSAB cement clinkers synthesized from reagent-grade chemicals and their relevant phase contents

Sample	$C_4A_3\overline{S}$	C_4AF	$C\overline{S}$	**Measured Gypsum**	**Calculated Gypsum**
HS	65.3%	3.2%	8.9%	**25%**	**22.5%**
MS	42.0%	6.1%	6.8%	**15%**	**17.7%**
LS	15.4%	7.2%	6.6%	**8%**	**7.4%**

Rate of heat evolution and cumulative heat results for the synthesized CSAB cements containing their optimum gypsum contents and a commercial Type I/II portland cement are shown in Figures 6.7 and 6.8. The results show that the synthesized cements with higher $C_4A_3\overline{S}$ contents had higher maximum rates of heat evolution and cumulative heats than the synthesized cements with lower $C_4A_3\overline{S}$ contents. The commercial Type I/II portland cement reacted slower and had a lower maximum rate of heat evolution than the synthesized cements. The differences can be attributed to the different hydration

mechanisms between $C_4A_3\overline{S}$ in CSAB cement and C_3S in portland cement, which both are fast-reacting and are responsible for the early-age hydration behavior and property development. The cumulative heat for the commercial Type I/II portland cement was initially lower than the synthesized cements, but it eventually caught up.

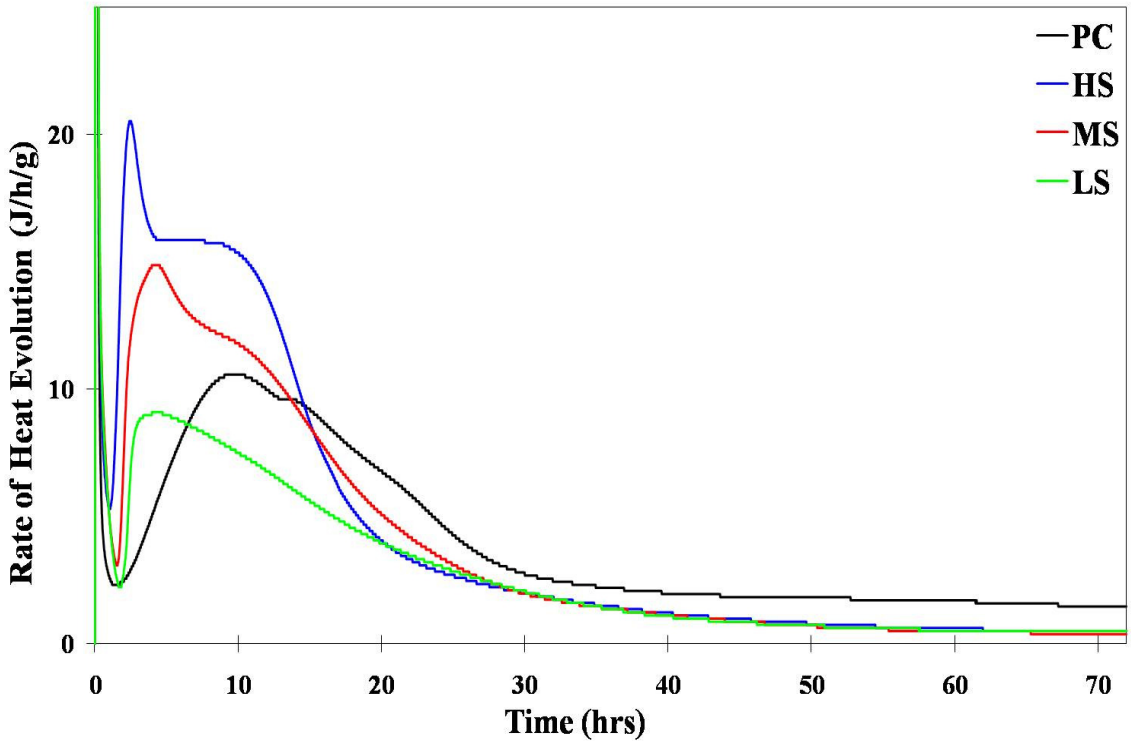

Figure 6.7 – Rate of heat evolution for a commercial Type I/II portland cement (PC) and the synthesized CSAB cements from reagent-grade chemicals

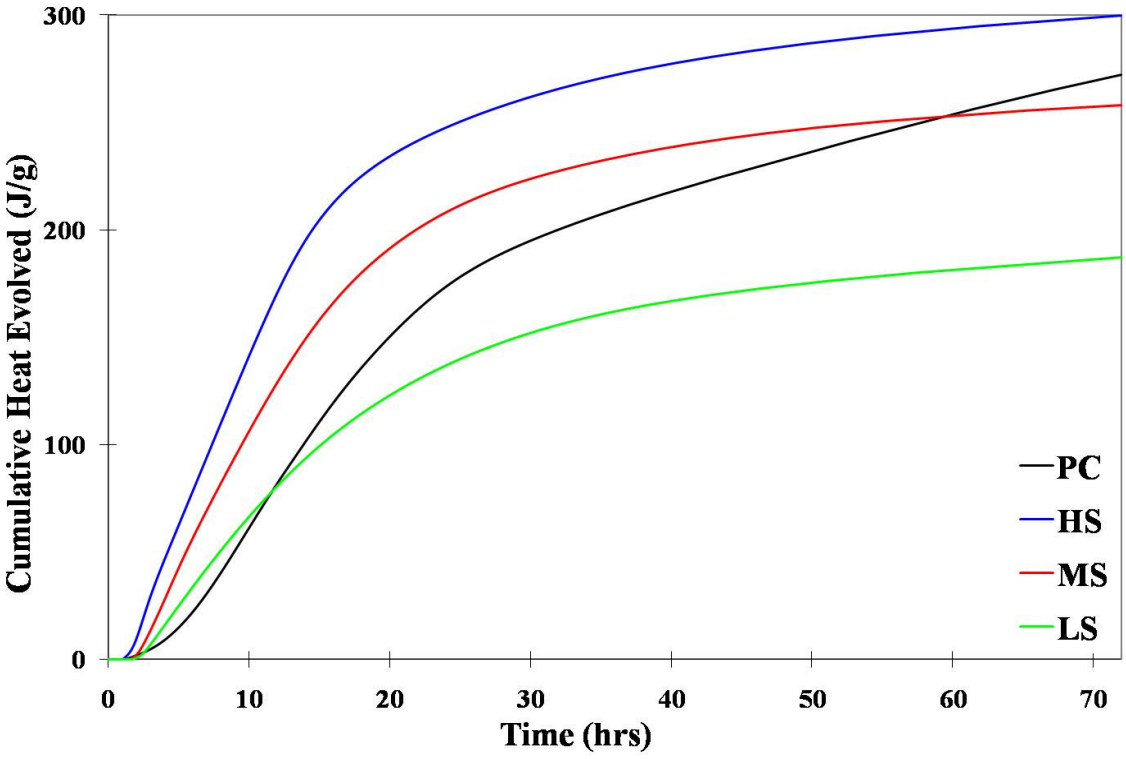

Figure 6.8 – Cumulative heat for a commercial Type I/II portland cement (PC) and the synthesized CSAB cements from reagent-grade chemicals

Rate of heat evolution and cumulative heat results for the synthesized CSAB cements at 5˚C, 23˚C, and 38˚C are shown in Figures 6.9 and 6.10. The results show that the synthesized cements reacted faster and had higher maximum rates of heat evolution and cumulative heats at 38˚C and reacted slower and had lower maximum rates of heat evolution and cumulative heats at 5˚C. However, it is interesting to note that the synthesized cements were actually able to react at temperatures as low as 5˚C, suggesting reasonably, yet marginal, cold-weather performance.

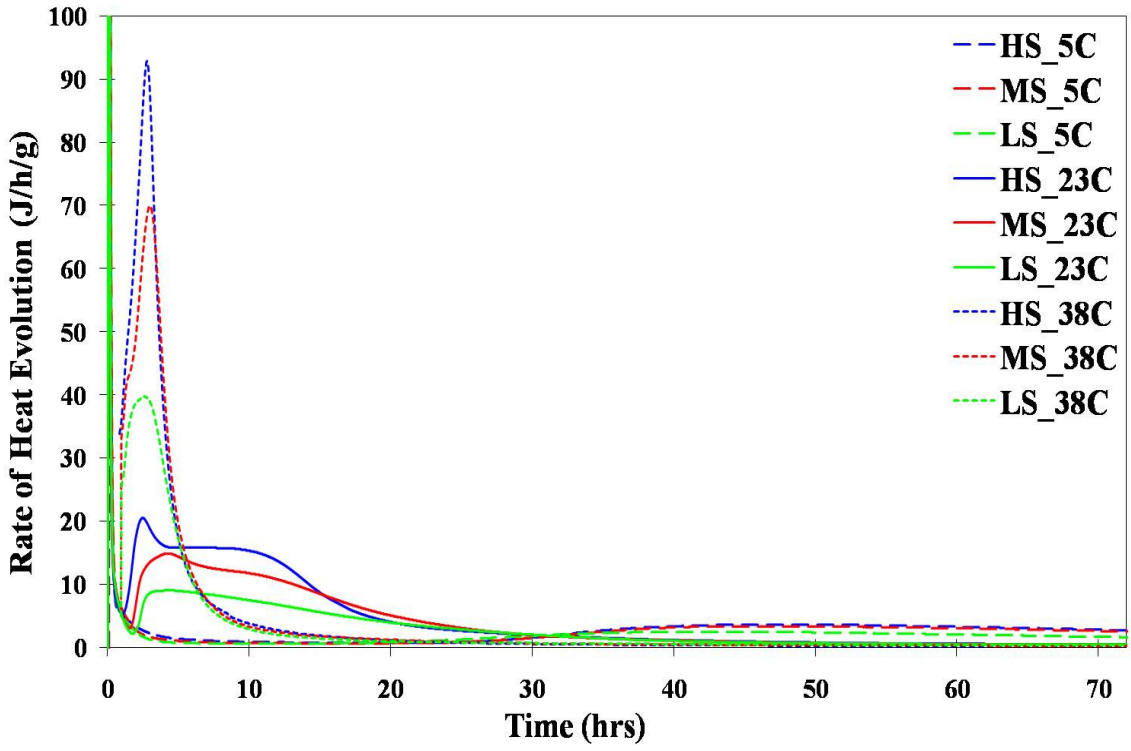

Figure 6.9 – Rate of heat evolution for the synthesized CSAB cements from reagent-grade chemicals at 5˚C, 23˚C, and 38˚C

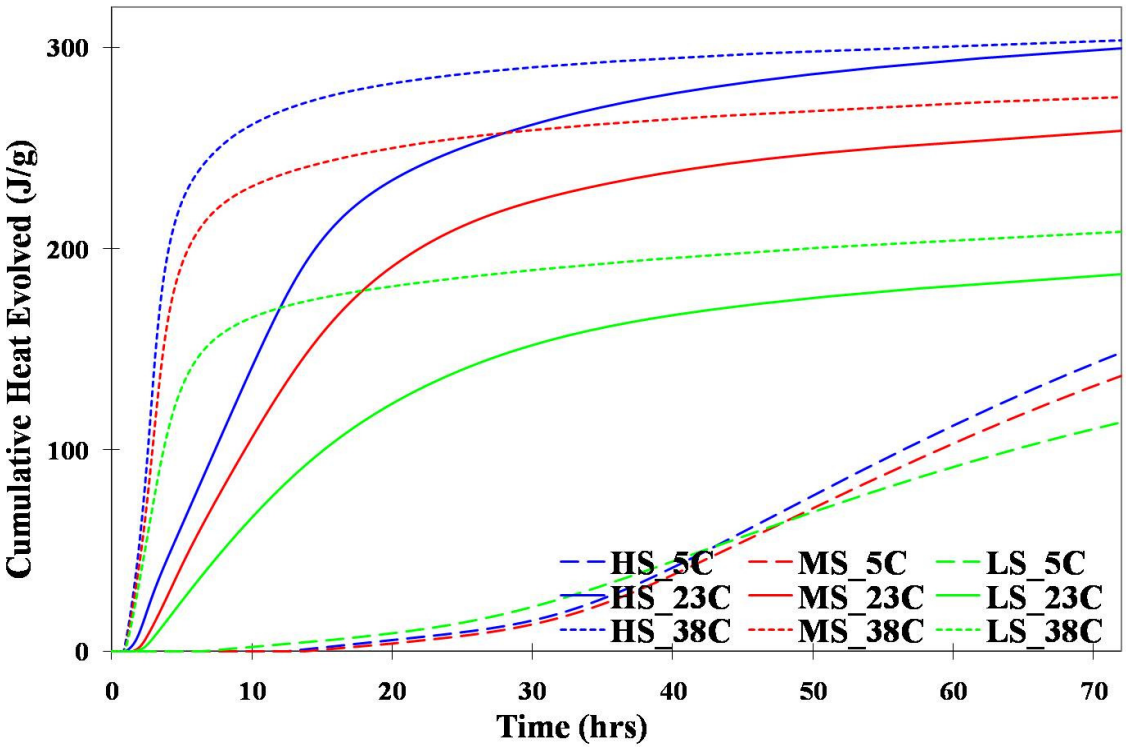

Figure 6.10 – Cumulative heat for the synthesized CSAB cements from reagent-grade chemicals at 5˚C, 23˚C, and 38˚C

Some alternative cement systems such as calcium aluminate cement system show dramatically different hydration product development with temperature (Ideker, 2008). In order to study the effect of temperature on hydration product development in CSAB cement system, the isothermal conduction calorimetry samples were tested with X-ray diffraction after 7 days of hydration. The synthesized cements showed similar hydration product development at the different temperatures tested. X-ray diffraction patterns for the synthesized CSAB cements after 7 days of hydration at 5˚C, 23˚C, and 38˚C (Figures 6.11-6.13) show that the only crystalline hydrated phase formed was ettringite. The other main hydrated phase, AH_3, appeared to be amorphous and cannot be detected by X-ray diffraction.

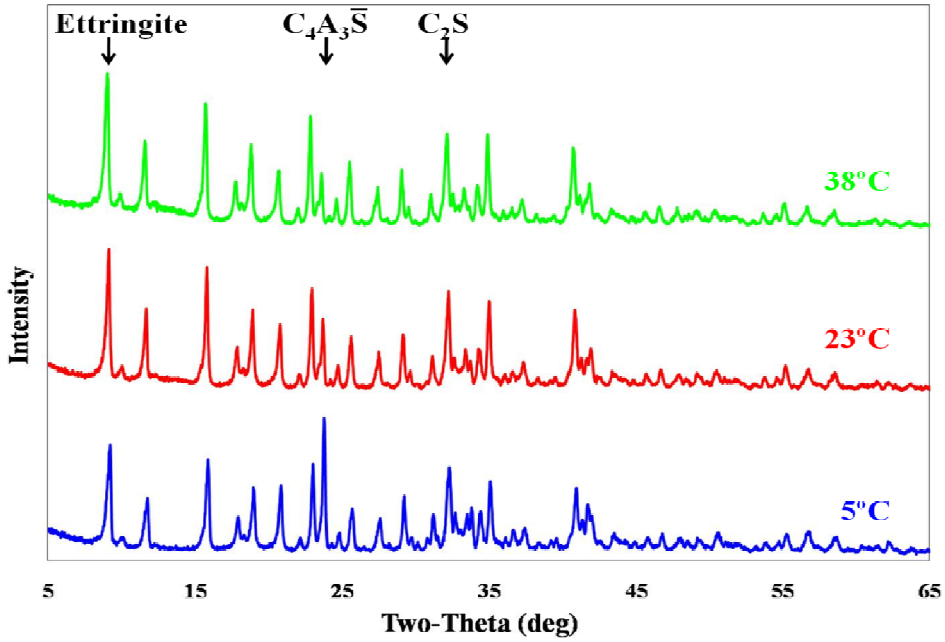

Figure 6.11 – X-ray diffraction patterns for the HS CSAB cement after 7 days of hydration at 5˚C, 23˚C, and 38˚C

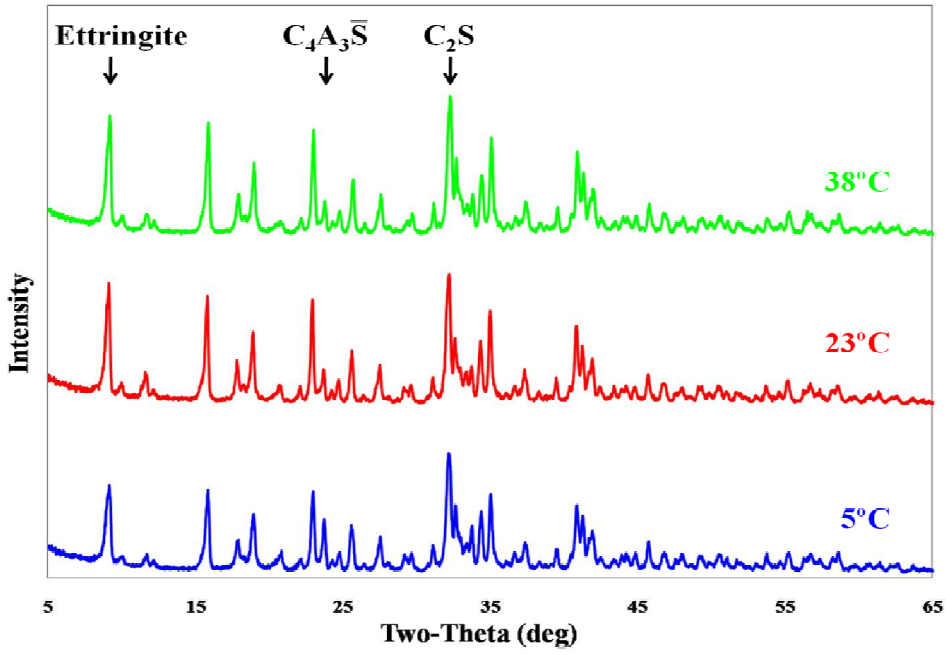

Figure 6.12 – X-ray diffraction patterns for the MS CSAB cement after 7 days of hydration at 5˚C, 23˚C, and 38˚C

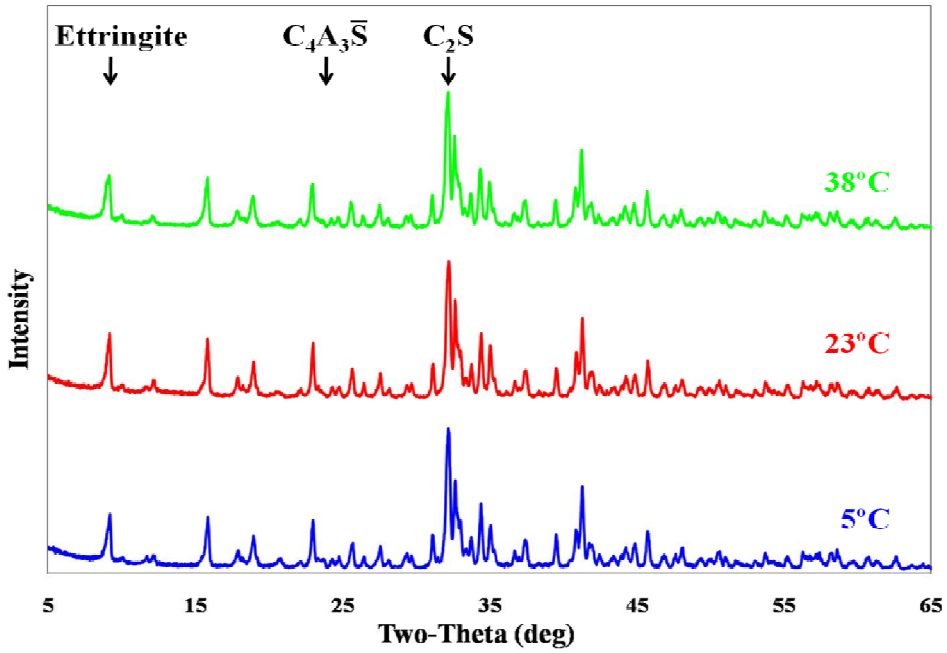

Figure 6.13 – X-ray diffraction patterns for the LS CSAB cement after 7 days of hydration at 5˚C, 23˚C, and 38˚C

6.3.2 Hydration Product Development

Quantitative X-ray diffraction results for the hydrated synthesized CSAB cements are shown in Table 6.2 (X-ray patterns listed in Appendix A). The results show that in all the hydrated synthesized cements, $C_4A_3\overline{S}$ and gypsum reacted quickly and contributed to the formation of ettringite (Equation 6.1). The amorphous content formed in these hydrated synthesized cements should be mainly composed of AH_3, the other main hydrated phase from the hydration reaction of $C_4A_3\overline{S}$ and gypsum besides ettringite (Equation 6.1). Most of the $C_4A_3\overline{S}$ and gypsum reacted by 7 days of hydration. However, C_2S remained mostly unhydrated at 90 days of hydration in all the synthesized cements. Furthermore, carbonation of the hydrated synthesized cements was observed as small amount of calcite formed in all the synthesized cements at 90 days of hydration.

Table 6.2 – Phase compositions for the hydrated synthesized CSAB cements from reagent-grade chemicals

Sample	**Phase Composition (weight %)**								
	C_2S	***$C_4A_3\overline{S}$***	***C_4AF***	***$C\overline{S}$***	***Lime***	***Gypsum***	***Ettringite***	***Amorphous***	***Calcite***
HS_3h	10.5	16.0	1.1	2.5	0	43.4	19.1	7.4	N/A
HS_1D	12.0	14.6	1.0	1.4	0	33.2	26.8	11.0	N/A
HS_3D	12.0	8.2	0.9	1.1	0	15.0	40.5	22.3	N/A
HS_7D	10.6	3.9	0.8	1.1	0	9.8	49.7	24.1	N/A
HS_28D	9.1	2.6	0.5	0.8	0	4.5	51.7	30.8	N/A
HS_90D	8.2	2.0	0.7	0.9	0	1.9	60.4	24.0	1.9
MS_3h	25.7	15.0	2.9	2.5	0	12.8	20.6	20.5	N/A
MS_1D	24.6	10.1	2.9	2.2	0.1	6.3	24.5	29.3	N/A
MS_3D	24.5	4.8	3.0	1.2	0	2.7	34.6	29.2	N/A
MS_7D	25.2	3.1	2.6	1.0	0.1	1.9	38.5	27.6	N/A
MS_28D	23.3	3.5	2.3	1.2	0.1	2.3	40.0	27.3	N/A
MS_90D	20.7	3.9	2.6	1.3	0	2.1	40.9	26.8	1.7
LS_3h	55.4	10.5	3.8	3.1	0	8.2	12.7	6.3	N/A
LS_1D	55.3	4.9	4.2	2.8	0.1	3.0	17.6	12.1	N/A
LS_3D	55.8	1.8	4.0	1.7	0.1	1.9	21.1	13.6	N/A
LS_7D	53.5	1.8	4.0	0.9	0.1	1.3	23.8	14.6	N/A
LS_28D	52.5	1.9	4.1	0.5	0.1	1.4	24.5	15	N/A
LS_90D	47.6	1.2	4.4	0.4	0.1	0.8	31.4	14.1	N/A

Backscattered electron images allowed the examination of phase distribution in the hydrated synthesized CSAB cements, as shown in Figures 6.14-6.16. The black areas represent pores and cracks. The dark gray background represents ettringite and the amorphous content (mainly AH_3), the dark gray particles represent unhydrated gypsum, the gray particles represent unhydrated $C_4A_3\overline{S}$, and the light gray particles represent unhydrated C_2S, as indicated in Figures 6.14-6.16. For the hydrated HS CSAB cement with high $C_4A_3\overline{S}$–C_2S ratio (Figure 6.14), substantial amounts of $C_4A_3\overline{S}$ and gypsum

remained unhydrated at 1 day of hydration. From 1–28 days of hydration, the amounts of $C_4A_3\overline{S}$ and gypsum decreased significantly. At 28 days of hydration, all the gypsum seemed to have reacted and only a few large $C_4A_3\overline{S}$ particles can be observed. Large $C_4A_3\overline{S}$ particles seemed to preferentially remain unhydrated. Moreover, rings were observed around the large unhydrated $C_4A_3\overline{S}$ particles starting at 3 days of hydration. Energy dispersive spectroscopy analysis showed that the rings had similar composition to the unhydrated $C_4A_3\overline{S}$ particles, perhaps indicating that the hydration of large $C_4A_3\overline{S}$ particles initiated from the outer layer but slowed down and became diffusion control after the paste developed a dense microstructure. The HS CSAB cement contained low C_2S content and small amount of C_2S remained unhydrated at 90 days of hydration. On the other hand, for the hydrated MS and LS CSAB cements with lower $C_4A_3\overline{S}$–C_2S ratios (Figures 6.15 and 6.16, respectively), at 1 day of hydration, substantial amounts of $C_4A_3\overline{S}$ and C_2S remained unhydrated; however, most of the gypsum seemed to have reacted and only a few gypsum particles can be observed. From 1–7 days of hydration, the amount of $C_4A_3\overline{S}$ decreased significantly and only a few large $C_4A_3\overline{S}$ particles can be observed at 7 days of hydration. Again, large $C_4A_3\overline{S}$ particles seemed to preferentially remain unhydrated. From 1–90 days of hydration, the amount of C_2S decreased and C_2S particles seemed to be reacting and breaking down. However, significant amount of C_2S remained unhydrated at 90 days of hydration. Hydration product development information shown in these images generally agrees with the quantitative X-ray diffraction results (Table 6.2).

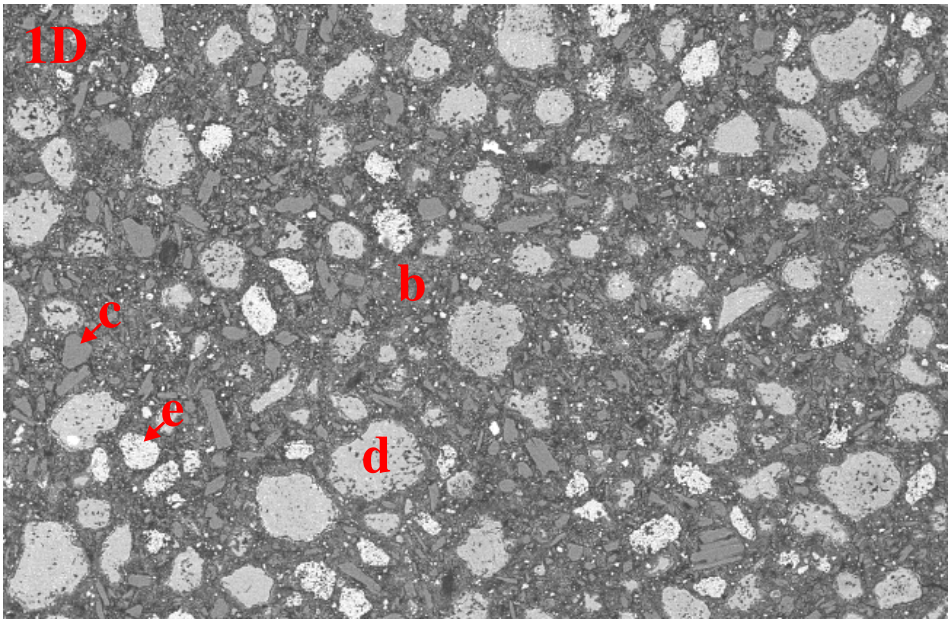
1D
b
c
e
d

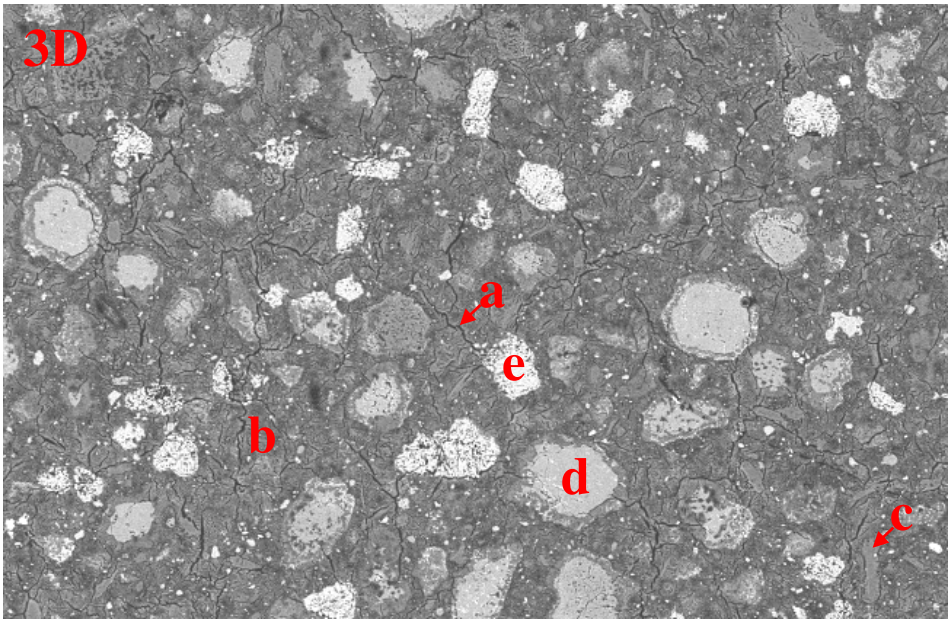
3D
a
e
b
d
c

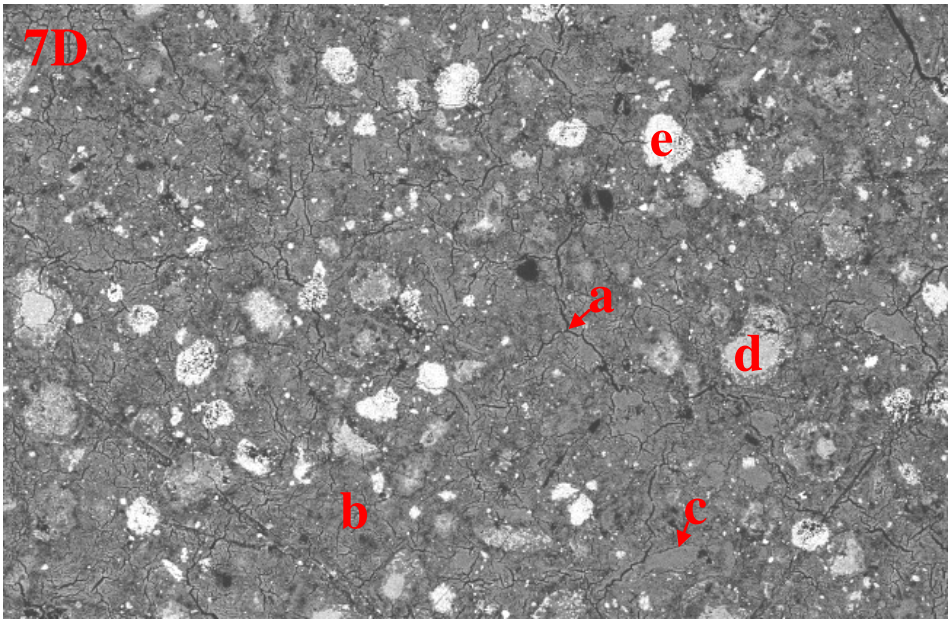
7D
e
a
d
b
c

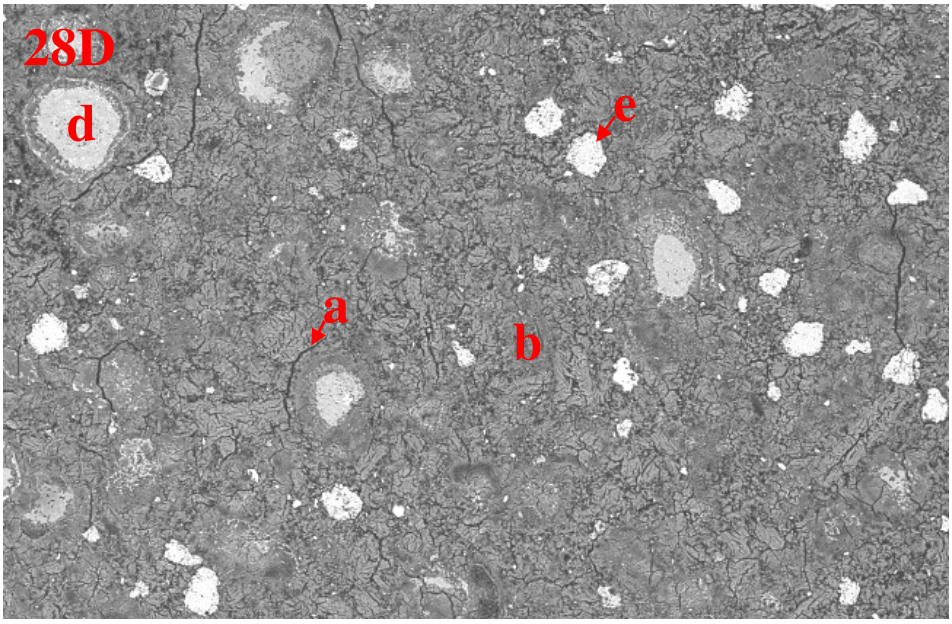
28D
d
e
a
b

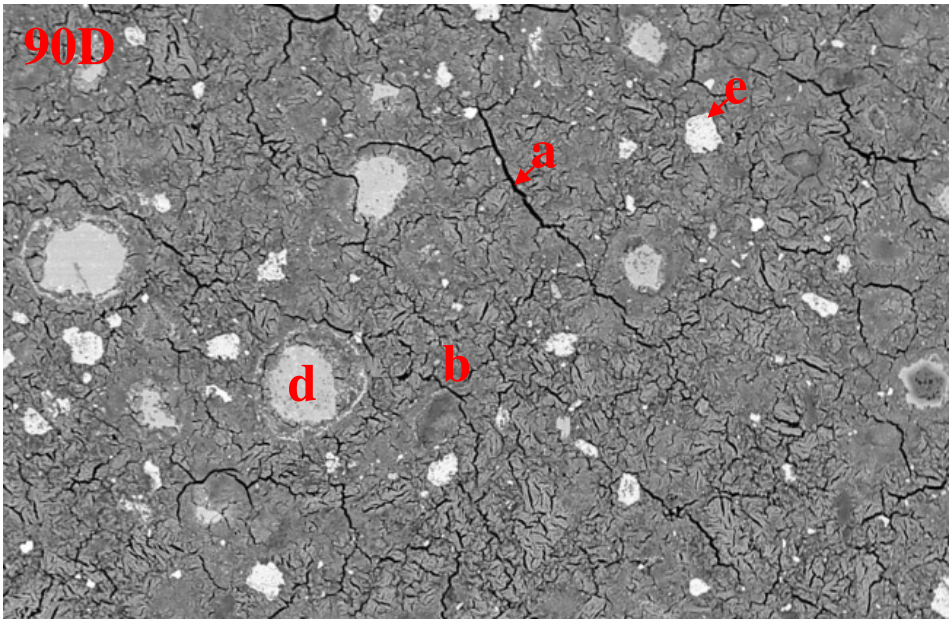

Figure 6.14 – Backscattered electron images for the hydrated HS CSAB cement from reagent-grade chemicals [a (black): pores and cracks, b (dark gray background): ettringite and amorphous content, c (dark gray particles): gypsum, d (gray): $C_4A_3\overline{S}$, and e (light gray): C_2S; field width: 1250 μm]

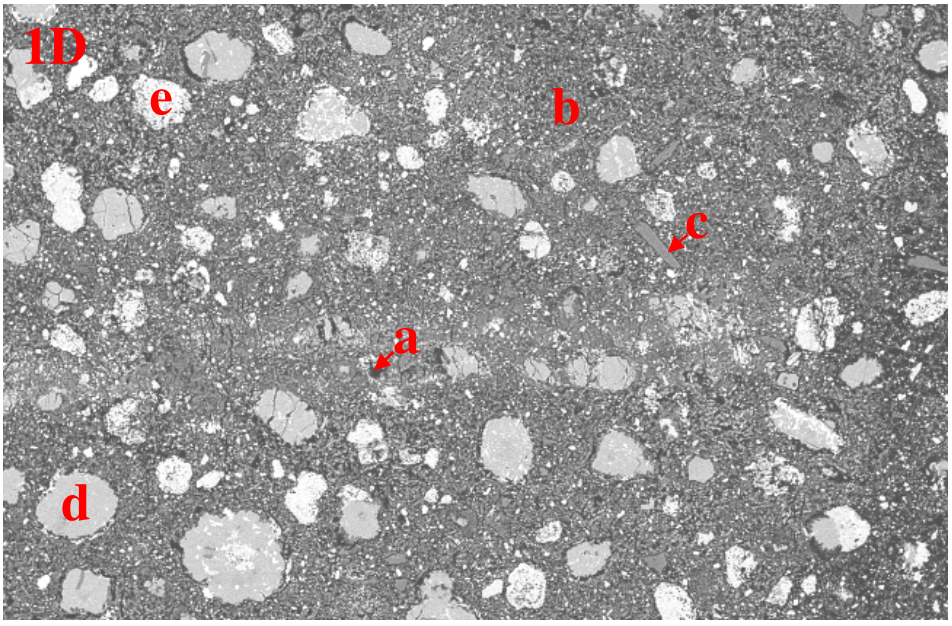

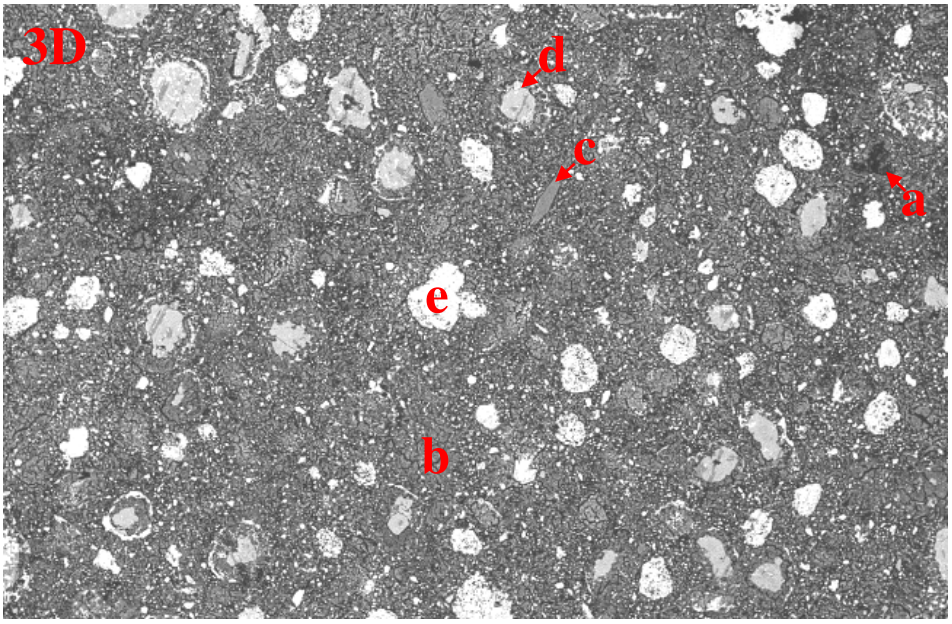
3D
d
c
a
e
b

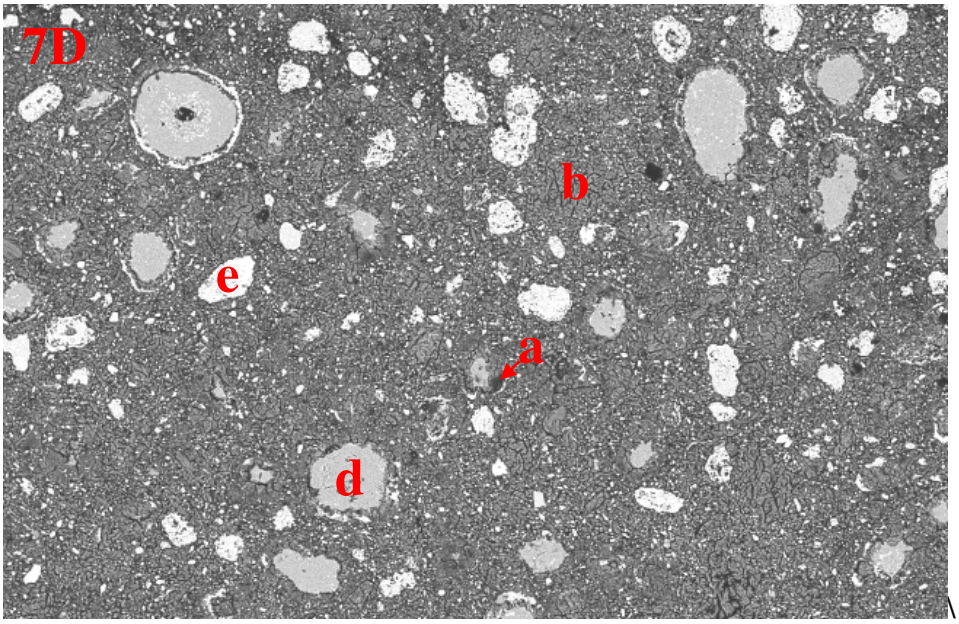
7D
b
e
a
d

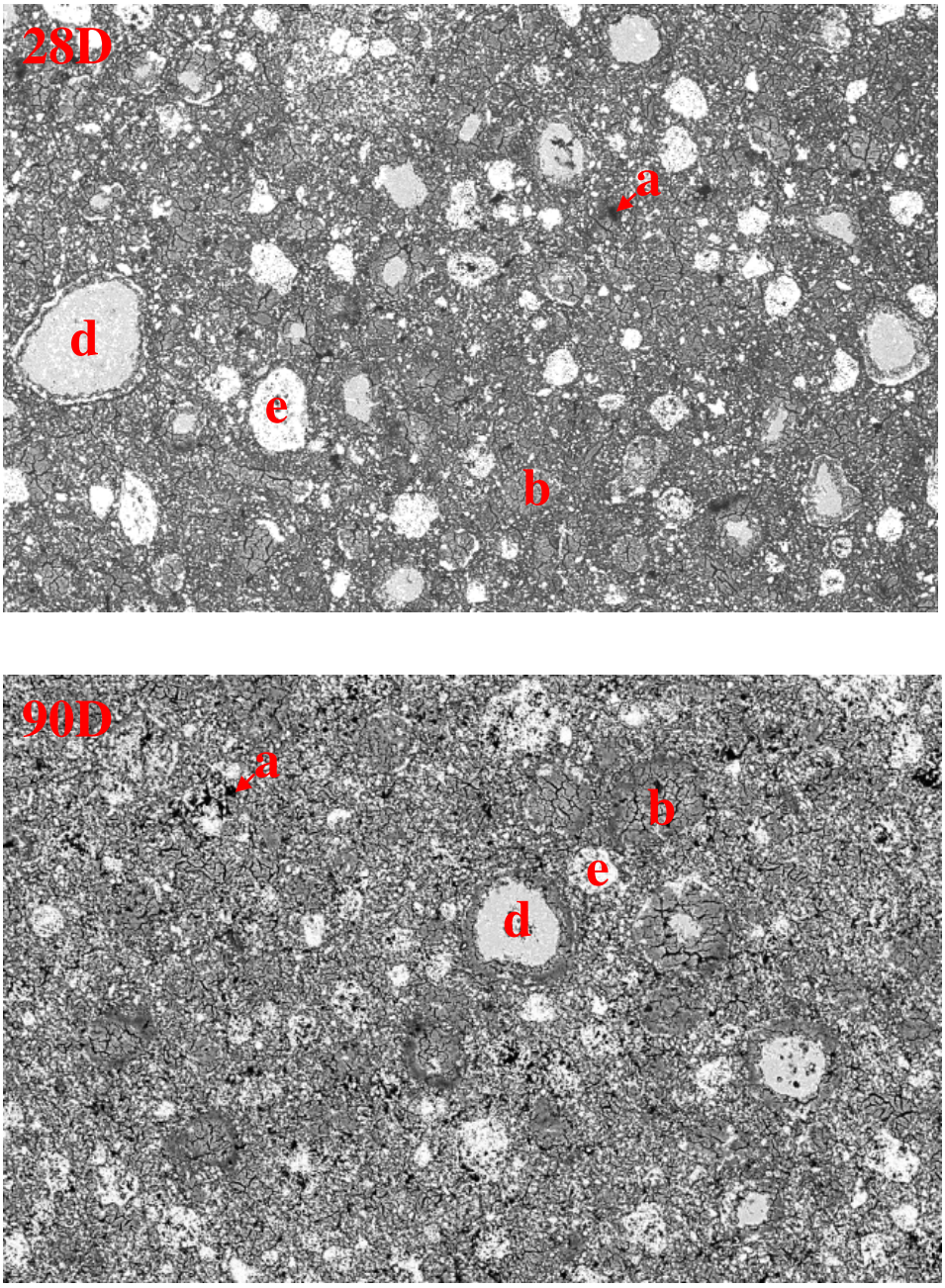

Figure 6.15 – Backscattered electron images for the hydrated MS CSAB cement from reagent-grade chemicals [a (black): pores and cracks, b (dark gray background): ettringite and amorphous content, c (dark gray particles): gypsum, d (gray): $C_4A_3\overline{S}$, and e (light gray): C_2S; field width: 1250 μm]

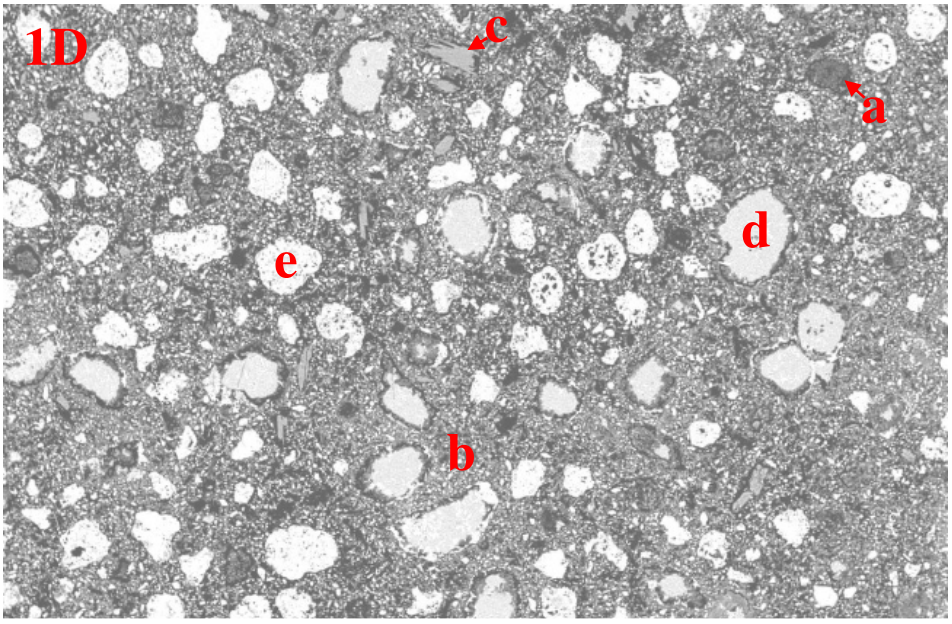
1D
c
a
d
e
b

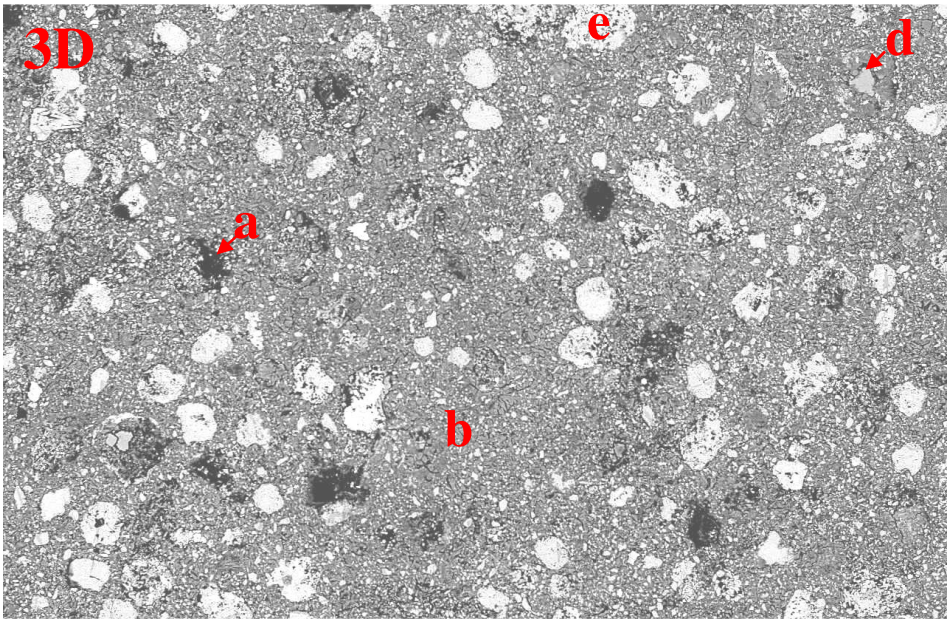
3D
e
d
a
b

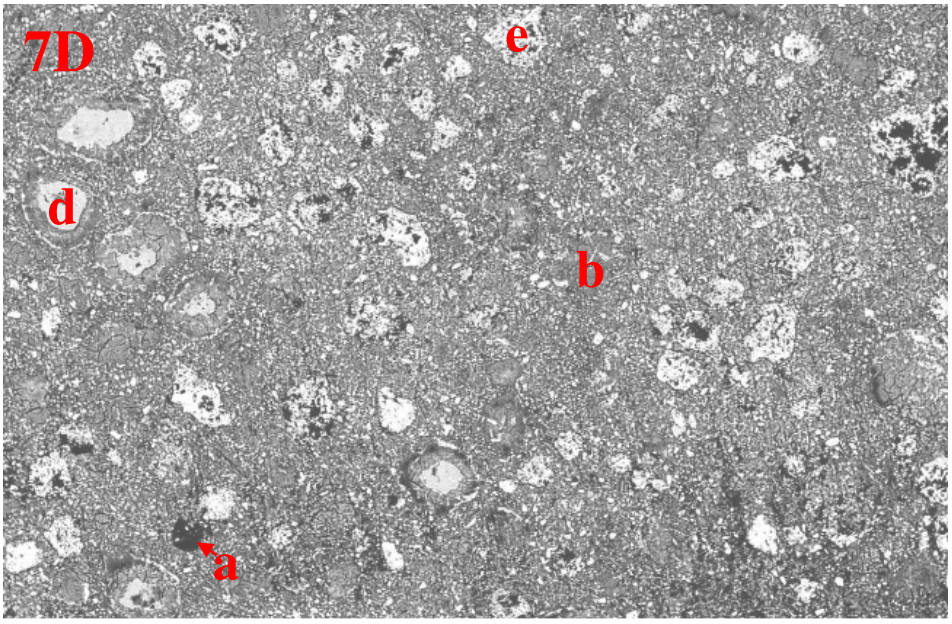
7D
e
d
b
a

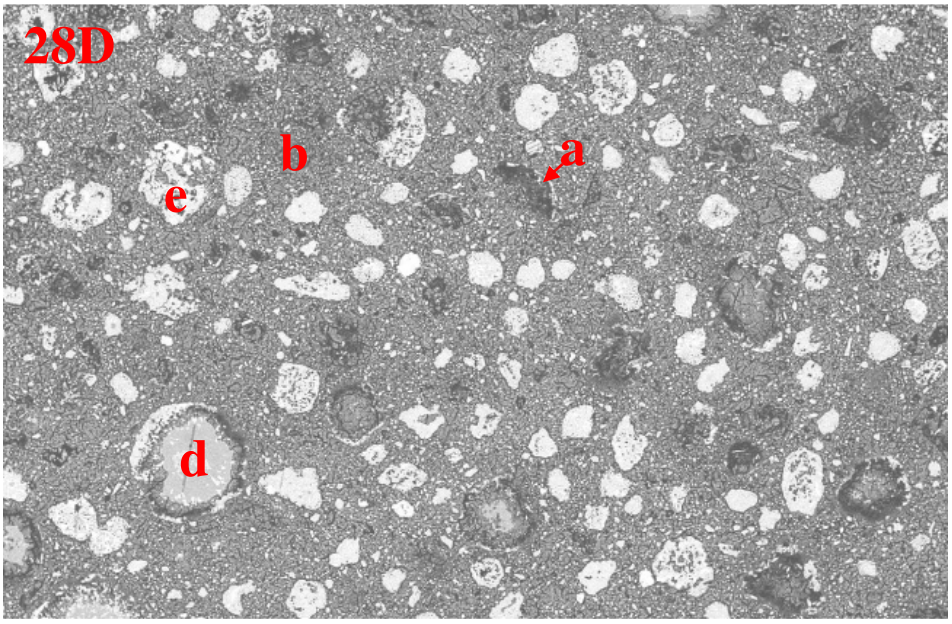
28D
b
a
e
d

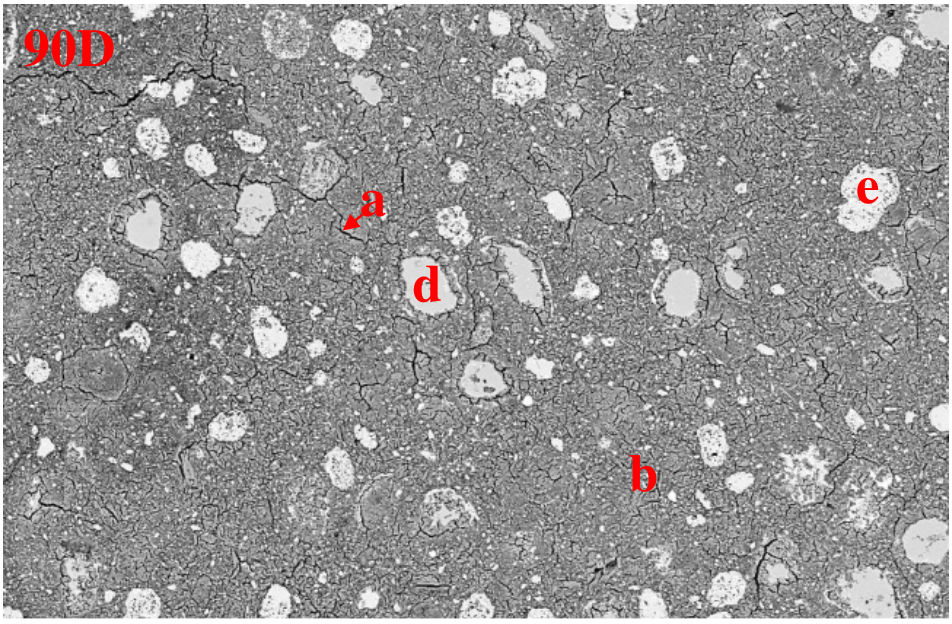

Figure 6.16 – Backscattered electron images for the hydrated LS CSAB cement from reagent-grade chemicals [a (black): pores and cracks, b (dark gray background): ettringite and amorphous content, c (dark gray particles): gypsum, d (gray): $C_4A_3\overline{S}$, and e (light gray): C_2S; field width: 1250 μm]

The microstructure of the hydrated HS and MS CSAB cements (Figure 6.14 and 6.15, respectively) seemed to be dense, indicating that ettringite and the amorphous content (mainly AH_3) were able to effectively fill in the space at early ages. However, the microstructure of the hydrated LS CSAB cement (Figure 6.16) seemed to be porous due to its low $C_4A_3\overline{S}$ content. Quantitative X-ray diffraction results (Table 6.2) show that 31.4% ettringite and 14.1% amorphous content formed in the LS CSAB cement compared to 60.4% and 40.9% ettringite, and 24.0% and 26.8% amorphous content formed in the HS and MS CSAB cements at 90 days of hydration, respectively.

Backscattered electron images for the hydrated HS CSAB cement with the highest $C_4A_3\overline{S}$ content (Figure 6.14) show significant cracking starting at 3 days of hydration perhaps due to the large amount of ettringite formed after cement hardened and caused

expansion (Ogawa and Roy, 1982). Quantitative X-ray diffraction results (Table 6.2) show that 21.4% ettringite formed from 3 h–3 days of hydration in the hydrated HS CSAB cement while only 14.0% and 8.4% ettringite formed in the MS and LS CSAB cements, respectively. Furthermore, 41.3% ettringite formed from 3 h–90 days of hydration in the HS CSAB cement while only 20.3% and 18.7% ettringite formed in the MS and LS CSAB cements, respectively.

6.3.3 Dimensional Stability

Dimensional stability in water results for the synthesized CSAB cements and a commercial Type I/II portland cement are shown in Figure 6.17. The HS CSAB cement that contained the highest $C_4A_3\overline{S}$ content expanded about 5% after demolding and curing in ultra-pure water for 3 days. The small bars slightly cracked after curing in ultra-pure water for 2 days. Figure 6.18 shows the picture of a cracked small bar made from the HS CSAB cement after demolding and curing in ultra-pure water for 6 days. On the other hand, the MS and LS CSAB cements that contained lower $C_4A_3\overline{S}$ contents showed limited expansion and were comparable to the commercial Type I/II portland cement.

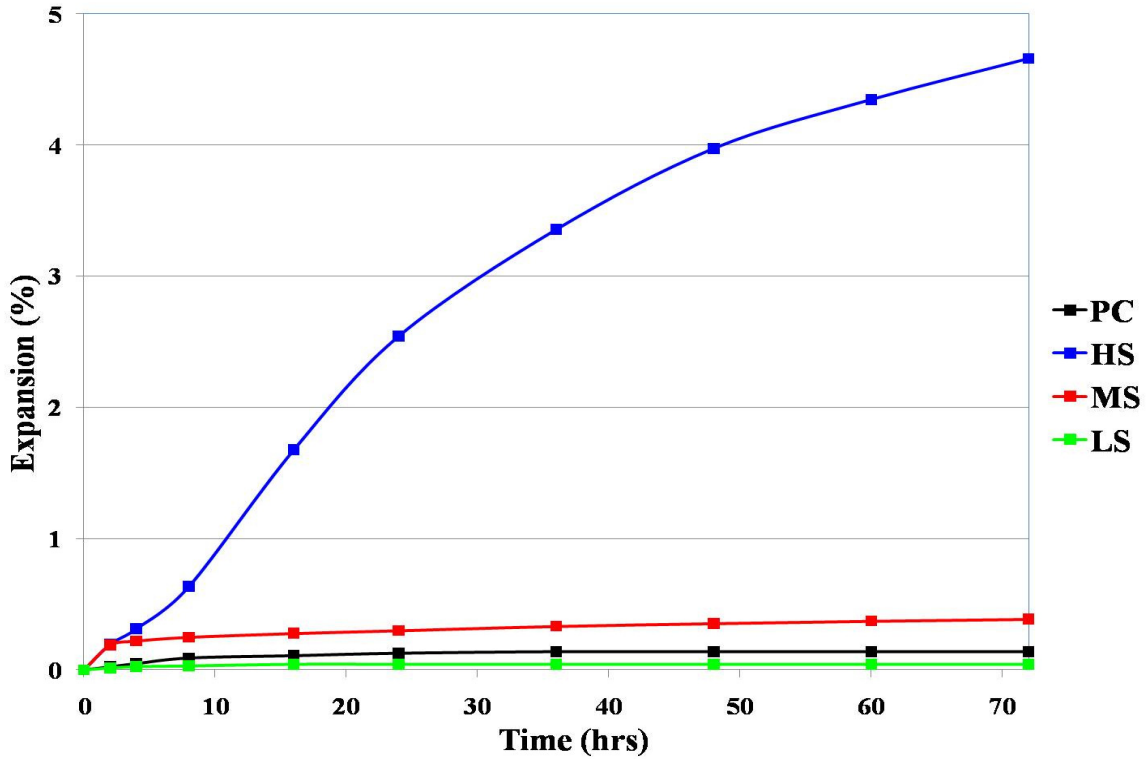

Figure 6.17 – Dimensional stability for a commercial Type I/II portland cement (PC) and the synthesized CSAB cements from reagent-grade chemicals cured in ultra-pure water after demolding at 1 day of hydration

Figure 6.18 – Picture of a slightly cracked small bar made from the HS CSAB cement from reagent-grade chemicals after 7 days of hydration

It is generally accepted in portland cement systems that expansion from ettringite formation happens when there is a significant amount of ettringite forming after cement hardens. Quantitative X-ray diffraction results (Table 6.2) show that about the same amount of ettringite formed in the HS and MS CSAB cements at 3 h of hydration (19.1% and 20.6%, respectively), which represents data from the systems close to setting. The amount of ettringite forming after cement hardened in the HS CSAB cement pastes is somewhat higher than that forming in the MS CSAB cement pastes, as 21.4% and 14.0% ettringite formed in the HS and MS CSAB cements from 3 h–3 days of hydration, respectively. However, given the large difference in expansion between the HS and MS CSAB cements, it does not appear that the difference in ettringite amounts could be the only determining factor. Therefore, the amorphous content (mainly AH_3) formed after cement hardened might also be a significant factor for expansion, as 14.9% and 8.7% amorphous content formed in the HS and MS CSAB cements from 3 h–3 days of hydration values, respectively. The 3-day values in Table 6.2 correspond to the amounts of ettringite and amorphous content in the samples at 48 h in Figure 6.17.

Glasser and Zhang (2001) showed that CSAB cement required a higher water-to-cement ratio for complete hydration than portland cement because the hydration reaction of $C_4A_3\overline{S}$ with gypsum in CSAB cement requires more water than the phases in portland cement. Therefore, it was hypothesized that perhaps the reason for the HS CSAB cement expanded and cracked during underwater curing was due to inadequate supply of mix water for complete hydration $C_4A_3\overline{S}$ during the first day. Quantitative X-ray diffraction results (Table 6.2) show that 14.6% $C_4A_3\overline{S}$ and 33.2% gypsum remained unhydrated at 1 day in the HS CSAB cement. In order to understand the effects of water-to-cement ratio on dimensional stability, the HS CSAB cement was tested using a higher water-to-cement ratio of 0.7 compared to the previous ratio of 0.45. However, the dimensional stability

results (Figure 6.19) show that the HS CSAB cement had about the same expansion after demolding and curing in ultra-pure water for 3 days using 0.45 and 0.7 water-to-cement ratios. Moreover, their small bars both slightly cracked after demolding and curing in ultra-pure water for 2 days. Therefore, the low water-to-cement ratio (0.45) was not the cause of the expansion and cracking observed in the HS CSAB cement.

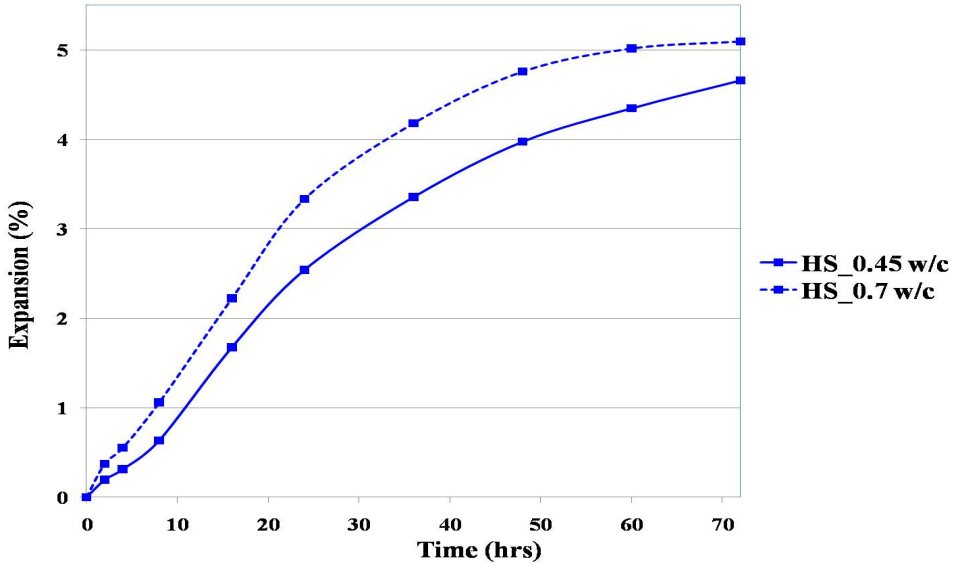

Figure 6.19 – Dimensional stability for the HS CSAB cement from reagent-grade chemicals using 0.45 and 0.7 water-to-cement ratio (w/c) cured in ultra-pure water after demolding at 1 day of hydration

Glasser and Zhang (2001) also showed that the dimensional stability of CSAB cement depended on the amount of gypsum available in the system. It was hypothesized that perhaps the optimal gypsum content determined through calorimetry in order to prevent formation of calcium monosulfoaluminate (discussed in section 6.3.1) was too high, thereby causing the expansion and associated cracking. In order to understand the effects of gypsum addition on dimensional stability, the HS CSAB cement clinker was tested with 10%, 15%, 20%, and 25% gypsum addition (with 25% being the optimum determined through isothermal calorimetry, Table 6.1). The dimensional stability results

(Figure 6.20) show that expansion for the HS CSAB cement clinker increased with increasing amount of gypsum added. The small bars for the CSAB cement clinker with 20% and 25% gypsum addition both slightly cracked after demolding and curing in ultra-pure water for 2 days.

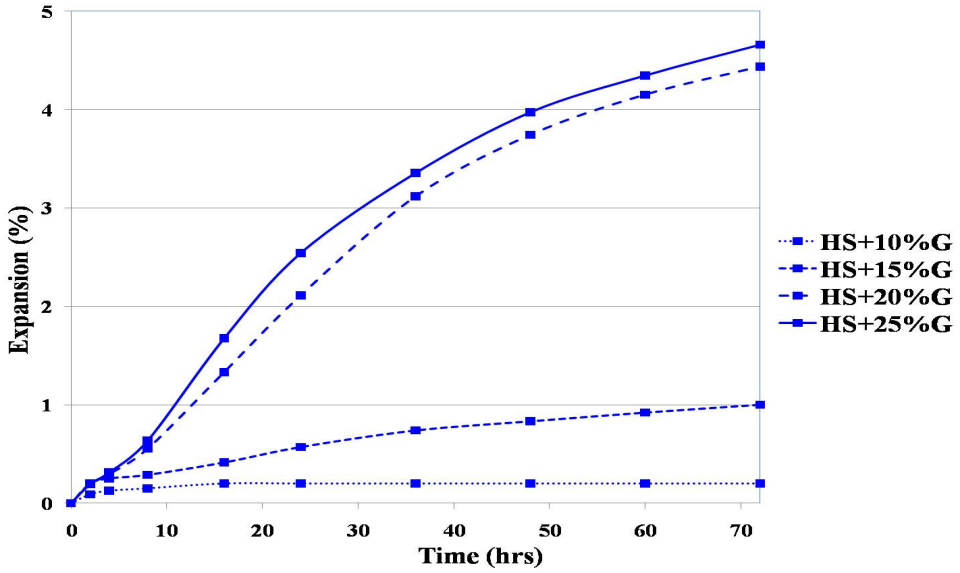

Figure 6.20 – Dimensional stability for the HS CSAB cement clinker synthesized from reagent-grade chemicals with different amounts of gypsum (G) addition cured in ultra-pure water after demolding at 1 day of hydration

In order to understand the mechanism for expansion, two cement paste samples were prepared from the HS CSAB cement clinker with 10% and 25% gypsum addition. Both samples were demolded at 1 day of hydration and cured in ultra-pure water from 1–7 days at room temperature. X-ray diffraction patterns (Figure 6.21) for the two cement paste samples show that less ettringite formed and more $C_4A_3\overline{S}$ remained unhydrated in the CSAB cement clinker with 10% gypsum addition, thereby explaining the decreased in expansion with decreasing amount of gypsum added. This phenomenon confirms to Wang et al.'s results (1992), which showed that the hydration reaction of $C_4A_3\overline{S}$ reached a lower degree of hydration with lower amounts of gypsum.

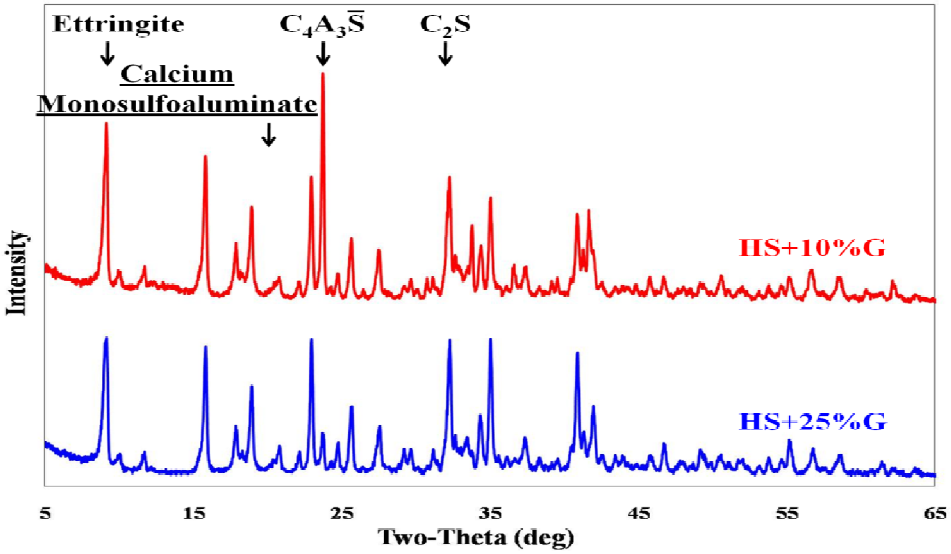

Figure 6.21 – X-ray diffraction patterns for the HS CSAB cement clinker with 10% and 25% gypsum (G) addition after 7 days of hydration; no calcium monosulfoaluminate formed

It is interesting to note that no calcium monosulfoaluminate formed even at very low amount of gypsum addition (10%), unlike in portland cement. Peng et al. (2006) showed that the transformation from ettringite to calcium monosulfoaluminate in portland cement after sulfate depletion had to overcome an energy barrier, which depended on the diffusion capability of aluminum ions. The transformation mostly took place at early ages before the development of a rigid microstructure. CSAB cement generally develops a denser microstructure at early ages compared to portland cement as shown by Bernardo et al. (2006). Therefore, aluminum ions might have a harder time diffusing, which stabilizes the unhydrated $C_4A_3\bar{S}$ and ettringite instead of forming calcium monosulfoaluminate. It should be noted, even though adding less gypsum than the optimal amount can improve dimensional stability, it might affect other property development in CSAB cement as more $C_4A_3\bar{S}$ remained unhydrated.

The lack of formation of calcium monosulfoaluminate in CSAB cement pastes, even at low gypsum additions (Figure 6.21), calls into question the typical assignment of peaks in calorimetry data. In portland cement systems, the additional heat evolution peak formed at gypsum addition lower than the optimal amount (even slightly lower), are typically described as representing the depletion of gypsum and subsequent formation of calcium monosulfoaluminate (Tenoutasse, 1968; Gaidis and Gartner, 1989). As shown in the rate of heat evolution results (Figures 6.1-6.3), these additional peaks are present in CSAB systems as well. However, they cannot represent the depletion of gypsum and the formation of calcium monosulfoaluminate because this phase does not form. The hydration mechanism associated with the additional heat evolution peak formation could be very complicated and requires further research. Minard et al. (2007) and Evju and Hansen (2001) showed that isothermal conduction calorimetry coupled with pore solution analysis and in situ X-ray diffraction, respectively, can provide detailed information of the hydration mechanism at early ages in portland cement system. These methods can be applied to CSAB cement system to better interpret the formation of the additional heat evolution peak and to understand its early-age hydration mechanism. Early-age hydration is of primary importance because of its implications in cement and concrete performance.

6.3.4 Sulfate Resistance

Sulfate resistance results for the synthesized CSAB cements and a commercial Type I/II portland cement after demolding and curing in ultra-pure water for 6 days are shown in Figure 6.22. The small bars for the HS CSAB cement that contained the highest $C_4A_3\overline{S}$ content had expanded and slightly cracked during curing in ultra-pure water, but remained intact when entering the sulfate resistance test (Figure 6.18).

However, the sulfate resistance results show that the HS CSAB cement expanded severely and the small bars completely failed after storing in 5% Na_2SO_4 solution for 5 days. On the other hand, the MS and LS CSAB cements that contained lower $C_4A_3\overline{S}$ contents showed no expansion and were comparable to the commercial Type I/II portland cement. Figure 6.23 shows pictures of the small bars made from the synthesized CSAB cements stored in 5% Na_2SO_4 solution; HS for 5 days, MS and LS for 90 days.

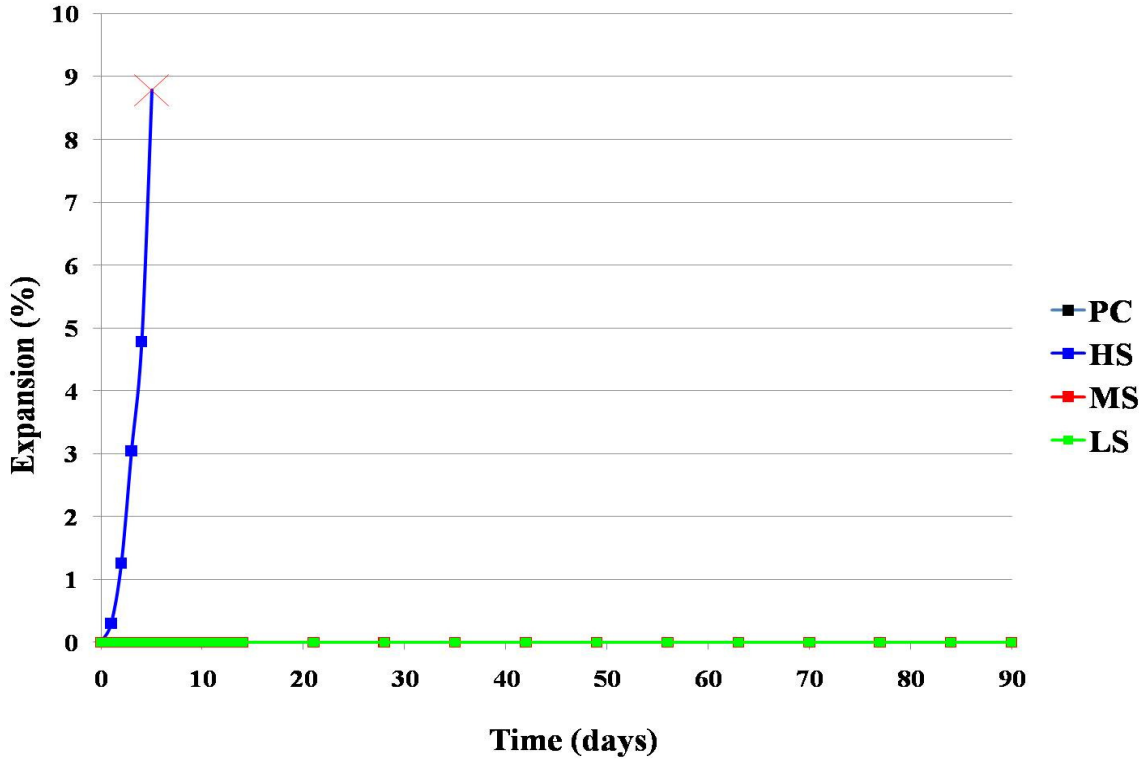

Figure 6.22 – Sulfate resistance for a commercial Type I/II portland cement (PC) and the synthesized CSAB cements from reagent-grade chemicals stored in 5% Na_2SO_4 solution after 7 days of hydration

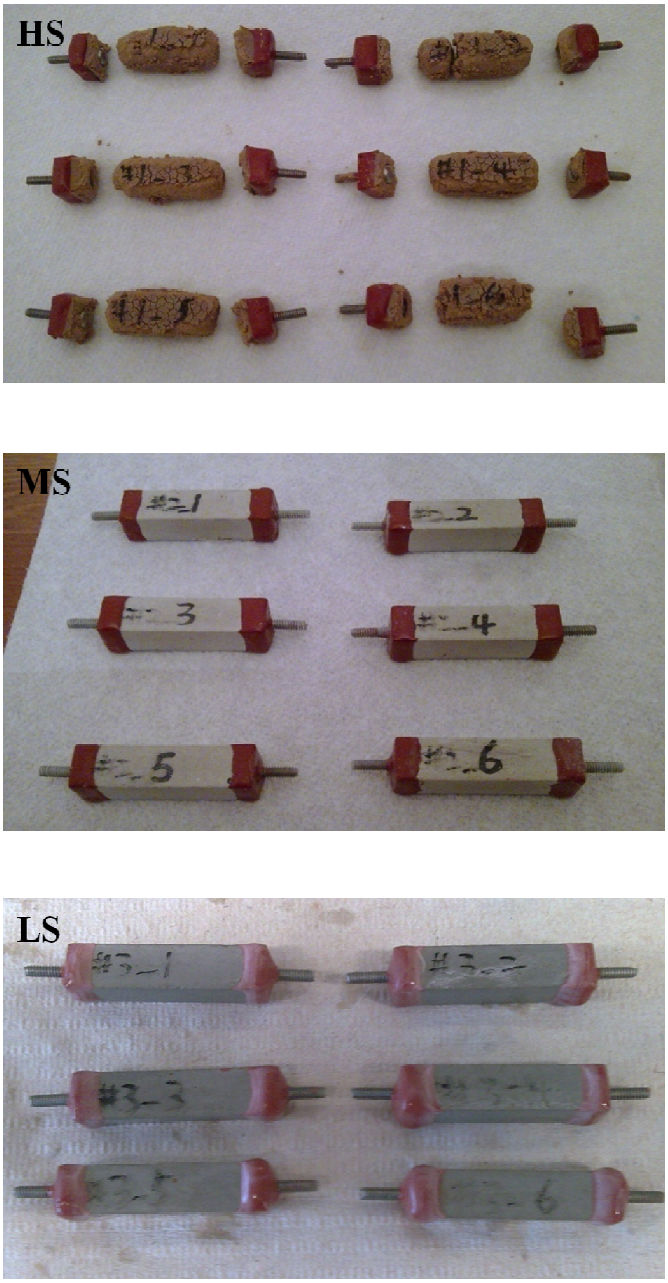

Figure 6.23 – Pictures of the small bars made from the synthesized CSAB cements from reagent-grade chemicals stored in 5% Na_2SO_4 solution; HS for 5 days (failed), MS and LS for 90 days

The hydrated HS CSAB cement contained no calcium monosulfoaluminate, as shown by quantitative X-ray diffraction (Table 6.2) and was not expected to expand in

the sulfate resistance test. In order to understand the mechanism for expansion, two cement paste samples were prepared from the HS CSAB cement. Both samples were demolded at 1 day of hydration and cured in ultra-pure water from 1–7 days at room temperature. One sample was continually stored in ultra-pure water from 7–10 days while the other was stored in 5% Na_2SO_4 solution. X-ray diffraction patterns for the two cement paste samples (Figure 6.24) show that more ettringite formed in the paste sample stored in 5% Na_2SO_4 solution than in the paste sample stored in ultra-pure water. The Na_2SO_4 solution accelerated the hydration reaction of the unhydrated $C_4A_3\overline{S}$ and gypsum contained in the hydrated HS CSAB cement to form ettringite and AH_3 and caused the severe expansion in the sulfate resistance test. Quantitative X-ray diffraction results (Table 6.2) show that the hydrated HS CSAB cement contained 3.9% $C_4A_3\overline{S}$ and 9.8% gypsum at 7 days of hydration.

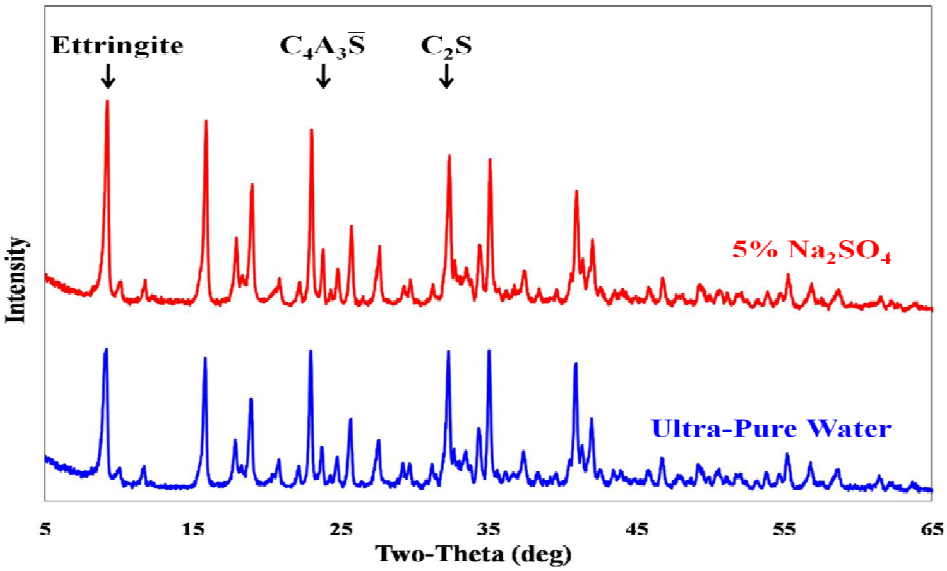

Figure 6.24 – X-ray diffraction patterns for the HS CSAB cement after 7 days of hydration and stored in 5% Na_2SO_4 solution and ultra-pure water for 3 days

In order to study the effects of water-to-cement ratio on sulfate resistance, the HS CSAB cement was tested using a higher water-to-cement ratio of 0.7 compared to the previous ratio of 0.45. The sulfate resistance results (Figure 6.25) show that the HS CSAB cement using 0.7 water-to-cement ratio expanded about 2% after curing and storing in 5% Na_2SO_4 solution for 7 days but stabilized afterwards, which was much less compared to the HS CSAB cement using 0.45 water-to-cement ratio (both had slightly cracked during curing in ultra-pure water). The microstructure of hydrated cement is more porous when using higher water-to-cement ratio and might be able to accommodate more ettringite and amorphous content (mainly AH_3) formation after cement hardens.

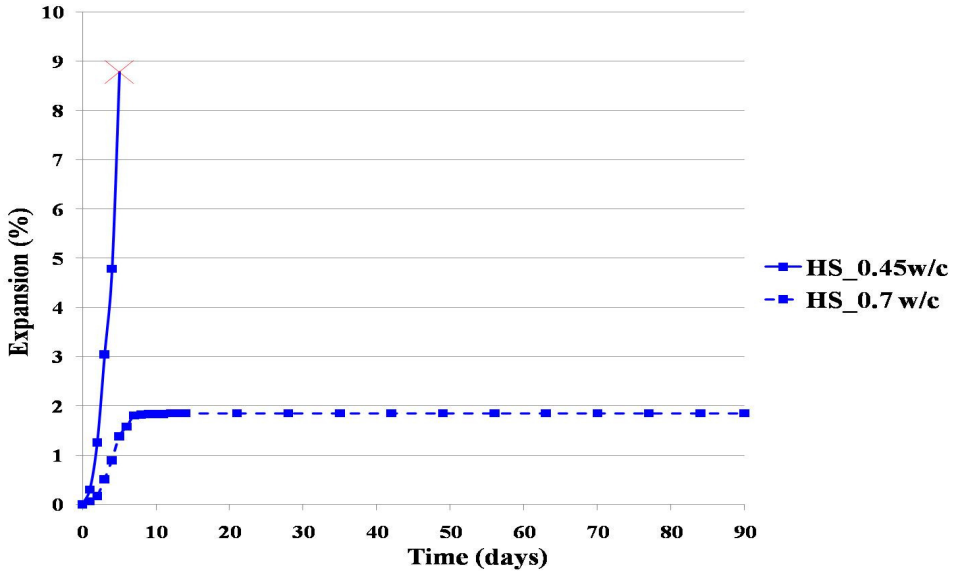

Figure 6.25 – Sulfate resistance for the HS CSAB cement from reagent-grade chemicals using 0.45 and 0.7 water-to-cement ratio (w/c) stored in 5% Na_2SO_4 solution after 7 days of hydration

The effects of gypsum addition on sulfate resistance for the HS CSAB cement clinker with 10%, 15%, 20%, and 25% gypsum addition were also investigated (with 25% being the optimum determined through isothermal calorimetry, Table 6.1). The sulfate resistance results (Figure 6.26) show that expansion for the HS CSAB cement

clinker increased with increasing amount of gypsum addition (20% and 25% gypsum addition had slightly cracked during curing in ultra-pure water). This is because with lower amounts of gypsum addition, less ettringite was able to form and more $C_4A_3\overline{S}$ remained unhydrated, as discussed in Section 6.3.3.

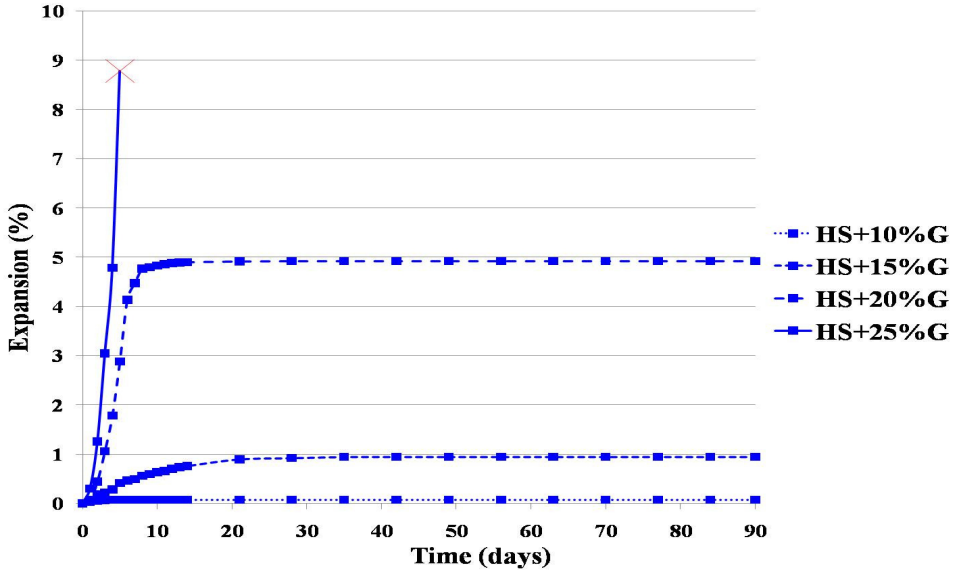

Figure 6.26 – Sulfate resistance for the HS CSAB cement clinker synthesized from reagent-grade chemicals with different amounts of gypsum (G) addition stored in 5% Na_2SO_4 solution after 7 days of hydration

Finally, the effects of type of sulfate solution on sulfate resistance for the HS CSAB cement were studied using 5% Na_2SO_4 and a saturated $CaSO_4$ solution. The sulfate resistance results (Figure 6.27) show that the HS CSAB cement had nearly no expansion after curing and storing in saturated $CaSO_4$ solution (had slightly cracked during curing in ultra-pure water), which might be caused by the different concentration of the sulfate solutions. The solubility of $CaSO_4$ in water is much lower than that of Na_2SO_4. On the other hand, Jawed and Skalny (1978) showed that alkalis increased the dissolution rate of the aluminate phases in portland cement. Therefore, it might possibly be the sodium ions in Na_2SO_4 solution that caused the acceleration of the unhydrated

$C_4A_3\overline{S}$ and gypsum contained in the hydrated HS CSAB cement to form ettringite and AH_3 and resulted in the severe expansion in the sulfate resistance test.

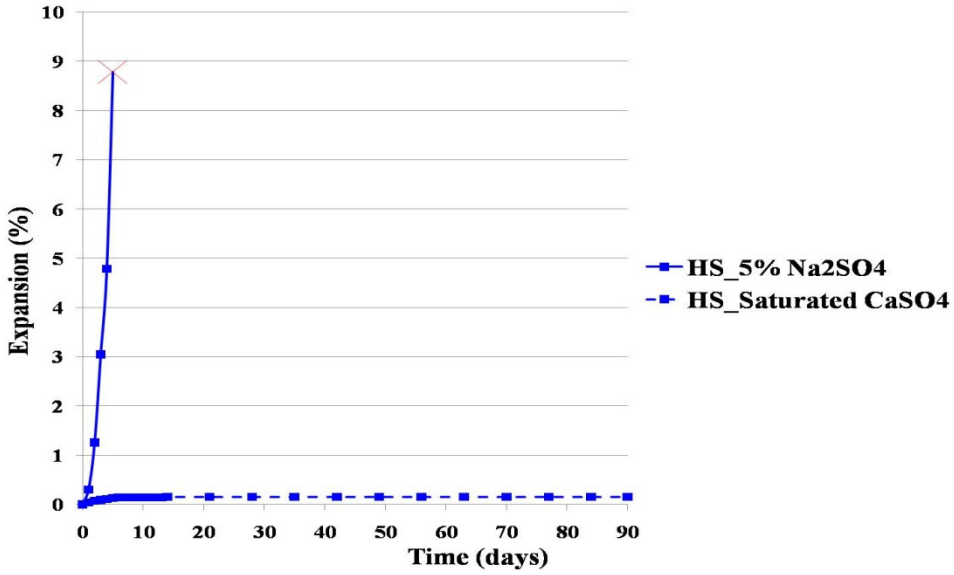

Figure 6.27 – Sulfate resistance for the HS CSAB cement from reagent-grade chemicals stored in 5% Na_2SO_4 solution and saturated $CaSO_4$ solution after 7 days of hydration

6.3.5 Compressive Strength Development

Compressive strength results for the synthesized CSAB cements and a commercial Type I/II portland cement are shown in Figure 6.28. The results show that the HS CSAB cement developed high compressive strength at 1 day due to its high fast-reacting $C_4A_3\overline{S}$ content; however, no significant strength gained was shown from 1–7 days because the large amounts of ettringite and amorphous content (mainly AH_3) formed after cement hardened caused expansion and therefore affected compressive strength development, as shown in the hydration product development and the dimensional stability results (Table 6.2 and Figure 6.14, and Figure 6.22, respectively). The LS CSAB cement showed sluggish compressive strength development due to its low $C_4A_3\overline{S}$ –C_2S ratio. The slow-reacting C_2S remained mostly unhydrated even at later ages, as

shown in the quantitative X-ray diffraction results (Table 6.2), and did not seem to contribute significantly to the long-term compressive strength development. The MS CSAB cement that contained medium $C_4A_3\overline{S}$ and C_2S contents showed good compressive strength development and was comparable to the commercial Type I/II portland cement.

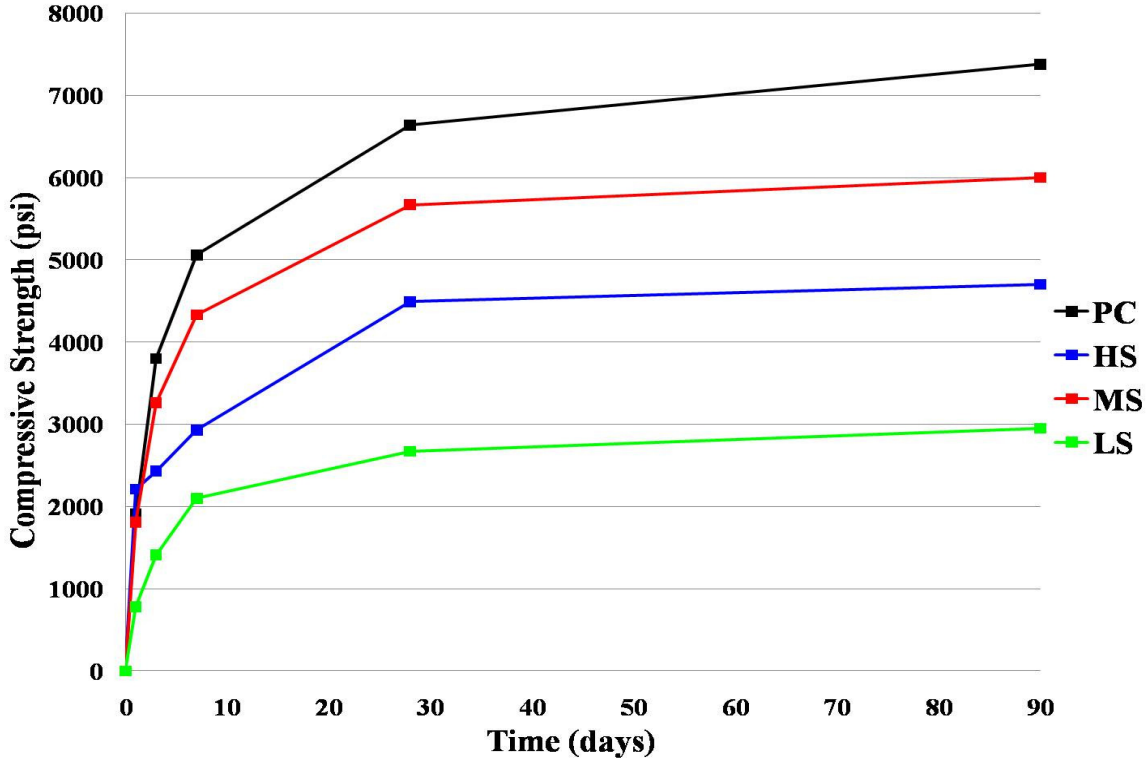

Figure 6.28 – Compressive strength development for a commercial Type I/II portland cement (PC) and the synthesized CSAB cements from reagent-grade chemicals

6.4 CONCLUSION

Rate of heat evolution and cumulative heat results showed that the optimum gypsum contents for the CSAB cement clinkers synthesized from reagent-grade chemicals mainly depended on their $C_4A_3\overline{S}$ contents. Optimum gypsum content (percentage of cement) was defined as the lowest amount of gypsum that produced only

one main heat evolution peak in calorimetry while the shape of the main heat evolution peak no longer changes with gypsum addition higher than the optimal amount. Furthermore, the CSAB cement clinkers showed the highest cumulative heat with their optimum gypsum contents added. Equation 6.3 was developed to predict the optimum gypsum content based on the phase composition of CSAB cement clinker. However, the additional heat evolution peak formed at gypsum addition lower than the optimal amount (even slightly lower) was not because of the depletion of gypsum and the formation of calcium monosulfoaluminate. The hydration mechanism associated with the additional heat evolution peak formation could be very complicated and requires further research. Isothermal conduction calorimetry coupled with pore solution analysis and in situ X-ray diffraction should be able to provide more detailed information of the early-age hydration mechanism of CSAB cement system. Early-age hydration is of primary importance because of its implications in cement and concrete performance.

The synthesized CSAB cements (defined as clinkers with their optimum gypsum contents added) with higher $C_4A_3\overline{S}$ contents had higher maximum rates of heat evolution and cumulative heat than the CSAB cements with lower $C_4A_3\overline{S}$ contents. Hydration product development results from X-ray diffraction for the synthesized CSAB cements showed that $C_4A_3\overline{S}$ and gypsum reacted quickly and contributed to the formation of ettringite and amorphous AH_3. Most of the $C_4A_3\overline{S}$ and gypsum reacted by 7 days of hydration. However, C_2S remained mostly unhydrated at 90 days of hydration in all the synthesized CSAB cements.

Results of dimensional stability testing in water showed that the HS CSAB cement (with the highest $C_4A_3\overline{S}$ content) expanded and slightly cracked perhaps due to the large amounts of ettringite and amorphous content (mainly AH_3) that formed after cement hardened. However, the MS and LS CSAB cements that contained lower $C_4A_3\overline{S}$

contents showed limited expansion and were comparable to the commercial Type I/II portland cement.

Sulfate resistance results showed that the HS CSAB cement that contained the highest $C_4A_3\overline{S}$ content expanded severely and failed after storing in 5% Na_2SO_4 solution for 5 days. However, the MS and LS CSAB cements that contained lower $C_4A_3\overline{S}$ contents showed no expansion and were comparable to the commercial Type I/II portland cement. It is thought that it is the sodium ions in the Na_2SO_4 solution accelerated the hydration reaction of the unhydrated $C_4A_3\overline{S}$ and gypsum contained in the hydrated HS CSAB cement to form ettringite and amorphous AH_3 and caused the severe expansion.

Finally, compressive strength results showed that the HS CSAB cement that contained the highest $C_4A_3\overline{S}$ content developed high compressive strength at 1 day of hydration; however, no significant strength gained was shown from 1–7 days because of the large amounts of ettringite and amorphous content (mainly AH_3) formed after cement hardened caused expansion and therefore affected compressive strength development. The LS CSAB cement showed sluggish compressive strength development due to its low $C_4A_3\overline{S}$ –C_2S ratio. The slow-reacting C_2S remained mostly unhydrated even at later ages and did not seem to contribute significantly to the long-term compressive strength development. However, the MS CSAB cement that contained medium $C_4A_3\overline{S}$ and C_2S contents showed good compressive strength development and was comparable to the commercial Type I/II portland cement. The MS CSAB cement that contained medium $C_4A_3\overline{S}$ and C_2S contents also showed good dimensional stability and sulfate resistance, and was therefore considered the optimum phase composition for CSAB cement in terms of comparable performance characteristics to portland cement.

Chapter 7: Calcium Sulfoaluminate-Belite Cement: Incorporation of Waste Materials

7.1 INTRODUCTION

A potential problem facing the widespread adoption and production of CSAB cement is the cost and availability of alumina bearing raw materials such as bauxite. Therefore, it is desirable to find alternative raw materials to keep costs competitive. If the raw materials are waste products of other industries, the environmental benefit of CSAB cement becomes even greater than simply a reduction in energy usage and CO_2 emissions because the cement becomes a useful repository for waste materials that would otherwise enter landfills. Furthermore, incorporating waste materials high in CaO rather than $CaCO_3$ further reduces energy consumption and CO_2 emissions, thereby further reducing the environmental impact.

As reported in Chapter 6, the MS CSAB cement synthesized from reagent-grade chemicals with medium $C_4A_3\overline{S}$ and C_2S contents showed good dimensional stability, sulfate resistance, and compressive strength, and was considered the optimum phase composition for CSAB cement. Therefore, CSAB cement clinkers were then synthesized from suitable natural and waste materials proportioned for a target phase composition according to the MS CSAB cement clinker. The synthetic clinkers from natural and waste materials were ground into fine powder form and tested for particle fineness and particle size distribution, phase composition, and phase distribution by Blaine fineness and laser light scattering particle size distribution analysis, X-ray diffraction, and scanning electron microscopy, respectively. Different amounts of gypsum were added to the synthetic clinkers and the resulting cements were tested for heat evolution rate using isothermal conduction calorimetry to study their optimum gypsum contents and early-age

hydration behavior. The synthesized CSAB cements from waste materials containing their optimum gypsum contents were monitored for hydration product development using X-ray diffraction and scanning electron microscopy. Phase composition and phase distribution information for the hydrated synthesized cements were collected. Finally, dimensional stability, sulfate resistance, and compressive strength development for the synthesized cements were studied. The results were compared to the MS CSAB cement synthesized from reagent-grade chemicals and a commercial Type I/II portland cement. The final goals were to produce satisfactory CSAB cements with minimal limestone and bauxite contents and maximal waste material content, and to evaluate the effects of impurities from the natural and waste materials on phase formation, hydration chemistry, and properties.

7.2 MATERIALS SELECTION AND PROPORTIONING

The natural and waste materials used to synthesize CSAB cement clinkers were limestone (Texas Lehigh Cement), bauxite (C-E Minerals), flue gas desulfurization sludge (Boral Material Technologies), Class C fly ash (Headwaters/ISG; ASTM C 618, 2005), and fluidized bed ash (Tucson Electric Power); their oxide compositions from X-ray fluorescence analysis are shown in Table 7.1. The reason for using flue gas desulfurization sludge, Class C fly ash and fluidized bed ash was because of their high CaO, Al_2O_3, or SO_3 contents. The Class C fly ash and fluidized bed ash chosen had high CaO contents instead of $CaCO_3$, which could reduce CO_2 emissions from cement manufacturing. Moreover, Class C fly ash and fluidized bed ash are less used in concrete as supplementary cementing materials to directly replace a portion of the portland cement in concrete than Class F fly ash. High calcium Class C fly ash has shown to be less effective to promote pozzolanic reaction in portland cement concrete than low calcium

Class F fly ash (Mehta and Monteiro, 2005). Furthermore, fluidized bed ash had a high sulfur content, which could cause durability problems in portland cement concrete (Neville, 2004).

Table 7.1 – Chemical compositions for the natural materials and industrial waste materials used

Oxide	**Amount in Sample (weight %)**				
	Limestone	***Bauxite***	***Flue Gas Desulfurization Sludge***	***Class C Fly Ash***	***Fluidized Bed Ash***
SiO_2	5.95	6.21	2.81	33.58	21.27
Al_2O_3	1.69	85.88	0.15	18.51	11.23
Fe_2O_3	0.64	2.16	0.16	6.56	3.50
CaO	49.02	0.47	37.87	27.08	37.74
MgO	0.94	0.15	0.21	6.10	3.70
Na_2O	0.07	0.06	0.09	1.89	1.99
K_2O	0.29	0.19	0.02	0.39	0.39
TiO_2	0.04	4.04	0.00	1.34	0.80
MnO_2	0.02	0.02	0.00	0.03	0.01
P_2O_5	0.08	0.25	0.01	1.15	0.91
SrO	0.07	0.09	0.01	0.48	0.21
BaO	0.02	0.00	0.02	0.74	0.43
SO_3	0.77	0.00	52.02	1.83	10.23
LOI*	40.39	0.49	6.63	0.34	7.54
Moisture	0.49	0.05	0.30	0.07	0.44

*LOI is mass lost on ignition to 750°C

Two CSAB cement clinkers were synthesized according to the phase composition of the MS CSAB cement clinker synthesized from reagent-grade chemicals. Materials

were proportioned using the adapted Bogue method for CSAB cement clinker developed in Chapter 5 including impurity contents, as shown in Equations 7.1-7.7:

$$\%C_4AF = 3.043(\%Fe_2O_3) \quad (7.1)$$

$$\%C_4A_3\overline{S} = 1.995(\%Al_2O_3) - 1.273(\%Fe_2O_3) \quad (7.2)$$

$$\%C_2S = 2.867(\%SiO_2) \quad (7.3)$$

$$\%C\overline{S} = 1.700(\%SO_3) - 0.445(\%Al_2O_3) + 0.284(\%Fe_2O_3) \quad (7.4)$$

$$\%C = 1.000(\%CaO) - 1.867(\%SiO_2) - 1.054(\%Fe_2O_3) - 0.550(\%Al_2O_3) - 0.700(\%SO_3) \quad (7.5)$$

$$\%M = 1.000(\%MgO) \quad (7.6)$$

$$\%\text{Other Impurities} = 1.000(\%\text{Other Impurities}) \quad (7.7)$$

The proportions of raw ingredients for the two CSAB cement clinkers are shown in Table 7.2. The MC CSAB cement clinker was synthesized from limestone, bauxite, flue gas desulfurization sludge, and Class C fly ash while the MF CSAB cement clinker was synthesized from limestone, bauxite, flue gas desulfurization sludge, and fluidized bed ash. Waste materials composed 30% and 41% of the raw ingredients for the MC and MF CSAB cement clinkers, respectively.

Table 7.2 – Proportion of raw ingredients for the CSAB cement clinkers synthesized from Class C fly ash (MC) and fluidized bed ash (MF)

Raw Materials	**Proportion of Materials (weight %)**	
	MC	***MF***
Limestone	56	45
Bauxite	14	14
Flue Gas Desulfurication Sludge	10	6
Class C Fly Ash	20	0
Fluidized Bed Ash	0	35

7.3 SYNTHESIS

The laboratory synthesis processes mimicked the processes that take place in industrial manufacturing, only on a much smaller scale. The proportioned raw ingredients were dispersed in ultra-pure water (1:2 ratio) and mixed using a rotary jar mill (U.S. Stoneware) for 8 h at 120 rpm in an HDPE bottle using 5-15 mm sphere high-purity ZrO_2 (Y_2O_3 stabilized) grinding media (Richerson, 1992). The solution was poured in a steel pan and dried in a 105˚C oven for 72 h. The resulting product was hand-crushed into fine powder form using a mortar and pestle. The raw ingredients were then placed in alumina crucibles and fired in an electric muffle furnace (Sentrotech). Two cycles of firing were run, with a 5˚C/min heating rate and a 2˚C/min cooling rate. In the first cycle, the raw ingredients were fired at 850˚C for 4 h to dehydrate and calcine the raw ingredients. Intermediate grinding by hand was performed between cycles to homogenize the raw ingredients. In the second cycle, covers were applied to the alumina crucibles to prevent sulfur emissions and the raw ingredients were fired at 1250˚C for 12 h. The firing time in the furnace was much longer compared to the firing time in a rotary kiln used in industrial manufacturing because the raw ingredients remained stationary

inside the crucibles during the firing process, which prevented materials from efficiently reacting with each other. Finally, the resulting clinker was ground into fine powder form using a micro mill grinder (Scienceware/Bel-Art).

7.4 ANALYSIS

7.4.1 Particle Fineness and Particle Size distribution

The ground synthetic clinkers from natural and waste materials were tested by an air-permeability test, called Blaine fineness, according to ASTM C 204 (2007) to assure uniform median particle fineness before testing with the laser light scattering particle size distribution analysis. Blaine fineness measures the rate of air passing thorough pressed powder and is the most common technique used by cement manufacturers to measure cement fineness. A laser light scattering particle size distribution analyzer (Fritsch Analysette 22) was used to study the particle size distribution for the CSAB cement clinkers (Ferraris et al., 2006). Both the Blaine fineness and the particle size distribution results were compared to the MS CSAB cement clinker synthesized from reagent-grade chemicals and a commercially-produced Type I/II portland cement (TXI Hunter).

7.4.2 X-Ray Diffraction

X-ray diffraction (Siemens D500 Powder Diffractometer; Cu $K_{\alpha 1}$, λ=1.5046 Å) was used to determine phase compositions for the CSAB cement clinkers and the hydrated synthesized CSAB cements from natural and waste materials (water-to-cement ratio of 0.45) at 3 h, 1, 3, 7, 28, and 90 days hydration. The synthesized cements were cast in plastic cups using a water-to-cement ratio of 0.45, demolded at 1 day of hydration, and stored in ultra-pure water at room temperature until testing. Hydration of the synthesized cements was stopped using ethanol and a vacuum dessicator. The instrument was operated under 40 keV and 30 mA, the step size used was 0.02˚/6 sec, and the scan

range used was 10˚-80˚ 2θ for the synthetic clinkers and 5˚-70˚ 2θ for the hydrated synthesized cements. 10% rutile (TiO_2) was ground into the hydrated synthesized cements to serve as an internal standard in order to quantify their amorphous contents. Qualitative information for the phases present in the CSAB cement clinkers was obtained using the Hanawalt manual and the Jade program (MDI) (JCPDS–International Centre for Diffraction Data, 1989). Quantitative information was collected using Rietveld analysis (accuracy about 1%) by fitting the lattice parameters of the phases present in the synthetic clinkers to their X-ray diffraction patterns, which was performed with TOPAS-Academic software (Bruker AXS) (Young, 1995; Stutzman and Leigh, 2002).

7.4.3 Scanning Electron Microscopy

Scanning electron microscopy (JEOL JSM-5610 SEM) was used to study phase distribution in the CSAB cement clinkers and the hydrated synthesized CSAB cements from natural and waste materials. Test samples for the synthetic clinkers were prepared by mixing the ground synthetic clinkers with optical-grade epoxy and casting in cylindrical epoxy sample disks that had four holes drilled into the surface. Test samples for the hydrated synthesized cements were prepared by placing a paste at the bottom of a cylindrical mold (30 mm diameter). 1, 3, 7, 28, and 90 day old paste samples were prepared. The synthesized cements were cast in plastic cups using a water-to-cement ratio of 0.45, demolded at 1 day of hydration, and stored in ultra-pure water at room temperature until testing. Hydration of the synthesized cements was stopped using ethanol and a vacuum dessicator. Optical-grade epoxy was then slowly poured in the cylindrical mold to cover the paste. Both the synthetic clinker and hydrated synthesized cement sample were then placed under vacuum to draw the remaining air out of the samples and were brought back to atmospheric pressure to allow epoxy to fill in the voids

of the paste. The samples were then cured in a 40˚C oven for 24 hrs, and the surface was polished and coated with silver before backscattered electron imaging and compositional examination by energy dispersive spectroscopy (Stutzman, 2004).

7.4.4 Isothermal Conduction Calorimetry

The heat produced by cementitious materials in exothermic hydration reactions is a good indication of their early-age hydration behavior (Gartner et al., 2002). The CSAB cement clinkers from natural and waste materials were made into cements by adding different amounts of gypsum (99% $CaSO_4 \cdot 2H_2O$; Arcos) to control the hydration reaction of $C_4A_3\overline{S}$. The resulting cements were tested for heat evolution rate using isothermal conduction calorimetry (Thermometric TAM Air) to determine the gypsum contents (percentage of cement) and to study early-age hydration behavior. Hydration was evaluated for 3 days at 23˚C using a water-to-cement ratio of 0.45. The results were compared to the MS CSAB cement synthesized from reagent-grade chemicals and a commercially-produced Type I/II portland cement (TXI Hunter Cement).

7.4.5 Dimensional Stability and Sulfate Resistance

Dimensional stability and sulfate resistance for the synthesized CSAB cements from natural and waste materials with 1% citric acid addition (retarder) were tested by adopting a new test method for concrete sulfate resistance developed at the National Institute of Standard and Technology (Ferraris et al. 2006). Small bars (40×10×10 mm) were made from the synthesized cement using a water-to-cement ratio of 0.45, demolded at 1 day of hydration, and cured in ultra-pure water from 1 to 7 days of hydration at room temperature. Dimensional stability of the synthesized CSAB cements was tested by measuring expansion of the small bars from 1 to 4 days of hydration.

At 7 days of hydration, two threaded studs were screwed into the pins embedded in each end of the small bars and sealed with epoxy to prevent sulfate penetration from the ends. The small bars were stored in 5% Na_2SO_4 solution at room temperature. Sulfate resistance of the synthesized CSAB cements was tested by measuring the expansion of the small bars from 7 to 97 days of hydration. For both the dimensional stability and the sulfate resistance tests, six small bars were measured from each batch of paste and the expansion was averaged. The results were compared to the MS CSAB cement synthesized from reagent-grade chemicals and a commercially-produced Type I/II portland cement (TXI Hunter).

7.4.6 Compressive Strength Development

Compressive strength development of the synthesized CSAB cements from natural and waste materials with 1% citric acid addition (retarder) was tested with cubes (50×50×50 mm) of standard mortar (cement + sand + water; water-to-cement ratio of 0.45) according to ASTM C 109 (2007). The mortar cubes were demolded at 1 day of hydration and cured in ultra-pure water at room temperature. Compressive strength was tested at 1, 3, 7, 28, and 90 days. Three mortar cubes were tested at each age for each sample type and the strengths were averaged. The results were compared to the MS CSAB cement synthesized from reagent-grade chemicals and a commercially-produced Type I/II portland cement (TXI Hunter).

7.5 RESULTS AND DISCUSSION

7.5.1 Particle Size and Distribution

Measuring the particle fineness and distribution of the synthetic clinkers are critical because these factors strongly affect performance. The MC and MF CSAB cement clinkers from natural and waste materials had uniform Blaine fineness after

grinding with the micro mill grinder, as shown in Table 7.3. Their Blaine values were about 325 m^2/kg, which is nearly identical to the MS CSAB cement clinker from reagent-grade chemicals. However, the synthetic clinkers had Blaine values about 20% lower than the commercial Type I/II portland cement (403.4 m^2/kg). Curiously, the particle size distributions obtained from laser light scattering particle size distribution analysis for the MC, MF, and MS CSAB cement clinkers were similar to the commercial Type I/II portland cement; all had median particle sizes (d_{50}) of approximately 45 μm, as shown in Figure 7.1. However, the MC and MF CSAB cement clinkers contained more fine particles (<20 μm) than the MS CSAB cement clinker and the commercial Type I/II portland cement.

Table 7.3 – Blaine fineness values for a commercial Type I/II portland cement (PC) and the CSAB cement clinkers synthesized from reagent-grade chemicals (MS) Class C fly ash (MC), and fluidized bed ash (MF)

Sample	**Specific Surface Area (m^2/kg)**
PC	403.4
MS	322.6
MC	323.6
MF	312.4

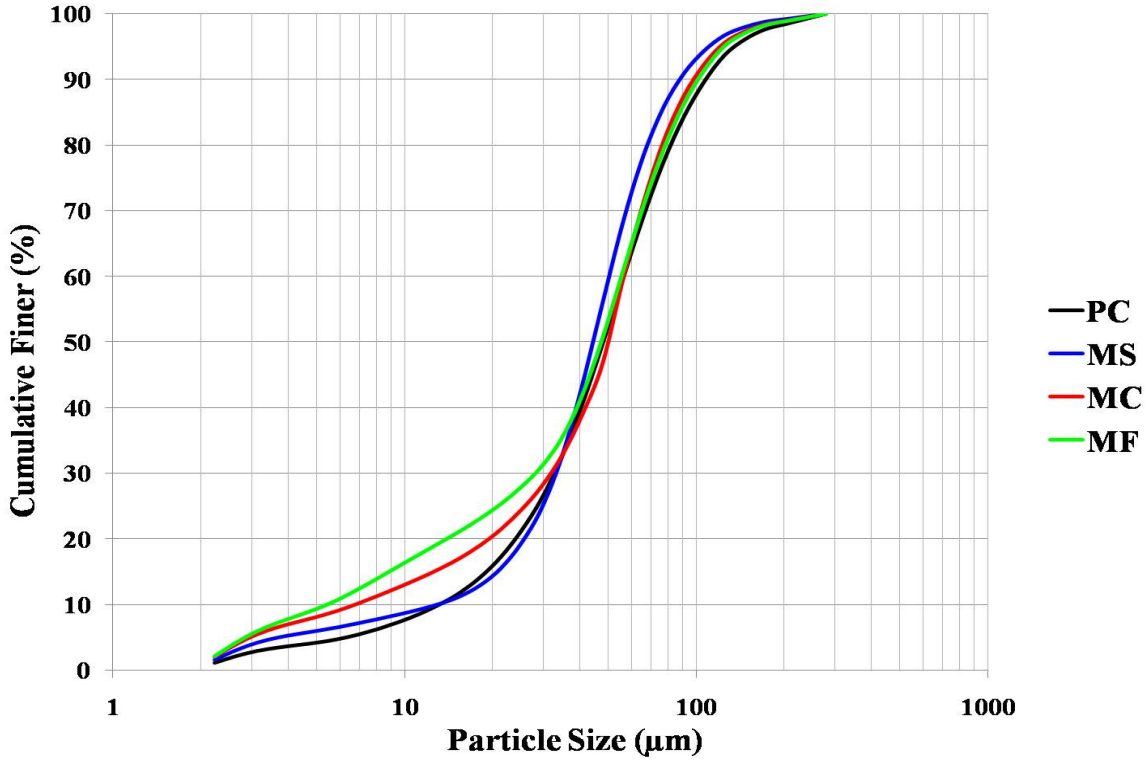

Figure 7.1 – Particle size distribution for a commercial Type I/II portland cement (PC) and the CSAB cement clinkers synthesized from reagent-grade chemicals (MS), Class C fly ash (MC), and fluidized bed ash (MF)

Blaine fineness measures the rate of air passing through pressed powder and its results could be affected by particle surface chemistry, morphology, and porosity, which could be different between CSAB cement and portland cement, resulting in different measured surface area values (Iyer and Stanmore, 1995).

7.5.2 Phase Composition and Distribution

The refined X-ray diffraction patterns for the MC and MF CSAB cement clinkers from natural and waste materials obtained through Rietveld analysis are shown in Figures 7.2-7.3, respectively. A comparison of the X-ray diffraction patterns for the MC and MF CSAB cement clinkers and the MS CSAB clinker from reagent-grade chemicals is shown

in Figure 7.4 and their quantitative phase compositions are shown in Table 7.4. The phase analysis results show that the four major CSAB cement phases formed in the MC and MF CSAB clinkers. The MC and MF CSAB clinkers had low free lime (C) contents indicating that the 1250˚C firing temperature was sufficient for CSAB cement clinker synthesis when using natural and waste materials as raw materials. The phase compositions for the MC and MF CSAB cement clinkers were reasonably close to their target phase compositions and the MS CSAB cement clinker, indicating that the Bogue method refined for this research can effectively predict CSAB cement clinker phase composition from its raw materials oxide composition when using natural and waste materials as raw materials. The slight deviations from the target phase compositions were perhaps caused by the ability of phases to accommodate substitute ions (Taylor, 1997). The impurities contained in the natural and waste materials slightly affected phase formation as $C_5S_2\overline{S}$ and periclase (M; MgO) formed in both the MC and MF CSAB cement clinkers. However, their contents were about 2% and should not seriously affect performance.

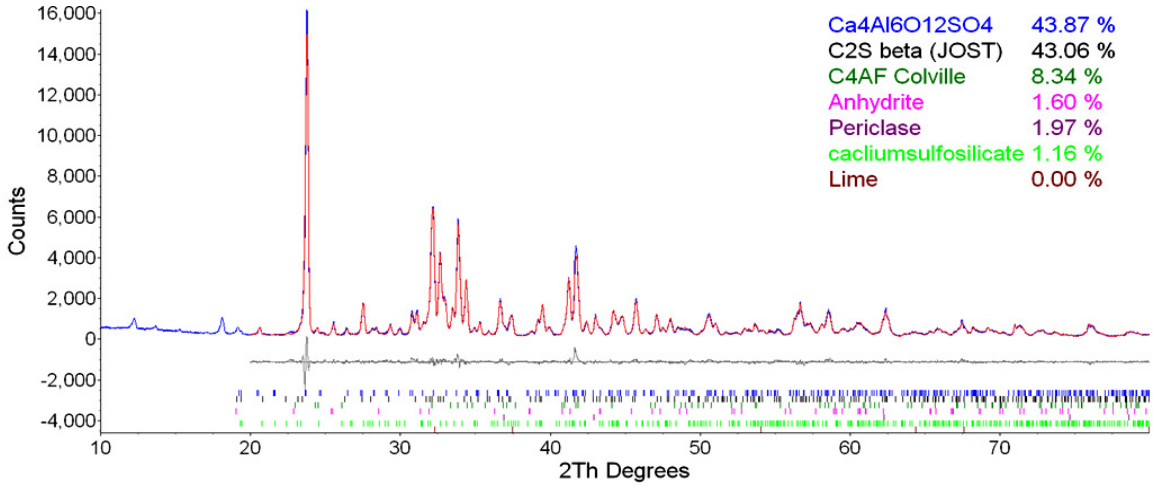

Figure 7.2 – Rietveld analysis results for the MC CSAB cement clinker synthesized from Class C fly ash

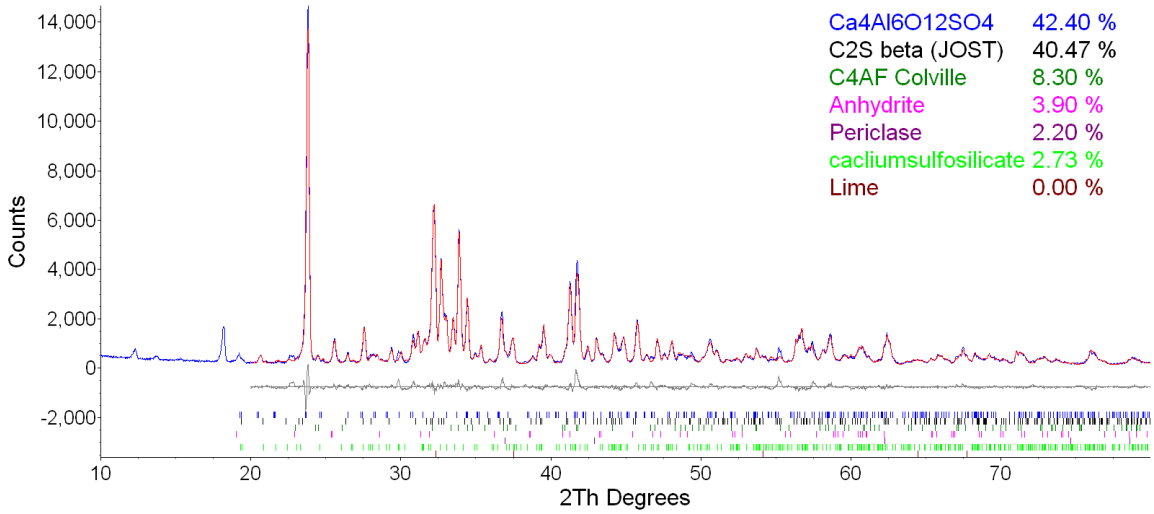

Figure 7.3 – Rietveld analysis results for the MF CSAB cement clinker synthesized from fluidized bed ash

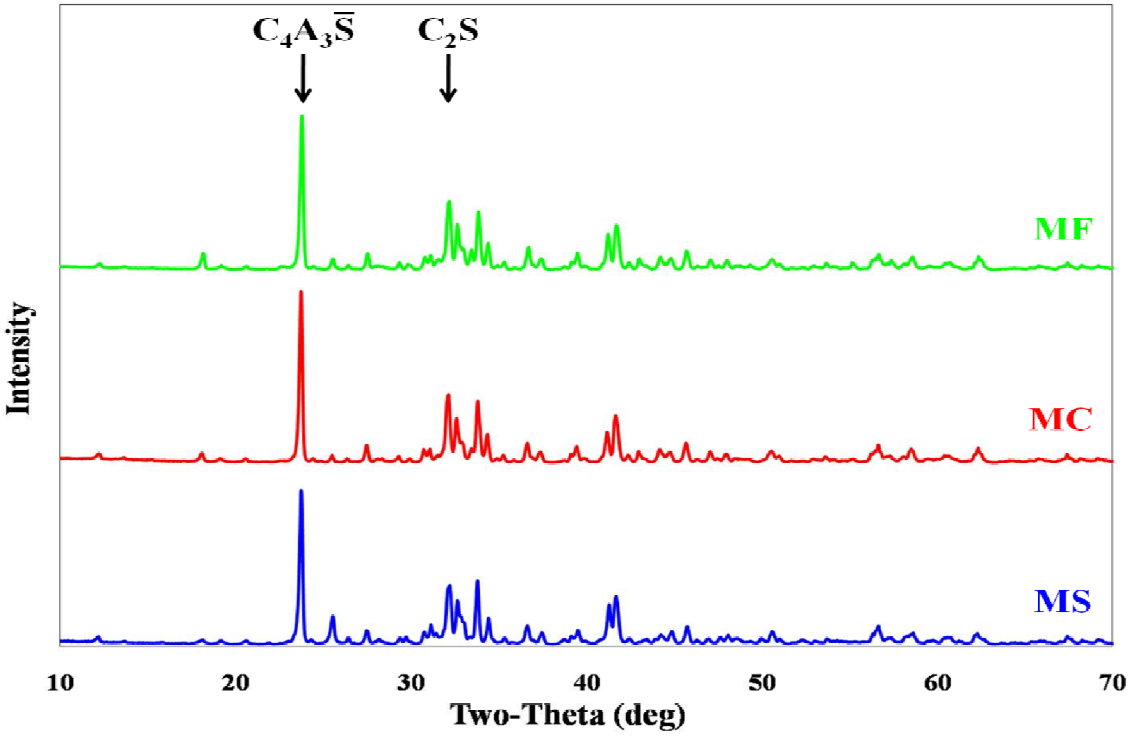

Figure 7.4 – X-ray diffraction patterns comparison for the CSAB cement clinkers synthesized from reagent-grade chemicals (MS), Class C fly ash (MC), and fluidized bed ash (MF)

Table 7.4 – Phase compositions for the CSAB cement clinkers synthesized from reagent-grade chemicals (MS), Class C fly ash (MC), and fluidized bed ash (MF) (TG: target calculated from the Bogue equations; R: Rietveld analysis)

Phase	**Phase Composition (weight %)**					
	MS		***MC***		***MF***	
	TG	***R***	***TG***	***R***	***TG***	***R***
C_2S	40	44.9	41.9	43.1	40.6	40.5
$C_4A_3\overline{S}$	40	42.0	40.1	43.8	39.4	42.4
C_4AF	10	6.1	7.9	8.3	7.1	8.3
$C\overline{S}$	10	6.8	4.4	1.6	6.5	3.9
Periclase	0	0	2.3	2.0	0.9	2.2
$C_5S_2\overline{S}$	0	0	0	1.2	0	2.7
C	0	0.2	0.5	0	2.2	0
Others	0	0	2.9	0	3.3	0

Backscattered electron images clearly show phase distribution in the MC and MF CSAB cement clinkers from natural and waste materials and the MS CSAB clinker from reagent-grade chemicals, as shown in Figures 7.5-7.7, respectively. The lighter gray areas in the images represent C_2S while the darker gray areas represent $C_4A_3\overline{S}$. The small amount of white areas that formed individually and inside the light gray (C_2S) and dark gray ($C_4A_3\overline{S}$) areas represent C_4AF. The MC, MF, and MS CSAB cement clinkers contained similar amounts of light gray (C_2S) and dark gray ($C_4A_3\overline{S}$) areas, which agree with the quantitative X-ray diffraction results (Table 7.4). Furthermore, the MC and MF CSAB cement clinkers contained more fine particles than the MS CSAB cement clinker, which conform to the laser light scattering particle size distribution analysis results (Figure 7.1) that show higher fine particle (<20 μm) contents in the MC and MF CSAB cement clinkers.

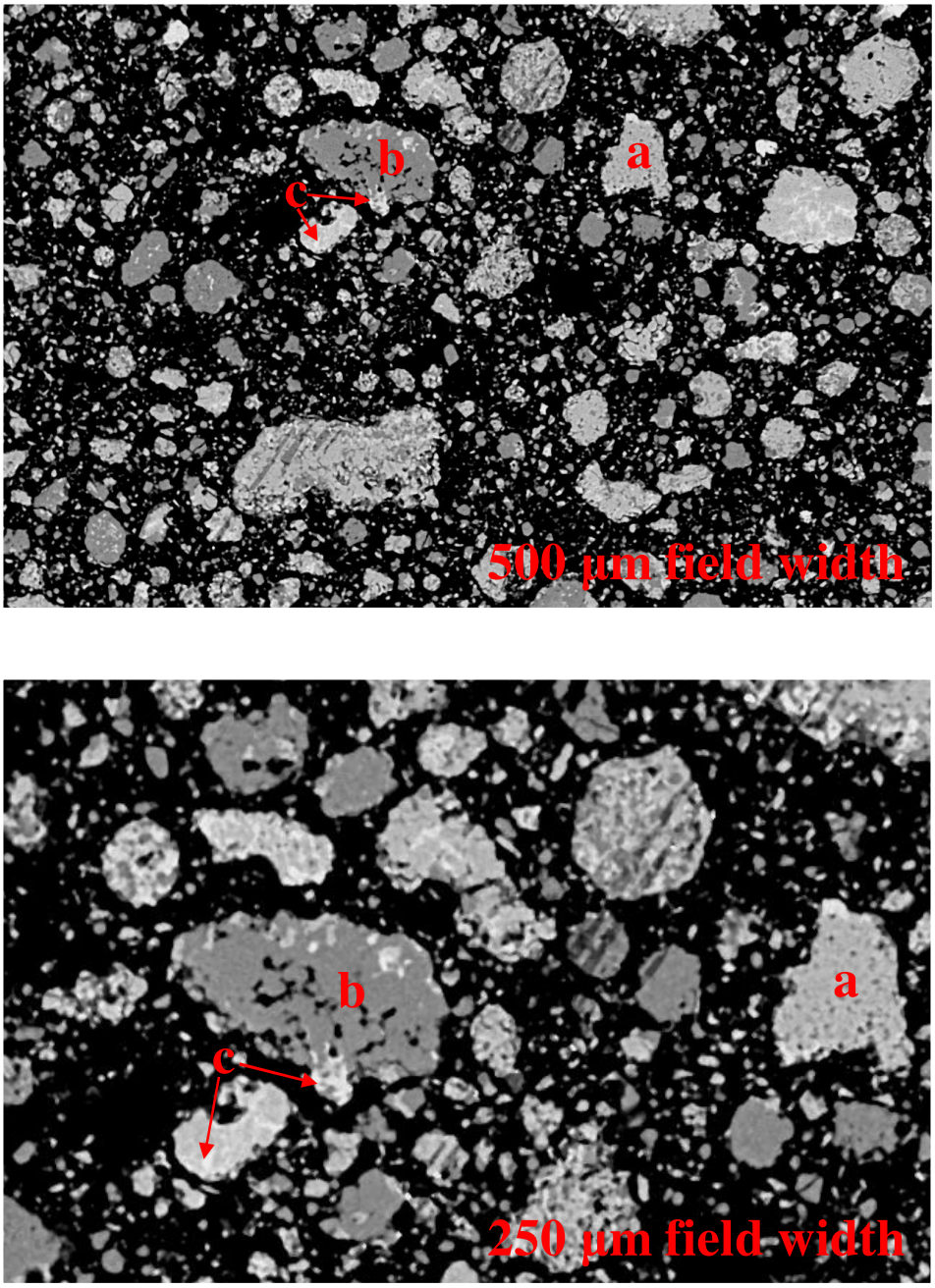

Figure 7.5 – Backscattered electron image for the MC CSAB cement clinker synthesized from Class C ash [a (light gray): C_2S, b (dark gray): $C_4A_3\overline{S}$, and c (white): C_4AF]

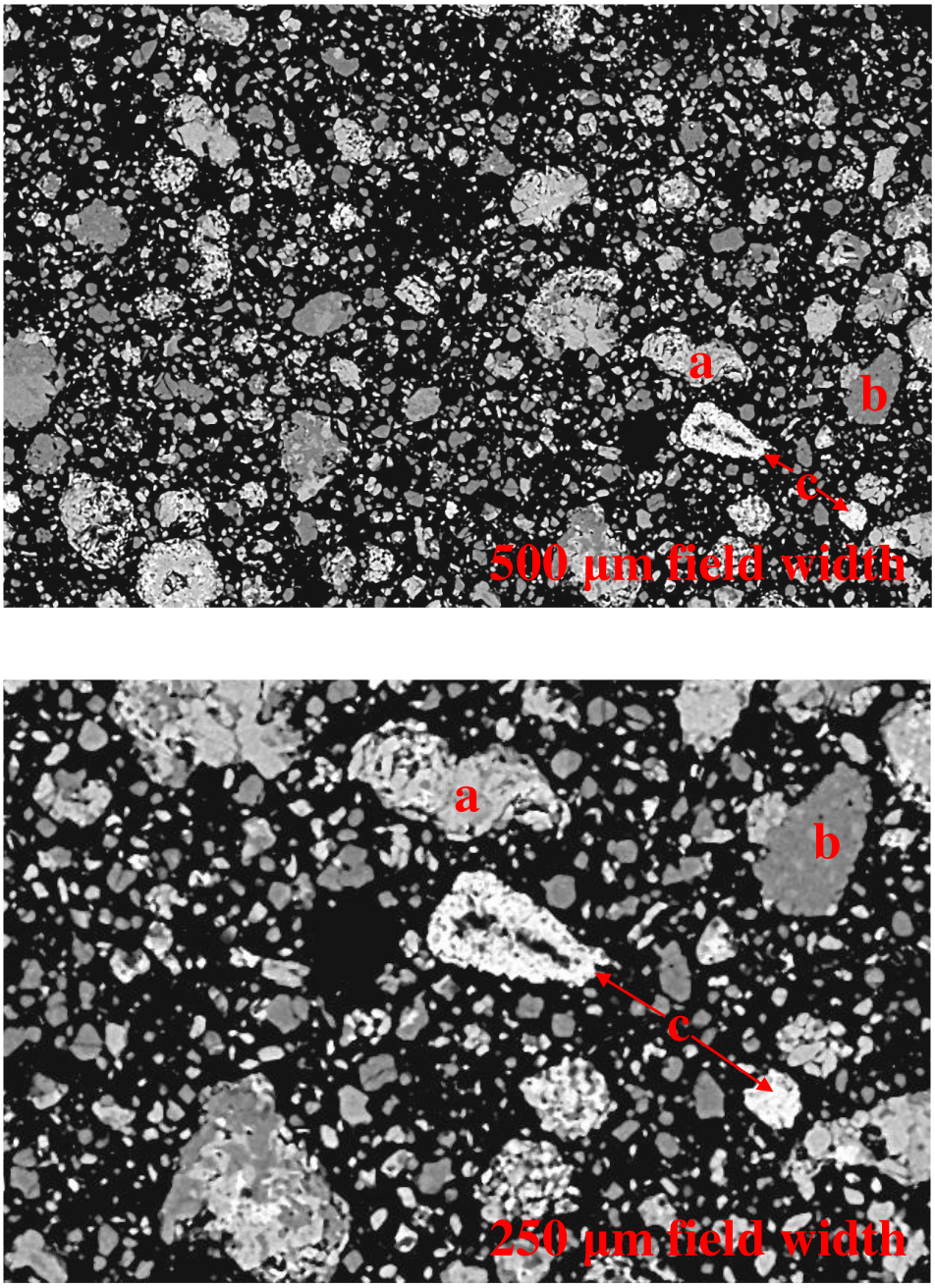

Figure 7.6 – Backscattered electron image for the MF CSAB cement clinker synthesized from fluidized ash [a (light gray): C_2S, b (dark gray): $C_4A_3\overline{S}$, and c (white): C_4AF]

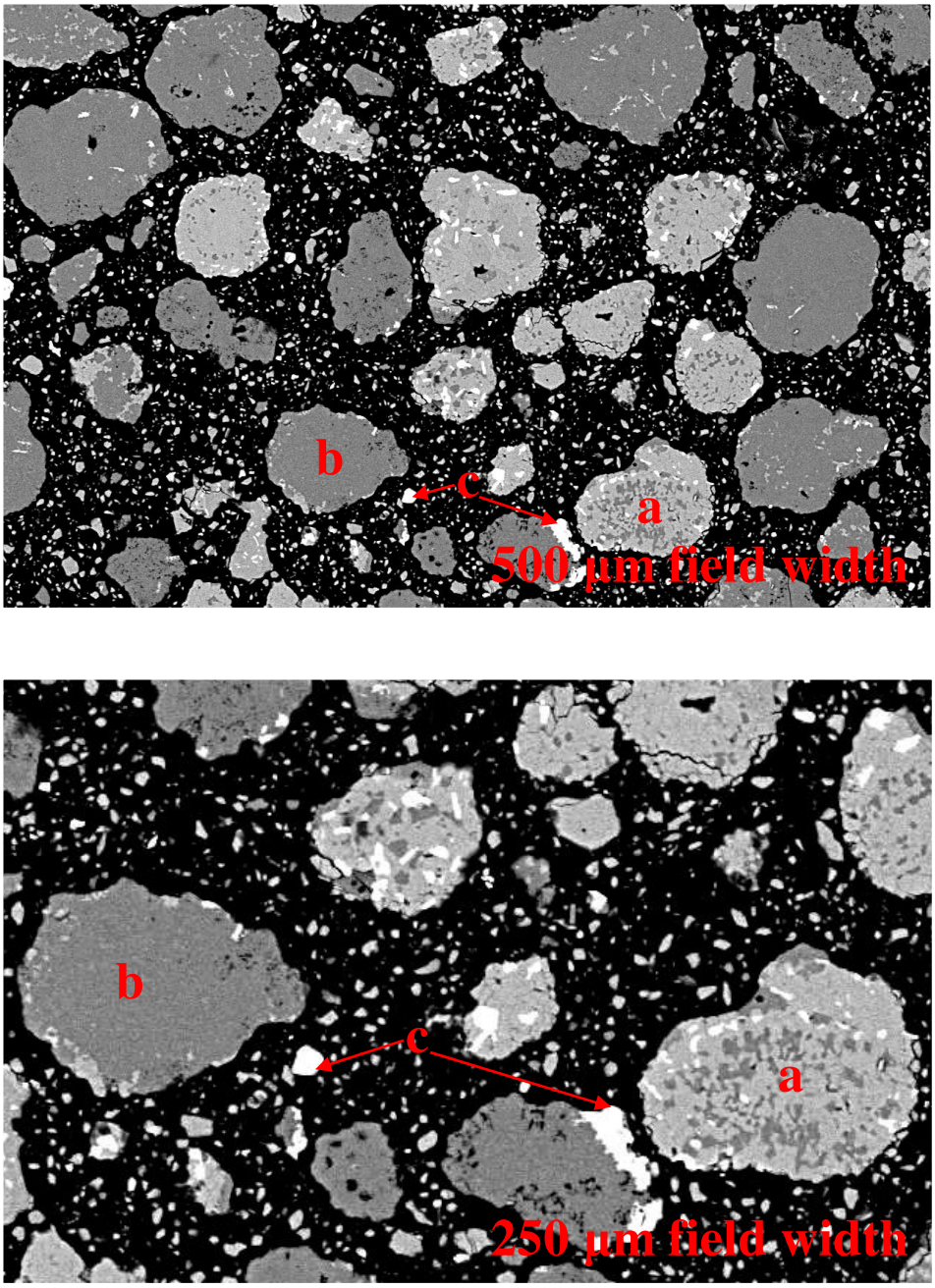

Figure 7.7 – Backscattered electron image for the MS CSAB cement clinker synthesized from reagent-grade chemicals [a (light gray): C_2S, b (dark gray): $C_4A_3\overline{S}$, and c (white): C_4AF]

7.5.3 Early-Age Hydration Behavior and Hydration Product Development

Rate of heat evolution and cumulative heat results for the MC and MF CSAB cement clinkers from natural and waste materials with 0-25% gypsum addition show that 20% gypsum addition was their optimum gypsum contents (Figures 7.8 and 7.9; Figures 7.10 and 7.11, respectively). The optimum gypsum contents (percentage of cement) for the MC and MF CSAB cement clinkers were determined using the method discussed in Chapter 6. The shape of the main heat evolution peak no longer changes with gypsum addition higher than the optimal amount. Moreover, with the optimum gypsum content added, CSAB cement clinker shows the highest cumulative heat. The optimum gypsum contents for the MC, MF, and MS CSAB cement clinkers and their relevant phase contents for ettringite formation are shown in Table 7.5. The optimum gypsum additions for the MC and MF CSAB cement clinkers were 5% higher than the MS CSAB cement clinker due to their lower $C\overline{S}$ contents. Furthermore, the calculated optimum gypsum contents (Table 7.5) from the equation developed in Chapter 6 based on the hydration reactions of $C_4A_3\overline{S}$ and C_4AF with gypsum to form ettringite agreed well with their measured optimum gypsum contents, indicating that the equation can effectively predict the optimum gypsum content for CSAB cement clinker. However, it is suggested to actually measure the optimum gypsum content using isothermal conduction calorimetry.

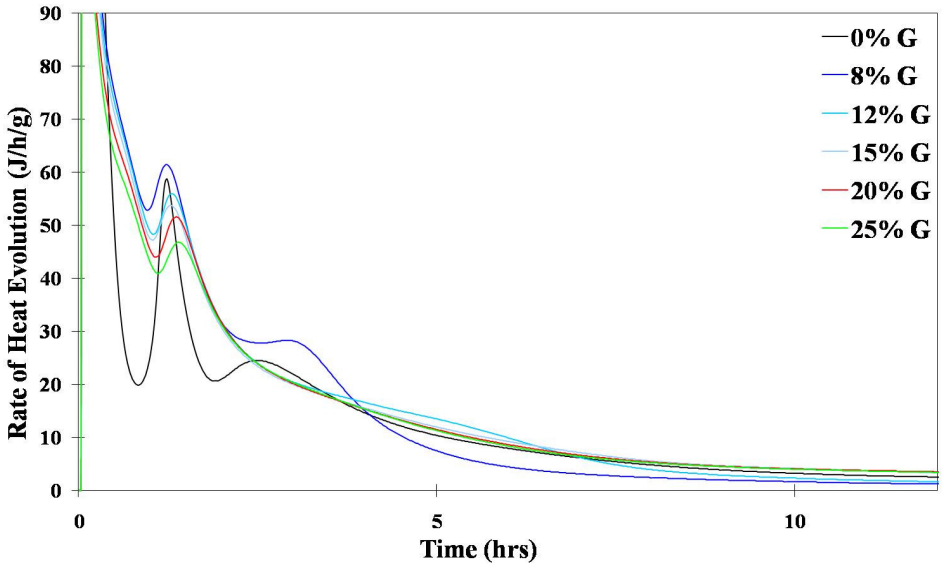

Figure 7.8 – Rate of heat evolution for the MC CSAB cement clinker synthesized from Class C fly ash with different amounts of gypsum (G) addition

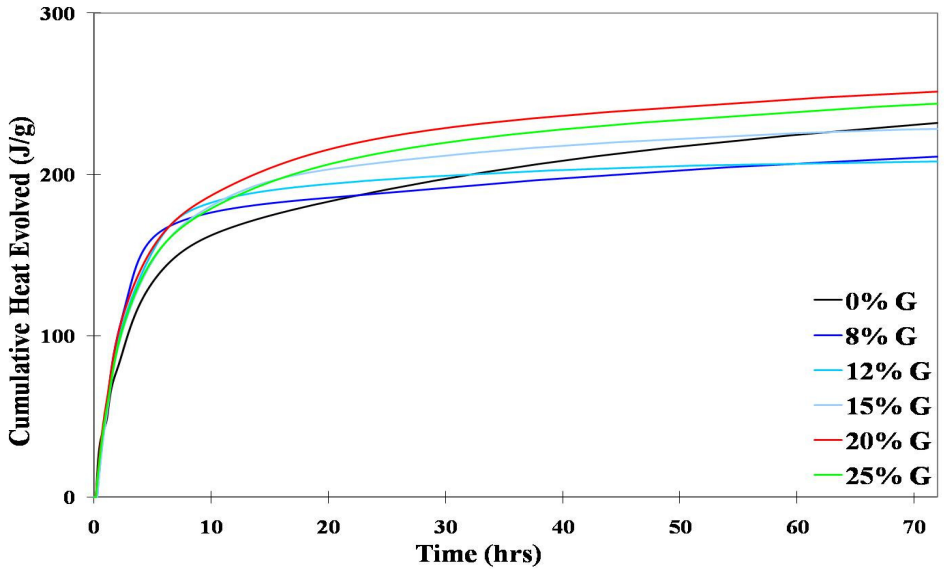

Figure 7.9 – Cumulative heat for the MC CSAB cement clinker synthesized from Class C fly ash with different amounts of gypsum (G) addition

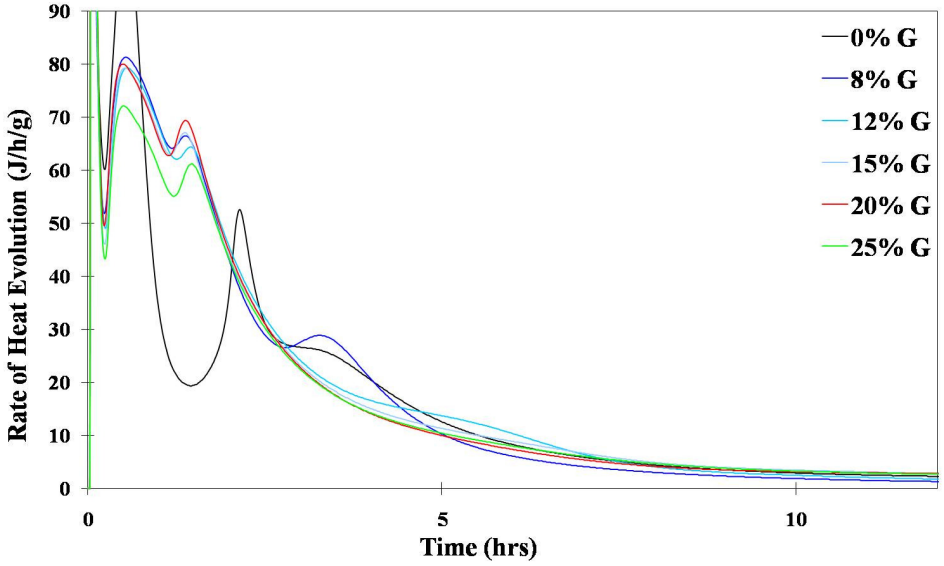

Figure 7.10 – Rate of heat evolution for the MF CSAB cement clinker synthesized from fluidized bed ash with different amounts of gypsum (G) addition

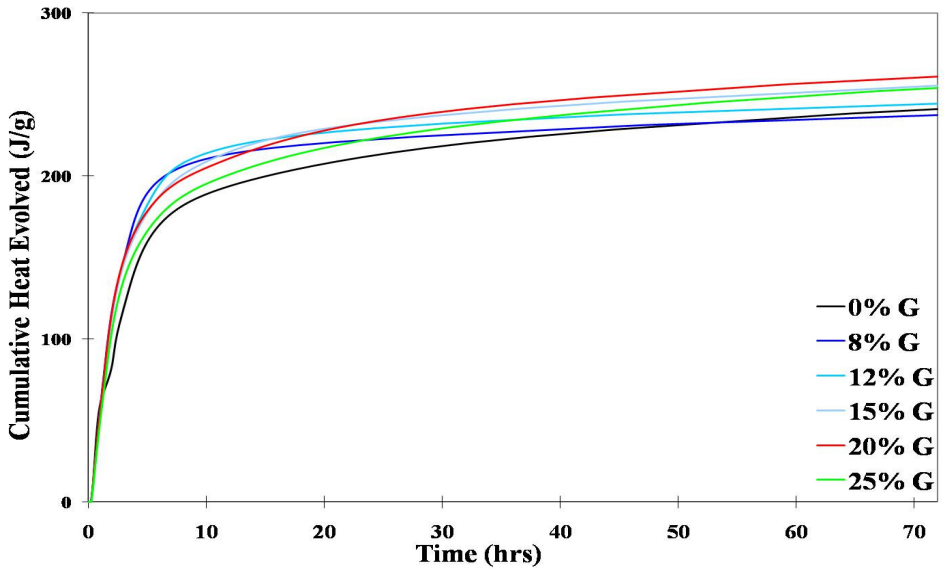

Figure 7.11 – Cumulative heat for the MF CSAB cement clinker synthesized from fluidized bed ash with different amounts of gypsum (G) addition

Table 7.5 – Calculated and measured optimum gypsum contents for the synthesized CSAB cements from reagent-grade chemicals (MS), Class C fly ash (MC), and fluidized bed ash (MF) and their relevant phase contents for ettringite formation

Sample	$C_4A_3\overline{S}$	C_4AF	$C\overline{S}$	**Measured Gypsum**	**Calculated Gypsum**
MS	42.0%	6.1%	6.8%	**15%**	**17.7%**
MC	43.8%	8.3%	1.6%	**20%**	**24.0%**
MF	42.4%	8.3%	3.9%	**20%**	**21.8%**

Rate of heat evolution results for the MC and MF CSAB cements from natural and waste materials containing their optimum gypsum contents showed that the pastes reacted extremely quickly and had much higher maximum heat evolution rates than the MS CSAB cement from reagent-grade chemicals even though they had similar clinker phase compositions, as shown in Figure 7.12. However, cumulative heat results after three days for the MC, MF, and MS CSAB cements were similar, as shown in Figure 7.13.

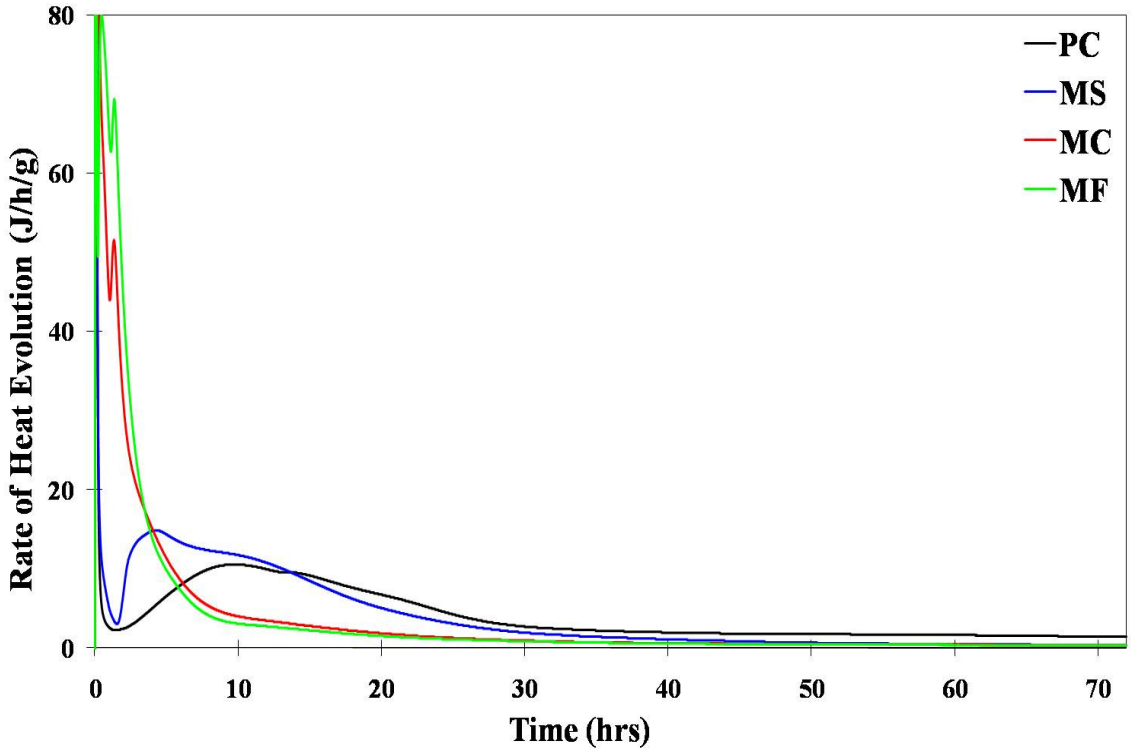

Figure 7.12 – Rate of heat evolution for a commercial Type I/II portland cement (PC) and the synthesized CSAB cements from reagent-grade chemicals (MS), Class C fly ash (MC), and fluidized bed ash (MF)

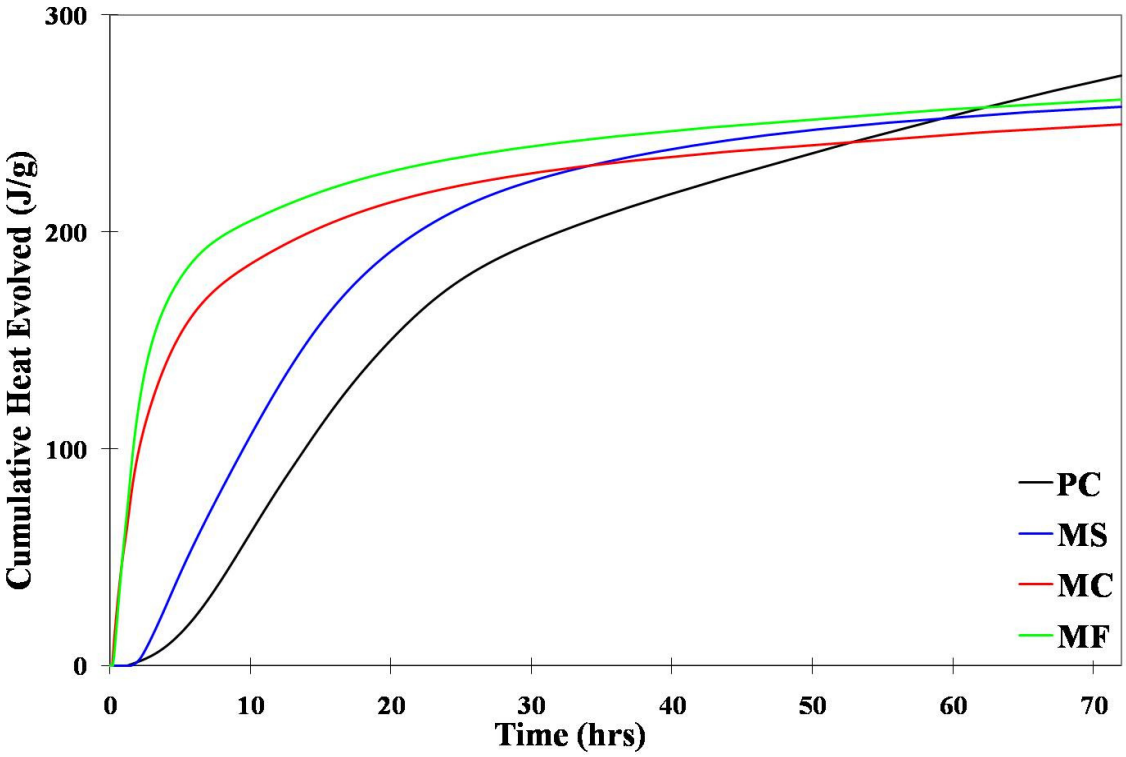

Figure 7.13 – Cumulative heat for a commercial Type I/II portland cement (PC) and the synthesized CSAB cements from reagent-grade chemicals (MS), Class C fly ash (MC), and fluidized bed ash (MF)

In order to understand the mechanism for the accelerating effect, the MC and MF CSAB cements were examined for hydration product development. However, the paste samples for the hydration product development study expanded, cracked, and totally turned into mush after demolding and curing in ultra-pure water for 2 days, as shown in Figure 7.14. Quantitative X-ray diffraction results for the hydrated MC, MF, and MS CSAB cements are shown in Table 7.6 (X-ray patterns listed in Appendix A). The MC and MF CSAB cements contained only 3.7% and 2.8% unhydrated $C_4A_3\overline{S}$ and 8.8% and 9.6% unhydrated gypsum, respectively, while the MS CSAB cement contained 15.0% unhydrated $C_4A_3\overline{S}$ and 12.8% unhydrated gypsum at 3 h of hydration. Moreover, at 3 h of hydration, more ettringite and amorphous content (mainly AH_3) formed in the MC and

MF CSAB cements (24.1% and 25.3%, 24.1% and 26.0%, respectively) than in the MS CSAB cement (20.6% and 20.5%). The rapid initial reaction of $C_4A_3\overline{S}$ and gypsum to form ettringite and AH_3 in the hydrated MC and MF CSAB cements caused the paste samples to harden quickly. It was visually observed that the MC and MF CSAB cements hardened within 2 h of hydration while the MS CSAB cement remained unset at 3 h of hydration. These results indicate that perhaps more ettringite and AH_3 formed in the MC and MF CSAB cements after cement hardened and resulted in the expansion and cracking in the paste samples.

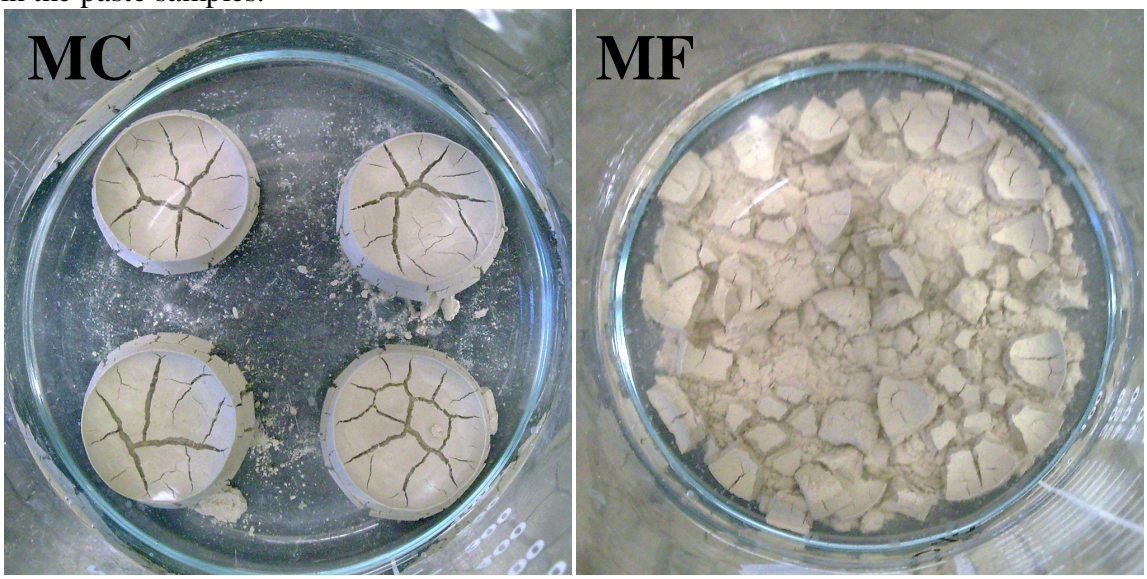

Figure 7.14 – Pictures for the hydrated synthesized CSAB cement samples from Class C fly ash (MC) and fluidized bed ash (MF) after 3 days of hydration

Table 7.6 – Phase compositions for the hydrated synthesized CSAB cements from reagent-grade chemicals (MS), Class C fly ash (MC), and fluidized bed ash (MF)

Sample	**Phase Composition (weight %)**										
	C_2S	$C_4A_3\bar{S}$	C_4AF	$C\bar{S}$	*Lime*	*Periclase*	$C_5S_2\bar{S}$	*Gypsum*	*Ettringite*	*Amorphous*	*Calcite*
MS_3h	25.7	15.0	2.9	2.5	0	N/A	N/A	12.8	20.6	20.5	N/A
MS_1D	24.6	10.1	2.9	2.2	0.1	N/A	N/A	6.3	24.5	29.3	N/A
MS_3D	24.5	4.8	3.0	1.2	0	N/A	N/A	2.7	34.6	29.2	N/A
MS_7D	25.2	3.1	2.6	1.0	0.1	N/A	N/A	1.9	38.5	27.6	N/A
MS_28D	23.3	3.5	2.3	1.2	0.1	N/A	N/A	2.3	40.0	27.3	N/A
MS_90D	20.7	3.9	2.6	1.3	0	N/A	N/A	2.1	40.9	26.8	1.7
MC_3h	29.2	3.7	4.4	2.5	0.1	1.2	0.7	8.8	24.1	25.3	N/A
MC_1D	28.3	3.4	4.9	1.9	0	1.0	1.0	7.2	31.1	21.2	N/A
MC_3D	28.0	1.2	4.7	1.8	0.1	0.8	1.1	1.9	40.3	20.1	N/A
MC_7D	28.2	1.7	5.0	1.1	0	0.9	1.1	1.2	44.4	16.4	N/A
MC_28D	21.3	0.9	4.9	2.0	0.1	0.8	1.2	1.3	49.6	16.7	1.2
MC_90D	12.5	1.1	3.8	1.0	0	0.3	0.9	1.5	47.5	29.6	1.8
MF_3h	28.7	2.8	3.4	3.2	0	1.0	1.2	9.6	24.1	26.0	N/A
MF_1D	29.6	2.4	3.8	2.7	0.1	1.0	1.3	7.2	29.6	22.3	N/A
MF_3D	27.6	1.3	3.9	1.8	0.1	1.0	1.2	3.6	41.5	18.0	N/A
MF_7D	27.9	1.1	4.2	1.5	0.1	0.9	1.4	2.3	43.9	16.7	N/A
MF_28D	24.0	0.7	4.1	2.2	0	1.0	1.0	1.3	47.5	17.1	1.1
MF_90D	14.4	0.7	3.5	1.2	0	0.7	0.7	0.7	46.0	29.7	2.4

The MC and MF CSAB cements from natural and waste materials and the MS CSAB cement from reagent-grade chemicals had similar clinker phase compositions. The only difference is that the MC and MF CSAB cements synthesized from natural and waste materials had higher impurity contents. Table 7.1 shows that the Class C fly ash and fluidized bed ash used both had high alkali contents. Alkalis contained in the MC and MF CSAB cements (about 1%) might have accelerated the dissolution rate of $C_4A_3\overline{S}$. Jawed and Skalny (1978) showed that alkalis can increase the dissolution rate of the aluminate phases in portland cement. To confirm this in the CSAB cement, 1% and 2% NaOH (percentage of cement) were added to the MS CSAB cement from reagent-grade chemicals to evaluate the effect of alkali on heat evolution rate. Rate of heat evolution results (Figure 7.15) show that with 1% and 2% NaOH addition, the MS CSAB cement reacted much faster and had much higher maximum heat evolution rates, which were similar to the MC and MF CSAB cements. The results demonstrate, therefore, that alkalis can significantly affect hydration kinetics of the CSAB cement system.

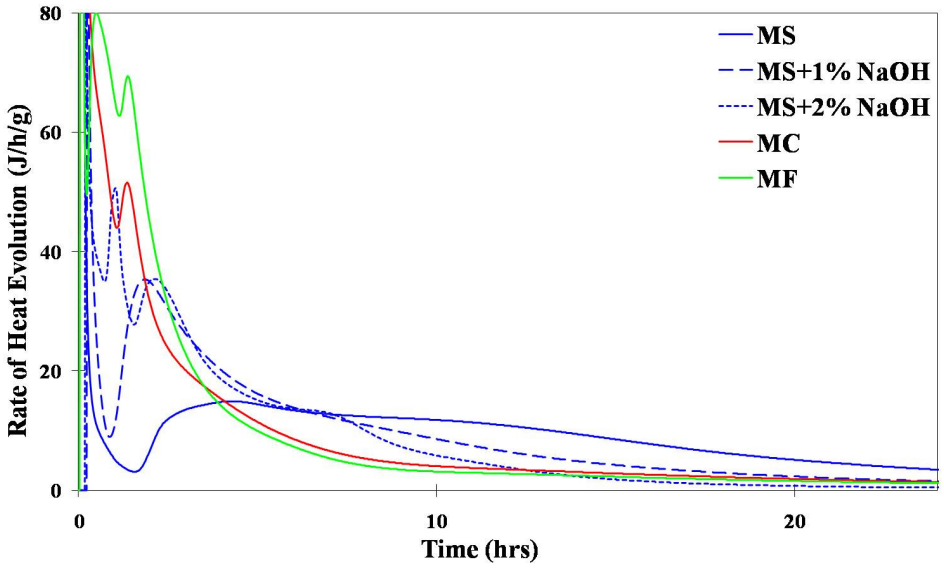

Figure 7.15 – Rate of heat evolution for the MS CSAB cement from reagent-grade chemicals with 1%, 2%, and 5% NaOH addition and the CSAB cements form Class C fly ash (MC) and fluidized bed ash (MF)

To slow down the reaction of $C_4A_3\overline{S}$ and gypsum, different amounts of citric acid, which is a common retarder used for both portland cement (Moschner et al., 2009) and CSAB cement (Hanley et al., 2004), were added to the MC and MF CSAB cements and tested for heat evolution rate. Rate of heat evolution results (Figure 7.16) show that 1% citric acid addition (percentage of cement) was enough to effectively retard the hydration reaction of both the MC and MF CSAB cements to about the same time as the MS CSAB cement; however, their maximum heat evolution rates were much higher. Cumulative heat results (Figure 7.17) show that the MC and MF CSAB cements had lower cumulative heat evolved with increasing amounts of citric acid addition, which could affect CSAB cement performance at higher dosage.

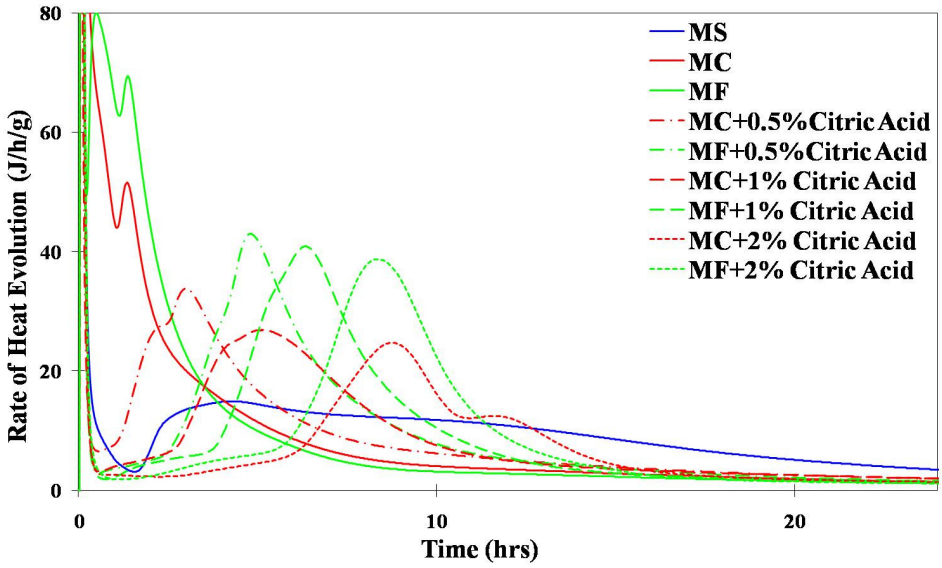

Figure 7.16 – Rate of heat evolution for the MS CSAB cement from reagent-grade chemicals and the CSAB cements form Class C fly ash (MC) and fluidized bed ash (MF) with 0.5%, 1%, and 2% citric acid (retarder) addition

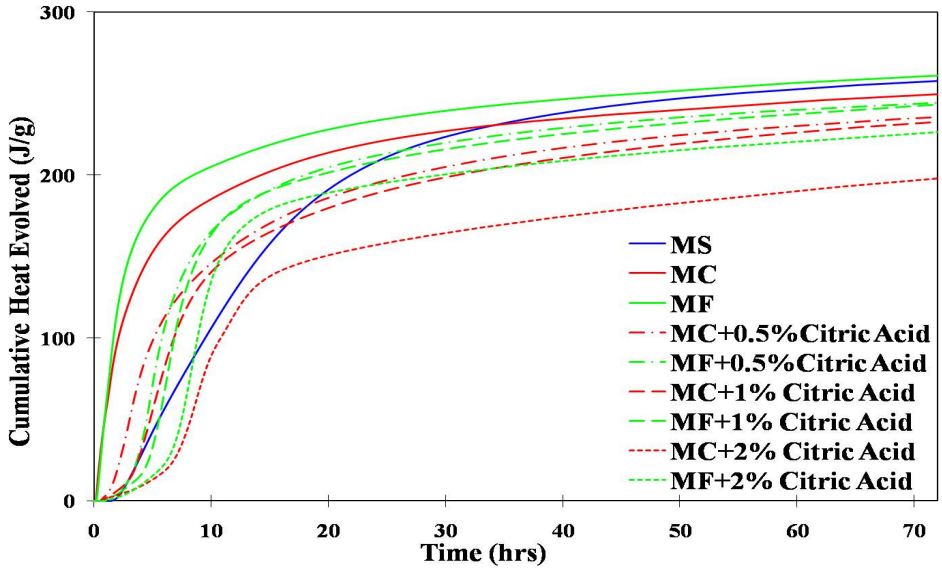

Figure 7.17 – Cumulative heat for the MS synthesized CSAB cement from reagent-grade chemicals and CSAB cements form Class C fly ash (MC) and fluidized bed ash (MF), respectively, with 0.5%, 1%, and 2% citric acid (retarder) addition

Quantitative X-ray diffraction results for the MC and MF CSAB cements from natural and waste materials and with and without 1% citric acid addition (retarder) and the hydrated MS CSAB cement from reagent-grade chemicals and are shown in Tables 7.6 and 7.7, respectively (X-ray patterns listed in Appendix A). The results show that less $C_4A_3\overline{S}$ and gypsum reacted and less ettringite formed in the MC and MF CSAB cements at early ages (before 3 days) with 1% citric acid addition than without citric acid addition. However, $C_4A_3\overline{S}$ and gypsum in the MC and MF CSAB cements with 1% citric acid addition still reacted faster and more ettringite formed at early ages (before 3 days) than in the MS CSAB cement. Furthermore, more C_2S reacted at later ages (after 7 days) in the MC and MF CSAB cements with and without 1% citric acid addition than in the MS CSAB cement. The MC, MF, and MS CSAB cements had similar clinker phase compositions. The only difference is that the MC and MF CSAB cements synthesized from natural and waste materials had higher impurity contents, as shown in Table 7.1. Gies and Konfel (1986) showed that incorporation of impurities in C_2S lattice can increase its hydraulic reactivity. It should also be noted that carbonation of the hydrated synthesized cements was observed as small amounts of calcite started to form in the MC and MF cements at 28 days of hydration with and without 1% citric acid addition.

Table 7.7 – Phase compositions for the hydrated synthesized CSAB cements from reagent-grade chemicals (MS), Class C fly ash (MC), and fluidized bed ash (MF); MC and MF with 1% citric acid (retarder) addition

Sample	**Phase Composition (weight %)**										
	C_2S	$C_4A_3\bar{S}$	C_4AF	$C\bar{S}$	*Lime*	*Periclase*	$C_5S_2\bar{S}$	*Gypsum*	*Ettringite*	*Amorphous*	*Calcite*
MS_3h	25.7	15.0	2.9	2.5	0	N/A	N/A	12.8	20.6	20.5	N/A
MS_1D	24.6	10.1	2.9	2.2	0.1	N/A	N/A	6.3	24.5	29.3	N/A
MS_3D	24.5	4.8	3.0	1.2	0	N/A	N/A	2.7	34.6	29.2	N/A
MS_7D	25.2	3.1	2.6	1.0	0.1	N/A	N/A	1.9	38.5	27.6	N/A
MS_28D	23.3	3.5	2.3	1.2	0.1	N/A	N/A	2.3	40.0	27.3	N/A
MS_90D	20.7	3.9	2.6	1.3	0	N/A	N/A	2.1	40.9	26.8	1.7
MC_3h	27.4	12.0	4.4	1.8	0	1.2	0.8	17.4	16.4	18.6	N/A
MC_1D	26.3	5.1	4.3	1.4	0	1.1	1.2	9.7	25.2	25.7	N/A
MC_3D	27.8	1.9	4.0	1.7	0.1	1.1	0.8	4.7	34.4	23.5	N/A
MC_7D	27.4	1.0	3.6	1.3	0	0.9	1.1	2.6	38.3	23.8	N/A
MC_28D	22.1	0.5	3.8	1.5	0	0.9	1.0	1.6	40.2	28.0	0.4
MC_90D	18.1	1.3	3.9	1.3	0	0.9	0.5	1.8	42.2	28.4	1.6
MF_3h	27.8	11.1	3.4	2.2	0	1.1	1.6	15.7	18.1	19.0	N/A
MF_1D	27.0	4.1	3.3	1.8	0	1.1	1.5	9.1	26.8	25.3	N/A
MF_3D	27.6	1.4	3.6	1.7	0.1	0.9	1.2	5.6	34.7	23.2	N/A
MF_7D	26.9	0.9	3.2	1.3	0.1	0.9	1.0	3.6	39.7	22.4	N/A
MF_28D	22.8	0.7	3.5	1.0	0.1	1.0	1.1	1.9	41.8	25.4	0.7
MF_90D	18.7	0.7	3.6	1.0	0	0.8	0.8	1.5	42.5	27.8	2.6

Backscattered electron images allowed the examination of phase distribution in the hydrated MC and MF CSAB cements from natural and waste materials with 1% citric acid addition, as shown in Figures 7.18 and 7.19, respectively. Only the paste samples with 1% citric acid addition were prepared because the paste samples without 1% citric acid addition expanded, cracked, and totally turned into mush at early age. The black areas represent pores and cracks. The dark gray background represents ettringite and the amorphous content (mainly AH_3), the dark gray particles represent unhydrated gypsum, the gray particles represent unhydrated $C_4A_3\overline{S}$, and the light gray particles represent unhydrated C_2S, as indicated in Figures 7.18 and 7.19. At 1 day of hydration, substantial amounts of $C_4A_3\overline{S}$ and C_2S remained unhydrated; however, most of the gypsum seemed to have reacted and only a few gypsum particles can be observed. From 1–3 days of hydration, the amount of $C_4A_3\overline{S}$ decreased significantly and only a few $C_4A_3\overline{S}$ particles can be observed at 3 days of hydration. From 1–90 days of hydration, the amount of C_2S decreased and C_2S particles seemed to be reacting and breaking down. However, significant amount of C_2S remained unhydrated at 90 days of hydration. On the other hand, microstructure of the hydrated MC and MF CSAB cements seemed to be very dense, indicating that ettringite and the amorphous content (mainly AH_3) were able to effectively fill in the space at early ages. The MC and MF CSAB cements from natural and waste materials showed similar trend of hydration product development compared to the MS CSAB cement from reagent-grade chemicals (Figure 7.20). Moreover, hydration product development information shown in these images generally agrees with the quantitative X-ray diffraction results (Table 7.7).

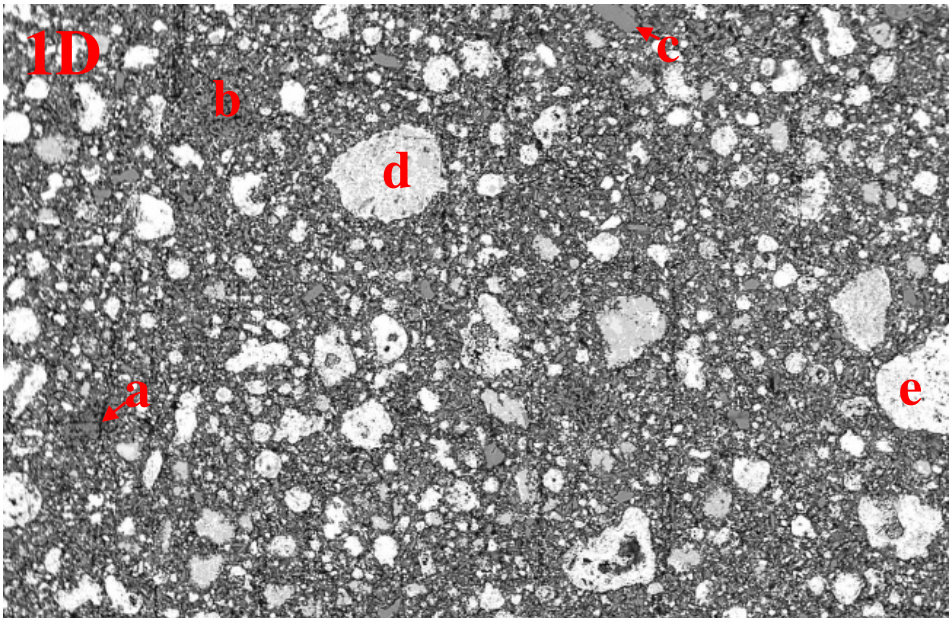
1D
b
c
d
a
e

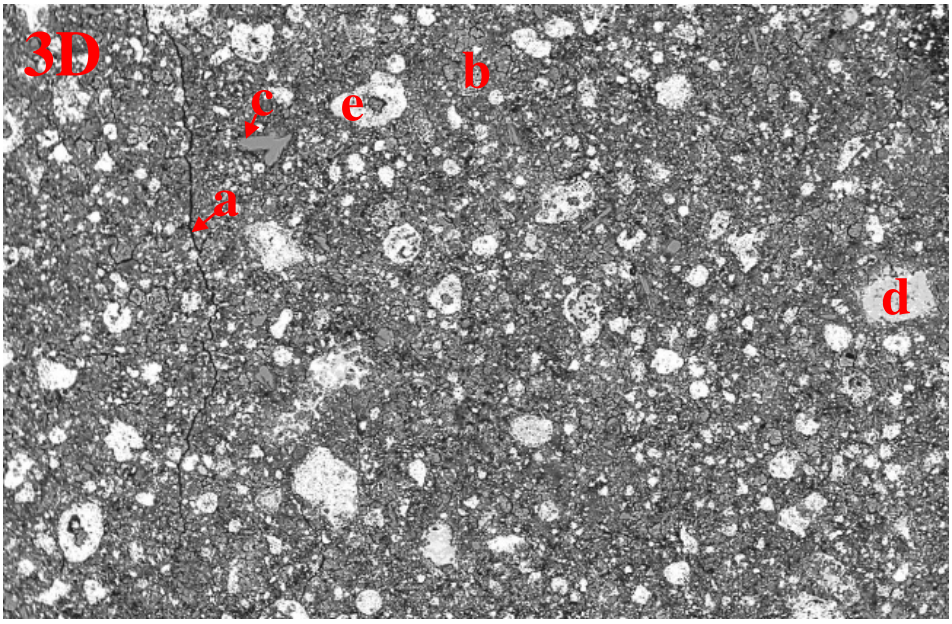
3D
c
e
b
a
d

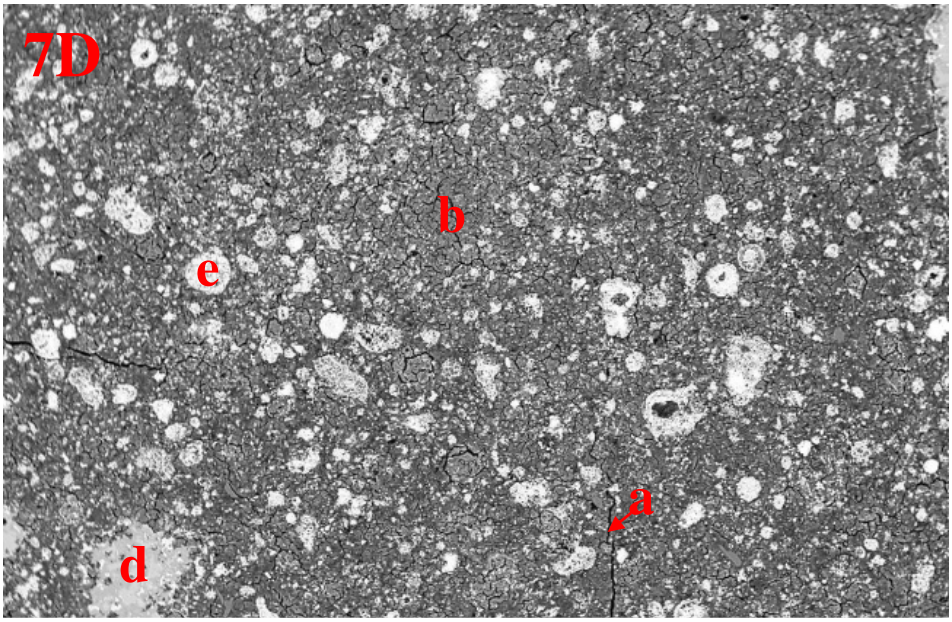
7D
b
e
a
d

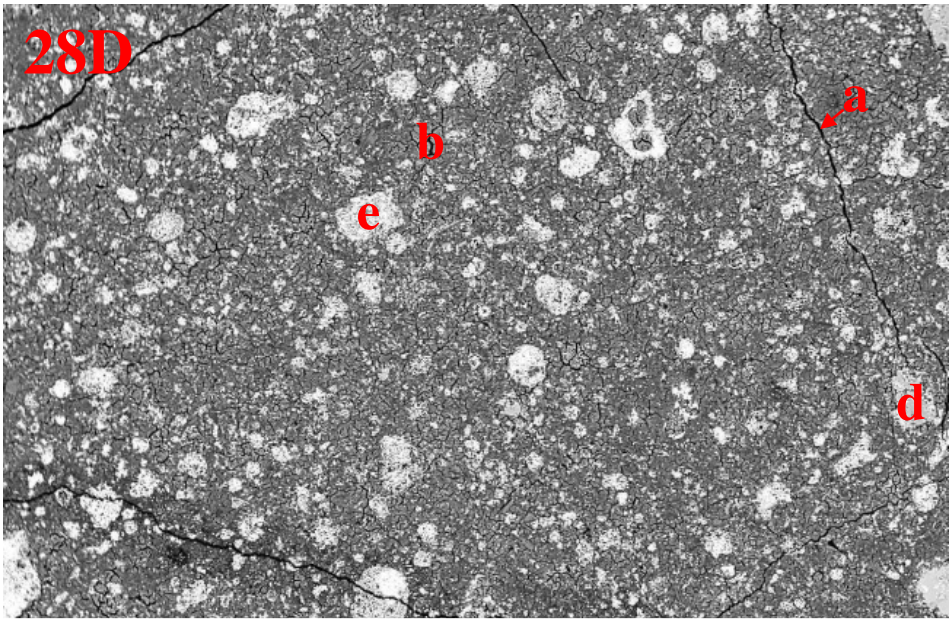
28D
a
b
e
d

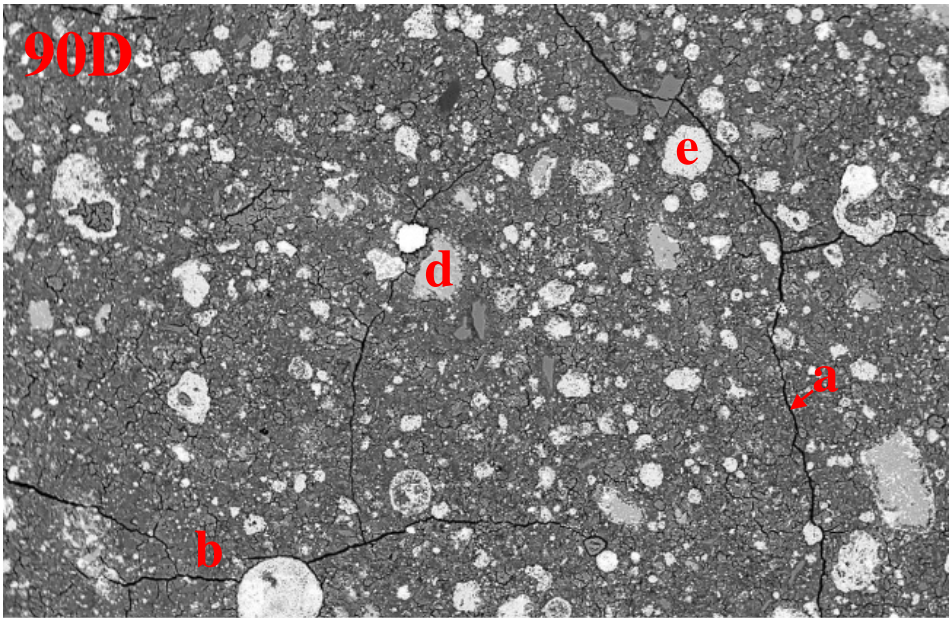

Figure 7.18 – Backscattered electron images for the hydrated MC CSAB cement from Class C fly ash [a (black): pores and cracks, b (dark gray background): ettringite and amorphous content, c (dark gray particles): gypsum, d (gray): $C_4A_3\overline{S}$, and e (light gray): C_2S; field width: 1250 μm]

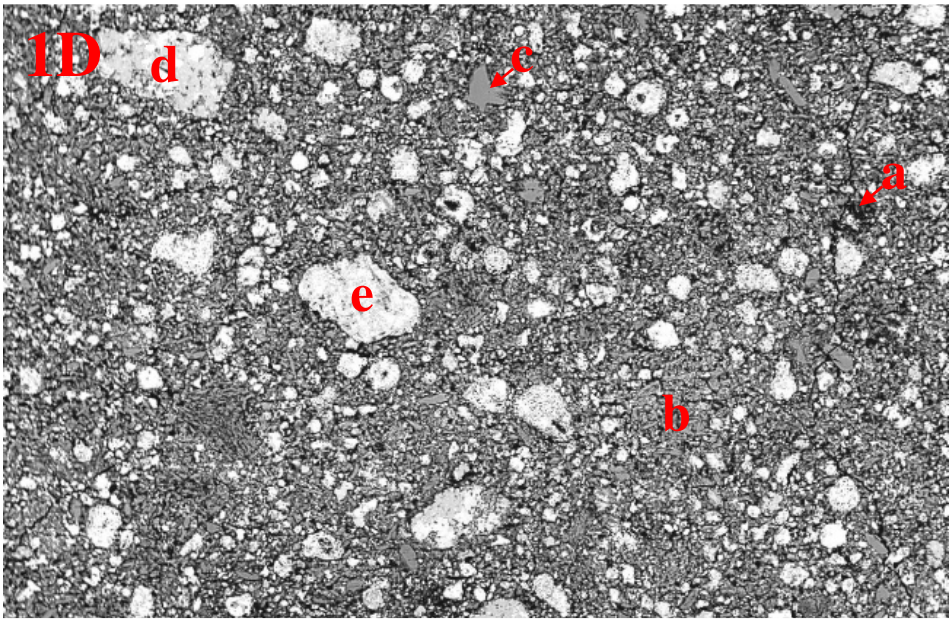

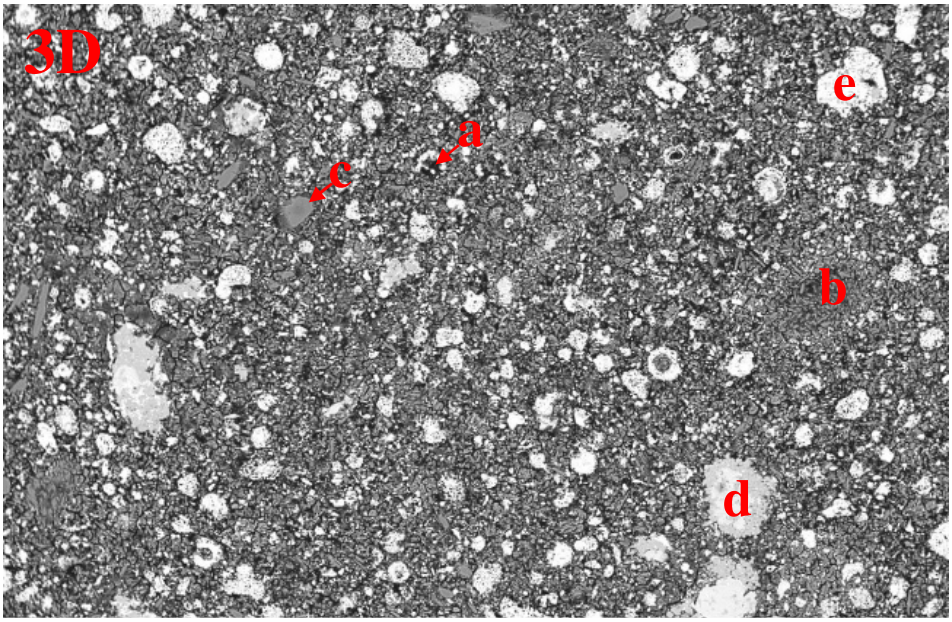
3D
e
a
c
b
d

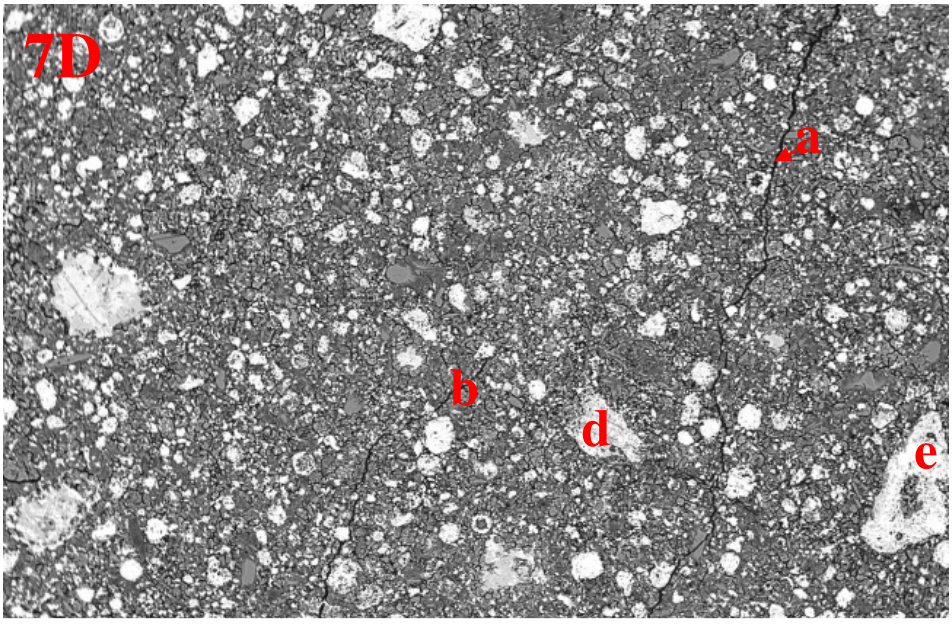
7D
a
b
d
e

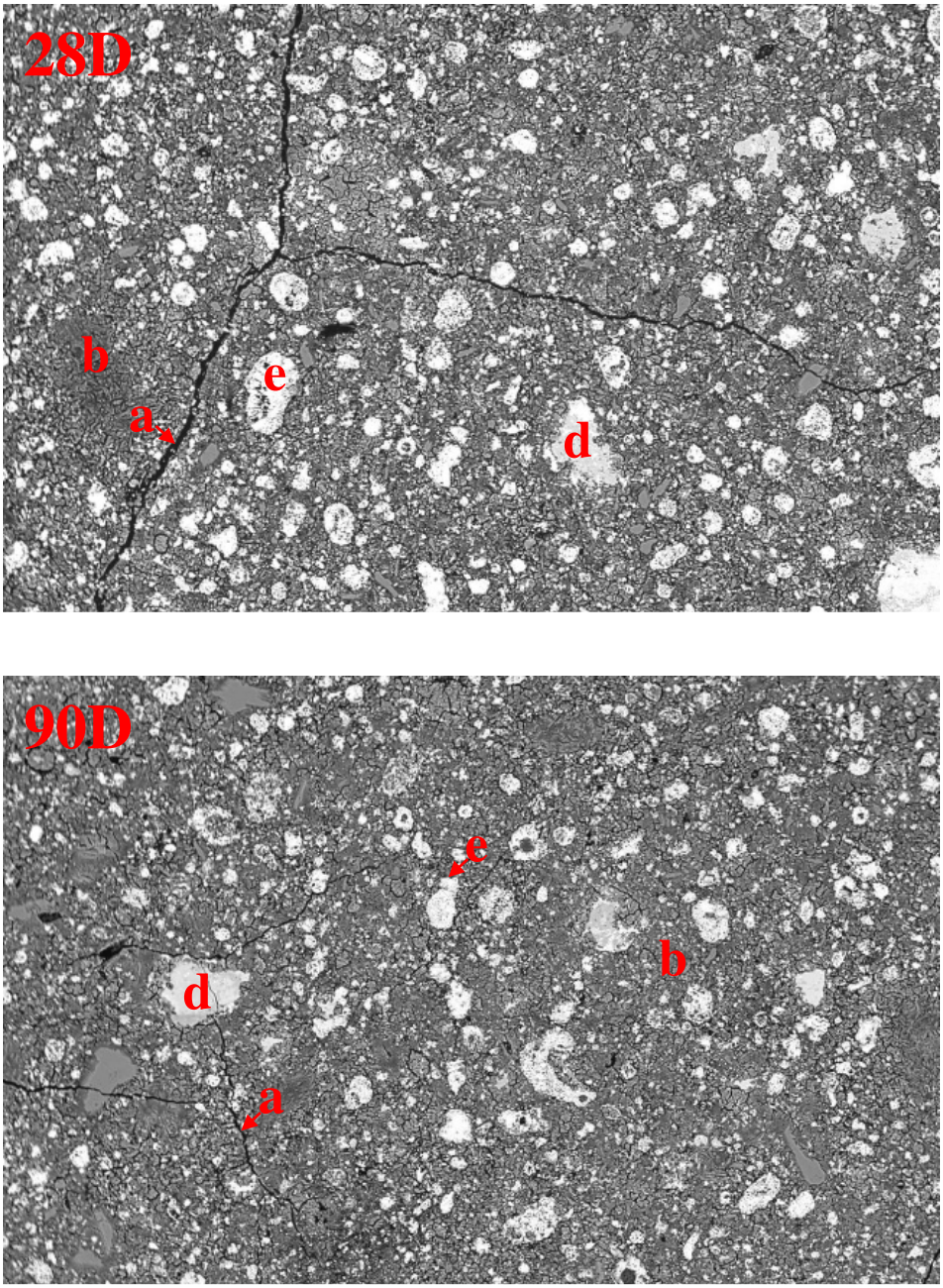

Figure 7.19 – Backscattered electron images for the hydrated MF CSAB cement from fluidized bed ash [a (black): pores and cracks, b (dark gray background): ettringite and amorphous content, c (dark gray particles): gypsum, d (gray): $C_4A_3\overline{S}$, and e (light gray): C_2S; field width: 1250 μm]

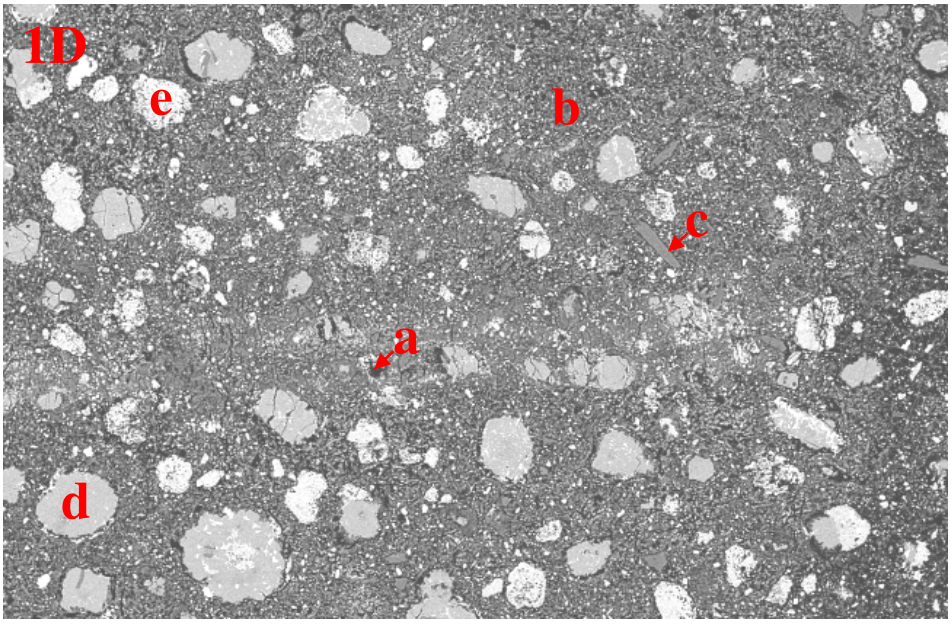
1D
e
b
c
a
d

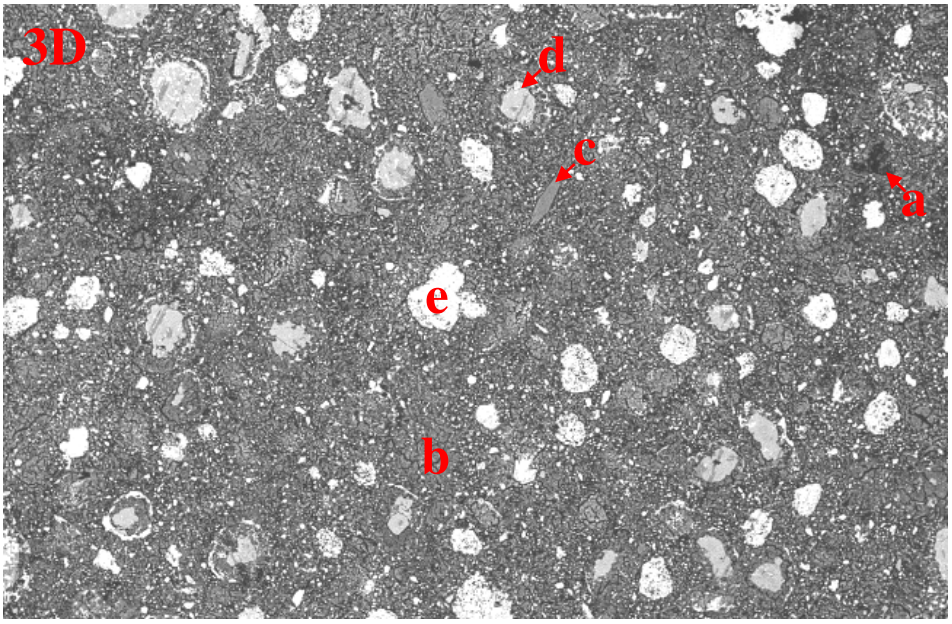
3D
d
c
a
e
b

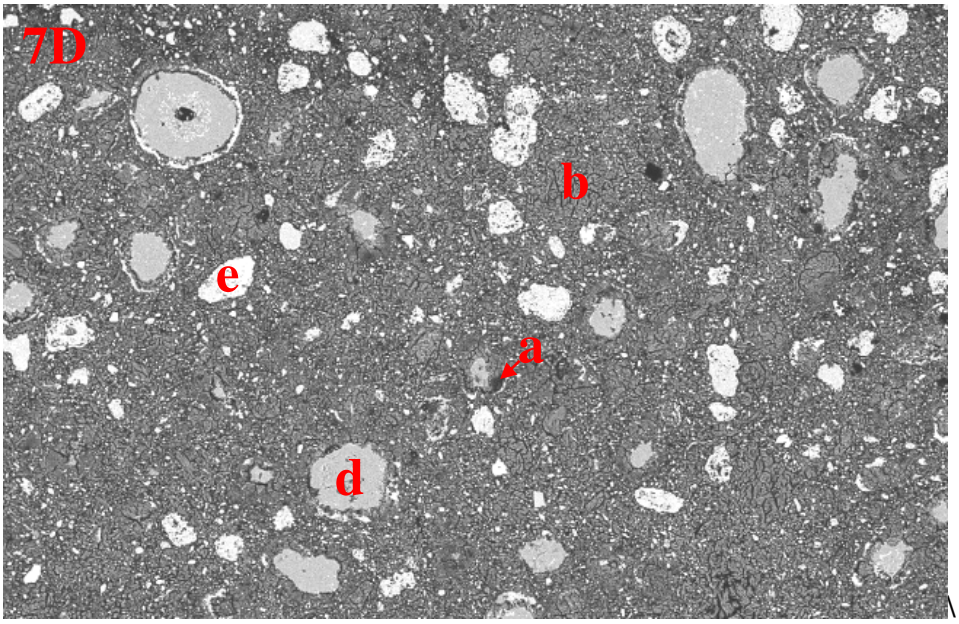
7D
b
e
a
d

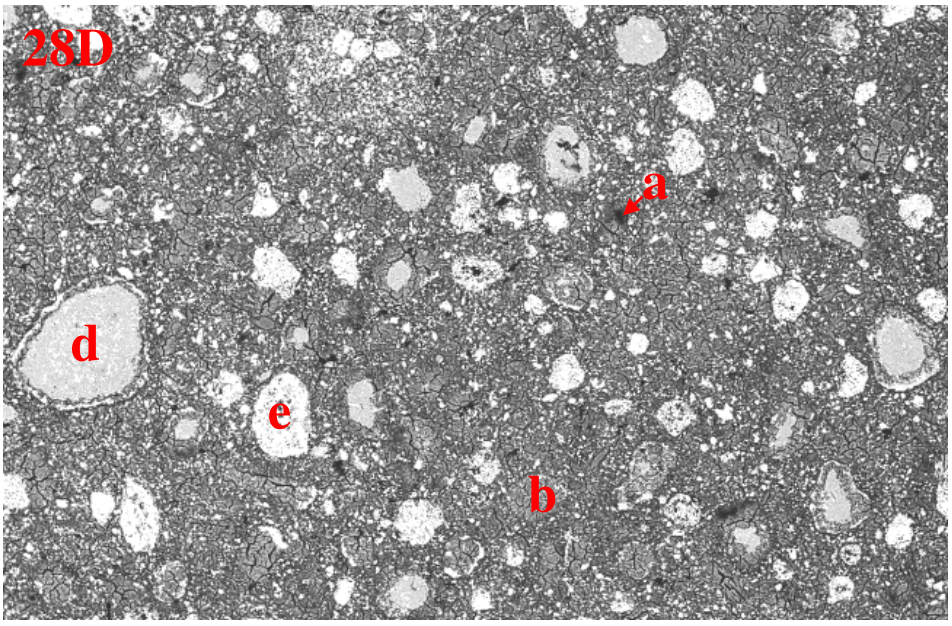
28D
a
d
e
b

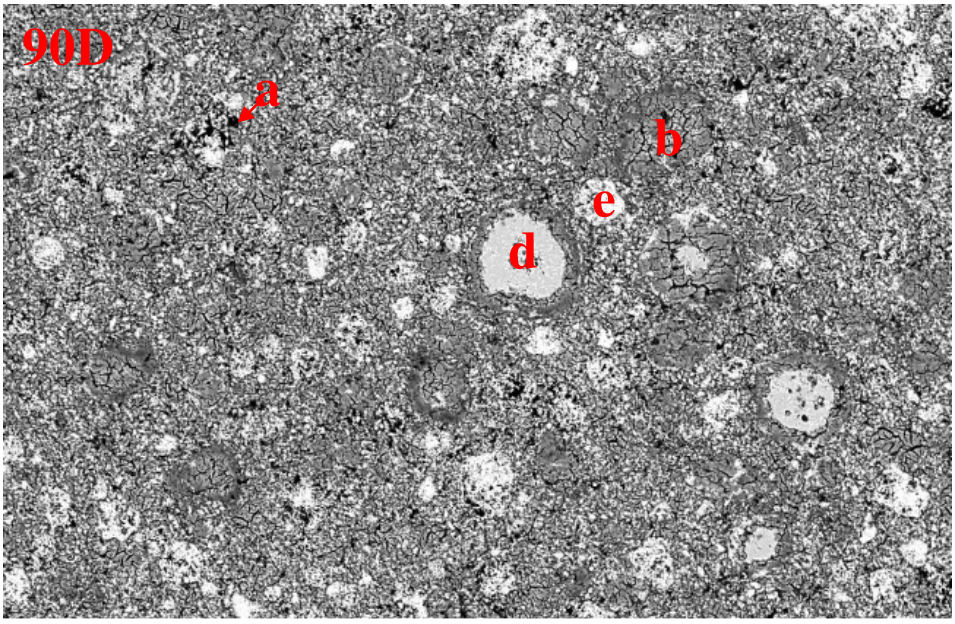

Figure 7.20 – Backscattered electron images for the hydrated MS CSAB cement from reagent-grade chemicals [a (black): pores and cracks, b (dark gray background): ettringite and amorphous content, c (dark gray particles): gypsum, d (gray): $C_4A_3\overline{S}$, and e (light gray): C_2S; field width: 1250 μm]

7.5.4 Dimensional Stability and Sulfate Resistance

Dimensional stability for the MC and MF CSAB cements from natural and waste materials with 1% citric acid addition (retarder), the MS CSAB cement from reagent-grade chemicals, and a commercial Type I/II portland cement are shown in Figures 7.21. The MC and MF CSAB cements showed no sign of cracking and expanded about 0.5% after demolding and curing in ultra-pure water for 3 days, which was about the same to the MS CSAB cement and should not seriously affect performance. However, the synthesized CSAB cements expanded about three times more than the commercial Type I/II portland cement.

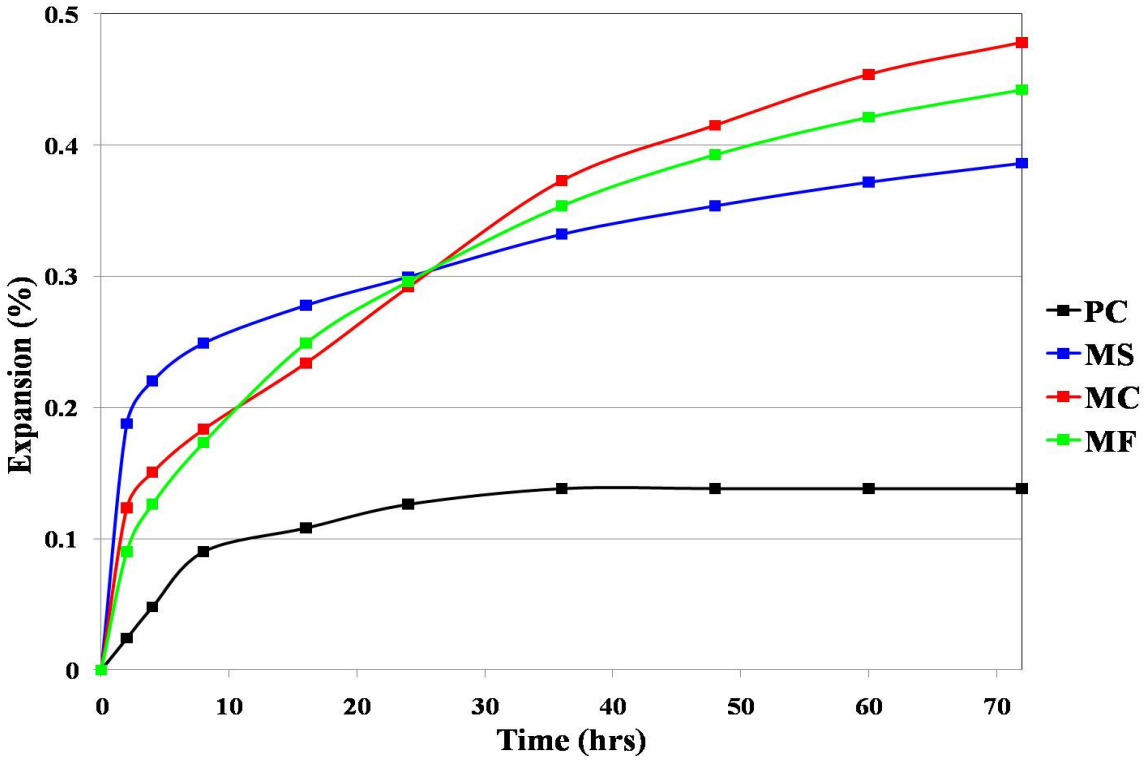

Figure 7.21 – Dimensional stability for a commercial Type I/II portland cement (PC) and the synthesized CSAB cements from reagent-grade chemicals (MS), Class C fly ash (MC), and fluidized bed ash (MF) stored in ultra-pure water after demolding at 1 day of hydration; MC and MF with 1% citric acid (retarder) addition

Sulfate resistance results for the MC and MF CSAB cements from natural and waste materials with 1% citric acid addition (retarder), the MS CSAB cement from reagent-grade chemicals, and a commercial Type I/II portland cement are shown in Figure 7.22. The MC and MF CSAB cements showed no expansion and were comparable to the MS CSAB cement and the commercial Type I/II portland cement.

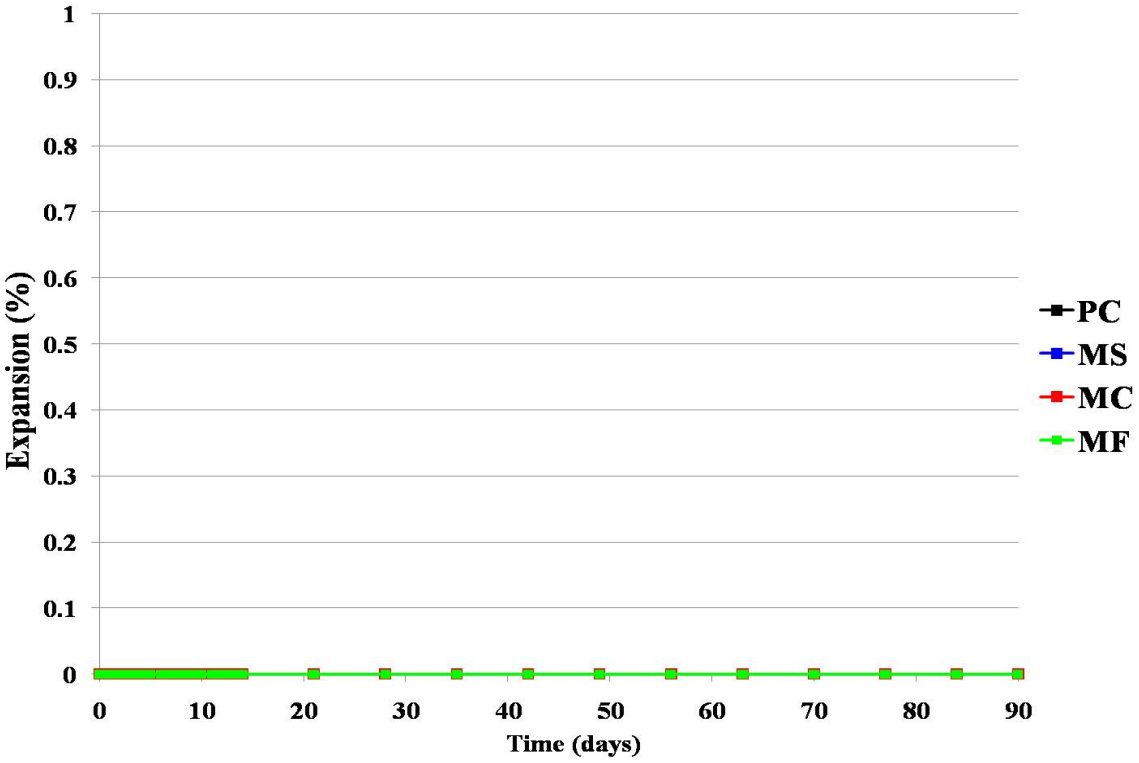

Figure 7.22 – Sulfate resistance for a commercial Type I/II portland cement (PC) and the synthesized CSAB cements from reagent-grade chemicals (MS), Class C fly ash (MC), and fluidized bed ash (MF) stored in 5% sodium sulfate solution after 7 days of hydration; MC and MF with 1% citric acid (retarder) addition

7.5.5 Compressive Strength Development

Compressive strength results for the MC and MF CSAB cements from natural and waste materials with 1% citric acid addition (retarder), the MS CSAB cement from reagent-grade chemicals, and a commercial Type I/II portland cement are shown in Figure 7.23. The MC and MF CSAB cements developed compressive strength exceeding the MS CSAB cement even though they had similar phase compositions. This is because more C_2S reacted in the hydrated MC and MF CSAB cements at later ages and contributed to the long-term compressive strength development, as shown in the hydration product development results (Table 7.7). Furthermore, the MC and MF CSAB

cements showed similar compressive strength development to the commercial Type I/II portland cement.

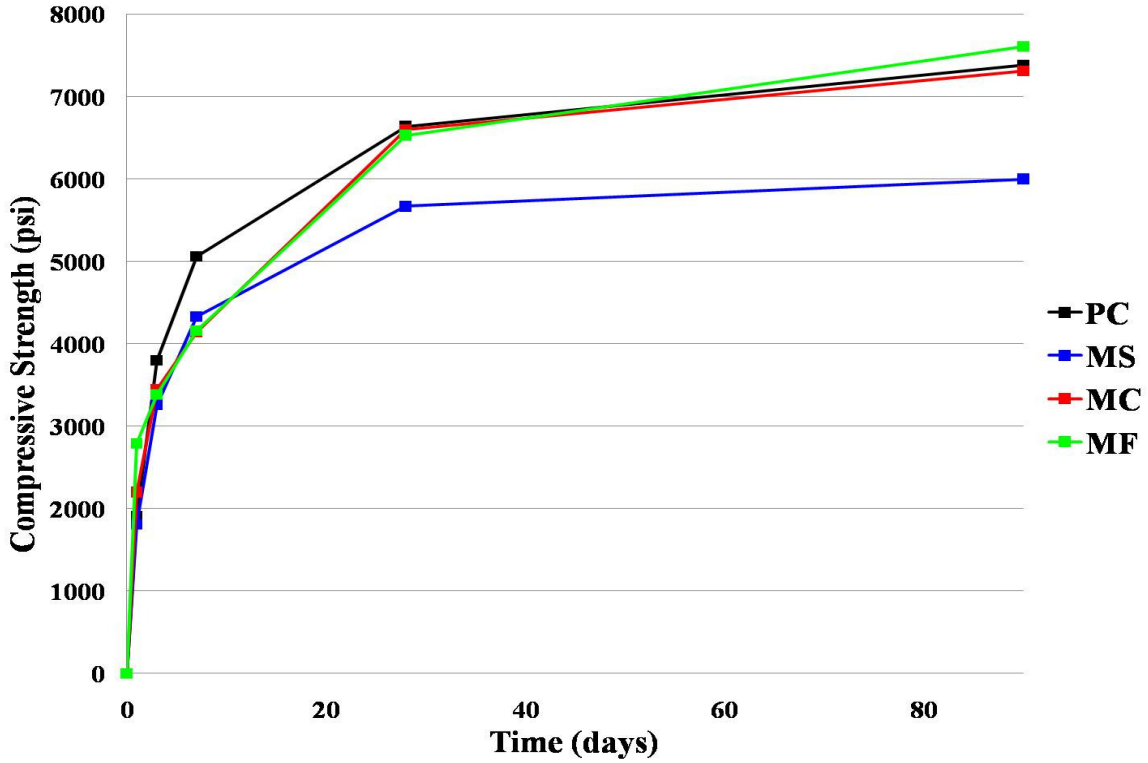

Figure 7.23 – Compressive strength development for a commercial Type I/II portland cement (PC) and the synthesized CSAB cements from reagent-grade chemicals (MS), Class C fly ash (MC), and fluidized bed ash (MF); MC and MF with 1% citric acid (retarder) addition

7.6 CONCLUSIONS

Two CSAB cement clinkers (MC and MF) were successfully synthesized from limestone, bauxite, flue gas desulfurization sludge, Class C fly ash, and fluidized bed ash that were proportioned according to the MS CSAB cement clinker synthesized from reagent-grade chemicals. Waste materials composed 30% and 41% of the raw ingredients for the MC and MF CSAB cement clinkers, respectively. The phase compositions for the MC and MF CSAB cement clinkers were reasonably close to their

target phase compositions and the MS CSAB cement clinker, indicating that the adapted Bogue method can effectively predict CSAB cement clinker phase composition from its raw materials oxide composition when using natural and waste materials as raw materials. Impurities contained in the natural and waste materials slightly affected phase formation as $C_5S_2\overline{S}$ and periclase (MgO) formed; however, their contents were about 2% and should not seriously affect performance. The MC and MF CSAB cements (defined as clinkers with their optimum gypsum contents added) reacted extremely quickly and had much higher maximum heat evolution rates than the MS CSAB cement even though they had similar clinker phase compositions. The accelerating effect was caused by the alkali impurities from waste materials contained in the MC and MF CSAB cements. However, 1% citric acid was shown to be enough to effectively retard the hydration reaction. Hydration product development results from X-ray diffraction showed that C_2S reacted faster at later ages in the MC and MF CSAB cement than in the MS CSAB cement. The impurities incorporated in C_2S lattice increased its hydraulic reactivity. Dimensional stability and sulfate resistance results showed that the MC and MF CSAB cements with 1% citric acid addition had limited expansion and was comparable to the MS CSAB cement and the commercial Type I/II portland cement. Finally, compressive strength results showed that the MC and MF CSAB cements with 1% citric acid addition developed compressive strength exceeding the MS CSAB cement and were comparable to the commercial Type I/II portland cement.

The MF and MC CSAB cement clinkers from natural and waste materials were successfully synthesized at a maximum temperature of 1250ºC, which is 200ºC lower than the maximum temperature used for portland cement clinker synthesis. The lower synthesis temperature reduces energy consumption and CO_2 emissions from cement manufacturing. Moreover, raw ingredients for the MC and MF CSAB cement clinkers

synthesized from natural and waste materials composed of 49.0% and 39.4% $CaCO_3$, which are 34.3% and 47.2% less than the portland cement clinker synthesized from natural materials (gray limestone and yellow limestone; 74.6% $CaCO_3$), respectively. The low lime requirement for CSAB cement production further reduces energy consumption and CO_2 emissions ($CaCO_3 \rightarrow CaO + CO_2$, $\Delta H = 178$ kJ/mol) from cement manufacturing. Finally, the use of high aluminum-containing waste materials such as Class C fly ash and fluidized bed ash reduces the use of expensive alumina bearing raw materials such as bauxite, thereby reducing cost and the environmental impact of cement manufacturing.

Chapter 8: Conclusions and Future Research

8.1 CONCLUSIONS

In the portland cement part of the research, portland cement clinkers conforming to the compositional specifications in ASTM C 150 for Type I cement were successfully synthesized from reagent-grade chemicals, reagent-grade chemicals with up to 40% fly ash and 60% slag incorporation (with 10% intervals), natural materials (gray limestone and yellow limestone), 72.5% limestone with 27.5% fly ash, and 65% limestone with 35% slag. However, waste materials significantly affected cement phase formation. The C_3S–C_2S ratio decreased with increasing amounts of waste materials incorporated. Periclase (MgO) was the only impurity phase formed; however, the quantities formed were less than the limit specified in ASTM C 150. On the other hand, the incorporation of waste materials had little to no effect on the spatial distribution of phases. The synthesized portland cements had similar early-age hydration behavior to commercial portland cement; however, their heat evolution rates and cumulative heat were lower.

Manufacturing portland cement with waste materials incorporation can reduce energy consumption, CO_2 emissions, and landfilling of wastes, thereby reducing the environmental impact of the portland cement production. Moreover, manufacturing portland cement from waste materials does not preclude it from being replaced with SCMs in concrete. These two methods can be applied simultaneously to further reduce the environmental impact of the concrete production.

In the calcium sulfoaluminate-belite (CSAB) cement part of the research, three CSAB cement clinkers with a range of phase compositions were successfully synthesized from reagent-grade chemicals. However, special care should be taken during the firing process because sulfur contained in the raw ingredients evaporated at high temperature.

The phase compositions for the CSAB cement clinkers were reasonably close to their target phase compositions, indicating that the adapted Bogue method can effectively predict CSAB cement clinker phase composition from its raw materials oxide composition. Rate of heat evolution and cumulative heat results showed that the optimum gypsum contents for the CSAB cement clinkers mainly depended on their $C_4A_3\overline{S}$ contents. An equation was developed to predict the optimum gypsum content based on the phase composition of CSAB cement clinker. The synthesized CSAB cements with higher $C_4A_3\overline{S}$ contents had higher maximum rate of heat evolution and cumulative heat than the synthesized CSAB cements with lower $C_4A_3\overline{S}$ contents. Hydration product development results from X-ray diffraction for the synthesized CSAB cements showed that $C_4A_3\overline{S}$ and gypsum reacted quickly and contributed to the formation of ettringite and amorphous AH_3. Most of the $C_4A_3\overline{S}$ and gypsum reacted by 7 days of hydration. However, C_2S remained mostly unhydrated at 90 days of hydration in all the synthesized CSAB cements. The synthesized CSAB cement with high $C_4A_3\overline{S}$ – C_2S ratio showed poor dimensional stability and sulfate resistance perhaps due to the large amounts of ettringite and amorphous AH_3 that formed after cement hardened caused expansion and cracking. The synthesized CSAB cement with low $C_4A_3\overline{S}$ –C_2S ratio showed sluggish compressive strength development. However, the synthesized CSAB cement with medium $C_4A_3\overline{S}$ –C_2S ratio showed good dimensional stability, sulfate resistance, and compressive strength development and was considered the optimum phase composition for CSAB cement in terms of comparable performance characteristics to portland cement.

Two CSAB cement clinkers were successfully synthesized from natural and waste materials such as limestone, bauxite, flue gas desulfurization ash, Class C fly ash, and fluidized bed ash proportioned to the optimum CSAB cement clinker synthesized from

reagent-grade chemicals. Waste materials composed 30% and 41% of the raw ingredients. The phase compositions for the CSAB cement clinkers synthesized from natural and waste materials were reasonably close to their target phase compositions and the optimum CSAB cement clinker synthesized from reagent-grade chemicals, indicating that the adapted Bogue method can effectively predict CSAB cement clinker phase composition from its raw materials oxide composition when using natural and waste materials as raw materials. Impurities contained in the natural and waste materials slightly affected phase formation as $C_5S_2\overline{S}$ and periclase (MgO) formed; however, their contents were about 2% and should not seriously affect performance. The synthesized CSAB cements from natural and waste materials reacted extremely quickly and had much higher maximum heat evolution rates than the optimum synthesized CSAB cement from reagent-grade chemicals even though they had similar clinker phase compositions. The accelerating effect was caused by the alkali impurities from the waste materials. However, 1% citric acid was shown to be enough to effectively retard the hydration reaction. Hydration product development results from X-ray diffraction showed that C_2S reacted faster at later ages in the synthesized CSAB cement from natural and waste materials than in the synthesized optimum CSAB cement from reagent-grade chemicals. The impurities incorporated in C_2S lattice increased its hydraulic reactivity. The two synthesized CSAB cements from natural and waste materials with 1% citric acid addition showed good dimensional stability, sulfate resistance, and compressive strength development exceeding the optimum synthesized CSAB cement from reagent-grade chemicals and were comparable to commercial portland cement.

All the CSAB cement clinkers were successfully synthesized at a maximum temperature of 1250ºC, which is 200ºC lower than the maximum temperature used for portland cement clinker synthesis. The lower synthesis temperature reduces energy

consumption and CO_2 emissions from cement manufacturing Moreover, raw ingredients for the two CSAB cement clinkers synthesized from natural and waste materials composed of 49.0% and 39.4% $CaCO_3$, which are 34.3% and 47.2% less than the portland cement clinker synthesized from natural materials (gray limestone and yellow limestone; 74.6% $CaCO_3$), respectively. The low lime requirement for CSAB cement production further reduces energy consumption and CO_2 emissions ($CaCO_3 \rightarrow CaO + CO_2$, $\Delta H = 178$ kJ/mol) from cement manufacturing. Finally, the use of high aluminum-containing waste materials such as Class C fly ash and fluidized bed ash reduces the use of expensive alumina bearing raw materials such as bauxite, thereby reducing cost and the environmental impact of cement manufacturing.

8.2 FUTURE RESEARCH

Portland cement properties are mainly governed by its phase composition. However, the presence of sulfur impurities in waste materials can significantly affect phase formation in portland cement clinker. The contents of C_2S and CaO increase, while the content of C_3S decreases when increasing amount of SO_3 is incorporated in portland cement clinker synthesis due to the changes in phase equilibria in the CaO–SiO_2–Al_2O_3–Fe_2O_3 system, which renders the standard and modified Bogue method inaccurate. Therefore, a model that is more precise than the currently used Bogue method in addition to empirical experience will be necessary to accurately predict portland cement clinker phase composition when using materials with high SO_3 content as raw ingredients.

Early-age hydration mechanism of CSAB cement system requires further research to better interpret the isothermal conduction calorimetry data. Isothermal conduction calorimetry coupled with pore solution analysis and in situ X-ray diffraction should be

able to provide more detailed information of the early-age hydration mechanism of CSAB cement system. Early-age hydration is of primary importance because of its implications in cement and concrete performance.

Pore solution pH in CSAB cement is generally lower than in portland cement due to its different hydration chemistry. Furthermore, ettringite, the main hydration product in CSAB cement, is susceptible to carbonation, which further lowers the pore solution pH in CSAB cement at later ages. In steel reinforcement concrete, the passivated oxide layer that protects the reinforcement steel from corrosion breaks down when the surrounding pore solution pH is below approximately 11.5, leading to corrosion in the reinforcement steel and cracking in the concrete. Therefore, it is important to investigate the corrosion resistance of this type of system. For this purpose, the synthesized CSAB cements from reagent-grade chemicals (HS, MS, and LS) and natural and waste materials (MC and MF) were sent to the Institute for Research in Construction at the National Research Council of Canada for corrosion resistance study.

Before CSAB cement can be fully utilized, long-term durability behavior such as freeze-thaw resistance, alkali-silica reaction, and delayed ettringite formation should be investigated. Most of the durability testing methods require large amount of cement; however, the amount of cement that can be produced in a laboratory furnace is very limited. Therefore, it is necessary to scale up the production using a small-scale kiln by adapting the synthesis procedures developed in this dissertation.

Appendix A: X-Ray Patterns for the Hydrated Synthesized Calcium Sulfoaluminate-Belite Cements

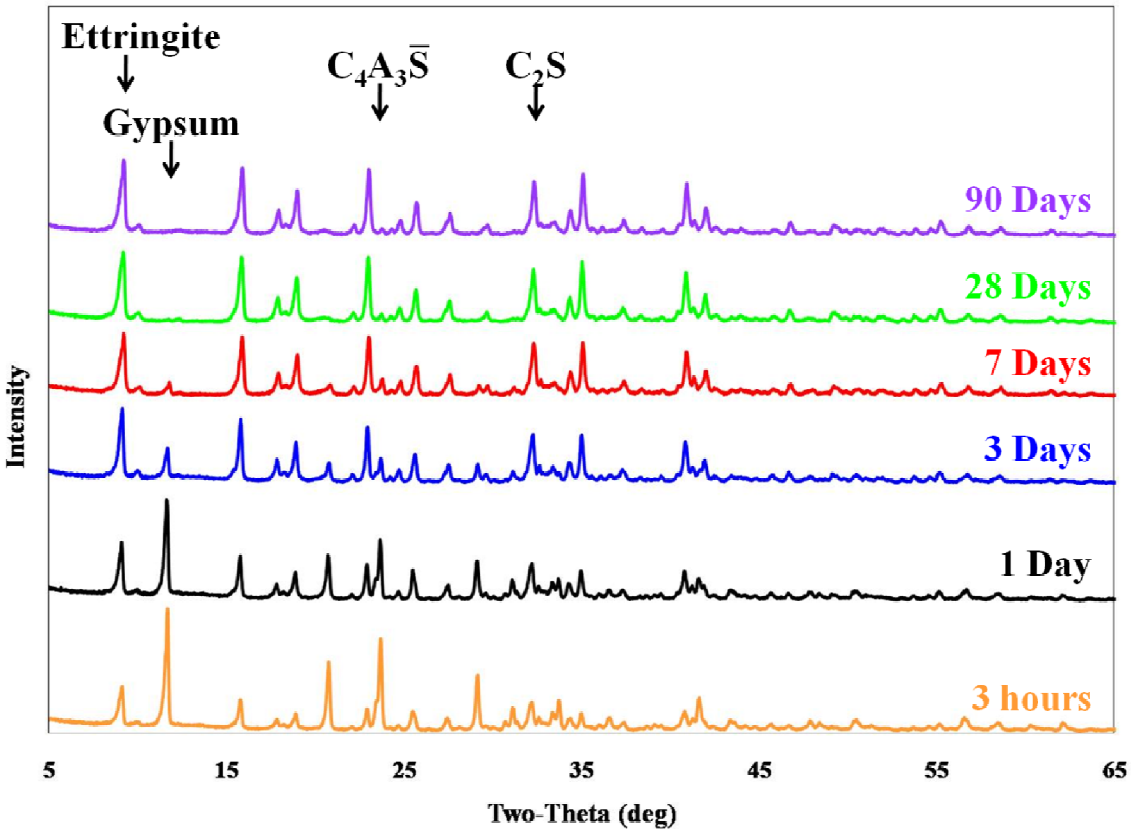

Figure A.1 – X-ray patterns for the hydrated HS CSAB cement synthesized from reagent-grade chemicals

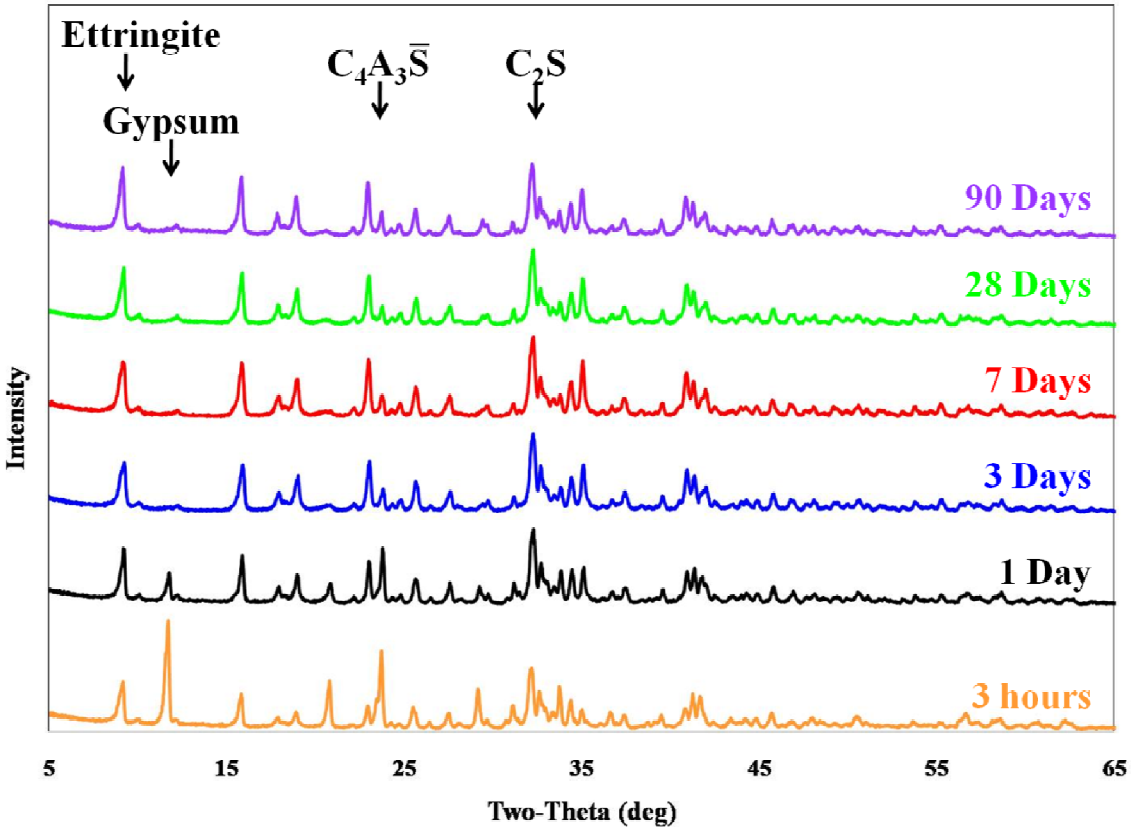

Figure A.2 – X-ray patterns for the hydrated MS CSAB cement synthesized from reagent-grade chemicals

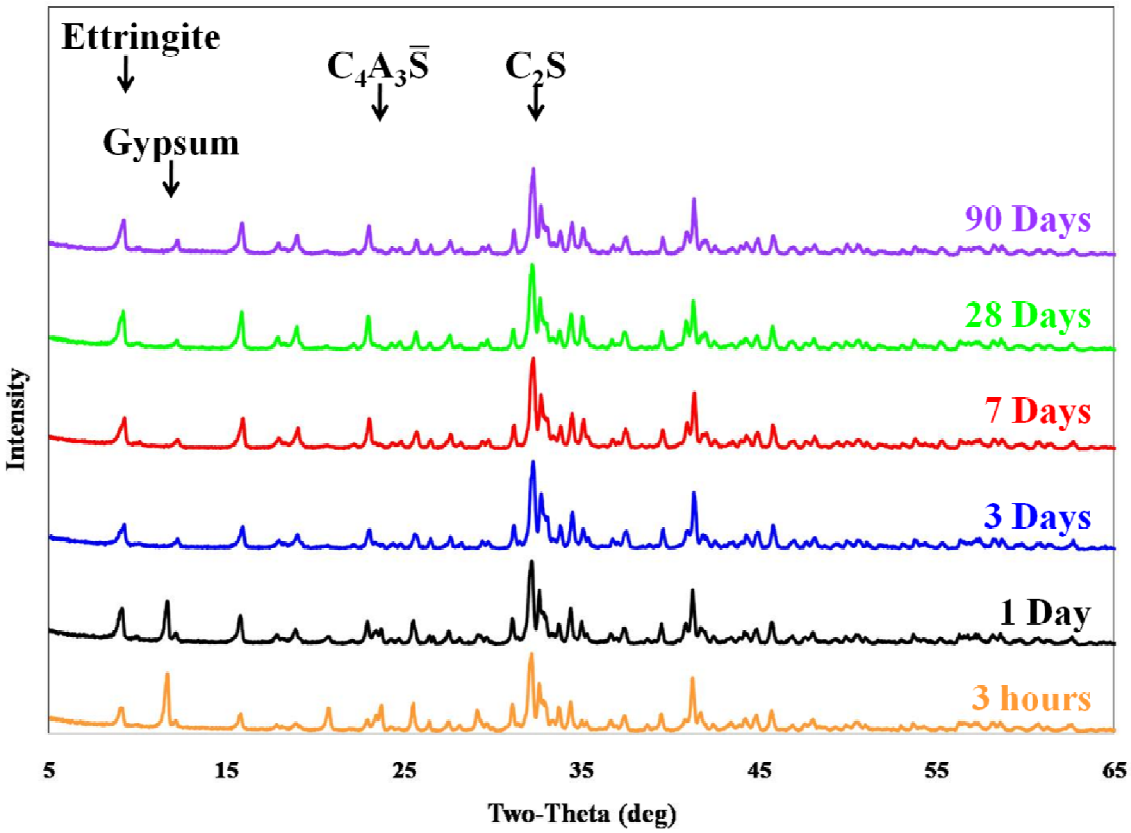

Figure A.3 – X-ray patterns for the hydrated LS CSAB cement synthesized from reagent-grade chemicals

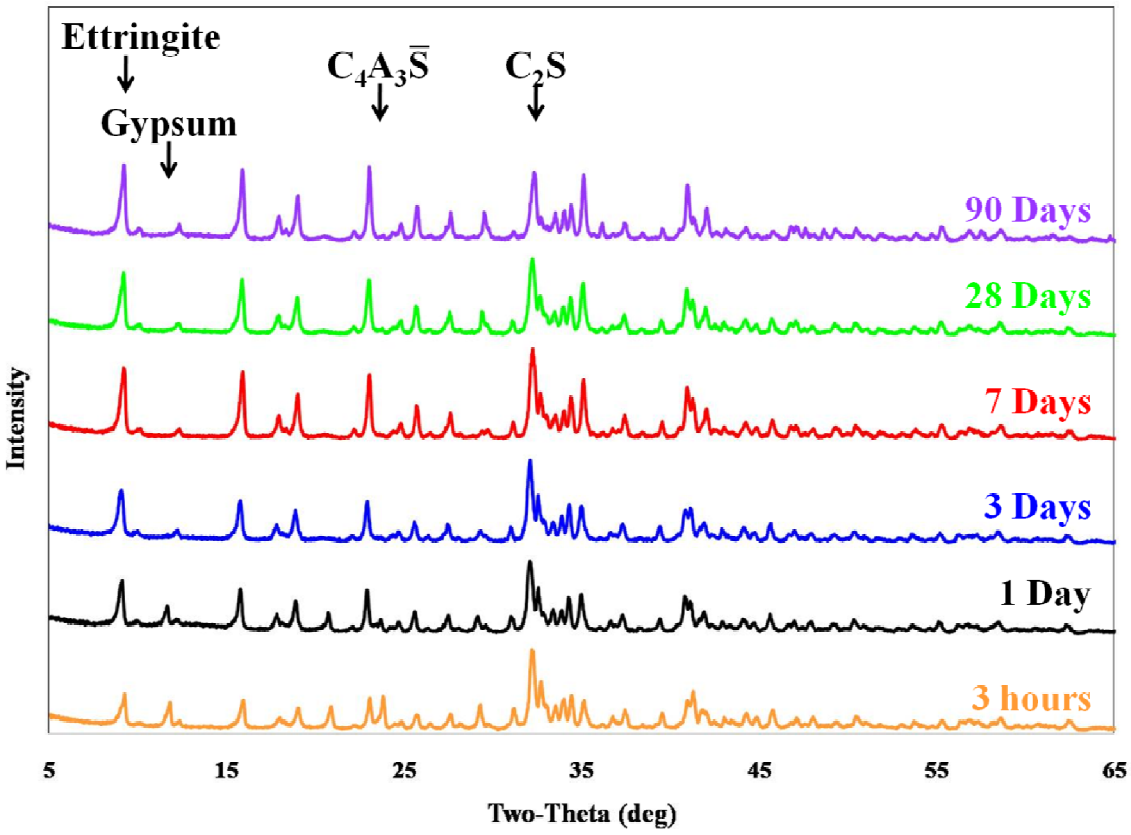

Figure A.4 – X-ray patterns for the hydrated MC CSAB cement synthesized from Class C fly ash

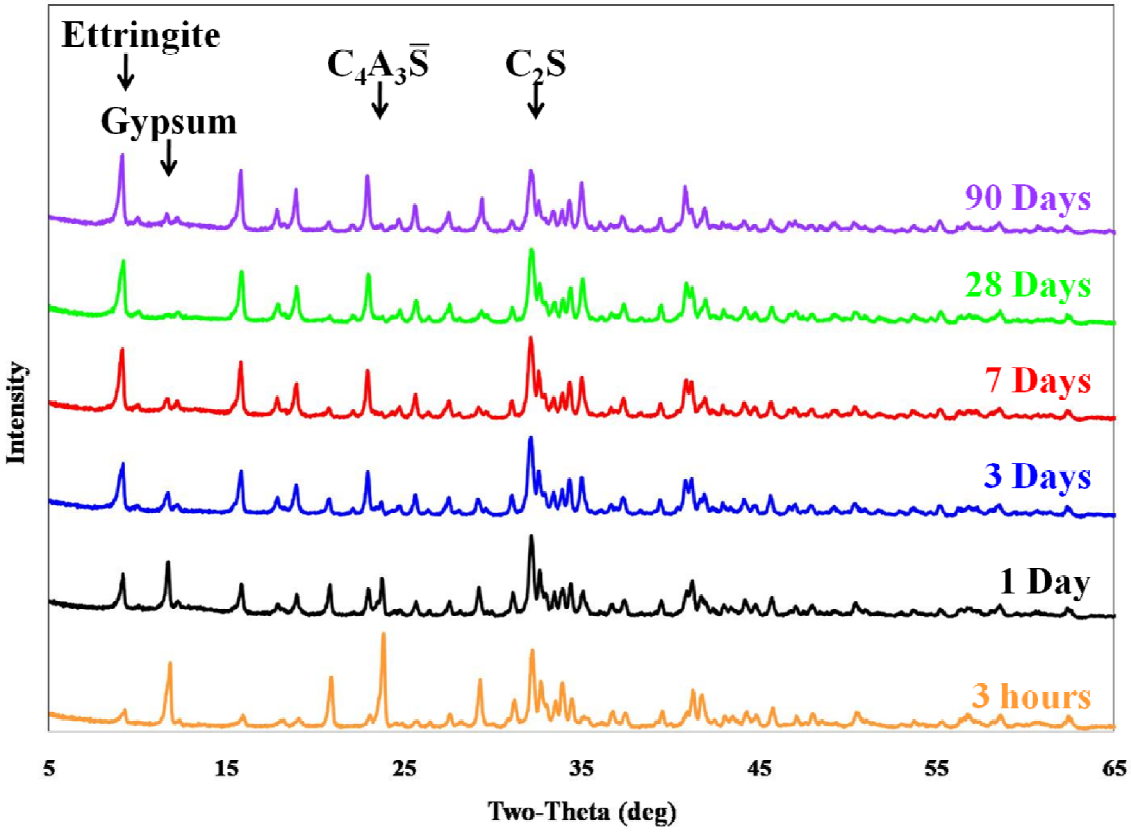

Figure A.5 – X-ray patterns for the hydrated MC CSAB cement synthesized from Class C fly ash with 1% citric acid (retarder) addition

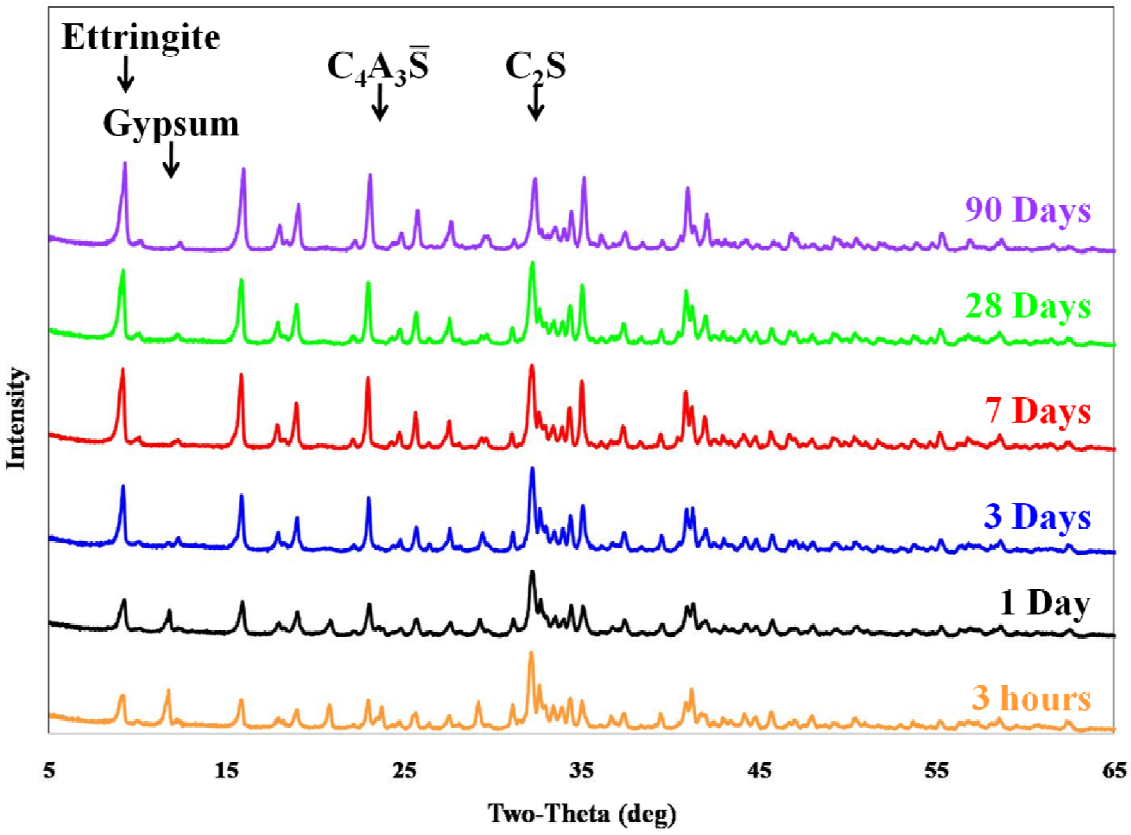

Figure A.6 – X-ray patterns for the hydrated MF CSAB cement synthesized from fluidized bed ash

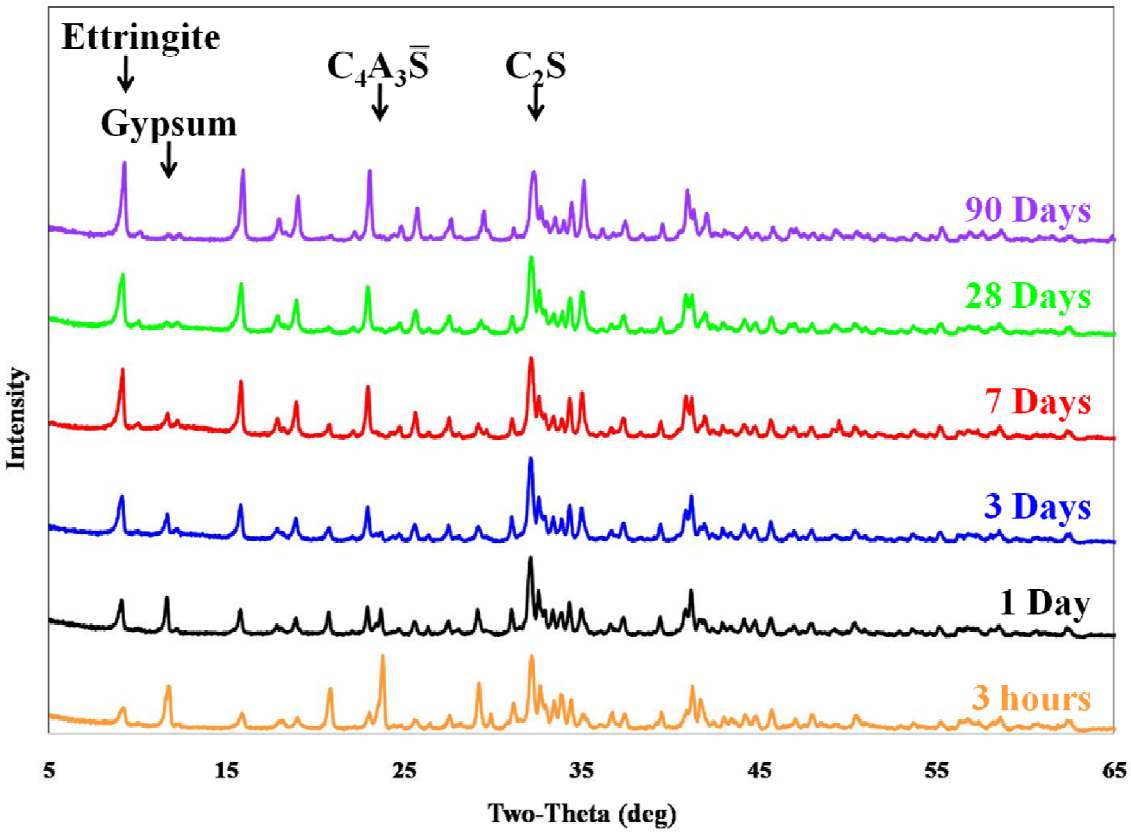

Figure A.7 – X-ray patterns for the hydrated MF CSAB cement synthesized from fluidized bed ash with 1% citric acid (retarder) addition

Bibliography

Arjunan, P., Silsbee, M.R., and Roy, D.M. (1999). "Sulfoaluminate-Belite Cement from Low-Calcium Fly Ash and Sulfur-Rich and other Indistrial By-Products." *Cement and Concrete Research*, 29, 1305-1311.

ASTM C 109. (2007). "Standard Test Method for Compressive Strength of Hydraulic Cement Mortars (Using 2-in. or [50-mm] Cube Specimens)." American Society of Testing and Materials, West Conshohocken, PA.

ASTM C 150. (2005). "Standard Specification for Portland Cement." American Society of Testing and Materials, West Conshohocken, PA.

ASTM C 204. (2007). "Standard Test Methods for Fineness of Hydraulic Cement by Air-Permeability Apparatus." American Society of Testing and Materials, West Conshohocken, PA.

ASTM C 618. (2005). "Standard Specification for Coal Fly Ash and Raw or Calcined Natural Pozzolan for Use in Concrete." American Society of Testing and Materials, West Conshohocken, PA.

ASTM C 1365. (2006). "Standard Test Method for Determination of the Proportion of Phases in Portland Cement and Portland-Cement Clinker Using X-Ray Powder Diffraction Analysis." American Society of Testing and Materials, West Conshohocken, PA.

Bentz, D.P., Garboczi, E.J., Haecker, C.J., and Jensen, O.M. (1999). "Effects of Cement Particle Size Distribution on Performance Properties of Portland Cement-Based Materials." *Cement and Concrete Research*, 29, 1663-1671.

Bernardo, G., Telesca, A., and Valenti, G.L. (2006). "A Porosimetric Study of Calcium Sulfoaluminate Cement Pastes Cured at Early Ages." *Cement and Concrete Research*, 36, 1042-1047.

Beretka, J., Santoro, L., Sherman, N., and Valenti, G.L. (1992). "Synthesis and Properties of Low Energy Cements Based on $C_4A_3\overline{S}$." in *Proceedings of the 9th International Congress on the Chemistry of Cement*, New Delhi, India, 1992.

Beretka, J., Vito, B. de, Santoro, L., Sherman, N., and Valenti, G.L. (1993). "Hydraulic Behavior of Calcium Sulfoaluminate-Based Cements Derived from Industrial Process Wastes." *Cement and Concrete Research*, 23, 1205-1214.

Beretka, J., Marroccoli, M., Sherman, N., and Valenti, G.L. (1996). "The Influence of $C_4A_3\overline{S}$ Content and W/S Ratio on the Performance of Calcium Sulfoaluminate-Based Cements." *Cement and Concrete Research*, 26, 1673-1681.

Bogue, R.H. (1929). "Calculation of the Compounds in Portland Cement." *Industrial and Engineering Chemistry*, 1, 192-197.

Chancey, R.T. (2008). "Characterization of Crystalline and Amorphous Phases and Respective Reactivities in a Class F Fly Ash." Ph.D. Dissertation, The University of Texas at Austin, Austin, TX.

Chen, I.A., and Juenger, M.C.G. (2008). "Calcium Sulfoaluminate-Belite Cement: Effect of Composition on Hydration Behavior." in *Proceedings of the U.S. – South America Workshop, Innovative Materials for Civil Infrastructure Research and Education*, Santiago, Chile.

Chen, I.A., and Juenger, M.C.G. (2009). "Incorporation of Waste Materials into Portland Cement Clinker Synthesized from Reagent-Grade Chemicals." *International Journal of Applied Ceramic Technology*, 6, 270-278.

Chen, I.A., and Juenger, M.C.G. (2009). "Incorporation of Waste Materials into Portland Cement Clinker Synthesized from Natural Raw Materials." *Journal of Materials Science*, 44, 2617-2627.

Dan, E., and Janotka, I. (2003). "Chemical Resistance of Portland Cement, Blast-Furnace Slag Portland Cement and Sulphoaluminate-Belite Cement in Acid, Chloride and Sulphate Solution: Some Preliminary Results." *Ceramics-Silikaty*, 47, 141-148.

Evju, C., and Hansen, S. (2001). "Expansive Properties of Ettringite in a Mixture of Calcium Aluminate Cement, Portland Cement and β-Calcium Sulfate Hemihydrate." *Cement and Concrete Research*, 31, 257-261.

Ferraris, C.F., Bullard, J.W., and Hackley, V. (2006). "Particle Size Distribution by Laser Diffraction Spectrometry: Application to Cementitious Powders." in *Proceedings of the 5th World Congress on Particle Technology*, Orlando, FL.

Ferraris, C.F., Stutzman, P., and Snyder, K. (2006). "Sulfate Resistance of Concrete: a New Approach." PCA Publication R&D Serial No. 2486, http://ciks.cbt.nist.gov/garbocz/monograph/SN248611.pdf.

Fierens, P., and Trilocq, J. (1983). "Effect of Synthesis Temperature and Cooling Conditions of Beta-Dicalcium Silicate on its Hydration Rate." *Cement and Concrete Research*, 13, 41-48.

Fierens, P., and Trilocq, J. (1983). "Nature and Concentration Effect of Stabilizing Elements of Beta-Dicalcium Silicate on its Hydration Rate." *Cement and Concrete Research*, 13, 267-276.

Gaidis, J.M., and Gartner, E.M. (1989). "Hydration Mechanisms II." pp. 9-39 in *Materials Science of Concrete II*, Edited by Skalny, J., and Mindess, S., American Ceramic Society, Westerville, OH.

Gartner, E.M., Young, J.F., Damidot D.A., and Jawed, I. (2002). "Hydration of Portland Cement." pp. 57-113 in *Structure and Performance of Cements*, Edited by Bensted, J., and Barnes, P., Spon Press, New York.

Gartner, E. (2004). "Industrially Interesting Approaches to "Low-CO_2" Cements." *Cement and Concrete Research*, 34, 1489-1498.

Gies, A., and Konfel, D. (1986). "Influence of Alkalis on the Composition of Belite-Rich Cement Clinkers and the Technological Properties of the Resulting Cements." *Cement and Concrete Research*, 16, 411-422.

Glasser, F.P., and Zhang, L. (2001). "High-Performance Cement Matrices Based on Calcium Sulfoaluminate-Belite Compositions." *Cement and Concrete Research*, 31, 1881-1886.

Hanley, W., Constantiner, N., and Goldbrunner, J. (2004). "Retarder for Calcium Sulfoaluminate Cements." US Patent 6818057.

Hendricks, C.A., Worrell, E., Price, L., Martin, N., Ozawa Meida, L., de Jager, D., and P. Riemer, P. (1998). ''Emission Reduction of Greenhouse Gases from the Cement Industry.'' in *Proceedings of the 4th International Conference on Greenhouse Gas Control Technologies*, Interlaken, Austria.

Ideker, J.H. (2008). "Early-Age Behavior of Calcium Aluminate Cement Systems." Ph.D. Dissertation, The University of Texas at Austin, Austin, TX.

Iyer, R.S., and Stanmore, B.R. (1995). "Surface Area of Fly Ashes." *Cement and Concrete Research*, 25, 1403-1405.

Janotka, I., Krajci, L., and Mojumdar, S.C. (2007). "Performance of Sulphoaluminate-Belite Cement with High $C_4A_3\overline{S}$ Content," *Ceramics-Silikaty*, 51, 74-81.

Jawed, I., and Skalny, J. (1978). "Alkalies in Cement: A Review." *Cement and Concrete Research*, 8, 37-51

JCPDS–International Centre for Diffraction Data. (1989). *Powder Diffraction File Search Manual (Hanawalt Method): Inorganic*.

Jones, D.A. (1996). *Principles and Prevention of Corrosion*, 2nd. ed., Prentice Hall, Upper Saddle River, NJ.

Kalogridis, D., Kostogloudis, G.Ch., Ftikos, Ch., and Malami, Ch. (2000). "A Quantitative Study of the Influence of Non-Expansive Sulfoaluminate Cement on the Corrosion of Steel Reinforcement." *Cement and Concrete Research*, 30, 1731-1740.

Kasselouri, V., Tsakiridis, P., Malami, Ch., Georgali, B., and Alexandridou, C. (1995). "A Study on the Hydration Products of a Non-Expansive Sulfoaluminate Cement." *Cement and Concrete Research*, 25, 1726-1736.

Klein, A. (1966). "Expansive and Shrinkage-Compensated Cements." US Patent 3251701.

Komljenovic, M., Jovanovic, N., Petrasinovic-Stojanovic, Lj., Bascarevic, Z., and Rosic, A. (2007). "Fly Ash as an Alternative Raw Materials for Portland Cement Clinker Synthesis." in *Proceedings of the 12th International Congress on the Chemistry of Cement*, Montreal, Canada.

Kurtis, K.E., Shomglin, K., Monteiro, P.J.M., Harvey, J., and Roesler, J. (2001). "Accelerated Test for Measuring Sulfate Resistance of Calcium Sulfoaluminate, Calcium Aluminate, and Portland Cements." *Journal of Materials in Civil Engineering*, 13, 216-221.

Lerch, W. (1947). "The Influence of Gypsum on the Hydration and Properties of Portland Cement Pastes." in *Proceedings of the American Society for Testing Materials* 46, 1252.

Lydon, J.W. (2005). "The Measurement of the Modal Mineralogy of Rocks from SEM Imagery: the use of Multispec© and ImageJ Freeware." Geological Survey of Canada, Open File 4941, 37p.

Majling, J., Sahu, S., Vlna, M., and Roy, D.M. (1993). "Relationship between Raw Mixture and Mineralogical Composition of Sulfoaluminate Belite Clinkers in the System CaO-SiO_2-Al_2O_3-Fe_2O_3-SO_3." *Cement and Concrete Research*, 23, 1351-1356.

Majling, J., Strigac, S., and Roy, D.M. (1999). "Generalized Bogue Computations to Forecast the Mineralogical Composition of Sulfoaluminate Cements Based of Fly Ashes." *Advances in Cement Research*, 11, 27-34.

McKeever, K.J. (2005). "Methods of Portland Cement Production from Pure Chemicals." Master Thesis, The University of Texas at Austin, Austin, TX.

Mehta, P.K. (1980). "Investigation on Energy-Saving Cements." *World Cement Technology*, 11, 167-177.

Mehta, P.K., and P.J.M., Monteiro (2005). *Concrete: Microstructure, Properties, and Materials*, 3rd. ed., McGraw-Hill, New York.

Minard, H., Nonat, A., and Garrault, S. (2007). "Understanding of Reactional Sequences and Limiting Stages during Tricalcium Aluminate Hydration with and without Gypsum." in *Proceedings of the 12th International Congress on the Chemistry of Cement*, Montreal, Canada.

Mindess, S., Young, J.F., and Darwin, D. (2003). *Concrete*, 2nd. ed., Pearson Education, Inc., Upper Saddle River, NJ.

Moschner, G., Lothenbach, B., Figi, R., and Kretzschmar, R. (2009). "Influence of Citric Acid on the Hydration of Portland Cement." *Cement and Concrete Research*, 39, 275-282.

Mohamed, B.M., and Sharp, J.H. (2002). "Kinetics and Mechanism of Formation of Tricalcium Aluminate, $Ca_3Al_2O_6$." *Thermochimica Acta*, 388 105-114.

Monshi, A., and Asgarani, M.K. (1999). "Producing Portland Cement from Iron and Steel Slags and Limestone." *Cement and Concrete Research*, 29, 1373-1377.

Neville, A. (2004). "The Confused World of Sulfate Attack on Concrete." *Cement and Concrete Research*, 34, 1275-1296.

Odler, I. (1998). "Hydration, Setting and Hardening of Portland Cement." pp. 241-297 in *Lea's Chemistry of Cement and Concrete*, Edited by Hewlett, P.C., Arnold, London.

Odler, I., and Colan-Subauste, J. (1998). "Investigations on Cement Expansion Associated with Ettringite Formation." *Cement and Concrete Research*, 29, 731-735.

Ogawa, K., and Roy, D.M. (1982). "$C_4A_3\overline{S}$ Hydration, Ettringite Formation, and its Expansion Mechanisms: III. Effect of CaO, NaOH, and NaCl; Conclusions." *Cement and Concrete Research*, 12, 247-256.

Palou, M.T., and Majling, J. (1995). "Preparation of the High Iron Sulfoaluminate Belite Cements from Raw Mixtures Incorporating Industrial Wastes." *Ceramics-Silikaty*, 39, 41-48.

Palou, M., Majling, J., Doval, M., Kozankova, J., and Mojumdar, S.C. (2005). "Formation and Stability of Crystallohydrates in the Non-Equilibrium System during Hydration of SAB Cements." *Ceramics-Silikaty*, 49, 230-236.

Peng, J., Zhang, J., and Qu, J. "The Mechanism of the Formation and Transformation of Ettringite." *Journal of Wuhan University of Technology-Materials Science Edition*, 21, 158-161.

Phair, J.W. (2006). "Green Chemistry for Sustainable Cement Production and Use." *Green Chemistry*, 8, 763-780.

Quillin, K. (2001). "Performance of Belite-Sulfoaluminate Cements." *Cement and Concrete Research*, 31, 1341-1349.

Quillin, K. (2007). *Calcium Sulfoaluminate Cements – CO_2 Reduction, Concrete Properties and Applications*, IHS BRE Press, Berkshire, UK.

Ramachandran, V.S. (1969). *Applications of Differential Thermal Analysis in Cement Chemistry*, Chemical Publishing Co. Inc., New York.

Rasband, W.S. (1997-2009). "ImageJ." U.S. National Institutes of Health, Bethesda, MD, http://rsb.info.nih.gov/ij/.

Richerson, D.W. (1992). *Modern Ceramic Engineering: Properties, Processing, and Use in Design*, 2nd ed., Marcel Dekker Inc., New York.

Rodrigues, F.A. (2003). "Low-Temperature Synthesis of Cements from Rice Hull Ash." *Cement and Concrete Research*, 33, 1525-1529.

Romano, J.S., Rodrigues, F.A., Bernardi, L.T., Rodrigues, J.A., Segre, N. (2006). "Calcium Silicate Cements Obtained from Rice Hull Ash: A Comparative Study." *Journal of Materials Science*, 41, 1775-1779.

Roy, D.M., Silsbee, M.R., and Xie, Z. (1999). "Influences of Surplus SO_3 in FBC Ash on Formation of Belite-Rich Sulfoaluminate Clinker," in *proceedings of the 1999 International Ash Utilization Symposium*, Center for Applied Energy Research, University of Kentucky, Lexington, KY.

Sahu, S., and Majling, J. (1994). "Preparation of Sulphoaluminate Belite Cement from Fly Ash." *Cement and Concrete Research*, 24, 1065-1072.

Sharp, J.H., Lawrence, C.D., and Yang, R. (1999). "Calcium Sulfoaluminate Cements—Low-Energy Cements, Special Cements or What?" *Advances in Cement Research*, 11, 3-13.

Shih, P.H., Chang, J.E., and Chiang, L.C. (2003) "Replacement of Raw Mix in Cement Production by Municipal Solid Waste Incineration Ash." *Cement and Concrete Research*, 33, 1831-1836.

Singh, M., Upadhayay, S.N., and Prasad, P.M. (1996). "Preparation of Special Cements from Red Mud." *Waste Management*, 16, 665-670.

Singh, M., Upadhayay, S.N., and Prasad, P.M. (2000). "Making Anhydrite Cement from Waste Gypsum." *Cement and Concrete Research*, 30, 571-577.

Stephan, D., and Wilhelm, P. (2004). "Synthesis of Pure Cementitious Phases by Sol-Gel Process as a Precursor." *Journal of Inorganic Chemistry,* 630, 1477-1483 (2004).

Strigac, J., Kristin, J., Sahu, S., Palou, M.T., and Majling, J. (1997). "An Approach to Refine the Bogue's Phase Composition of Sulphoaluminate Belite Cement." in *Proceedings of the 10th International Congress on the Chemistry of Cement*, Gothenburg, Sweden.

Strigac, J., Palou, M.T., Kristin, J., and Majling, J. (2000). "Morphology and Chemical Composition of Minerals inside the Phase Assemblage C-C_2S-$C_4A_3\overline{S}$-C_4AF-C$\overline{S}$ Relevant to Sulphoaluminate Belite Cements." *Ceramics-Silikaty*, 44, 26-34.

Stutzman, P. (2004). "Scanning Electron Microscopy Imaging of Hydraulic Cement Microstructure." *Cement and Concrete Composites*, 26, 957-966.

Stutzman, P., and Leigh, S. (2002). "Phase Composition Analysis of the NIST Reference Clinkers by Optical Microscopy and X-Ray Powder Diffraction." NIST Technical Note 1441, 44p.

Taylor, H.F.W. (1997). *Cement Chemistry*, 2nd ed., Thomas Telford, London, 1997.

Tenoutasse, N. (1968). "The Hydration Mechanism of C_3A and C_3S in the Presence of Calcium Chloride and Calcium Sulphate." in *Proceedings of the 5th International Symposium on the Chemistry of Cement*, Part II: Hydration of Cements, Volume II, Tokyo.

Uda, S., Asakura, E., and Nagashima, M. (1998). "Influence of SO_3 on the Phase Relationship in the System $CaO–SiO_2–Al_2O_3–Fe_2O_3$." *Journal of the American Ceramic Society*, 81, 725-729.

Valenti, G.L., Marroccoli, M., Montagnaro, F., Nobili, M., and Telesca, A. (2007). "Synthesis, Hydration Properties and Environmental Friendly Features of Calcium Sulfoaluminate Cements." in *Proceedings of the 12th International Congress on the Chemistry of Cement*, Montreal, Canada.

Wang, Y., Su, M., Yang, R., and Liu, B. (1992). "A Quantitative Study of Paste Microstructure and Hydration Characteristics of Sulfoaluminate Cement." in *Proceedings of the 9th International Congress on the Chemistry of Cement*, New Delhi, India.

Whitfield, P.S., and Mitchell, L.D. (2003). "Quantitative Rietveld Analysis of the Amorphous Content in Cements and Clinkers." *Journal of Materials Science*, 38, 4415-4421.

Young, R.A. (1995). *IUCr Monographs of Crystallography, Vol. 5, the Rietveld Method*, Oxford University Press, New York.

Zhang, L., Su, M., and Wang, Y. (1999). "Development of the Use of Sulfo- and Ferroaluminate Cements in China." *Advances in Cement Research*, 11, 15-21.

Zhang, L., and Glasser, F.P. (2005). "Investigation of the Microstructure and Carbonation of $C\bar{S}A$-Based Concretes Removed from Service." *Cement and Concrete Research*, 35, 2252-2260.

Vita

Irvin Allen Chen was born in Champaign, IL on May 16, 1983, the son of David M. Chen and Chenghwa Hsu. He graduated from National Panchiao Senior High School in Taipei, Taiwan in 2001. He then entered National Cheng-Kung University in Tainan, Taiwan and received a Bachelor of Science degree in Resources Engineering in 2005. Irvin enrolled in the University of Texas at Austin in 2006 to pursue a Doctor of Philosophy degree in Materials Science and Engineering.

Permanent address: 6F-1, 156 Sez-Wei Rd., Linkou, Taipei County 24441, Taiwan

This dissertation was typed by the author.